THESIS FOR THE DEGREE OF DOCTOR OF PHILOSOPHY (PHD)

Macrophage polarization signals-induced mechanisms of transcriptional and post-transcriptional repression

by Zsolt Czimmerer

Supervisor: Professor Dr. László Nagy

UNIVERSITY OF DEBRECEN

DOCTORAL SCHOOL OF MOLECULAR CELL AND IMMUNE BIOLOGY

DEBRECEN, 2018

Table of contents

1. Abbreviations

3C	chromosome conformation capture
3'UTR	3'-untranslated region
AGO	Argonaute
AP-1	activator protein 1
Arg1	arginase-1
ATAC-seq	Assay for Transposase Accessible Chromatin sequencing
Bcl6	B-cell lymphoma 6 protein
BMDM	bone marrow-derived macrophages
CBP proteins	CREB-binding proteinCEBP CCAAT/enhancer binding
ChIA-PET	chromatin interaction analysis by paired-end tag sequencing
ChIP-seq	Chromatin Immunoprecipitation sequencing
CTCF	CCCTC-binding factor
CLR	C-Type lectin receptor
CXCL	C-X-C motif chemokine
CXCR3	C-X-C motif chemokine receptor 3
ERK	extracellular signal-regulated kinase
eRNA	enhancer RNA
GM-CSF	granulocyte macrophage colony-stimulating factor
GPS2	G protein pathway suppressor 2
GRα	glucocorticoid receptor alpha
GRO-seq	Global Run-On sequencing
H3K4m1	histone H3 lysine 4 mono-methylation
H3K4m2	histone H3 lysine 4 di-methylation
H3K4m3	histone H3 lysine 4 tri-methylation
H3K27Ac	histone H3 lysine 27 acetylation
HAT	histone acetyltransferase
HDAC	histone deacetylase

Hi-C	chromatin conformation capture sequencing
IL-4	interleukin-4
IFNγ	interferon-gamma
IFNGR1	Iinterferon-gamma receptor 1
iNOS	inducible nitric oxide synthase
IPA	Ingenuity Pathway Analysis
IRF-1	interferon regulatory factor 1
Jak1	Janus kinase 1
KLF4	Kruppel-like factor 4
LDTF	lineage determining transcription factor
LPS	Lipopolysaccharide
LXR	Liver X Receptor
MAOA	monoamine oxidase A
M-CSF	macrophage colony-stimulating factor
miRNA	microRNA
Mmp9	matrix metalloproteinase-9
MRC1	mannose receptor 1
MyD88	myeloid differentiation primary response 88
NCoR	nuclear receptor corepressor 1
NFkB	nuclear factor kappa-light-chain-enhancer of activated B cells
NFY	nuclear transcription factor Y
NGS	next generation sequencing
NK cells	natural killer cells
PI3K	phosphoinositide 3-kinase
RISC	RNA-induced silencing complex
RNAPII	RNA Polymerase II
ROS	reactive oxygen species
RUNX	Runt-related transcription factor
SMRT	silencing mediator of retinoic acid and thyroid hormone receptor

SOCS3	suppressor of cytokine signaling 3
Sp1	specificity protein 1
SRTF	stimulus-regulated transcription factors
STAT1	signal transducer and activator of transcription 1
TAD	Topological Associating Domain
TGM2	transglutaminase 2
Tirap	Toll/IL-1 receptor associated protein
TLR	Toll-like-receptor
TNFα	tumor necrosis factor alpha
TSS	transcription start site
YY-1	ying yang 1

2. Introduction

2.1 The macrophage heterogeneity and plasticity in the body

2.1.1. Tissue and molecular microenvironment-dependent heterogeneity of macrophages

Metchnikoff discovered macrophages and described phagocytosis as the main macrophage function more than 100 years ago [1]. Since that time, the pagocytic capacity of macrophages was identified as the key process in the defense against infection and the regeneration following tissue injury and inflammation through the elimination of bacteria, injured host components and apoptotic cells [2]. However, macrophage function is not restricted to their phagocytic activity, they play complex role in the maintenance of tissue homeostasis and the control of immune response via presentation of antigens, production of cytokines and other biologically active molecules as well as regulation of T-cell activation [2-4]. Finally, they are also participating in the resolution of inflammation and wound helaing [2-4].

The phenotypic and functional properties of macrophages are largely dependent on their origin and tissue environment-derived molecular signals [5]. In adult, the majority of tissue macrophages have embryonic origin deriving from embryonic yolk sac and foetal liver precursors (Figure 1) [6]. They represent resident, self-maintaining populations which are associated with organ-specific trophic functions controlling the tissue homeostases under steady state conditions [6, 7].

Bone marrow-derived monocytes are also participating in the replenishment of tissue-resident populations with high turnover including gut and are recruited following tissue injury, infection and inflammation (Figure 1) [8]. In addition, monocyte recruitment is also observed in the host's response to atherogenic, metabolic and neoplastic stimuli. The monocyte-derived macrophages are participating in the regulation of angiogenesis, tumor growth and fibrosis (Figure 1) [9-11].

The phenotypic and functional plasticity of tissue-resident and monocyte-derived macrophages is depended on their dynamic and partially reversible responsiveness to different macrophage polarizing stimuli such as pathogen-derived molecules as well as cytokines and lipids [4]. The two well-characterized extreme outcomes of macrophage polarization are the Th1-type cytokine interferon-gamma (INFγ)-induced classical or M1 macrophage polarization and the Th2-type cytokines interleukin-4 (IL-4)-promoted alternative or M2 macrophage polarization with completely different molecular signatures and fuctional properties [3, 12, 13]. Nevertheless, recent studies show that the integration of various environmental signals are able to induce an entire spectrum of different polarization states besides the M1/M2 end-points and

macrophages can fine-tune their polarization state according to the changing microenvironment during disease progression [4, 12, 14-16].

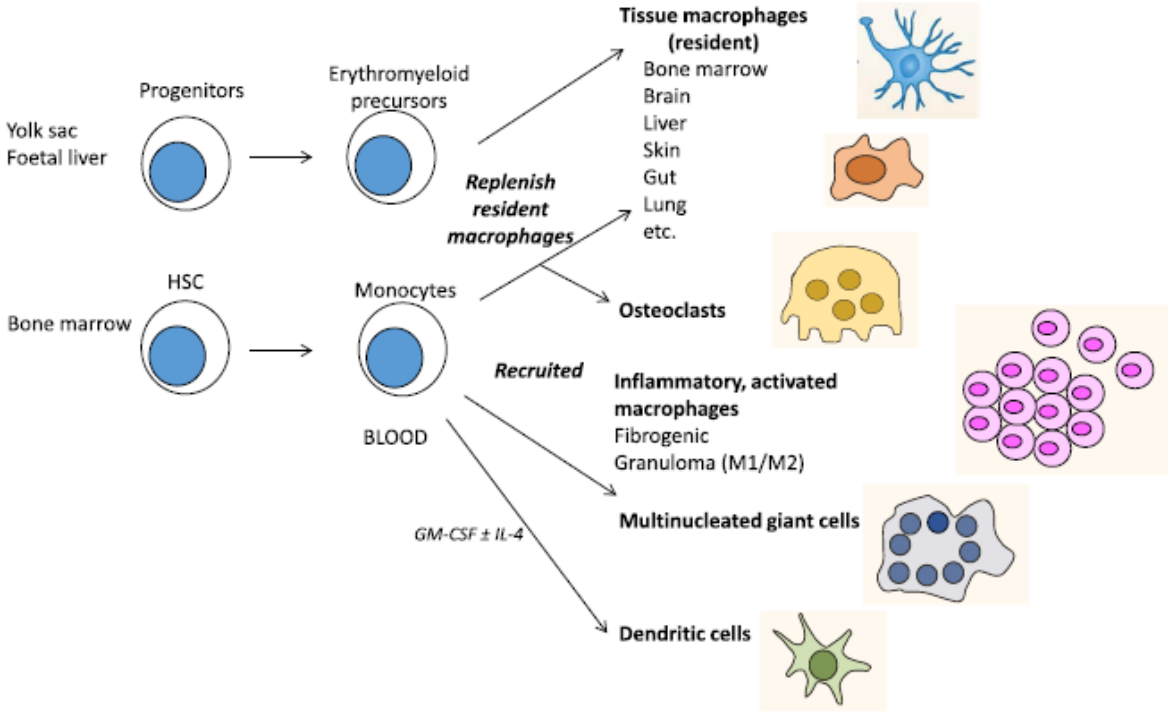

Figure 1. Origin and distribution of tissue macrophages (published in [5]**)**

(HSC: hematopoetic stem cell, GM-CSF: granulocyte macrophage colony-stimulating factor, IL-4: interleukin-4)

2.1.2. Classical macrophage polarization signals, markers and effector functions

The classical macrophage polarization is induced by Th1-type cytokine IFNγ, intracellular pathogens, bacterial cell wall components and granulocyte macrophage colony-stimulating factor (GM-CSF) [17]. Toll-like-receptor (TLR) or C-Type lectin receptor (CLR)-based recognition of invading pathogens leads to the production of inflammatory cytokines such as IFNγ by innate and adaptive immune cells including $CD4^+$ Th1-type T cells, $CD8^+$ T cells and natural killer (NK) cells [4]. Interestingly, INFγ, lipopolysaccharide (LPS), IL-12 or IL-18 stimulation in monocytes and macrophages can also induce INFγ secretion in human and/or mice [18, 19]. The immune cells-derived IFNγ can switch on the classical polarization-specific gene expression program in macrophages promoting the inflammatory response and the elimination of invading pathogens [12, 20]. IFNγ acts via interferon-gamma receptor 1 (IFNGR1) and IFNGR2 chains-containing IFNγ receptor recruiting Janus kinase 1 (Jak1) and Jak2 adaptors, and acticating signal transducer and activator of transcription 1 (STAT1), interferon regulatory factor 1 (IRF-1) as well as IRF-8 transcription factors (Figure 2) [20]. Several

INFγ-induced classical macrophage polarization markers are known including different C-X-C motif chemokines (CXCL9, CXCL10 and CXCL11), cytokines (IL-12), inducible nitric oxide synthase (iNOS) and suppressor of cytokine signaling 3 (SOCS3) [2, 4]. CXCL9, CXCL10 and CXCL11 are responsible for the trafficking $CD4^+$ Th1-type T cells, $CD8^+$ T cells and NK cells through their binding to a common receptor C-X-C motif chemokine receptor 3 (CXCR3) [2, 21]. Macrophage-produced IL-12 participates in the differentiation of naive T cells into Th1-type $CD4^+$ T cells [22]. In addition, IL-12-stimulaton leads to enhanced tumor necrosis factor alpha (TNFα) and IFNγ production in T cells and NK cells as well as elevated cytotoxic activity in NK cells and $CD8^+$ cytotoxic T cells [23, 24]. IFNγ-enhanced iNOS expression results NO production and elevated anti-bacterial capacities in classically polarized macrophages [2]. SOCS3 also contributes to the classical macrophage polarization via the attenuation of IL-4 responsiveness and inhibition of alternative macrophage polarization markers [25, 26].

Gram-negative bacterial cell wall-derived LPS is also an effective inductor of classical macrophage activation. LPS can act as TLR4 ligand and activates nuclear factor kappa-light-chain-enhancer of activated B cells (NFkB) and activator protein 1 (AP-1) transcription factor complexes as well as IRFs in myeloid differentiation primary response 88 (MyD88) and/or Toll/IL-1 receptor associated protein (Tirap)-dependent manner (Figure 2) [27, 28]. LPS-induced classical macrophage polarization are characterized with the elevated expression of pro-inflammatory cytokines (such as IL-1β, IL-6, IL-12, TNFα and IFNβ), chemokines (CCL2, CXCL10 and CXCL11), antigen presentation molecules as well as co-stimulatory molecules resulting leukocyte trafficking and Th1-type inflammation [17]. LPS also augments mitochondrial reactive oxygen species (ROS) production in macrophages leading increased bactericidal capacity [29]. In addition, one of the prominent effector functions of macrophages is the integration of pathogen-associated molecular patterns (PAMPs) including LPS and other microbial signals as well as different endogenous and exogenous danger signals such as uric acid crystal, peptide aggregates, ROS and extracellular ATP into inflammasome activation [30-32]. This two-step activation of macrophages leads to the assembly and activation of NLRP3 inflammasome from NOD-like receptor superfamily member NLRP3, apoptosis-associated speck-like protein containing a CARD (ASC) and pro-Caspase-1 [31, 32]. Activated inflammasomes play a key role in the generation of proinflammatory secreted forms of IL-1β and IL-18 from pro-IL-1β and pro-IL-18. The secreted IL-1β participates in the innate immune response to microbial infection including monocyte-dendritic cell/macrophage differentiation, enhanced bacterial killing and also has pyrogenic effect [33-35]. In parallel, macrophages undergo active Caspase-1-dependent cell death termed "pyroptosis" [31, 32]. This Caspase-1-mediated rapid cell death of bacterial-infected macrophages is associated with rapid cell swelling and membrane rapture similarly to necrosis, leading to the release of intracellular contents [36].

The granulocyte macrophage colony-stimulating factor (GM-CSF) is also able to act as a classical macrophage polarization signal in human and mice. GM-CSF receptor and JAK2 containing GM-CSF signaling pathway activates STAT5, IRF5 and NFkB transcription factors as well as extracellular signal-regulated kinase (ERK) and AKT

kinases resulting the development of classical macrophage polarization state (Figure 2) [17]. GM-CSF induces the expression of several pro-inflammatory cytokines including IL-6, IL-8, TNFα as well as IL-1β, and enhances leukocyte chemotaxis, antigen presentation, complement- and antibody-mediated phagocytosis and microbicidal capacity [37].

Taken together, the classical macrophage polarization is characterized by production of proinflammatory cytokines, reactive nitrogen and oxygen species, induction of Th1 response, and elevated microbicidal capacity.

2.1.3. Alternative macrophage polarization signals, markers and effector functions

The alternative macrophage polarization is induced by Th2-type cytokines, macrophage colony-stimulating factor (M-CSF) and various other signals including glucocorticoids [17, 38]. IL-4 and IL-13 cytokines are produced following the activation of Th2-type immune response. The main sources of these cytokines are $CD4^+$ Th2-type T cells, basophil and eosinophil granulocytes as well as macrophages themselves [17]. IL-4 and IL-13 can activate partially different receptor complexes. Both IL-4 and IL-13 bind to IL-4Rα1-γc and IL-4Rα1-IL-13Rα1 heterodimers while IL-13 is also able to bind to IL-13Rα2 chain. The interaction between IL-4 and its receptors leads to the JAK1 and JAK3 activation inducing STAT6 phosphorylation, dimerization and nuclear translocation (Figure 2) [3, 17]. The phosphorylated STAT6 dimers initiate the alternative macrophage polarization specific transcriptional program [3]. In addition, further IL-4/STAT6 signaling patway-induced transcriptional factors such as IRF4, Kruppel-like factor 4 (KLF4), c-Myc and peroxisome proliferator-activated receptor gamma (PPARγ) also participate in the transcriptional regulation of alternative macrophage polarization [39-42].

Although, the components of IL-4/STAT6 signaling pathway are identical in humans and mice but the IL-4-induced alternatively macrophage polarization markers show species-specific differences [3]. Ym1, Fizz1 and arginase-1 (Arg1) show IL-4-responsiveness in mice, while IL-4-dependent induction of monoamine oxidase A (MAOA) and CD180 expression is restricted to human macrophages [3, 43-45]. In contrast, transglutaminase 2 (TGM2), mannose receptor 1 (MRC1/CD206) and PPARγ are common IL-4-induced alternative macrophage polarization markers [42, 44]. Despite differences in gene expression, the IL-4/IL-13-induced alternative macrophage polarization is associated with anti-inflammatory action in both human and mice [3, 46-49].

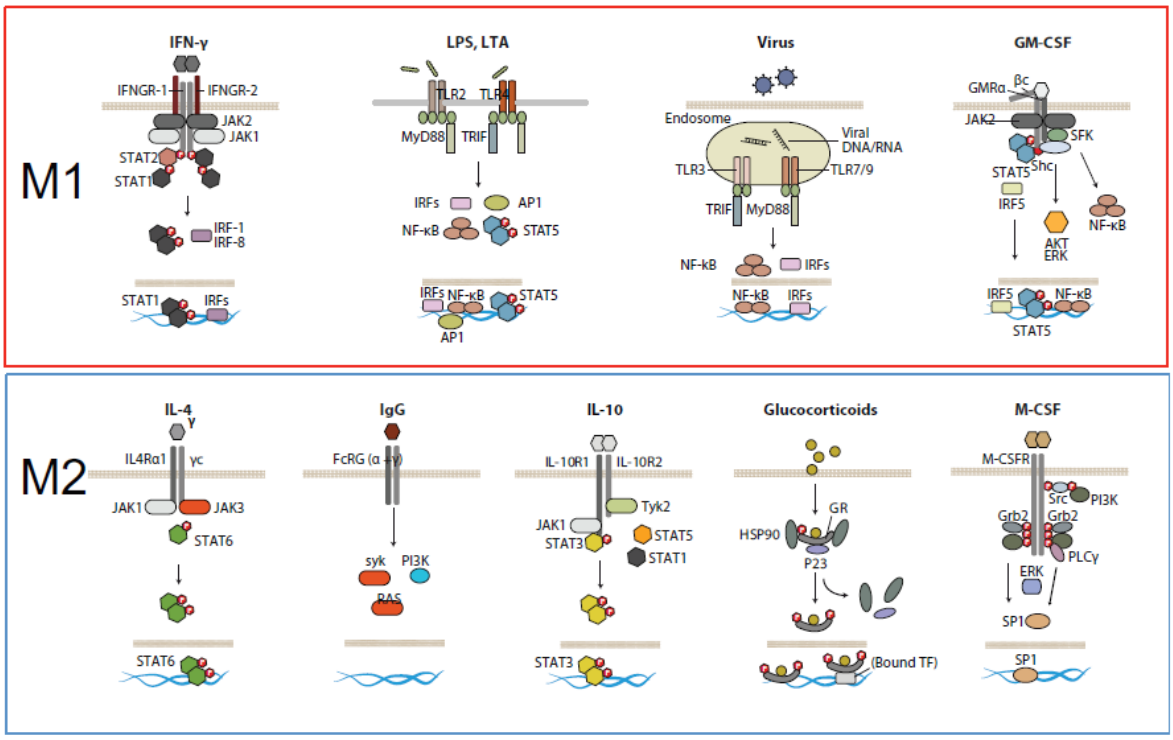

Figure 2. Different M1 and M2 macrophage polarization stimuli-activated signaling pathways (published in [17]**)**

(INFγ: interferon-gamma, IRF:interferon regulatory factor, IFNGR: interferon-gamma receptor, JAK: Janus kinase, STAT: signal transducer and activator of transcription, LPS: lipopolysaccharide, NFkB: nuclear factor kappa-light-chain-enhancer of activated B cells, AP-1: activator protein 1, MyD88: myeloid differentiation primary response 88, TRIF: TIR-domain-containing adapter-inducing interferon-β, LTA: lipoteicholic acid, TLR: Toll-like-receptor, GM-CSF: granulocyte macrophage colony-stimulating factor, ERK: extracellular signal-regulated kinase, SFK: Src family kinase, IL: interlukin, IL-10R: interleukin-10 receptor, PLCγ: Phospholipase C, gamma, PI3K: phosphoinositide 3-kinase)

The adrenal glands-secreted glucocorticoids are lipophilic molacules and activate glucocorticoid receptor alpha (GRα) following the diffusion through plasma membrane. The activated GR complex translocates to the nucleus and induces gene expression changes in macrophages via minimum two independent mechanisms. GR complex can promote/repress transcription directly following DNA binding or indirectly by interacting with NFkB and AP-1 transcription factor complexes (Figure 2) [17]. Glucocorticoid exposure induces the expression of several alternative macrophage polarization markers including MRC1 and CD163 as well as IL-10 production [50]. In addition, long-term glucocorticoid treatment can partially inhibit the LPS and/or IFNγ-induced transcriptional programs [51]. Although, the glucocorticoids-induced transcriptional changes are different from the IL-4-regulated gene expression program but both stimuli have anti-inflammatory properties and are categorized into the alternative macrophage polarization signals [17, 38].

Another alternative macrophage polarization inducer cytokine IL-10 is produced by virtually all leukocytes and inhibits Th1-type immune response. IL-10 acts on IL-10R1-IL-10R2 heterodimer activating STAT3 transcription factor (Figure 2) [17]. IL-10

enhances the expression of chemoattractants such as CXCL13 and CXCL4, as well as cell surface receptor TLR1 and endosomal receptor TLR8 in macrophages [52, 53]. In addition, IL-10 represses the pro-inflammatory cytokine production of macrophages [53].

M-CSF binds to its tyrosine kinase transmembrane receptor and activates ERK, phosphoinositide 3-kinase (PI3K) and phospholipase C leading to the nuclear translocation of specificity protein 1 (Sp1) transcription factor and the development of M2-like macrophage characteristics (Figure 2) [17, 54].

2.1.4. Macrophage polarization *in vivo*

Although, the gene expression signatures and functional properties of classically and alternatively polarized macrophages are well characterized *in vitro* and *ex vivo*, the microenvironmental signals-dependent regulation of phenotypic and functional characteristics of macrophages *in vivo* is more complex and less understood. Both classical and alternative macrophage polarization states can be clearly linked to *in vivo* macrophage functions in different physiological and pathological conditions. While the alternative macrophage polarization plays crutial role in the protection against nematode infections and Th2-type inflammation [55, 56], the classical macrophage activation is tightly associated with Th1-type inflammation and anti-microbial defense [57, 58]. However, several studies showed that M1 and M2 macrophage polarization have overlapping effects in these processes. For instance, classically polarised macrophages-produced reactive nitrogen intermediates may have antiparasitic activity or alternatively polarized macrophages potentiate the secretion of pro-inflammatory cytokines after *Neisseria meningitidis* infection [59, 60]. In addition, inflammatory (M1-like) and restorative (M2-like) macrophages may participate with different kinetics in same pathological process such as muscle injury and regeneration [16]. Neverthelless, most physiological and pathological processes are characterized *in vivo* by complex immunological milieu. The molecular microenvironment may lead to the development of broad spectrum of mixed macrophage polarization states in different pathological conditions including tumor development and different bacterial infection modulating disease progression and therapeutic responsiveness [4, 61, 62]. Therefore, the identification of the potential interactions between the different polarization signals is one of the most important challenges in macrophage biology.

2.2. Molecular and epigenetic bases of polarization signals-mediated transcriptional regulation in macrophages

2.2.1. Epigenomic background of cell type-specific transcriptional regulation

In the last decade, the development of next-generation sequencing-based methods allowed the identification of DNA methylation, histon modification, transcription factor binding, chromatin accessibility and nascent RNA expression on a whole-genome level [63-66]. The combination of these genom-wide assays facilitated the better understanding of the connection between the specific pattern of histone marks and genomic-regulatory regions including promoters and distal regulatory regions termed enhancers in different cell types [65, 66]. In addition, these studies provided an opportunity for the identification of cell type-sepcific enhancer repertoire and its responsiveness to different internal or external stimuli [65-67].

The promoters are located near to the transcription start sites (TSSs) of coding genomic regions towards the 5' region of sense strand, and play central role in the regulation of gene expression. The major function of the promoters is the direction of RNA Polymerase II (RNAPII)-dependent transcriptional initiation in tight cooperation with basal transcription factor machinery [68]. The promoter regions are generally associated with high level of histone H3 lysine 4 tri-methylation (H3K4m3) as well as low H3K4m1 and H3K4m2 [69]. In addition, the promoters contain the combination of binding sites of broadly expressed transcription factors including SP-1, ying yang 1 (YY-1) and nuclear transcription factor Y (NFY) and regulate the tissue and/or signal-specific gene expression signature in collaboration with the tissue and/or signal-specific enhancer repertoire [70, 71].

In general, enhancers are defined as distal regulatory elements in the genome that "enhance" transcription in collaboration with gene-proximal promoters. These distal regulatory elements may be located upstream and downstream from the regulated protein-coding or non-coding genes or within their gene bodies [67]. Enhancers have specific molecular characteristics including unmetylated DNA and nucleosome depletion at sites bound by transcription factors as well as post-translational histone modification pattern. Unlike promoters, the enhancers are associated with relatively high levels of H3K4m1 and low H3K4m3 [72]. The $H3K4m1^{high}/H3K4m3^{low}$ distal regulatory regions are bound by the lineage determining transcription factors (LDTFs), which are responsible for the establishment of cell type-specific enhancer repertoire [67, 73, 74]. These genomic regions serve as an important binding platform for external or internal stimulus-regulated transcription factors (SRTFs) regulating the cell- and signal-specific transcription in tight collaboration with the LDTFs [67, 75].

The actual activation state of the enhancers is strongly dependent on the composition of recruited cofactors including the ratio of coactivators and corepressors. Many coactivators including CREB-binding protein (CBP), p300, GCN5 and PCAF have

histone acetyl-transferase activities and catalyze the acetylation of histone H3 at lysine K27, K9, K14, and histone H4 at lysine K5, K8 and K12. The enrichment of these histone modifications correlates with enhancer activity and active transcription [76-80]. These coactivators are detected at the active enhancers or recruited to enhancers following SRTFs binding [72, 81, 82]. In contrast, the corepressor complexes such as nuclear receptor corepressor 1 (NCoR)/ silencing mediator of retinoic acid and thyroid hormone receptor (SMRT), Sin3 and polycomb complexes associate with histone deacetylase, H3K4 demethylase or histone lysine methylase activities and remove the active histone mark acetyl grops or methyl gropus from H3K4 and catalyse H3K27 trimethylation leading to transcriptional repression [83-85].

In the last decade, the combination of chromosome conformation capture (3C) studies including 3C, chromatin conformation capture sequencing (Hi-C) and chromatin interaction analysis by paired-end tag sequencing (ChIA-PET) with CCCTC-binding factor (CTCF)-specific chromatin immunoprecipitation sequencing (ChIP-seq) experiments contributed to the better understanding of 3D chromatin organization [86, 87]. These studies identified the megabase sized chromosomal regions so-called topological associating domains (TADs) as the functional units of chromosomes. The tissue-invariant TAD boundaries are marked by CTCF binding, which plays essential role in stable long-range loop formation between these genomic regions. These structural domains are characterized by favourable contacts between genomic loci inside the same TAD and insulation from loci in neighbouring TADs determining the potential promoter-enhancer interactions [88, 89]. The effective enhancer-mediated transcriptional activation/repression needs its close spatial proximity to susceptible gene/promoter. The three-dimensional chromatin loop formation between the enhancers and promoters usually occurs within the boundaries of TADs [89]. Two different enhancer-promoter loop types are distinguished such as constitutive and *de novo* loops [90]. The constitutive loops between enhancers and promoters are formed in a cell-type and transcriptional status independent manner. This type of loop formation is mediated by CTCF without the association of typical enhancer marks such as DNase hypersensitivity and histone acethylation [91-93]. In contrast, *de novo* or tissue-specific enhancer-promoter loops require the tissue-specific transcription factors-recruited mediator and cohesion complexes [94, 95].

Recently, the global run-on sequencing (GRO-seq) studies described that nascent RNA expression is observed at the RNAPII-bound active enhancers in different cell-types including breast cancer cells, B cells and macrophages [96-99]. In addition, enhancer RNA (eRNA) expression is dynamically regulated by different external signals including nuclear receptor and TLR4 ligands, as well as eRNA levels show high correlation with the transcription of neighboring genes suggesting that eRNA expression may be a good marker of enhancer activity [97, 99]. Although, the exact function of eRNAs is not fully understood in the transcriptional regulation but some findings indicate that eRNAs can participate in the *de novo* promoter-enhancer looping promoting the transcription of protein-coding genes [100-102].

2.2.2. Polarization signals-mediated transcriptional activation in macrophages

The rapid and dramatic alteration of transcriptional output in macrophages is necessary for the quick adaptation to abruptly changing environments during infections or tissue injuries. In addition, each macrophage subtipes have highly specialized functions in normal homeostatic conditions, which require the expression of function-specific gene subsets. The macrophage-specific transcriptome and its dynamic responsiveness to the microenvironmental changes are significantly determined by different epigenomic regulatory mechanisms including DNA methylation, post-translational histone modifications and overall 3D architecture of the genome [103].

Based on H3K4m1 and H3K4m3-specific ChIP-seq experiments, 35000-45000 H3K4m1^{high} and H3K4m3^{low} enhancers were identified in mouse macrophages [82, 104]. Importantly, many LDTF binding motifs including ETS-domain transcription factor PU.1, AP-1, IRF, CCAAT/enhancer binding proteins (CEBP) and Runt-related transcription factor (RUNX) are enriched significantly at these regions suggesting their important role in the determination of macrophage specific enhancers [82, 104]. Many experimental evidence indicate that PU.1 is a key LDTF for the determination of macrophage-specific enhancer landscape. It has been described that, the macrophages are completely abscent in PU.1 deficient mice and the majority of H3K4m1 positive enhancers are occupied in resting macrophages by PU.1 [82, 104, 105]. PU.1 depletion also leads to the decreased H3K4m1 enrichment at several PU.1-bound enhancers in macrophages as well as the ectopic expression of PU.1 in mouse fibroblast 3T3 cells results in an increased H3K4m1 enrichment and development of nucleosome-depleted region at the same region as in macrophages [82, 104]. In addition, further LDTFs including CEBPα and IRF8 show highly overlapping cistrome with PU.1 and regulate the development of macrophage-specific enhancer landscape in thight collaboration with PU.1 [104, 106].

The changing microenvironment leads to the activation of SRTFs including NFkB, AP-1, STAT1, STAT6 or nuclear receptors in macrophages. The activated SRTFs control the macrophage polarization-specific gene expression program by binding to the promoters and enhancers of their target genes (Figure 3) [75]. The ChIP-seq studies show that the most signal-induced DNA binding events of SRTFs are observed at macrophage-specific LDTF-bound H3K4m1 positive enhancers.

In parallel with SRTF binding, stimulus-induced recruitment of coactivator p300 and enhanced active histone mark H3K27Ac enrichment as well as elevated eRNA expression are also observed at the enhancers nearby the activated genes suggesting the SRTF-dependent activation of this enhancer subsets (Figure 3) [82, 97, 99, 107]. Despite the fact that the significant portion of signal-induced SRTF binding is observed at the pre-determined enhancers, small percentage SRTF binding is linked to closed genomic regions. The SRTF binding at these genomic regions results in the acquisition of active enhancer marks such as H3K4m1 and H3K27Ac. These “de novo” or “latent”

enhancers bind the SRTFs with macrophage-specific LDTFs following the SRTF activation suggesting their collaboration in this enhancer subset [99, 108].

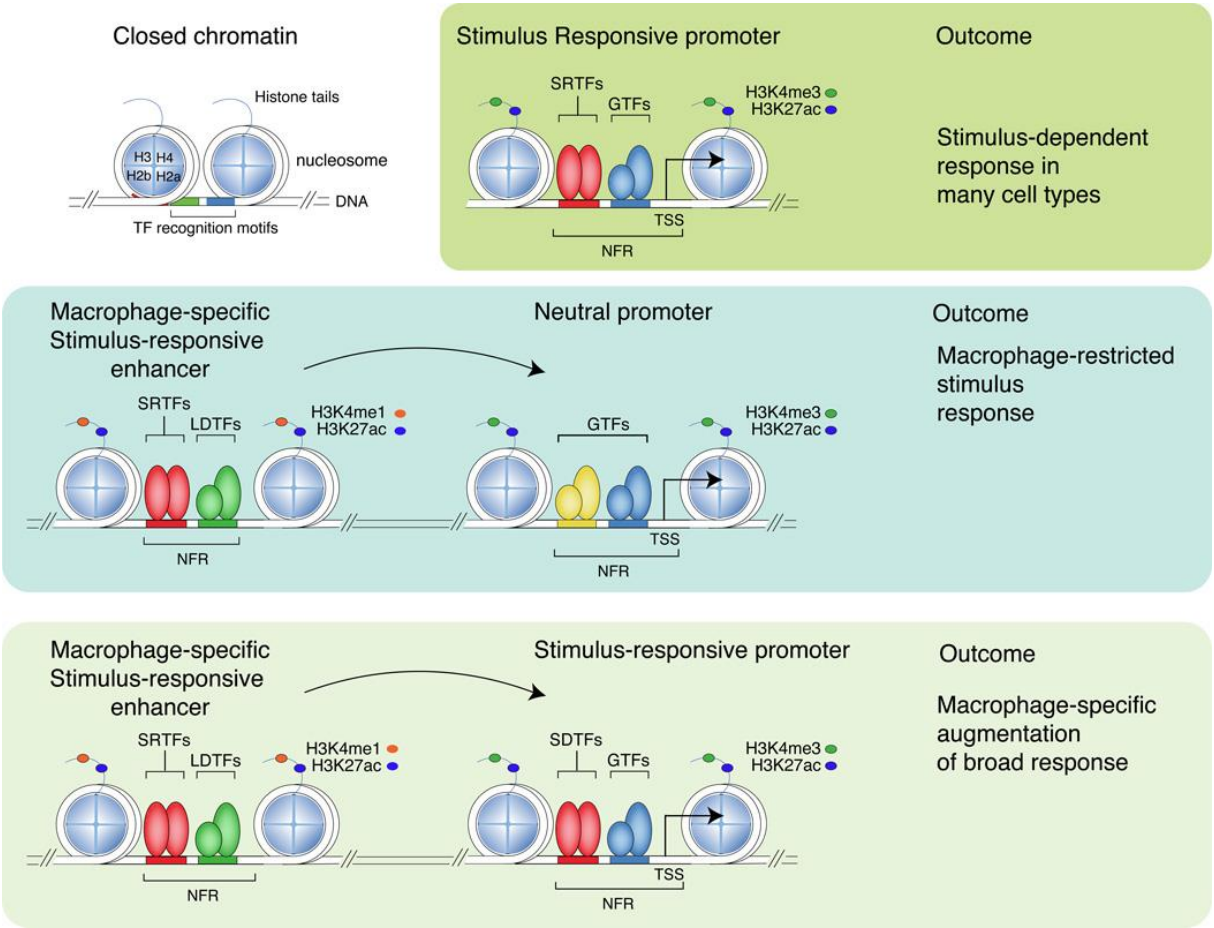

Figure 3. Mechanisms of macrophage polarization signals-induced transcriptional activation (published in [75]**)**

(H3K27Ac: H3 acetylated at lysine 27, H3K4me1: histone H3 monomethylation at lysine 4, NFR: nucleosome free region, TSS: transcriptional start site, SRTF: stimulus responsive transcription factor, GTF: general transcription factor, LDTF: lineage determining transcription factor, SRTF: stimulus responsive transcription factor, H2a, H2b, H3, H4: histones H2a, 2b, 3 and 4)

2.2.3. Molecular bases of transcriptional repression in macrophages

Several experimental evidence indicate that transcriptional repression mechanisms can also modulate the inflammatory status and the responsiveness to different microenvironmental stimuli in macrophages (Figure 4) [109].

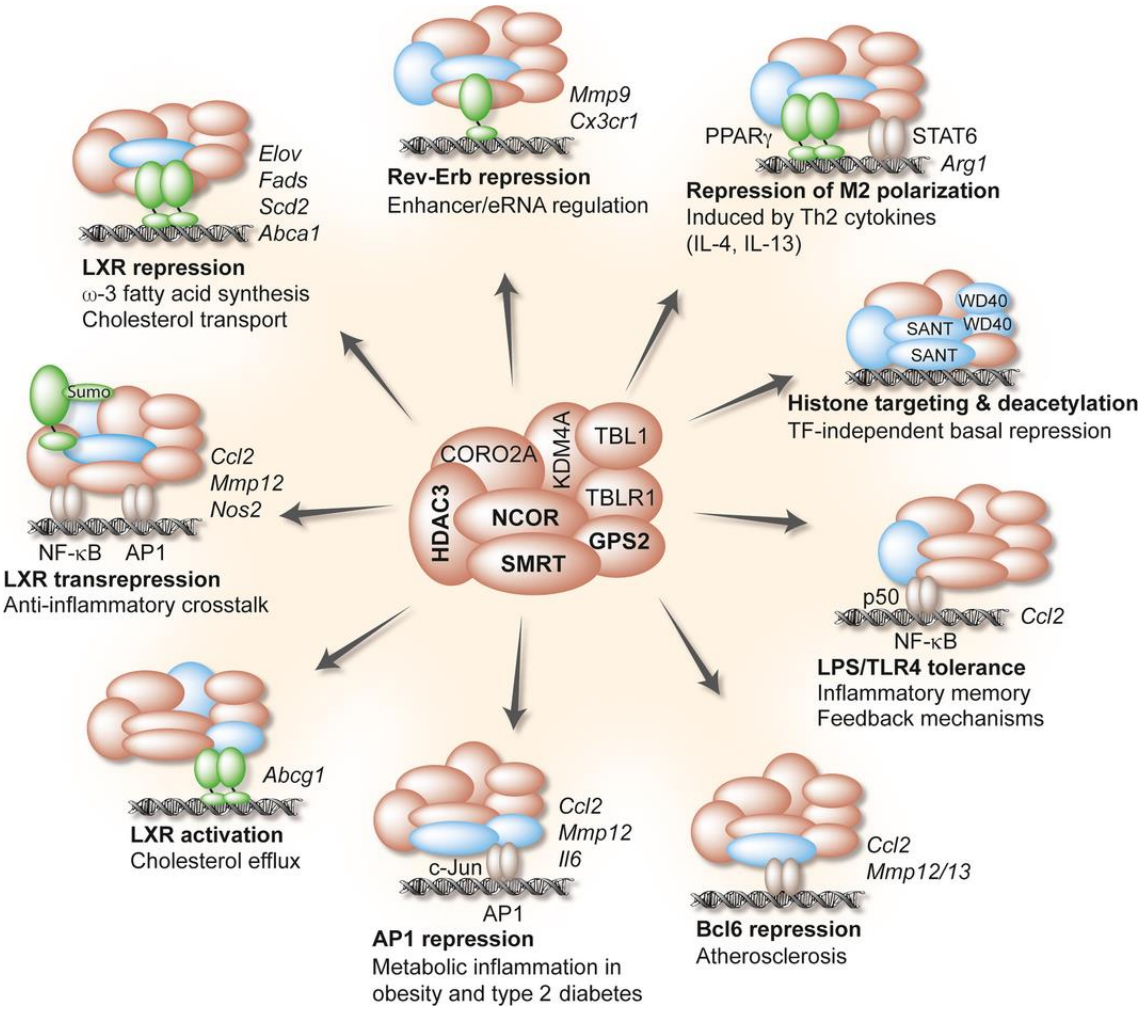

Figure 4. Different aspects of NCoR/SMRT corepressor complexes-mediated transcriptional repression in macrophages (published in [109]**)**

(LXR: Liver X Receptor, AP1: activator protein 1, Bcl6: B-cell lymphoma 6 protein, LPS: Lipopolysaccharide, TLR4: Toll-like-receptor 4, SMRT: silencing mediator of retinoic acid and thyroid hormone receptor, NCoR: nuclear receptor corepressor 1, NFkB: nuclear factor kappa-light-chain-enhancer of activated B cells, HDAC3: histone deacetylase 3, TBL1: transducin beta-like protein 1, TBLR1: transducin beta-like-related 1, KDM4A: Lysine-specific demethylase 4A, CORO2A: Coronin 2A)

It has been described, that Rev-Erb transcription factor binding is observed at the distal enhancers of many inflammatory genes including matrix metalloproteinase-9 (Mmp9) and Cx3cr1. These genes show increased expression levels in the Rev-Erbα and Rev-Erbβ double deficient macrophages suggesting the repressor function of Rev-Erbs [100]. The transcriptional repressor B-cell lymphoma 6 protein (Bcl6) transcription factor also have anti-inflammatory role in macrphages. ChIP-seq experiments display extensive overlap between genome-wide Bcl6 binding and NCoR/SMRT corepressor cistromes suggesting their tight collaboration in transcriptional repression of NFkB target genes [110, 111]. NCoR is also contributed to the regulation of inflammatory state of macrophages via the repression of Liver X Receptor (LXR) target genes including the members of ω-3 fatty acid biosynthesis pathway. The elevated ω-3 fatty acids production leads to the development of anti-inflammatory macrophage

phenotype in the absence of NCoR [112]. Furthermore, NCoR participates in LXRs-mediated transrepression in macrophages in which the ligand-activated LXR can attenuate LPS-induced expression of large set of genes without direct DNA binding of nuclear receptor. [113]. Finally, it has been described that, other members of NCoR/SMRT corepressor complexes including histone deacetylase 3 (HDAC3) and G protein pathway suppressor 2 (GPS2) also play important role in the control of inflammatory status of macrophages [114-116].

On the other hand, the polarization signals repress large sets of genes but the repressive activity of polarization-specific transcription factors has not been studied in detail [42, 44, 54, 117]. Importantly, the combination of next generation sequencing-based methods including GRO-seq and ChIP-seq provided opportunities for the characterization of direct transcription factor-mediated repression in different cell types including breast cancer cells and macrophages [96, 100]. It has also been described recently that LPS-dependent activation of macrophages is associated with significantly decreased eRNA expression at several enhancers. These TLR4-signaling-repressed enhancers are characterized by decreased binding capacity of the NF-κB subunit p65 but the exact mechanism of repression remained unknown [118].

2.3. MicroRNA-mediated post-transcriptional regulation of macrophage polarization

2.3.1. MicroRNA transcription and maturation

MicroRNAs (miRNAs) are single-stranded, 18-23 nucleotid-long, small non-coding RNA molecules acting as post-transcriptional regulators of gene expression in animals and plants [119, 120]. MiRNAs are located in both intronic/exonic regions of protein-coding genes and intergenic regions (Figure 5) [121]. Interestingly, approximately 50% of mammalian miRNAs are organized into miRNA transcription units and generated from primary polycistronic transcripts encoding more than one miRNA (Figure 5) [121]. They are usually transcribed by RNAPII but RNAPIII- mediated transcription has also been described in case of some miRNAs [122, 123]. Primary miRNA transcripts (pri-miRNAs) are long (usually over 1 Kb) and incorporate one or more mature miRNA-containing stem-loop structure [121].

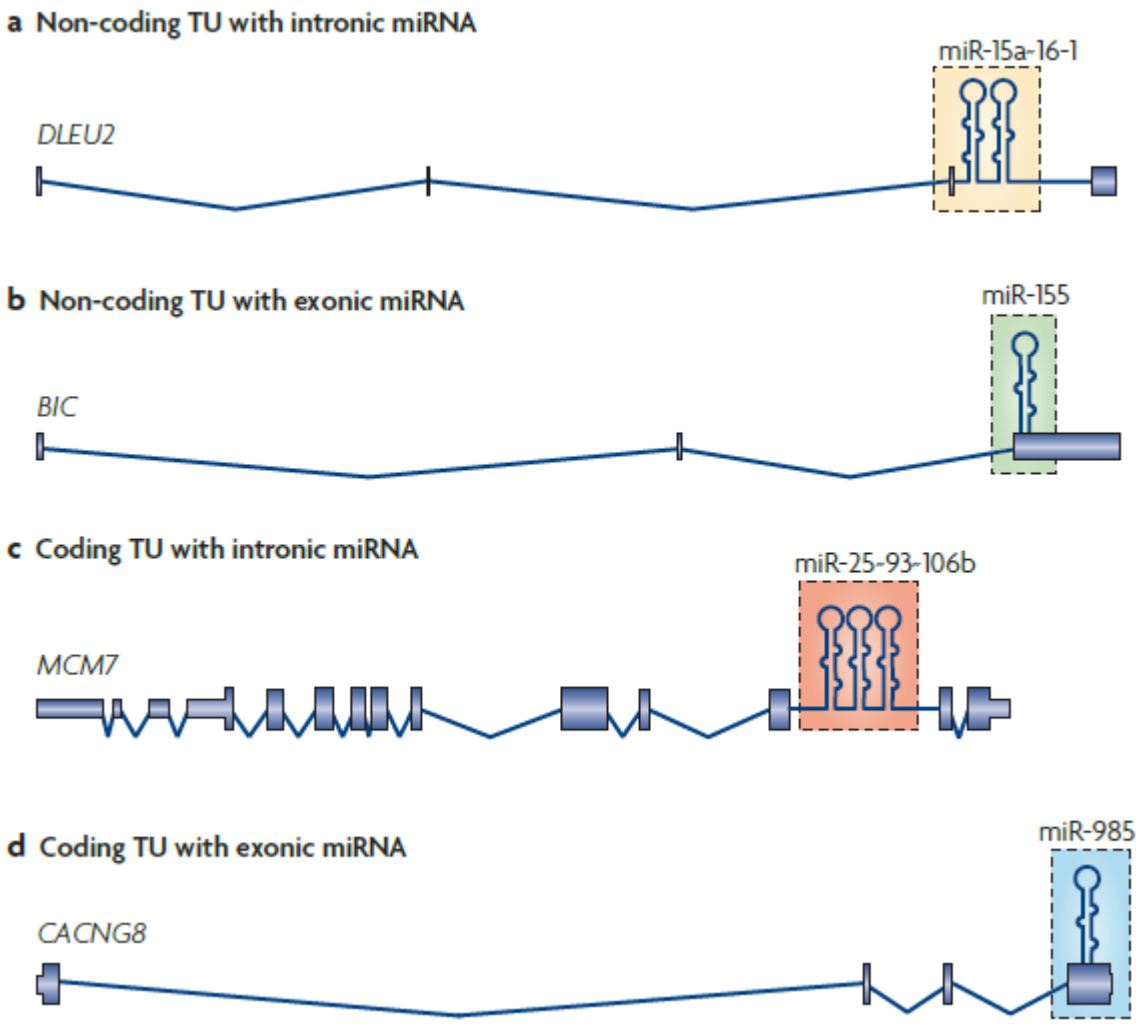

Figure 5. Genomic location and structure of the subtypes of miRNA genes (published in [121]**)**

These pri-miRNAs undergo several nuclear and cytoplasmic steps of maturation. First, pri-miRNAs are processed in the nucleus by the Drosha and DGCR8-containing Microprocessor complex (Figure 6) [121]. Drosha is a RNase III-type endonclease and is responsible for the clevage of pri-miRNAs [124]. DGCR8 also has important role in this process as the cofactor of Drosha [125-127]. Microprocessor complex precisely recognises a hairpin structure at the pri-miRNA transcript and the Microprocessor complex-mediated clevage results in the small haripin-shaped, approximately 65-70 nucleotids lenght miRNA precursor (pre-miRNA) [128, 129]. Interestingly, the Microprocessor complex-mediated processing of intronic miRNA does not influence the host pre-mRNA splicing and stability [130]. In contrast, Drosha-mediated clevage of exonic miRNAs induces the destabilization of host mRNA [131]. Following the Microprocessor complex-mediated processing, pre-miRNA is exported into the cytoplasm to the completing of miRNA maturation by Exportin 5 (Figure 6) [132, 133]. Pre-miRNAs are further processed in the cytoplasm by RNase III-type endonuclease Dicer and the Dicer-mediated clevage near to the terminal loop of pri-miRNA results approximately 20-22 nucleotides lenght small RNA duplexes which includes miRNA (guide strand) and its complementer strand (miRNA* or passenger strand) (Figure 6) [134, 135].

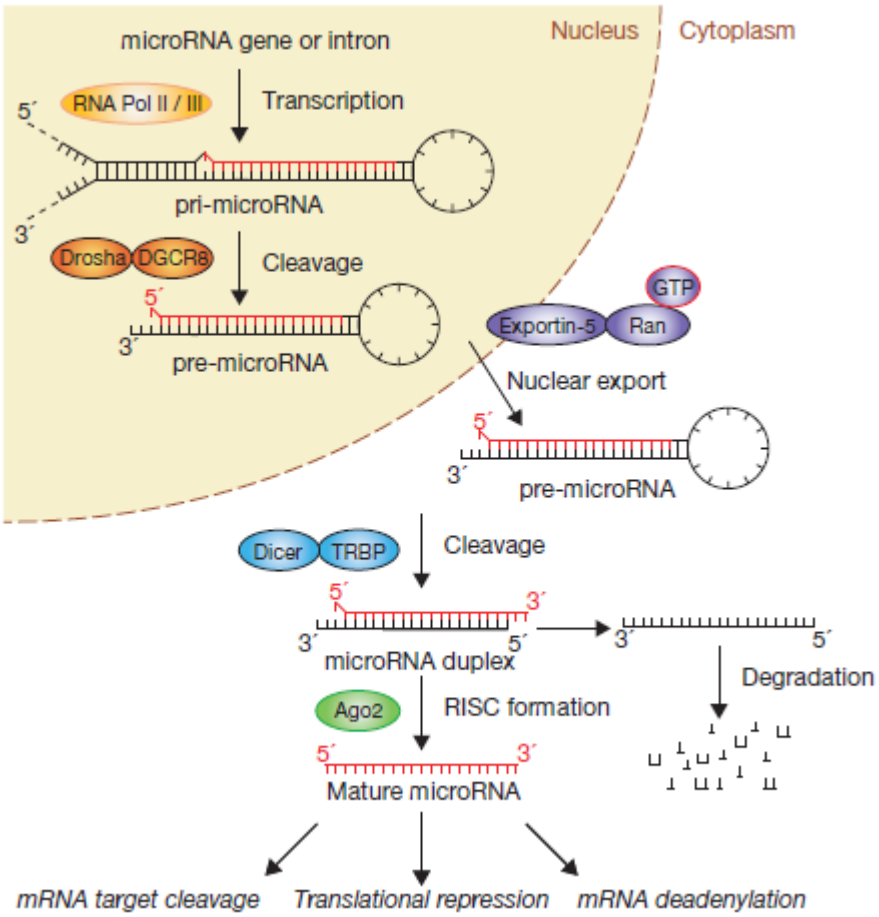

Figure 6. Canonical pathway of miRNA biogenesis (published in [136]**)**

(Ago2: Argonaute 2, RNA Pol II: RNA Polymerase II)

Finally, the miRNA/miRNA* duplex is loaded onto Argonaute (AGO) proteins forming RNA-induced silencing complex (RISC) (Figure 6) [137, 138]. One strand from the small RNA duplex remains bound by Ago proteins as miRNA, while miRNA* is degraded. Strand selection is depended on the thermodynamic of the two ends of the RNA duplex. Generally, the strand with relatively unstable base pairs at the 5' end remains functional but some duplexes produce miRNAs from both strands with similar frequencies [139, 140].

Although the majority of the miRNAs are processed by Drosha and Dicer-dependent cannonical miRNA biogenesis pathway but some miRNAs and miRNA-like small RNAs undergo through several alternative maturation processes. Some intronic miRNAs (so called mirtrons) are processed Drosha-independent manner, pre-miRNAs are generated through mRNA splicing [141, 142]. In addition, the biogenesis of the directly transcribed endogenous short hairpin RNA-derived miRNAs such as miR-320 is also Drosha independent [143, 144]. Interestingly, the processing of erythropoetic miR-451 does not require the participation of Dicer and instead pre-miR-451 is cleaved directly by AGO2 [145, 146].

In the last decade, many research groups focused on the identification of potential regulatory mechanisms in the miRNA biogenesis. These studies show that each steps of miRNA biogenesis may be regulated from the pri-miRNA transcription to the mature miRNA degradation in different physiological and pathological conditions [121, 136, 147]. Nevertheless, there are still a lot of questions that remained unanswered in this field.

2.3.2. Mechanisms of miRNA-induced post-transcriptional repression

The miRNAs are important components of the post-transcriptional fine-tuning of gene expression in animals and plants [119, 120]. They act as post-transcriptional repressors though the inhibition of mRNA translation and/or induction of mRNA degradation [148].

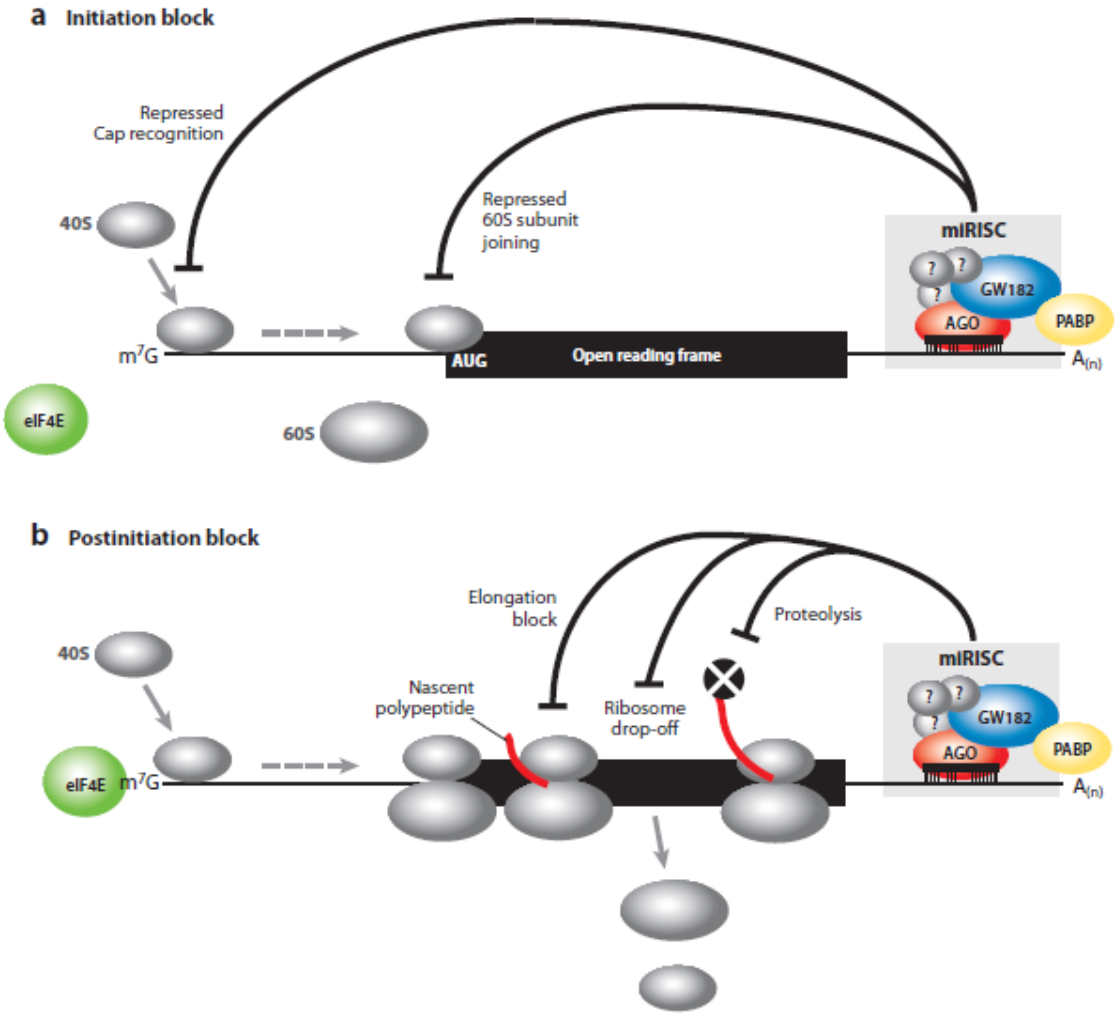

Figure 7. The mechanisms of miRNA-induced post-transcriptional repression at the translational level (published in [148]**)**

(AGO: Argonaute, A(n): poly(A) tail, m7G: the 5 -terminal cap, PABP: poly(A)-binding protein, eIF4E: eukaryotic translation initiation factor 4E)

The molecular bases of the interaction between miRNAs and target mRNAs is the complete (in plants) or imperfect (in animals) sequence complementarity. In general, the perfect base paring between the miRNA 5'-proximal seed region (nucleotide 2-8) and mRNA 3'-untranslated region (3'UTR) is required for the stable miRNA:mRNA interaction in metazoan [149, 150]. Furthermore, multiple miRNA binding sites (for same or different miRNAs) are necessary for effective repression, and these sites can cooperate with each other [151, 152].

In the last decade, several studies characterized the potential mechanisms of miRNA-supressed protein synthesis. Based on these findings, miRNAs can cause the inhibition of protein synthesis at the initiation and post-initiation levels (Figure 7) [148]. Two different mechanisms of the miRNA-induced initiation block were identified including (i) interference with 5'cap recognition and 40S small ribosomal subunit recruitment capacities of eIF4E and (ii) inhibition of 80S ribosomal complex formation (Figure 7) [153-157]. Several evidence also support the miRNA-induced translational block at the post-initiation level with the further potential mechanisms: (i) diminished translational elongation, (ii) induced ribosome drop-off and (iii) promoted proteolytic degradation of nascent polypeptides (Figure 7) [158-160].

Besides the translational block, miRNAs are also able to attenuate the RNA stability reducing the "steady-state" mRNA level of hundreds of their direct target genes. The miRNA-induced destabilization of mRNAs involves two different mechanisms including (i) the CCR4-NOT1 deadenylase complex-mediated deadenylation of poly(A) tail of mRNAs and (ii) the removal of 5' cap structure by the DCP1/DCP2 decapping complex (Figure 8) [148, 161].

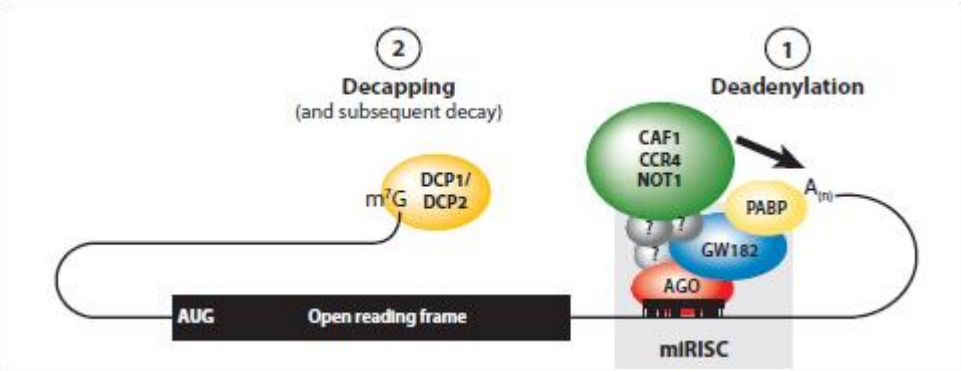

Figure 8. Mechanisms of miRNA-induced post-transcriptional repression at the mRNA degradation level (published in [148]**)**

(AGO: Argonaute, CAF1: CCR4-associated factor, CCR4: carbon catabolite repression 4 protein, NOT1: negative on TATA-less)

2.3.3. MicroRNAs as important regulators of macrophage polarization and function

In the last decade, several studies demonstrated that the macrophage-specific miRNome is responsible for different macrophage polarization signals and modulate the phenotypic and functional properties of myeloid cells *in vitro* and *in vivo*. Different inflammatory signals or bacterial pathogens can regulate the miRNA expression signature in macrophages and dendritic cells (Table 1) [162-170]. These miRNAs participate in controlling inflammatory response and bactericidal capacity of macrophages. The most studied inflammation-induced miRNA is miR-155, which plays a complex role in the macrophages. On the one hand, many papers reported that miR-155 enhances classical macrophage polarization and directly represses the expression of several anti-inflammatory proteins including SOCS1, SHIP1 and BCL6 [171-174]. In addition, miR-155 is able to suppress the alternative macrophage polarization via the direct inhibition of CEBPβ and IL-13Rα1 expression [175, 176].

	miRNA	Polarization signals or pathogens	Regulation	References
Classical macrophage polarization signals	miR-155	LPS, poly I:C, IFNβ, Candida albicans, Listeria monocytogenes	upregulated	[162-164, 166-168]
	miR-146a	LPS, Candida albicans, Listeria monocytogenes	upregulated	[162-164, 168]
	miR-132	LPS	upregulated	[162]
	miR-455	LPS, Candida albicans	upregulated	[163]
	miR-125a	LPS, Candida albicans, Listeria monocytogenes	upregulated	[163, 164]
	miR-147	LPS	upregulated	[169]
	miR-149	Listeria monocytogenes	upregulated	[164]
	miR-99b	Mycobacterium tubercolosis	upregulated	[165]
	miR-125b	LPS	downregulated	[167]
	miR-27*	LPS	downregulated	[168]
	miR-532-5p	LPS	downregulated	[168]
	miR-223	LPS, poly I:C	downregulated	[170]
Alternative macrophage polarization signals	miR-378-3p	IL-4, Brugia malayi	upregulated	[177]
	miR-125b	IL-4, Brugia malayi	upregulated	[177]
	miR-124	IL-4, IL-13	upregulated	[178]
	miR-511	IL-4, IL-13	upregulated	[179]
	miR-193b	IL-4	upregulated	[180]

Table 1. The list of macrophage polarization signals-regulated miRNAs

On the other hand, miR-155 acts as a negative regulator of overwhelmed inflammation via repression of some members of LPS-activated signaling pathways including IKKε and MyD88 [167, 181]. The LPS-induced miR-146a can also function as a negative feedback regulator of inflammatory response in macrophages via inhibition of downstream signaling molecules of TLR signaling including TRAF6 and IRAK1 [162]. In addition, miR-146 attenuates the RIG-I-dependent type I IFN production in macrophages via direct repression of IRAK2 [182]. Another LPS-induced miRNA, miR-147 also represses TLR2, TLR3 and TLR4 ligands-induced cytokine expression and inflammatory activation of mouse macrophages [169]. Although, miR-125a and miR-125b have same seed sequences and target genes but they are regulated differently in macrophages by inflammatory signals. While miR-125a is induced by several inflammatory stimuli [163, 164], until then the miR-125b expression level is reduced by LPS [167]. It has been described that miR-125a and miR125b are able to enhance the expression of classical polarization markers via direct repression of anti-inflammatory protein TNAFIP3 and IRF4 [180, 183, 184]. In contrast, it is also described that these miRNAs inhibit directly the KLF13 and TNFα protein expression limiting the inflammatory response in macrophages [185]. Furthermore, LPS-mediated repression of miR-223 directly regulates STAT3 transcription factor expression and promotes IL-6 and IL-1β production in macrophages [186]. Similarly to inflammatory stimuli, alternative macrophage polarization signals including Th2-type cytokine IL-4 and IL-13 as well as nematode infections are also able to regulate the miRNA expression pattern in macrophages, though their role is less characterized in the control of macrophage phenotype and functions [170, 177-179]. MiR-125b and miR-378-3p is induced during both nematode infection-induced *in vivo* and IL-4-induced *in vitro* alternative macrophage polarization and the elevated miR-378-3p expression contributes to the proper regulation of *in vivo* proliferation of alternatively polarized macrophages [177]. It has been also shown that IL-4/IL-13-induced miR-193b, miR-124 and miR-511 participate in the development of alternatively polarized macrophage phenotype [165, 178, 179]. Finally, some recent *in vivo* studies showed that the miRNAs play important role in the regulation of functional properties of macrophages in the complex tumor microenvironment [187-189].

3. Hypothesis and Research Questions

The molecular microenvironment-dependent dynamic transcriptional and post-transcriptional regulations of gene expression are essential for the phenotypic and functional plasticity of macrophages. Several aspects of macrophage polarization signals-induced regulatory mechanisms including SRTF-mediated transcriptional activation and miRNA-mediated post-transcriptional repression are well characterized in macrophages. However, the molecular bases of macrophage polarization signal-dependent repression and transcriptional regulation of miRNA expression are less characterized. Here, we combined the next generation sequencing (NGS)-based transcriptomic and epigenomic approaches with functional methods for the better understanding of alternative macrophage activation signal IL-4-induced transcriptional and post-transcriptional repression and LPS-dependent classical macrophage activation-triggered transcriptional regulation of miRNome.

Based on our preliminary global transcriptomic data we hypothesized that IL-4 represses a large gene set at the transcriptional level in mouse bone marrow-derived macrophages (BMDMs). We sought to investigate the direct role of STAT6 transcription factor in the IL-4-dependent transcriptional repression. Finally, we hypothesized that IL-4/STAT6 signaling pathway-mediated transcriptional repression modulates the inflammatory responsiveness of macrophages.

We also hypothesized the conserved, IL-4/STAT6 signaling pathway-mediated regulation of miRNome during alternative macrophage activation. We sought to identify the potential role of the selected IL-4-induced miRNA in the alternative macrophage polarization-linked biological functions.

Lastly, we integrated different NGS-based methods to systematically evaluate the transcriptional basis underlying the inflammation-mediated regulation of macrophage miRNome.

4. Aims

Our work focused on investigating the transcriptional and post-transcriptional mechanisms of polarization signals-induced repression in macrophages. Our long-term goals were (i) to characterize the macrophage polarization signals-dependent transcriptomic and epigenomic changes using unbiased genomic approaches (RNA-seq, small RNA-seq, microarray, ATAC-seq, GRO-seq, ChIP-seq and 3C-seq), (ii) to integrate the transcriptomic and epigenomic informations using bioinformatics approaches and (iii) to identify the functional consequences of macrophage polarization signals-induced transcriptional and post-transcriptional repression.

Specific aims:

1. Investigation of the IL-4/STAT6 signaling pathway-induced transcriptional repression in mouse macrophages:

- Identifying the gene set repressed by the IL-4/STAT6 signaling pathway.
- Identifying the STAT6-bound enhancer subsets repressed or activated by IL-4.
- Characterizing the direct transcriptional repression mediated by the IL-4/STAT6 signaling pathway.
- Studying the partial repression of inflammatory responsiveness induced by IL-4 pretreatment.

2. Identification of the IL-4 responsive miRNAs and their role in mouse and human alternatively polarized macrophages:

- Investigating the miRNAs in mouse alternatively polarized macrophages.
- Identfying the expression pattern of the selected miRNAs regulated by IL-4 during *in vivo* alternative macrophage polarization in mice.
- Studying the IL-4-dependent regulation of the selected miRNAs in human macrophages.
- Characterizing the molecular bases of IL-4-dependent regulation of the selected miRNAs in mouse and human macrophages.
- Identifying the alternative macrophage polarization-linked function of the selected IL-4 responsive miRNA.

3. Characterization of the transcriptional regulation of inflammation-responsive miRNAs in mouse macrophages.

- Identifying miRNAs regulated at the transcriptional level in LPS-stimulated mouse macrophages.

- Identifying and characterizing the inflammation-responsive pri-miRNAs-associated enhancer subset.
- Investigating the loop formation between the distal-enhancers and promoter of pri-miR-155 regulated by LPS.

5. Materials and Methods

Animals

Wild-type (WT; C57BL/6J or BALB/c), Stat6-deficient (S6 KO) mice on C57BL/6J and IL-4 receptor-α–deficient (IL-4Rα KO) mice on a BALB/c background were housed under minimal disease conditions and experiments were carried out under institutional ethical guidelines and licenses (file number: 120/2009/DE MAB). Surgical implant of adult *Brugia malayi* parasites into WT (C57BL/6) mice was carried out as described previously in accordance with the UK Animals (Scientific Procedures) Act of 1986 [177].

Brugia malayi in vivo infection model

Surgical implantation of adult *Brugia malayi* parasites was performed by the same group and at the same facilities like in case of the results presented by Jenkins et al. (2011) [190]. Peritoneal exudate cells from *B. malayi* infected animals were seeded at $5x10^6$ cells per well to 6-well cell-culture plates (NUNC, Roskilde, Denmark) in RPMI, 5% FCS, 2 mM L-glutamine, 0.25 U/mL penicillin and 100 mg/mL streptomycin. After 4 hours incubation at 37 °C / 5% CO_2 non-adherent cells were washed off and the adherent cells lysed in 700 µl Qiazol. (Dominik Rückerl)

Heligmosomoides polygyrus in vivo infection model

Heligmosomoides polygyrus life cycle was maintained in house and infective third-stage larvae (L3) were obtained as described elsewhere [191]. Mice were infected with 200 *H. polygyrus* L3 by oral gavage. The attenuated, aroA deficient *Salmonella enterica enterica* serovar Typhimurium strain SL3261 [192] was cultured as stationary overnight culture from frozen stock in Luria-Bertani broth. Co-infections were carried out as described previously [193]. Briefly, animals were injected i.p. with ~$1x10^6$ CFU *Salmonella* Typhimurium diluted in PBS or received 1 mg/kg LPS from *Salmonella enterica* ser. Minnesota (Sigma-Aldrich, Saint Louis, Mo, USA, L4641) 9 days after *H. polygyrus* infection. 6h after bacterial inoculation peritoneal macrophages were isolated by lavage, purified by adherence for 2 h to cell culture plastic and total RNA extracted. (Dominik Rückerl)

Differentiation of bone marrow-derived macrophages

Bone marrow was isolated from 8-12 weeks old male mice. Isolation and differentiation were completed as described earlier [97]. Isolated bone marrow-derived cells were differentiated for 6 days in the presence of L929 supernatant. For alternative macrophage activation we differentiated the freshly isolated bone-marrow cells in the

presence of IL-4 (5 ng/ml; PreproTech, London, UK) and/or treated BMDMs with IL-4 (20 ng/ml) on the 6th day of the differentiation for the indicated period of time. Differentiated BMDMs were treated with LPS (100 nM, Sigma-Aldrich, Saint Louis, Mo, USA, L4641) and/or ATP (5mM) for the indicated period of time. (Zsolt Czimmerer, Bence Dániel, Tímea Silye-Cseh)

Immortalization of mouse bone marrow-derived macrophages

Bone marrow-derived cells were immortalized using the J2 cell line continuously producing the J2 virus encoding v-raf and v-myc oncogenes [194]. J2 cells were grown in DMEM containing 20% FBS. Bone marrow cells were seeded in immortalization media I. (90% J2 supernatant, 5% HyClone FBS, 10 µg/ml Polybrene 0.1%, L929 supernatant 5%) and incubated overnight. On the second day supernatant was collected and spun down to pellet floating cells. Adherent cells were scraped and re-plated in a new petri dish using immortalization media II. (20% J2 supernatant, 10% HyClone FBS, 10 µg/ml Polybrene 0.1%, L929 supernatant 10%, 60% DMEM) and incubated for 6 days. After the immortalization cells were kept in regular macrophage differentiation media (20% FBS, 30% L929 supernatant and 50% DMEM containing 1% antibiotics). (Bence Dániel, Zsolt Czimmerer, Tímea Silye-Cseh)

Human monocyte isolation and culture

Isolation of human monocytes, mouse bone marrow cells and mouse peritoneal macrophages were completed as described earlier with minor modifications [43, 177, 195]. CD14+ human monocytes were isolated from platelet-free buffy coats from healthy donors by Ficoll gradient centrifugation followed by immunomagnetic cell separation with anti-CD14-conjugated microbeads (VarioMACS Separation System, Miltenyi Biotec., Bergisch Gladbach, Germany). Monocytes were cultured in multiwell culture plates in RPMI 1640 (Sigma-Aldrich, Saint Louis, Mo, USA) supplemented with 10% fetal bovine serum (Invitrogen, Carlsbad, CA, USA) and penicillin/streptomycin (Sigma-Aldrich, Saint Louis, Mo, USA). For macrophage differentiation and alternative macrophage activation freshly plated monocytes were treated with IL-4 (100 ng/ml; PreproTech, London, UK). Cells were harvested 12 and 72 hours after cytokine treatment. (Zsolt Czimmerer, Ibolya Fürtös)

RNA-seq

cDNA library for RNA-Seq was generated from 1µg total RNA using TruSeq RNA Sample Preparation Kit (Illumina, San Diego, CA, USA) according to the manufacturer's protocol. Briefly, poly-A tailed RNAs were purified by oligodT conjugated magnetic beads and fragmented on 94 C degree for 8 minutes, then 1st strand cDNA was transcribed using random primers and SuperScript II reverse

transcriptase (Lifetechnologies, Carslbad, CA, USA). Following this step second strand cDNA synthesized, double stranded cDNA end repaired and 3' ends adenylated then Illumina index adapters were ligated. After adapter ligation enrichment PCR was performed to amplify adapter ligated cDNA fragments. Fragment size distribution and molarity of libraries were checked on Agilent BioAnalyzer DNA1000 chip (Agilent Technologies, Santa Clara, CA, USA). Paired read 100bp sequencing runs were performed on Illumina HiScan SQ instrument (Illumina, San Diego, CA, USA). (Szilárd Póliska)

Small RNA-seq

Small RNA-sequencing libraries were generated from 1 μg of total RNA using TruSeq Small RNA Sample Preparation Kit (Illumina, San Diego, CA, USA) according to manufacturer's protocol. Briefly, after ligation of 3' and 5' RNA adapters, reverse transcription was performed to synthesize cDNA and then using Illumina specific index adapter primers, cDNA was amplified. The amplified library was excised from 6% Novex TBE PAGE gel (Invitrogen, Carlsbad, CA, USA) and after purification the libraries were quantified by Qubit fluorometer and checked on BioAnalyzer 2100 using DNA1000 chip (Agilent Technologies, Santa Clara, CA, USA). Single read 50bp sequencing was performed on HiScanSQ instrument (Illumina, San Diego, CA, USA). (Szilárd Póliska)

ATAC-seq

ATAC-seq was carried out as described earlier with minor modification [196]. Cells were scraped and counted to achieve 50k/ml in ice-cold PBS. Cell suspension was further diluted to 25k/ml and nuclei were isolated with ATAC-LB (10mM Tris-HCl pH7.4, 10mM NaCl, 3mM MgCl2, 0.1% IGEPAL). Nuclei from 25k cells were used for tagmentation using Nextera DNA Library Preparation Kit (Illumina, San Diego, CA, USA) from two biological replicates. After tagmentation DNA was purified with Minelute PCR Purification Kit (Qiagen, Hilden, Germany). Tagmented DNA was amplified with Kapa Hifi Hot Start Kit using 9 PCR cycle. Amplified libraries were purified again with Minelute PCR Purification Kit. Fragment distribution of libraries was assessed with Agilent Bioanalyzer and libraries were sequenced on a HiSeq 2500 platform. (Bence Dániel)

GRO-seq

GRO-seq was performed as described earlier [97] but the libraries were prepared with NEBNext Small RNA Library Prep set for Illumina. (Bence Dániel)

ChIP-seq and ChIP-qPCR

ChIP was performed essentially as previously described [97]. Libraries were prepared either with Ovation Ultralow Library Systems (Nugen, San Carlos, CA, USA) or TruSeq ChIP library systems (Illumina, San Diego, CA, USA) according to the manufacturer's instructions. ChIP antibodies are listed in Table 2. In all cases, 1.5 µg antibodies were used for ChIP-qPCR and 3 µg for ChIP-seq experiments.

Antibody	Identifier
IgG	Millipore, 12-370
H3K27Ac	ab4729
P300	sc-585
PU.1	sc-352
JunB	sc-46x
IRF8	sc-32528x
STAT6	sc-981
C/EBPα	sc-61X
HDAC1	ab7028
HDAC2	ab7029
HDAC3	ab4729
RNAPII-pS5	ab5131
RNAPII-pS2	ab5095
p65	sc-372

Table 2. List of antibodies for ChIP

Primer sequences for ChIP-qPCR analysis are listed in Table 3.

qPCR assay	FW primer	Rev primer
IL-18_+25Kb	tgaaaagaaagctgtgttcacatt	agcccgagaagcttatgaaa
Fcgr1_-7.7Kb	acatcagcaaaaggcttggt	ggctactctgctaacctgctaca
Irak3_+10Kb	acagaaatcgtgtctccatatgc	tggggtgtgttgcgttattc
IL1b_-7.7Kb	agcaggattgctggctagag	ccatgtcagcagcacagtgta
pri-miR-155_-62Kb	aagaaggaagtcgtggcagt	ggttgcccaggtagctttaag
pri-miR-155_-76Kb	gccaggactgctgaagaatg	ctgggaatatcccacttgttatct
pri-miR-155_-96Kb	aaaacctaaatgtgtgggtcttcta	cccatttataaaagcaggatgg
pri-miR-155_-116Kb	ggggaaacattcaagaagca	cctttagccaagcagatgattt
pri-miR-147_+27Kb	ctggggcacaatgagagaa	cacacccagtgtgaaatgatg
pri-miR-147_+14Kb	tgctctgcccttctcactg	tggctacactgaacttcccaat
Prmt8e	cgtgagcagaggtgaggagt	ggttaacccaagcttcttgct
Evl_-4 Kb	tggttcacaggaggcagatc	ctctcacatgcacagacagc
Evl_+4 Kb	ctagggaacagggcttgaca	agggaagtgaactggctcat
EVL_+0.3 Kb	caattcccctagatggctca	tagaaattagcacctgcctctca

Table 3. List of primer sequences for ChIP-qPCR analyses

(Zsolt Czimmerer, Bence Dániel, Zsuzsanna Nagy, Ágnes Kriston)

RNA-seq analysis

TopHat and Cufflinks toolkits [197] were used for mapping spliced reads to the mm10 mouse assembly with default parameters, making transcript assemblies, and getting and sorting gene expression data. Genes with at least 1 FPKM (Fragments Per Kilobase per Million mapped reads) expression value in at least one sample were considered to be expressed. In the downstream analysis 2-way anova and post-hoc tests were performed on WT and STAT6KO macrophages exposed to IL-4 for 1, 3, 6 and 24 hours in R using the aov() and TukeyHSD() functions of the MASS package. Differences were considered statistically significant at p-value<0.05 and FC>2. For IL-4 pretreatment-LPS datasets, LPS-induced genes were considered statistically significant at p-value<0.05 compared to the control and then these genes were clustered based on their sensitivity (p-value<0.05) to IL-4 pretreatment as follows: attenuated response - Cluster 1; insensitive - Cluster 2; increased response - Cluster 3. K-means clustering was performed in R using the function kmeans from package stats. Gene Set Enrichment Analysis was done by GSEA v2.2.0 [198]. KEGG pathway enrichment analyses were done using the DAVID web application [199]. Heat maps were drawn using the R package pheatmap. (Attila Horváth)

3C-seq and analysis

Experiments were carried out as previously described [200]. After the first digestion and ligation the 3C DNA pool was purified with phenol/chloroform/ isoamyl alcohol (25:24:1) (Sigma-Aldrich, Saint Louis, Mo, USA). Second restriction digestion was performed by using DpnII (NEB, Ipswich, MA, USA) for 16 hours per manufacturer's instruction. Second ligation was performed at 16C° for 6 hours with 200U of T4 DNA ligase. DNA was then purified again with phenol/chloroform/isoamyl alcohol (25:24:1) followed by QIAquick gel purification columns (Qiagen, Hilden, Germany). Bait specific inverse PCRs were performed using primers coupled to Universal Illumina adapters and Barcode sequences. Reactions were purified by QIAquick gel purification columns. Amplicon libraries were quantified and qualified by Agilent using DNA 7500 chip cartridge. Primers are available upon request. Amplicon libraries were sequenced on Illumina HiSeq sequencer. Raw reads were demultiplexed using FASTX-Toolkit and then aligned to mm10 genome assembly (GRCm38.p1.) by BWA [201]. Bedgraph and TDF files for visualization were generated as previously described. The R package r3Cseq (pvalue<=0.05) was used to predict the putative interactions [202]. (Bence Dániel, Attila Horváth)

Small RNA-seq data analysis for the identification of LPS responsive miRNome

Small RNA-seq samples were aligned by novoalign (with –r Random and –m options) to mm10 genome assembly (GRCm38.p1.) and converted into BAM files with

SAMtools [203, 204]. The Rsubread and edgeR packages were used to quantify and infer the statistically significant miRNAs using mature miRNA collection from MirBase (v21), respectively. CPM (counts per million) scores were normalized by using TMM method. For the downstream analysis only the expressed miRNAs (CPM>=10 at least in two samples) and significantly changed (p-value<=0.05 and FDR <= 0.1) miRNAs were used. (Attila Horváth)

Small RNA-seq data analysis for the identification of IL-4-regulated miRNAs

The processed sRNA-Seq reads were mapped to all available *Mus Musculus* mature-miRNA sequences (miRBase v21, [204]). Read mapping was performed using Bowtie [205]. The mapping process for reads longer than 10 nucleotides allows 2 mismatches. Quantification of mapped reads with minimum and maximum length of 18 and 24 nucleotides overlapping to mature miRNA regions (miRBase v21) was performed using the R package *GenomicRanges* [206, 207]. Minimum overlapping between mapped reads and mature regions was 16. We filtered out mature microRNAs with counts per million (CPM) lower or equal than 4 cpm across at least 3 libraries. Differential expression analysis was performed using 'edgeR' package [208] fitting a negative binomial generalized linear model for each mature microRNA, and then the likelihood ratio test was performed. The contrasts used were: wild type IL-4 vs. wild type control, wild type IL-4 vs. STAT6 KO IL-4, STAT6 KO IL-4 vs. STAT6 KO control and wild type control vs. STAT6 KO control. The Benajmini and Hochberg method was used to calculate FDRs [209]. (Attila Horváth)

ATAC-seq, ChIP-seq and GRO-seq analyses

The primary analysis of the ATAC-seq, ChIP-seq and GRO-seq raw sequence reads was carried out using our ChIP-seq analysis command line pipeline [210]. Briefly, Burrows-Wheeler Alignment Tool (BWA, [201]) was used to align the reads to mm9 and mm10 genome assembly with default parameters. MACS2 [211] (with '-B' and '-SPMR' options) was used for predicting transcription factor peaks and nucleosome free regions (q-value<=0.01), and findPeaks.pl (with '-size 1000', '-minDist 2500' and '-style histone' options) for histone regions. Artifacts were removed using the ENCODE blacklist [212]. Predicted peaks were sorted by average coverage (RPKM, Reads Per Kilobase per Million mapped reads). Average coverage of the predicted peaks and significantly changing regions (p-value<=0.05) were calculated by DiffBind v2.0.5 [213]. Intersections, subtractions and merging of the predicted peaks were made with BedTools. Proportional Venn diagrams were generated with VennMaster [214]. Genome coverage files (bedgraph files) for visualization were generated by makeUCSCfile.pl (HOMER) and then converted into tdf files using igvtools with 'toTDF' option. *De novo* motif discovery was performed on the 100 bp vicinity of the peak

summits using findMotifsGenome.pl with options '–len "10,12,14,16"' and '-size 200' on the repeat-masked mouse genome (mm10r) from HOMER. The HOMER option '-style groseq' was used for GRO-seq samples. Integrative Genomics Viewer (IGV2.3, Broad Institute) was used for data browsing [215] and creating representative snapshots. Normalized tag counts for Meta histograms and RD plots were generated by annotatePeaks.pl from HOMER (with option '-hist 10' for histograms and with options '-ghist' and '-hist 10' for RD plots) and visualized by R using package ggplot2 or by Java TreeView, respectively. Gene body metaplots were created using ngs.plot software [216]. Pearson's correlation coefficients between GRO-seq, RNAPII-pS2, RNAPII-pS5 and H3K27ac ChIP-seq data (fold change of RPKM values upon 1h IL-4 treatment on the merged replicates using a custom bash script) were calculated in R using function cor() from package stats. Changes on boxplots were considered significant at $p<0.00001$ using paired t-test and the average of fold differences at the individual enhancers ≥1.15. (Attila Horváth)

Identification of pri-miRNAs using GRO-seq and H3K4m3-specific ChIP-seq data sets

GRO-seq transcripts were predicted by findPeaks,pl with '-style groseq' option of HOMER (with parameters minBodySize=1000, maxBodySize=80000, tssFold=5, bodyFold=1.5 endFold=6.5) and merged with known gene bodies within a window of 1000bp in a strand specific manner. Finally to make the prediction of TSSs of predicted transcripts more precise they were split by the union of control and LPS treated H3K4m3 regions (3000bp distance between features allowed for features to be merged) dealing with the cases when there is more than active promoter regions on the same transcript. TSS predictions from FANTOM5 data set aligned to mm9 was converted to mm10 genome using liftOver [217]. (Attla Horváth)

Enhancer annotation and eRNA expression analysis for the characterization of LPS-responsive miRNA expression

Enhancer transcripts were predicted based on the pool of the sequence reads derived from the (2x4) LPS-treated time-course GRO-seq samples according to our previous work [97]. From nearby enhancers within 1 Kb, those were used in the further analyses showing the highest expression calculated in RPKM. Enhancers were filtered based on their expression level (over 0.5 RPKM in at least one sample per replicate), expression change (at least 1.3 fold change in the same time point(s) in both replicates as compared to time 0) and the overlap with H3K4m1 enrichment upon LPS treatment (according to the region prediction of HOMER). Intergenic H3K4m1/eRNA "double positive" enhancers farther than 1 Kb and within 50 Kb compared to LPS-responsive pri-miRNA TSSs and/or within the predicted domains around the pri-miRNA TSSs and flanked by the highest CTCF/Cohesin peaks were assigned to the associated gene. RPKM values for H3K4m1 enrichment were calculated within the 1 Kb wide region around the annotated enhancers. (Attila Horváth, Gergely Nagy)

Domain prediction

ChIP-seq raw reads of 47 CTCF and 42 Cohesin (RAD21, SMC1/3 or SA1/2) samples were downloaded from the Sequence Read Archive of NCBI and processed using our ChIP-seq analysis command line pipeline [210]. Consensus CTCF peak summits were defined as the average genomic location of at least two summits within 51 bp. Consensus peak summits for Cohesin were defined in the same manner. Insulator peak summits were determined from those consensus CTCF peak summits that were closer to a consensus Cohesin peak summit than 51 bp. Motif enrichments were calculated in two rounds by findMotifsGenome.pl (HOMER) from the 100 bp region around the 5000 most ubiquitous insulator peak summits. Having mapped the putative elements matching with the CTCF motif of the first search by annotatePeaks.pl (HOMER), we used those top 5000 regions that lacked these hits. Score 6 was set as a threshold for both CTCF motif matrices, and to filter putative CTCF elements in the case of multiple occurrences at the same region those hits were preferred that followed the direction of the CTCF/Cohesin peak location compared to each other [91] and had the highest motif score. Insulators showing clear protein-binding direction without predicted element were also included in domain prediction. Average coverage (RPKM) of CTCF and RAD21 ChIP-seq derived from bone marrow-derived macrophages was calculated on the 100 bp region around insulators, and those regions were filtered out that had an RPKM value exceeding the hundred-thousandth of the summed density of all regions per sample in both samples. The closest insulators showing convergent direction within 1Mb distance but farther than 1kb were assigned to each other and called domains if their coverage showed less than 2-fold difference for both proteins. In the case of overlapping domains, those were filtered having the highest insulator coverage. “Negative” domains with divergent insulators were defined between the final convergent domains. Association scores between STAT6-bound enhancers and IL-4-regulated gene clusters were calculated and visualized by package pheatmap using option scale="column" (scaling by RNA-seq clusters). (Gergely Nagy)

mRNA microarray and computational target identification

The Raw Sample CEL files were processed within R, using ‘affy’, ‘org.Mm.eg.db’ and ‘mogene10stv1cdf’ packages [218-220] Similarly to the miRNA microarray processing, raw expression values were processed with robust multi-array average (RMA) procedure [221]. Interquartile Range was calculated across all samples for each probe in an identical way as miRNA microarray methodology, to remove probes mapping to the same transcript. Quality control was performed using Principal Component Analysis. Differential expression analysis was performed as mentioned in microRNA microarray analysis. Using ‘limma’ package [222] to fit a linear model to each probe, then using an empirical Bayes method to get moderate t-statistics. The contrast used here was transfection with miR-342-3p vs mir-negative control miRNA mimics in mouse macrophage cell line RAW264.7. The Benjamini and Hochberg method was used to calculate FDRs [221]. The contrast was used to verify direct effect due to miR-

342-3p regulation. Sylamer [223] was used to quantify the enrichment or depletion of miRNA seed matches in the 3'UTRs of genes. These 3'UTRs genes are ordered given t statistic (differential expression). Prediction of functional miRNA targets was performed by TargetExpress [224]. TargetExpress is a Support Vector Machine combination based on TargetScan [225] and microT-CDs [226] predictions and an expression profile. In this case, the mir-negative control expression profile was included in the TargetExpress model.

3'UTR sequences corresponding to selected down-regulated and computationally predicted anti-apoptotic mmu-miR-342-3p target genes were obtained using 'TxDb.Mmusculus.UCSC.mm10.ensGene' and 'GenomicFeature' packages [206, 227] Conservation scores for these 3'UTR sequences where obtained from UCSC GenomeBrowser using 'rtracklayer' package [228] selecting the track 'cons60way' to get the 'phastCons60wayPlacental' table. (Cesaré Ovando Vázquez, Cei Abreu-Goodger)

Real-time quantitative PCR-based measurement of mRNA, eRNA and pri-miRNA expression

Total RNA was isolated from cells using Tri Reagent (MRC, Cincinnati, OH, USA) according to manufacturer's protocol. For quantification of mRNAs, eRNA and pri-miRNAs reverse transcription was performed by using High-Capacity cDNA Reverse Transcription Kit (Applied Biosystems, Foster City, CA, USA). RT primers for mature miRNAs were supplied by Applied Biosystems. Transcript quantification was performed by quantitative real-time RT (reverse transcriptase) PCR (polymerase chain reaction) using SYBR Green assays (selfmade assays). Primer sequences are listed in Table 4.

qPCR assay	FW primer	Rev primer
mCd14	aaagaaactgaagcctttctcg	agcaacaagccaagcacac
mTlr2	ggggcttcacttctctgctt	agcatcctctgagatttgacg
mAbca1	tccaatttcccatccatttg	acaggtaccaaaccaccagc
mClec4d	agtaacgtgcatccgagagg	taacaggacagcaggtccaa
mNlrp3	cccttggagacacaggactc	ggtgaggctgcagttgtcta
mFos	cagcctttcctactaccattcc	acagatctgcgcaaaagtcc
mLyz1	ggcaaaaccccaagatctaa	tctctcaccaccctctttgc
mLyz2	gaatggaatggctggctact	cgtgctgagctaaacacacc
mSmad3	tccattcccgagaacactaac	ccaggaggtgggtttct
mIL1b	agttgacggaccccaaaag	tttgaagctggatgctctcat
mKlf4	cgggaagggagaagacact	gagttcctcacgccaacg
mEdn1	ggacatcatctgggtcaacac	tgggaagtaagtctttcaaggaa
mHbegf	tcttcttgtcatcgtgggact	cacgcccaacttcactttct
mPpia	tctgctgtctttggaacttt	cgatgacgagcccttgg
Hbegf_+43Kb	cagcagggaggacttcatgt	ggaaagccttcatcgactgt
Edn1_-42Kb	gctctttgctagggttttagacg	atcacgaggcagccactc
Klf4_-34Kb	ggactccaaaagatggatcg	gaatggactcaaggggtcag

Cd14_+25Kb	tgctatgtatccctggaacct	tgcctgaaaatggtgcctac
Tlr2_+29Kb	acgatctgacctgaccatacc	gcccctcgatgttaaaaccc
Fos_-5Kb	tcctccttttcgcctctctc	ggaatgtggggttatcttgagc
Abca1_-27Kb	tggctacaaagggtcaggtc	tcaccaaaaatccagttgctt
Clec4d_-9Kb	tagtggtccctgggcaagta	tggaaagaagagaaatggagggg
Nlrp3_-1.3Kb	acagcatctactcagggtgg	gctctttacattagctgcccc
Tlr2_-21Kb	aagcaagagtttgtgtaccctctta	cctgtcttccctctggtcac
Cxcl11_-11Kb	gccgggtcagctcttatcta	accaaggacaaaaccaaccg
Fcgr1_-7.7Kb	ccctttctccctagccgtag	agtgactagtgccatgcgaa
IL1b_-9.7Kb	gctggaccgttttcttatagaca	tgtagaaacacaggagcagaat
pri-miR-155_-76Kb	tgatttagataggacagcaaaaagc	gcttgttatcctggctcgac
pri-miR-155_-96Kb	caaaactgggaatgctagtgc	cgtgctactcaggggtctgt
pri-mir-147_+14Kb	tgctctgcccttctcactg	tggctacactgaacttcccaat
pri-miR-147_+27Kb	cctgctttcctctgactgct	tgtccctgggtcatccaa
pri-miR-223_-12Kb	tgcaaaaagagaatcacataaacc	aaagagagccaacaattaaagagg
pri-mir-223_+16Kb	tgaacaccagcattctctgc	tctgggctcagctcaaagat
pri-miR-155	acaggaaacagcaaattcatctt	aaagagctctgactcaagggact
pri-miR-147	tgttttgcctcacactatcagc	tccttatatggaatctcaacgaaa
pri-miR-223	catgcaagaataggagacattcc	gccacaaattcagggaacc

Table 4. List of primer sequences for mRNA, pri-miRNA and eRNA-specific qPCR analyses

(Zsolt Czimmerer, Bence Dániel, Máté Kiss, Zsuzsanna Kolostyák,Beáta Szalka, Ágnes Kriston)

LDH release

LDH activity was measured in the supernatants of unstimulated and IL-4-pretreated WT and STAT6KO bone marrow-derived macrophages after IL-4 pretreatment and/or LPS/ATP costimulation (LPS-exposed BMDMs were treated with ATP for 30 min) by commercially available LDH UV assay on Cobas c 501 instrument (Roche Diagnostics, Mannheim, Germany). This measurement is based on the conversion of L-lactate to pyruvate along with the reduction of NAD+ to NADH. The initial rate of the NADH formation was directly proportional to the catalytic LDH activity determined by photometrically measuring the absorbance increment at 340 nm. (Béla Nagy Jr., Zsolt Czimmerer)

Measurement of IL-1β production

LPS-exposed BMDMs were treated with ATP for 45 min. Supernatants from ATP-treated macrophages were collected, centrifuged and stored at -20 ^{o}C until further use. IL-1β was measured from samples using ELISA kit (DY401-05, R&D System, Minneapolis, MN, USA) according to the manufacturer's instructions and analyzed on FlexStation 3 Microplate Reader (Molecular Devices, San José, CA, USA). The minimum detectable dose is 15.6 pg/ml. (Marietta M. Budai, Szilvia Benkő)

Western Blot analysis

Cells were harvested and centrifuged, then they were lysed in loading buffer (62,5mM Tris pH=8.8, 25% glycerol, 2% SDS, 1% β-mercaptoethanol and 1% BPB). Before loading all samples were boiled for 10 minutes. Proteins were separated by SDS-PAGE and transferred onto nitrocellulose membranes. Membranes were then blocked with 5% non-fat milk, washed briefly, incubated with primary antibodies at 4°C overnight. Pro-IL-1β (AF401-NA) was from R&D System, ASC (sc22514-R) was from Santa Cruz, pro-caspase-1 (AG-20B-0042) and NLRP3 (AG-20B-0014) antibodies were obtained from AdipoGen. Primary antibodies were incubated with corresponding horseradish peroxidase-conjugated secondary antibodies from BioRad for 1 hour at room temperature. Proteins were visualized by Supersignal West-Pico peroxide/luminol enhancer solution from Pierce. To verify the loading of equal amount of protein sample, the β-actin (Sigma-Aldrich, Saint Louis, Mo, USA) expression was detected. (Marietta M. Budai, Szilvia Benkő)

Caspase-1 assay and PI-based detection of pyroptotic cell death

Caspase-1 activity and pyroptotic cell death by propidium iodine staining was measured in single cells using imaging Laser Scanning Cytometry (LSC). Mouse macrophages were cultured, treated, stained and imaged in 8 well IBIDI (Martinsried, Germany) slides with an initial concentration of 15,000 cells per well. Sub-vital staining was performed in culture medium at room temperature for 20 minutes by Hoechst 34580 (10 microg/ml), propidium iodine (10 microg/ml), Alexa-488 tagged Annexin V (1 microg/ml) and caspase-1 specific FLICA® 660 (FLICA® 660 far-red fluorescence Caspase-1 Assay Kit was used according to the description of manufacturer; ImmunoChemistry Technologies, LLC). In some experiments specific Caspase-1/ICE Inhibitor Z-WEHD-FMK (R&D Systems, Inc. Minneapolis, MN, USA) was also used before FLICA labeling. For LSC imaging an iCys Research Cytometer (formerly CompuCyte; Thorlabs Imaging Systems, Sterling, VA) was used with its iNovator Application Development Toolkit software. Hoechst, Alexa, PI and FLICA fluorescence dyes were excited separately with 405, 488, 488, 633 nm laser lines and detected at 430-470, 515-545, 650-700, 650 and above nanometers, respectively. Single cell data were gated according to their area, DNA content and nuclear shape and fluorescence pixel integral, maximum pixel intensity and average pixel intensity parameters with raw images were recorded for all dyes. For cytoplasmic caspase-1 activity measurements dynamic background subtraction was applied. Gated single cell FCS data were exported from LSC software and contour plots were generated in FCS Express 5 flow and image cytometry data analysis software (De Novo Software, Glendale, CA, USA). (Zsolt Bacsó, Zsolt Czimmerer, Csaba Bankó)

Flow cytometry for the characterization of in vivo macrophage polarization

All antibodies were purchased from Biolegend UK unless otherwise indicated. Equal numbers of cells were stained with LIVE/DEAD cell viability assay (Life Technologies, Carlsbad, CA, USA) and blocked with 5 µg/mL anti- CD16/32 (2.4G2, BD Biosciences, San Jose, CA, USA) and heat-inactivated normal mouse serum (1:10) in FACS buffer (0.5% BSA and 2 mM EDTA in Dulbecco's PBS) before surface staining with antibodies to F4/80 (BM8), Siglec-F (E50-2440), Ly-6C (HK1.4), Ly-6G (1A8), TCRβ (H57-597), CD11b (M1/70), CD11c (N418), I-A/I-E (M5/114.15.2), CD19 (6D5) and CD115 (AFS98). Detection of intracellular Ym1 and NOS2 was performed directly *ex vivo*. Cells were stained for surface markers then fixed with 2% paraformaldehyde (Sigma Aldrich, Saint Louis, Mo, USA), permeabilized using Permeabilization Buffer (eBioscience, San Diego, CA, USA) and stained with directly labeled antibodies to NOS2 (CXNFT; eBioscience, San Diego, CA, USA) or biotinylated polyclonal goat anti-Ym1 (R&D Systems, Minneapolis, MN, USA) followed by streptavidin-PerCP (Biolegend, San Diego, CA, USA). Expression of Ym1 and NOS2 was determined relative to appropriate polyclonal or monoclonal isotype controls.

Samples were acquired on a BD LSR II using BD FACSDiva software (BD Bioscience, San Jose, CA, USA) and post-acquisition analysis performed using FlowJo v9 software (Tree Star Inc., Ashland, OR, USA). Macrophages were identified as lineage negative (CD19-,TCRb-,Ly6G-,SiglecF-), CD11b+ CD115+. (Dominik Rückerl)

Flow cytometry for the characterization of IL-4-induced in vitro alternative macrophage polarization

Macrophages were resuspended in staining medium (phenol-red free DMEM, 10 mM HEPES, 2% FBS) and incubated with anti-mouse CD206 (AbD Serotec, Hercules, CA, USA) or anti-human CD206 antibody (BD Biosciences, San Jose, CA, USA) or corresponding unspecific isotype control antibodies for 20 minutes at 4 °C. Cells were washed and resuspended in staining medium for flow cytometry. Data acquisition was performed using a FACS Aria III instrument (BD Biosciences, San Jose, CA, USA) and data were analyzed with FlowJo software. (Máté Kiss)

Arginase activity

Arginase activity measurement was performed as previously described with minor modifications [229]. (Zsolt Czimmerer)

Transient transfection

To determine potential function of miR-342-3p, RAW264.7 cells were transfected with 30 nM miR-342-3p precursor (Applied Biosystems, Foster City, CA, USA) or scrambled miRNA negative control (Applied Biosystems, Foster City, CA, USA) using DharmaFECT 3 (Thermo Scientific) in 12-well, 96 well plates (Sigma-Aldrich, Saint Louis, Mo, USA) and 8-well chamber slides (Thermo Scientific). (Zsolt Czimmerer)

Cell number analysis

Propidium iodide (PI)-based cell number analysis was performed as previously described with minor modifications [230]. Briefly, macrophages attached to the bottom of 96-well plates were permeabilized by Triton X-100, stained by propidium iodide (PI) and measured in a Synergy HT microplate reader (Bio-Tek Instruments, Winooski, VT) at 530/25 nm excitation and 645/40 nm emission. Cell numbers were determined using cell number reference curve. (Zsolt Czimmerer, Zsolt Bacsó)

Cell viability analysis

Resazurin-based viability staining (Promega, Mannheim, Germany) was carried out according to manufacturer's protocol. Neutral red staining was performed as previously described with minor modifications [231]. (Zsolt Czimmerer, Zsolt Bacsó)

Cell cycle analysis

$2x10^4$ cell/well were plated in Labtek 8-well chambered coverslips and transfected with appropriate miRNAs. 48 hours post-transfection cell fixation and PI staining was performed as previously described [232] with minor modifications. Raw264.7 cells were fixed on chamber slides using -20 °C methanol at -20 °C overnight. Fixed cells were covered with 5 µg/ml PI (Sigma-Aldrich, Saint Louis, Mo, USA) and 200 µg/ml RNase A (Sigma-Aldrich, Saint Louis, Mo, USA) in 0.4 ml PBS for 2 hours at room temperature in dark. Measurements were performed on a slide-based iCys Research Imaging Cytometer (CompuCyte Corporation, Westwood, MA). The DNA dye was excited by the 488 nm laser line and emission was collected in the red channel with a 650 nm longpass filter on linear scale. Single cells were recognized according to their size and circularity and cells were further gated according to their integral fluorescence intensity and maximum pixel intensity on 2D scattergram of PI signal. Data of the 1D histogram of the DNA staining was exported and fitted with the automatic one cycle diploid model of the Modfit LT 3.0 software (Verity Software House) with AutoDebris compensation, AutoAggregate Compensation and Apoptosis Model. In the measurements, the G1–G2 linearity ratio was around 1.8 and the R.C.S. of the fit (reduced $\chi 2$, a measure of goodness of fit) was less than 5. Measurements were repeated 3 times and approximately 1000-2000 cells were collected from each well. (Quang Minh Doan Xuan, Zsolt Bacsó)

Apoptosis assay

Raw264.7 cells were plated and treated in similar manner as in cell cycle analysis. Annexin V-FITC/PI staining was performed as previously described [233] with minor modifications. 48 hours following miRNA transfection, culture medium was replaced by 100 µl AB buffer (140 mM NaCl and 2.5 mM $CaCl_2$) and 10 µl Hoechst 33342 solution (50 µg/ml stock), 10 µl propidium iodide solution (50 µg/ml stock), and 5 µl FITC-conjugated Annexin V (AV) was added (according to the description of the MBL Apoptosis Detection Kit) for 15 minutes at 37 °C. Laser-scanning cytometric measurements were made by iCys Research Imaging Cytometer (CompuCyte Corporation, Westwood, MA). Hoechst, which stains all cells, was excited at 405 nm and detected via 463/20 bandpass filter; PI, which stains dead cells, was excited at 488 nm and collected via 650 nm longpass filter; and AV signal, which indicates apoptotic cells, was excited at 488 nm and detected with 530/30 bandpass filter. Single cells were selected by size and circularity and cells were additionally gated by their DNA content. Early apoptotic AV^+/PI^-, late apoptotic AV^+/PI^+,- and unapototic AV^-/PI^- cells were recognized by quadrant gate in the PI versus AV dot-plot with respect to unlabeled and miRNA untreated cells. (Quang Minh Doan Xuan, Zsolt Bacsó)

Plasmid construction

PsiCHECK2 dual luciferase vector (Promega, Mannheim, Germany) was used to confirm the function of the putative miR-342-3p binding sites in the Bcl2l1 3′-UTR. . For luciferase reporter assays, 320 bp (miR-342-3p_1) and 309 bp (miR-342-3p_2) from 3′UTR of Bcl2l1 gene, including the mir-342-3p target sites, were amplified by PCR using F1/R1 and F3/R3 primer pairs with XhoI and NotI sites. PCR was performed on mouse macrophages-derived genomic DNA. The XhoI/NotI-digested PCR product was cloned into the XhoI/NotI-digested psiCHECK2 dual luciferase vector. F1/R2 and F2/R1 as well as F3/R4 and F4/R3 primers were used to delete the mir-342-3p target sites from the 3′UTR. After mixing the two PCR products in case of both mir-342-3p binding sites, and digestion with XhoI and NotI, the 3′UTR fragment with a deleted mir-342-3p binding sites was cloned into XhoI/NotI-digested psiCHECK2 vector. (Zsolt Czimmerer)

Luciferase assay

Luciferase assays were measured as described previously [234]. Brifely, HEK293 cells were grown on 24-well plates to a 70-80% confluence. Transfection was performed using PEI with 0.1 µg of pRL-TK (Rr-luc) containing 3’UTR sequences and 0.1 µg of pGL3 control vector (Pp-luc) (Promega, Mannheim, Germany) for either a specific miR-342 or siRNA control. Cell lysates were collected 30–36 h post-transfection, and luciferase activity was determined using Dual-Luciferase® Reporter Assay System

(Promega, Mannheim, Germany). Renilla luciferase activity was normalized to firefly luciferase activity for each cell culture well and averaged across 6 well repetitions per condition. (Xin Yan, Sudhir Gopal Tattikota, Matthew N. Poy)

Statistical analysis

Statistical analysis for qRT-PCR, ChIP-qPCR, ELISA, LDH-release assay, FACS analysis, densitometry analysis of western blot, cell number analysis, cell viability analyses and luciferase assay: the error bars represent standard deviation (SD). The two-tailed Student's t test was used to evaluate the significance of differences between two groups.

Quantification and alignments of NGS analysis for RNA-seq, ChIP-seq and ATAC-seq as well as microarray analyses are also described in more detail in the material and methods section above. (Zsolt Czimmerer, Attila Horváth, László Steiner)

6. Results

6.1. IL-4-STAT6 signaling pathway-mediated direct transcriptional repression limits inflammatory responsiveness in alternatively polarized macrophages

6.1.1. Identification of IL-4-STAT6 signaling pathway-mediated gene expression changes in mouse BMDMs

In order to obtain a comprehensive understanding of STAT6-dependent transcriptional responses in IL-4 polarized mouse BMDMs, we determined the STAT6-dependent IL-4-regulated genes in a time course experiment in wild type (WT) and STAT6 KO BMDMs using RNA-seq (The experimental design is shown in Figure 9).

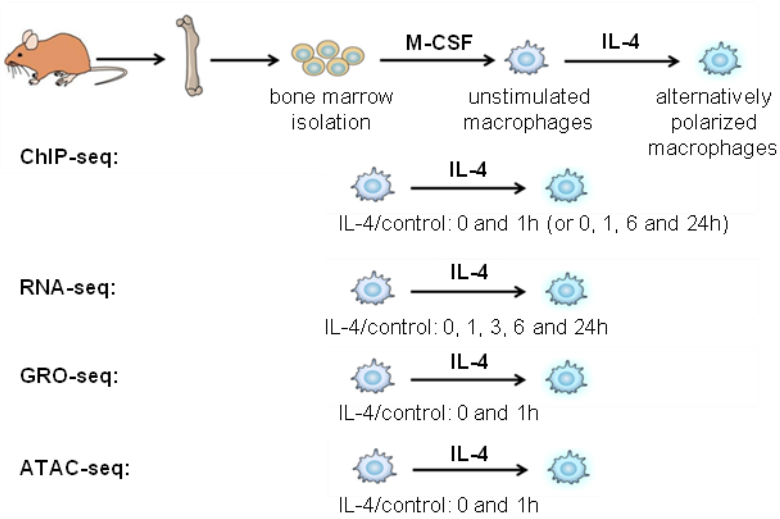

Figure 9. Schematic representation of the applied alternative macrophage polarization protocol and experimental system

We identified 1614 IL-4-regulated genes (Fc≥2, p-value<0.05) and classified into four IL-4-induced gene expression clusters based on fold changes and expression kinetics (Figure 10A, B and C). The IL-4-induced clusters include well established alternative macrophage activation-associated genes such as *Arg1*, *Socs1*, *Irf4,* and *Chil3* (Figure 10A) [3, 39, 235]. Unexpectedly, we observed that a relatively high portion of IL-4-responsive genes (39%) were repressed (Figure 10A, B and C). The IL-4-mediated repression was detected after 3 hours of stimulation and remained attenuated at later time points as well (6, 24h) (Figure 10A, B and C). Importantly, IL-4-dependent repression and activation were completely abolished in the STAT6-deficient BMDMs (Figure 10C).

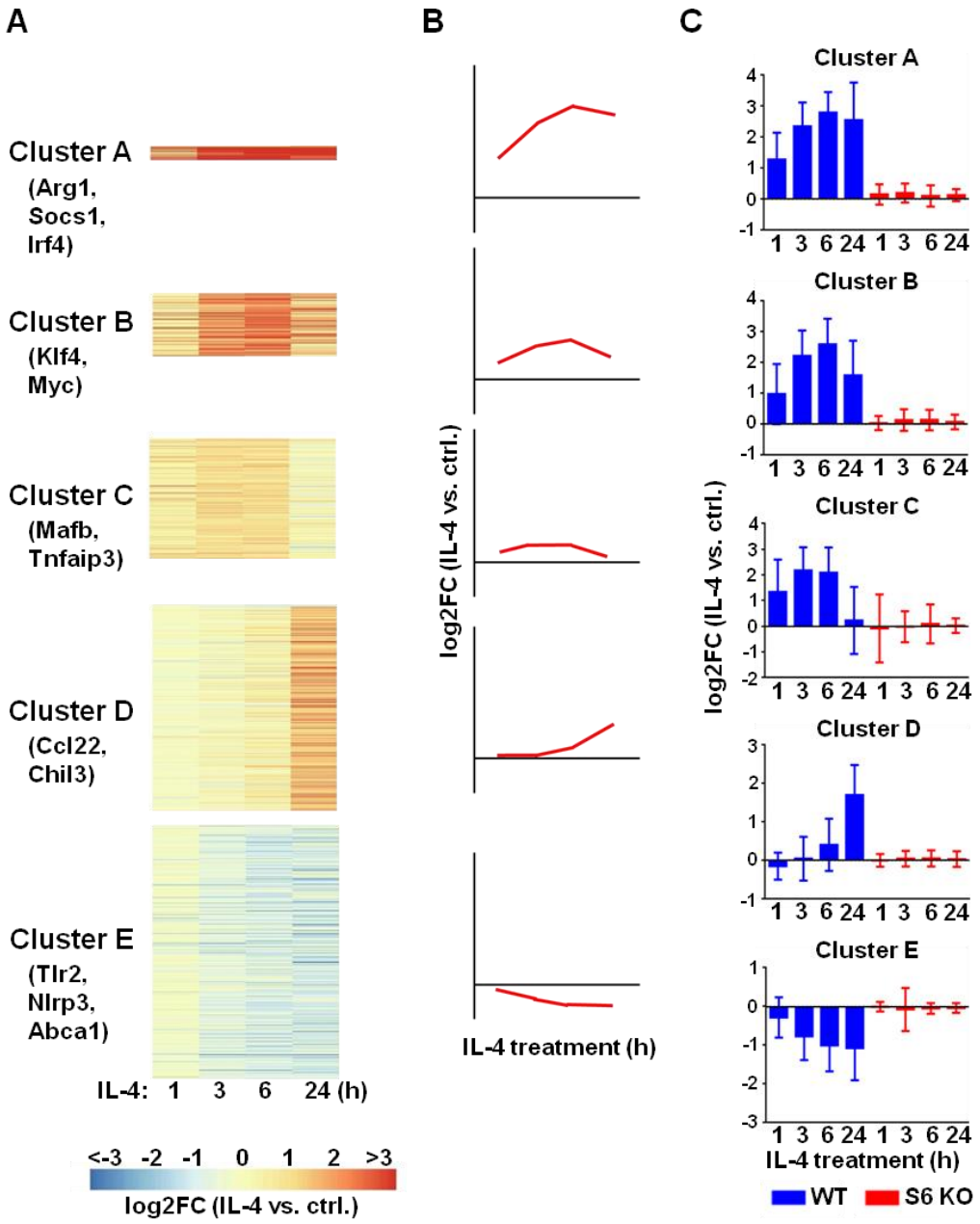

Figure 10. RNA-seq-based investigation of the IL-4/STAT6 signaling pathway-induced gene expression program during mouse alternative macrophage polarization

(A) Heat map representation of IL-4-regulated (p-value≤0.05, FC≥2) gene expression clusters in murine BMDMs (bone marrow-derived macrophages). Differentiated macrophages were treated with IL-4 for the indicated period of time and RNA-seq was performed. (B) Schematic representation of the dynamics of gene expression changes in IL-4-activated and repressed gene clusters. (C) Presentation of the average fold change from the IL-4-activated and repressed gene clusters at indicated time points following IL-4 stimulation in wild-type (WT) and STAT6-deficient (S6 KO) macrophages.

For validation, we examined the steady-state mRNA level of six IL-4-repressed (*Abca1*, *Clec4d*, *Fos*, *Tlr2*, *Cd14* and *Nlrp3*) and three activated (*Klf4*, *Hbegf* and *Edn1*) genes with RT-qPCR, and confirmed IL-4-mediated and STAT6-dependent regulation (Figure 11A and B).

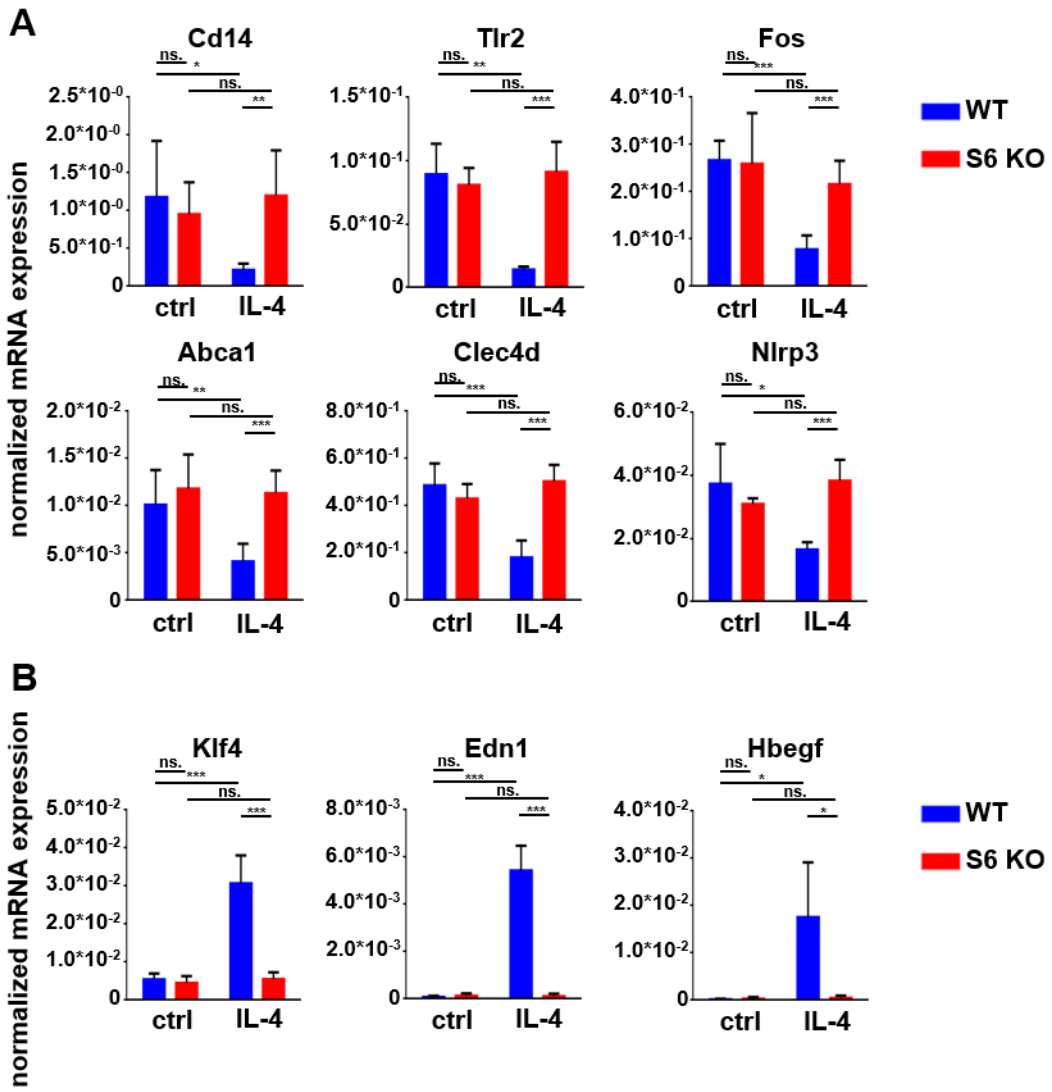

Figure 11. RT-qPCR-based validation of IL-4/STAT6 signaling pathway-mediated activation and repression

(A) RT-qPCR analysis of gene expression on a select set of IL-4-repressed genes in wild-type (WT) and STAT6 deficient (S6KO) BMDMs. Macrophages were treated with IL-4 for 6 hours. Each data point represents the mean and SD of five individual animals. **P*<0.05, ***P*<0.01, ****P*<0.001, n.s. indicates not significant change. (B) RT-qPCR measurement of selected IL-4-activated genes in wild-type (WT) and STAT6 deficient (S6KO) bone marrow-derived macrophages. Macrophages were treated with IL-4 for 6 hours. Each data point represents the mean and SD of five individual animals. **P*<0.05, ***P*<0.01, ****P*<0.001, ns. indicates not significant change.

As demonstrated previously, filarial nematode infection is associated with the accumulation of alternatively polarized macrophages, showing increased expression of *Ym1*, *Fizz1/RELM-α* and *Arg1* [56]. In order to study whether transcriptional repression in response to alternative macrophage polarization signals occurs *in vivo*, we compared the transcriptome of peritoneal macrophages from *Brugia malayi* nematode-implanted mice (Ne-Mac) and thioglycollate-elicited peritoneal macrophages (Thio-Mac) using publicly available RNA-seq data sets [236]. Gene Set Enrichment Analysis (GSEA) analysis showed that the *in vitro* IL-4-repressed gene set

was significantly enriched (FDR q-value<0.1, NER: -2.38) among the genes that were down-regulated in response to nematode infection in peritoneal macrophages (Figure 12A). In addition, the expression of all six selected IL-4/STAT6-repressed genes were significantly attenuated in Ne-Mac compared to Thio-Mac (Figure 12B).
Taken together, these results show the complex regulatory role of IL-4-STAT6 signaling pathway in the control of macrophage transcriptome during alternative macrophage polarization.

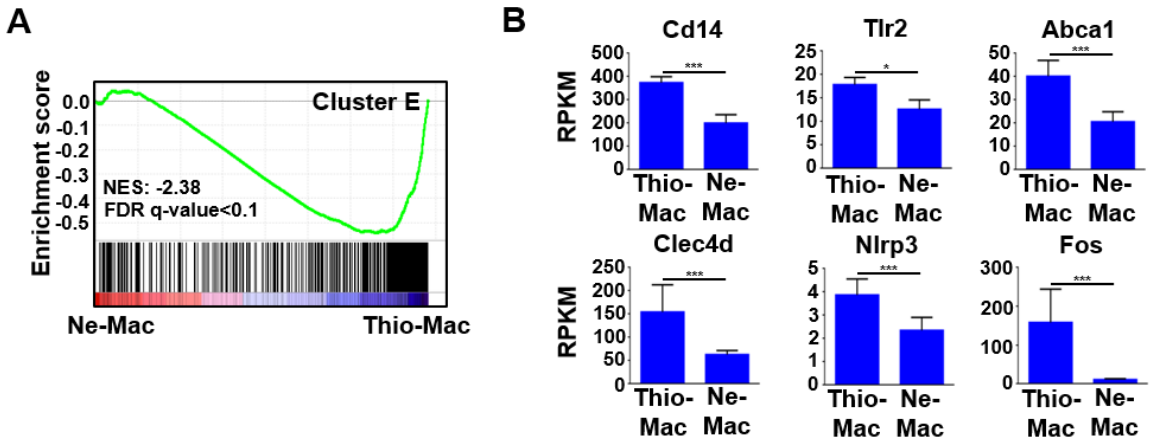

Figure 12. IL-4-repressed gene set is inhibited during nematode infection-induced in vivo alternative macrophage activation in mice
(A) GSEA showing enrichment of IL-4-repressed genes (*in vitro*) among the repressed genes in the *Brugia malayi*-implanted mice-derived alternatively polarized macrophages (Ne-Mac) compared to the intraperitoneal thioglycollate-administrated mice-derived peritoneal macrophages (Thio-Mac). Rank order of mouse genes from the most upregulated (position 1) to the most downregulated (position 11,726) between the Ne-Mac versus the Thio-Mac is shown on the *x*-axis; the barcode indicates the position of genes from the IL-4-repressed genes (*in vitro*). The *y*-axis corresponds to the running enrichment score generated by the cumulative tally of the IL-4-repressed genes. The total height of the curve indicates the extent of enrichment, with the normalized enrichment score (NES) and *P* values indicated. (B) Expression of the selected IL-4 repressed genes in the *Brugia malayi*-implanted mice-derived alternatively polarized macrophages (Ne-Mac) and the intraperitoneal thioglycollate-administrated mice-derived peritoneal macrophages (Thio-Mac). Reads per kilobase per million values (RPKM) are presented as the mean and SD of three individual animals quantified by RNA-seq. **P*<0.05, ***P*<0.01, ****P*<0.001.

6.1.2. IL-4 activates and represses the gene expression at transcriptional level

Next, we wanted to investigate whether IL-4/STAT6 signaling pathway regulates gene expression at the transcriptional or post-transcriptional level. We assessed the immediate early effect of IL-4 on the two serine phosphorylated forms of RNA polymerase II, the active histone mark H3K27Ac and analyzed nascent RNA expression by GRO-seq after 1 hour of cytokine exposure. Elongation-specific RNAPII-pS2 ChIP-seq revealed 5931 gene bodies, exhibiting significantly changing read enrichments (3008 down-regulated and 2923 up-regulated, p≤0.1) (Figure 13A).

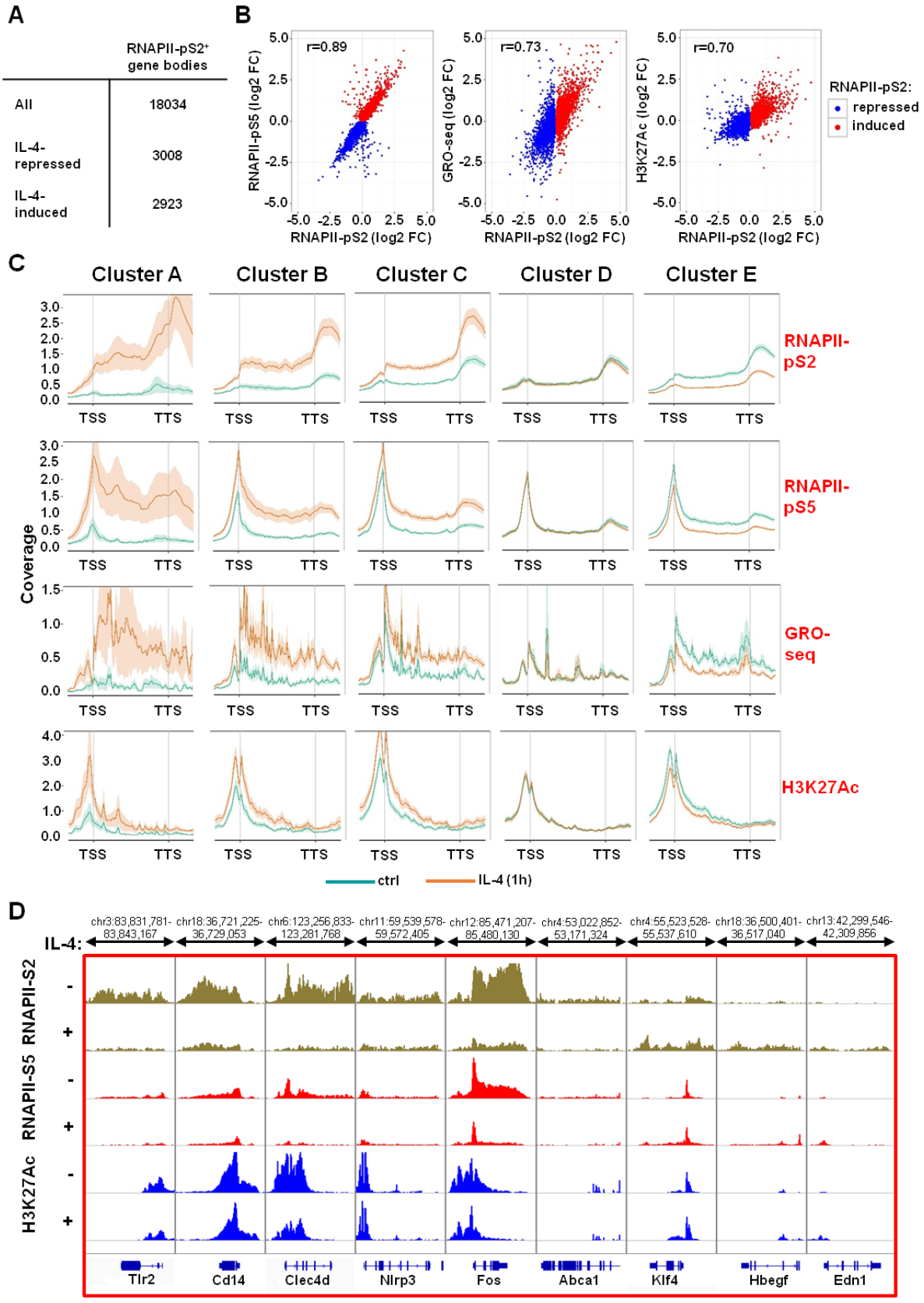

Figure 13. IL-4-STAT6 signaling pathway-induced transcriptional repression and activation
(A) The number of gene bodies associated with IL-4-dependent regulation of RNAPII-pS2 binding (p≤0.1) in BMDMs. Macrophages were treated with IL-4 for 1 hour. (B) Correlation of RNAPII-pS2 binding with RNAPII-pS5 binding, nascent RNA expression as well as H3K27Ac enrichment at the IL-4-

regulated RNAPII-pS2 binding-associated gene bodies. (C) Metaplot representation of RNAPII-pS5, RNAPII-pS2, H4K27Ac-specific ChIP-seq and GRO-seq signals at the gene bodies in the different IL-4-regulated gene clusters (Figure 10) in WT macrophages. Macrophages were treated with IL-4 for 1 hour. Coverage is defined as read count per million mapped reads. (D) H3K27Ac, RNAPII-pS5 and RNAPII-pS2 ChIP-Seq signals at the selected IL-4-repressed and activated gene bodies. ChIP-seq signals are visualized by the Integrative Genomics Viewer.

As expected, positive correlation was observed between RNAPII-pS2 binding and transcription initiation-specific RNAPII-pS5 binding, H3K27Ac enrichment as well as nascent RNA expression at the gene bodies (Figure 13B).
In additon, IL-4-dependent induction of RNAPII-pS2, RNAPII-pS5 and H3K27Ac enrichment as well as nascent RNA expression were detected at gene bodies of IL-4 induced gene clusters (Cluster A-C) and the selected IL-4-induced genes such as Klf4, Hbegf and Edn1 (Figure 13C and D). In contrast, the gene bodies of IL-4 repressed genes (Cluster E) were associated with attenuated RNAPII-pS2, RNAPII-pS5 and H3K27Ac enrichments and nascent RNA expression (Figure 14A and B). Taken together, these results show that IL-4/STAT6 signaling pathway directly activates and represses gene expression, primarily at the transcriptional level during the alternative polarization of mouse BMDMs.

6.1.3. IL-4-activated STAT6 binding is required for transcriptional activation and repression

To further characterize the role of STAT6 transcription factor in transcriptional activation and repression, we also investigated the STAT6 cistrome (the sum of all genomic binding sites) using a time course of 1, 6 and 24 hours of IL-4 stimulation (Figure 9). As expected, STAT6 binding was negligeable in untreated macrophages (Figure 14A) but as short as 1 hour of IL-4 stimulation dramatically enhanced the binding of STAT6, which was followed by a reduction after 6 and 24 hours (Figure 14A). The comparison of the STAT6 cistrome (20119 genomic regions in IL-4 stimulated cells) with the RNAPII-pS5-bound genomic regions revealed that 60.5% of STAT6 peaks overlapped with the union of the RNAPII-pS5 positive genomic sites in non-polarized and/or IL-4-treated macrophages (Figure 14B) suggesting that transcription could be directly regulated by STAT6 at these regions. Next, we categorized the RNAPII-pS5 positive STAT6 peaks based on IL-4-regulated RNAPII-pS5 binding and divided the STAT6-bound regulatory regions into three different clusters: "repressor", "neutral" and "activator" STAT6 peak clusters (Figure 14C). We observed that “repressor” and "neutral" STAT6 peaks were associated with typically lower occupancies compared to the IL-4-induced RNAPII-pS5-associated "activator" STAT6 peaks (Figure 14D). In addition, IL-4-dependent regulation of RNAPII-pS2 binding and H3K27Ac enrichment exhibited similar patterns to RNAPII-pS5 in all three STAT6 clusters (Figure 14E and F). These findings confirm the conclusion that STAT6 binding can be associated with either transcriptional activation or repression at different genomic sites.

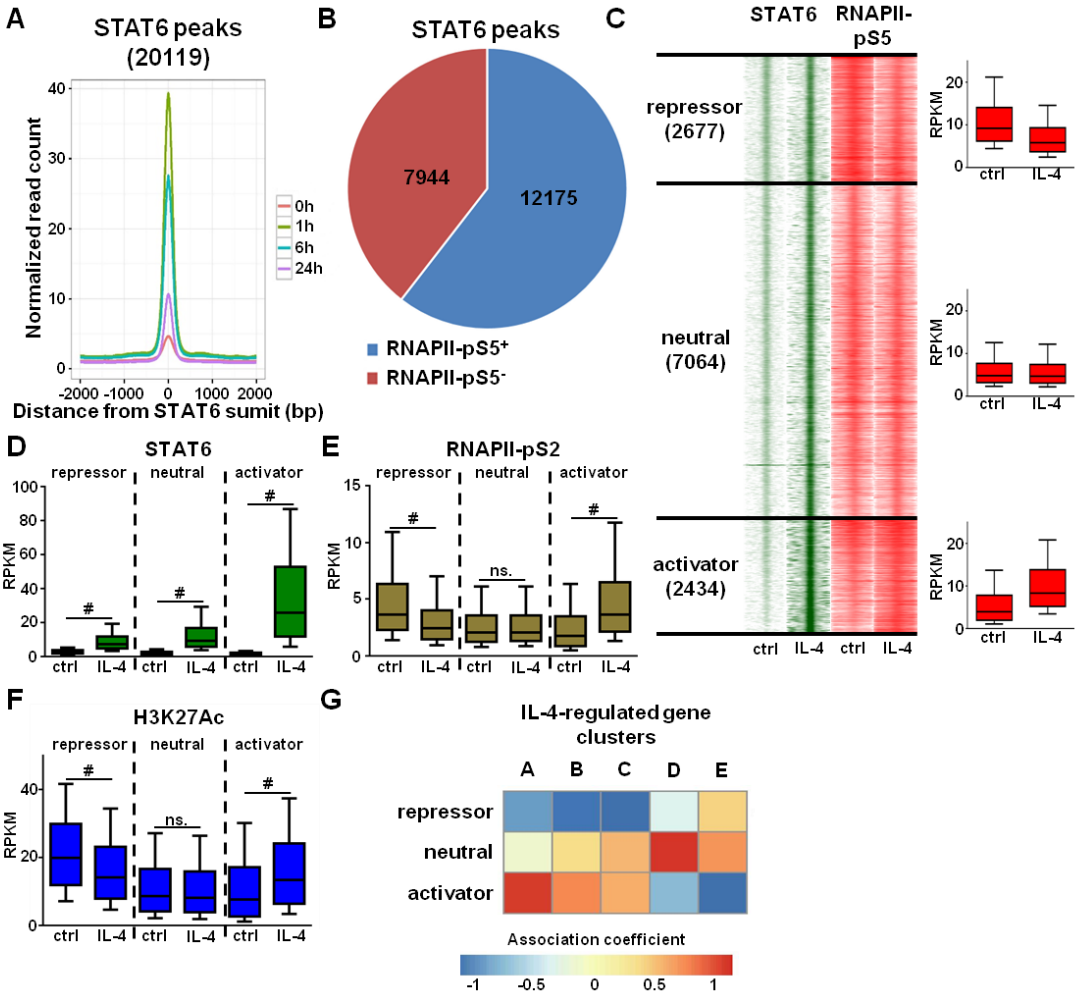

Figure 14. RNAPII-pS5-based functional characterization of IL-4-activated STAT6 cistrome in mouse macrophages

(A) Histogram depicting the average read count of STAT6 peaks at the indicated period of time following IL-4 treatment in wild-type macrophages. (B) Pie chart representing the RNAPII-pS5 positive and negative STAT6-bound regulatory regions following 1 hour of IL-4 stimulation. (C) Read distribution plot of ChIP-seq intensities for STAT6 and RNAPII-pS5 around the summit of the detected STAT6 peaks in a 4kb window (left). Macrophages were either treated with IL-4 for 1 hour or left untreated (ctrl). Clustering of STAT6/RNAPII-pS5 co-bound genomic regions was performed using DiffBind analysis ($p \leq 0.05$). Boxplots depicting the average RPKM values for RNAPII-pS5 in each clusters (right). (D) Box plot representation of STAT6 read enrichments (RPKM) around the identified STAT6 peak clusters in wild-type macrophages. Changes were considered significant at $p<0.00001$ using paired t-test and an average fold change cut off value of ≥1.15 was used between ctrl and IL-4 treated samples. # means significant difference, n.s. indicates not significant change. (E) Box plot representation of RNAPII-pS2 read enrichments (RPKM) around the identified STAT6 peak clusters in wild-type macrophages. Changes were considered significant at $p<0.00001$ using paired t-test and an average fold change cut off value of ≥1.15 was used between ctrl and IL-4 treated samples. # means significant difference, n.s. indicates not significant change. (F) Box plot representation of H3K27Ac read enrichments (RPKM) around the identified STAT6 peak clusters in wild-type macrophages. Changes were considered significant at $p<0.00001$ using paired t-test and an average fold change cut off value of ≥1.15 was used between ctrl and IL-4 treated samples. # means significant difference, n.s. indicates not significant change. (G) Heat map representation of correlations between STAT6 peak clusters (Figure 14C) and IL-4-regulated gene clusters (Figure 10A) based on genomic proximity and functional chromatin domain prediction.

Next we assigned STAT6-bound genomic regions to genes in order to assess the correlation between IL-4-repressed enhancer activity (RNAPII-pS5 - ChIP-seq) and gene expression (mRNA – RNA-seq). For this analysis, we predicted the subTADs in which gene regulation by STAT6 might take place, based on CTCF and RAD21 ChIP-seq data sets from BMDM, utilizing a previously described algorithm [91, 97, 237-239]. As shown in Figure 14G, we observed that "repressor" STAT6 peaks were tightly associated with the IL-4-repressed gene cluster (Cluster E), while "activator" STAT6 peaks were linked to the immediate early IL-4-induced genes containing Clusters A-C. These results indicate a tight connection between STAT6-dependent regulation of enhancer activity and neighboring gene expression in the same subTAD.

To further characterize the IL-4/STAT6 signaling-dependent transcriptional regulation, we examined the potential link between IL-4-regulated genes and the associated STAT6 peaks at the level of individual genes. We detected at least one repressed, STAT6-bound enhancer around the selected IL-4-repressed genes accompanied by reduced H3K27 acetylation and RNAPII binding (Figure 15A). The selected IL-4-induced genes were also associated with STAT6-bound enhancers from the "activator" cluster (*Klf4*_-34Kb, *Hbegf*_+43Kb and *Edn1*_-42Kb) (Figure 15A). In addition, enhancer RNA (eRNA) expression is an excellent marker of enhancer activity [240]. Thus, we measured the expression of eRNAs at the "repressor" and "activator" STAT6 peaks using RT-qPCR method. Indeed, eRNA expression was regulated in a similar manner as the binding of RNAPII-pS5, RNAPII-pS2 and changes of H3K27Ac levels at the "repressor" and "activator" STAT6 sites in wild-type BMDMs (Figure 15A, B and C). Interestingly, IL-4-dependent regulation of eRNA expression was completely abrogated in the STAT6 defficient mouse BMDMs at the examined enhancers (Figure 15B and C). Taken together, these results suggest that IL-4-activated STAT6 is essential for the transcriptional repression characterized by reduced RNAPII binding, histone acetylation and, consequently enhancer activity.

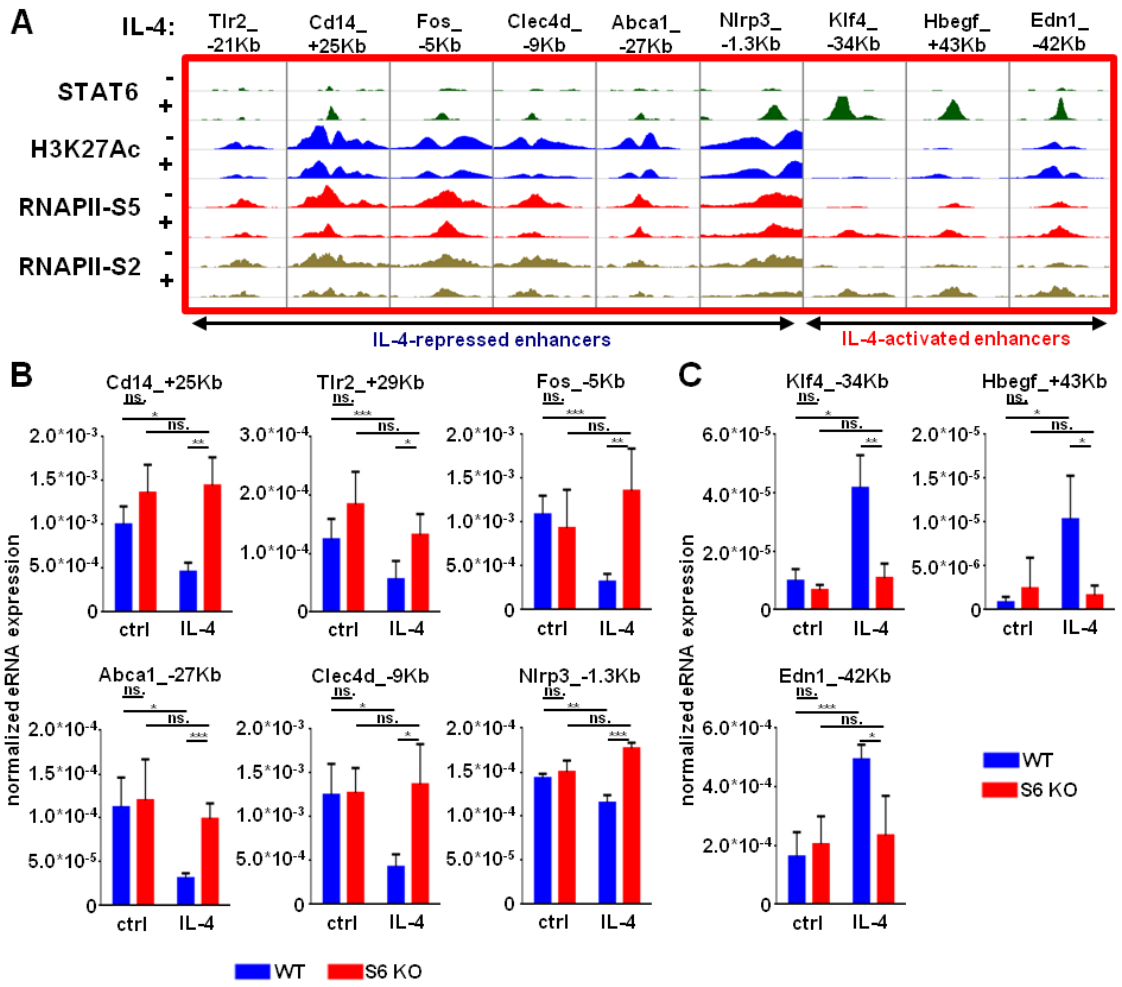

Figure 15. IL-4-STAT6 signaling pathway-mediated activation and repression at the selected enhancers

(A) Integrative Genomics Viewer snapshots of STAT6, H3K27Ac, RNAPII-pS5 and RNAPII-pS2 ChIP-seq signals on a select set of IL-4-repressed and activated genomic loci. (B) RT-qPCR-based measurement of eRNA expression at the selected IL-4-repressed enhancers in wild-type (WT) and STAT6 deficient (S6KO) bone marrow-derived macrophages following 1 hour of IL-4 stimulation. Each data point represents the mean and SD of five individual animals. **P*<0.05, ***P*<0.01, ****P*<0.001, n.s. indicates not significant change. (C) (B) RT-qPCR-based measurement of eRNA expression at the selected IL-4-activated enhancers in wild-type (WT) and STAT6 deficient (S6KO) bone marrow-derived macrophages following 1 hour of IL-4 stimulation. Each data point represents the mean and SD of five individual animals. **P*<0.05, ***P*<0.01, ****P*<0.001, n.s. indicates not significant change.

6.1.4. STAT6 binds to repressed sites in the absence of a canonical binding motif

In order to identfy whether the functional features of STAT6 binding are influenced by their genomic localization and/or the DNA sequences they are associated with, we investigated the genomic distribution of STAT6 peak clusters. We could not observe notable differences between the three STAT6 peak clusters regarding genomic localization relative to genes (Figure 16A). The majority of STAT6-bound genomic sets were detected in intergenic and intronic regions in the genome in all three clusters

(Figure 16A). About 10% of STAT6 binding sites were found at TSSs and in promoter regions (Figure 16A). We also investigated the enrichment of active histone mark H3K4m1 at the neighboring genomic regions of STAT6 peaks using a publicly available ChIP-seq data set [108]. Interestingly, H3K4m1 enrichment was detected on more than 98% of STAT6-bound genomic sites but changes were not significant following IL-4 treatment (Figure 16A and B). These results show that STAT6 transcription factor primarily binds enhancers and the functional features of different STAT6 peak clusters cannot be simply interpreted by their genomic localization relative to genes.

Next, we performed *de novo* motif analysis of the sequences under the different STAT6 peak clusters. As we expected, PU.1, TRE, RUNX and CEBP motifs were significantly enriched under all three clusters (Figure 16C). In contrast, the canonical STAT6 motif was under-represented under "repressor" and "neutral" STAT6 peaks compared to the "activator" STAT6 peaks (Figure 16C and D). Plotting the motif scores for PU.1, TRE, RUNX and CEBP did not show significant differences between the three STAT6 peak clusters (Figure 16E). However, motif score for STAT6 was lower in the “repressor” and "neutral" STAT6 peak clusters compared to the “activator” STAT6 peak cluster (Figure 16E). Considering that the presence of STAT6 is needed for repression (Figure 10B), these findings suggest that STAT6 is bound without direct DNA contact or it recognizes non-canonical binding motifs at repressed genomic reginos.

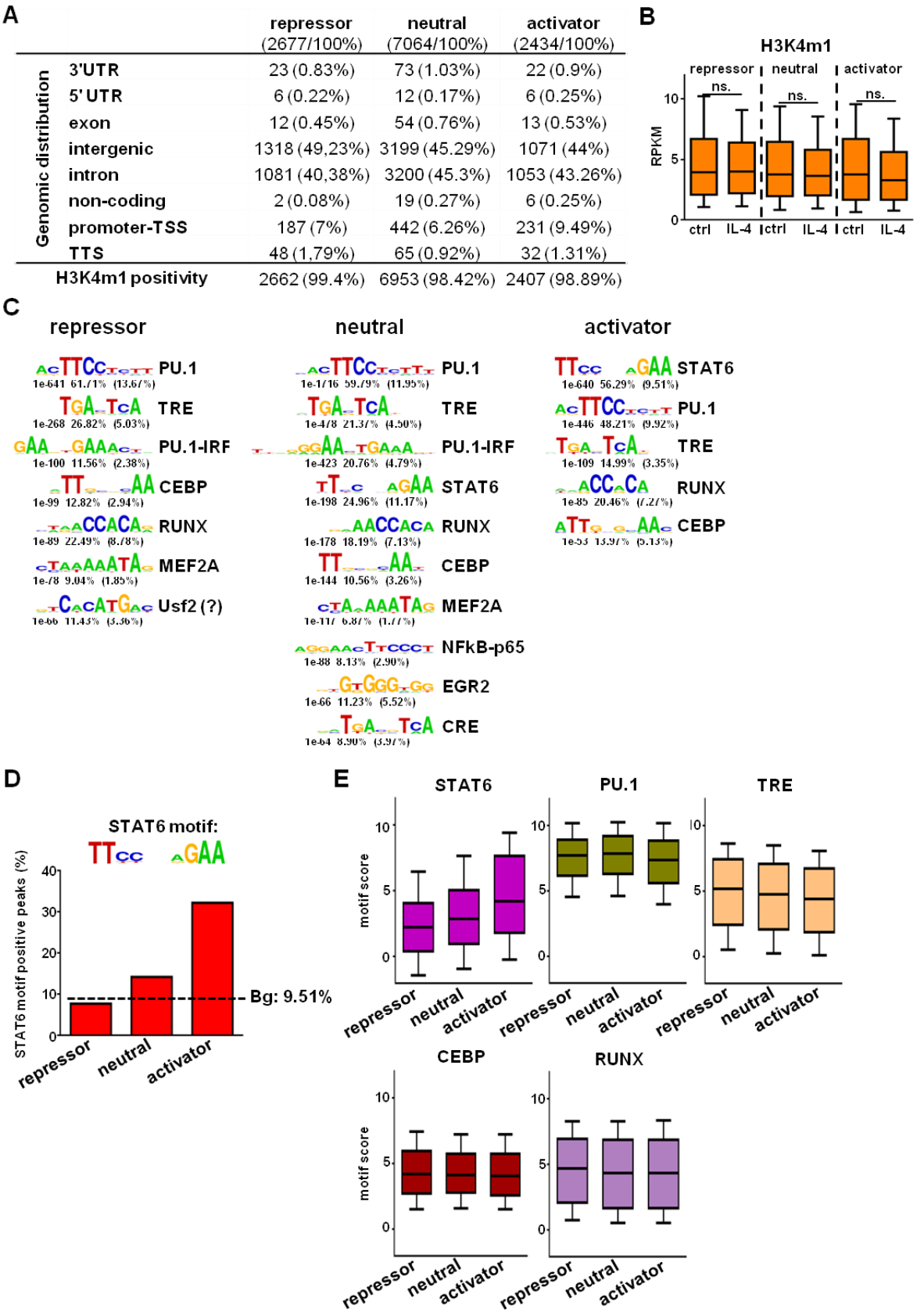

Figure 16. Genomic distribution and H3K4m1 positivity of RNAPII-pS5 positive STAT6 peak clusters as well as LDTF and STAT6 motif enrichment under the different STAT6 peaks

(A) Active histone mark H3K4m1 positivity and genome-wide distribution of STAT6 peaks from different clusters. (B) Box plot representation of H3K4m1 enrichment at the surrounding genomic regions of the identified STAT6 peak clusters in wild-type macrophages. Macrophages were treated with IL-4 for 4 hour. Changes were considered significant at $p<0.00001$ using paired t-test and an average fold change cut off value of ≥1.15 was used between ctrl and IL-4 treated samples. # means significant difference, n.s. indicates not significant change. (C) De novo motif enrichment identification under different STAT6 peak clusters from ChIP-seq data using HOMER. “Target %” refers to the ratio of the peaks having the given motif, and “Bg %” refers to the ratio of a random background. (D) Box plot representation of STAT6, PU.1, TRE, CEBP and RUNX motif scores at the functionally distinct STAT6 peak clusters. (E) Bar graph depicting the percentage of the STAT6 motif positive STAT6 peaks in the clusters defined on panel C. The logo of the STAT6 binding motif is also presented, which served as the basis of the targeted motif discovery under STAT6 peaks. Dashed line indicates background (Bg: 9.51%).

6.1.5. STAT6-mediated repression of enhancer activity is accompanied by decreased chromatin accessibility and linage-determining transcription factor binding

To characterize the IL-4/STAT6 signaling pathway-dependent transcriptional regulation in more detail, we investigated the chromatin accessibility at the STAT6-bound genomic regions by performing ATAC-seq experiments. As we expected, our genome-wide analysis indicated elevated chromatin accessibility at the “activator” STAT6-bound sites (Figure 17B), while significant reduction was observed in chromatin accessibility at the “repressor” STAT6-bound genomic regions (Figure 17B). These findings suggest that both STAT6-mediated enhancer activation and repression are associated with the alteration of chromatin openess in the alternatively polarized macrophages.

Chromatin accessibility determines enhancer activity in different cell types [241, 242]. Furthermore, binding of macrophage LDTFs, PU.1, JUNB, C/EBPα and IRF8 are associated with active enhancers in macrophages [82, 104]. Indeed, their binding motifs were significantly enriched under STAT6 peaks (Figure 16C). Therefore, we wanted to investigate whether IL-4/STAT6 signaling pathway-mediated activation and repression are associated with modified binding of LDTFs and examined their binding at activated and repressed enhancers in the absence or presence of IL-4 using ChIP-seq. As we expected, a high portion of the STAT6 peaks were overlapped with the examined LDTF cistromes in all three STAT6 peak clusters except for JUNB which showed moderated overlap (Figure 17A).

Interestingly, PU.1, JUNB and C/EBPα binding were significantly diminished, while IRF8 binding did not change at the "repressor" STAT6-bound genomic regions after 1 hour IL-4 treatment in BMDMs (Figure 17C, D, E and F). In contrast, all four LDTFs showed significantly increased binding at the activated STAT6-bound enhancers following IL-4 stimulation (Figure 17C, D, E and F). These findings indicate that IL-4/STAT6 signaling pathway influences the binding of LDTFs at the "activator" and "repressor" STAT6-bound enhancers into opposite directions.

A

STAT6 peak clusters	Overlap with STAT6 peaks (peak number/%)								
	ATAC-seq	PU.1	JunB	CEBPα	IRF8	P300	HDAC1	HDAC2	HDAC3
repressor (2677)	2418/ 90.3	2603/ 97.2	886/ 33.1	2154/ 80.5	2468/ 92.2	2671/ 99.8	2409/ 90	2456/ 91.8	2173/ 81.2
neutral (7064)	6007/ 85	6848/ 96.9	1568/ 22.2	5103/ 72.2	6580/ 93.2	7050/ 99.8	6296/ 89.1	6478/ 91.7	5293/ 74.9
activator (2434)	1876/ 77.1	2272/ 93.3	376/ 15.5	1704/ 70	2064/ 84.8	2410/ 99	1952/ 80.2	2090/ 85.9	1681/ 69.1

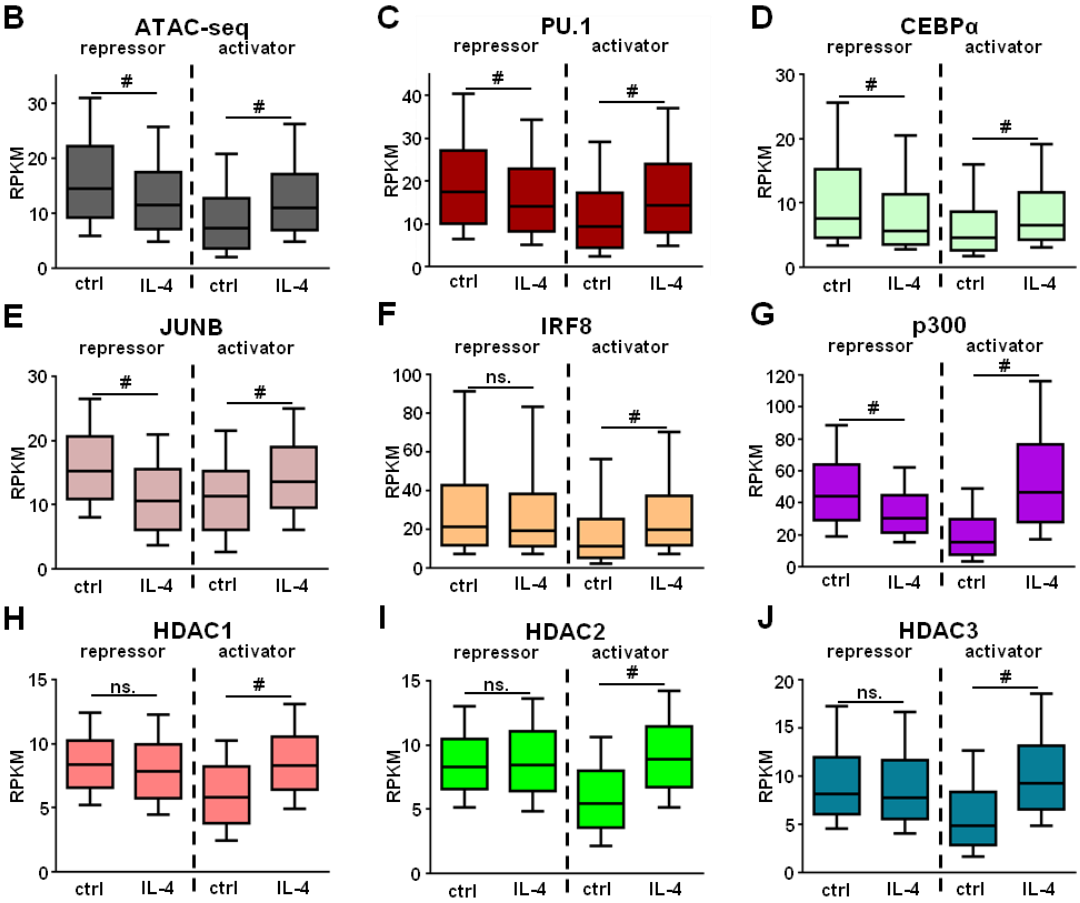

Figure 17. Characterization of the IL-4-induced epigenomic changes at repressor and activator STAT6 sites

(A) Overlap of LDTFs, p300 and classical HDACs binding with RNAPII-pS5 positive STAT6 peak clusters. (B) Box plot representation of ATAC-seq and (C-J) ChIP-seq signals for the indicated factors (PU.1, CEBPα, JUNB, IRF8, p300, HDAC1, HDAC2 and HDAC3) on the repressor and activator STAT6 sites in wild-type macrophages. Macrophages were treated with IL-4 for 1 hour. Changes were considered significant at $p<0.00001$ using paired t-test and an average fold change cut off value of ≥1.15 was used between ctrl and IL-4 treated samples. # means significant difference, n.s. indicates not significant change change.

6.1.6. IL-4/STAT6 signaling pathway-mediated repression of enhancers is characterized by an altered p300:HDAC ratio

The acetylation status and thus the activity of enhancers are tightly regulated by HAT and HDAC enzymes [243, 244]. Therefore, we studied the binding of the histone acetyltransferase p300 as well as classical histone deacetylases, including HDAC1, 2 and 3 at the STAT6-bound genomic sites after 1 hour of IL-4 exposure using ChIP-seq method. We observed that the majority of STAT6-bound genomic sites were either pre-loaded by p300 and classical HDACs or recruited these factors upon IL-4 stimulation (Figure 17A). The binding of p300 was significantly induced at the "activator" STAT6-bound genomic regions but significantly decreased at STAT6-repressed enhancers after 1 hour of IL-4 treatment (Figure 17G). Unexpectedly, classical HDACs occupancy were significantly increased at STAT6-activated enhancers in IL-4-stimulated BMDMs but STAT6-repressed enhancers were bound by HDAC1, 2 and 3 at the basal state and their occupancy did not change significantly upon IL-4 treatment (Figure 17H, I and J). Taken together, these findings show that STAT6-repressed enhancers are bound by both p300 and classical HDACs at the steady-state, and p300 binding is selectively decreased by IL-4 resulting in a modified equilibrium favoring HDAC binding.

6.1.7. The presence of HDAC3 is required for IL-4/STAT6-signaling pathway-mediated repression on a subset of genes

Direct interactions between STAT transcription factors and classical HDACs have been described previously in numerous cell types regulating STAT-mediated direct transcriptional regulation [245-247]. Furthermore, HDAC3 has been shown to contribute to the control of alternative macrophage polarization *in vitro* and *in vivo* [114]. Therefore, we wanted to study wheter HDAC3, which is present on STAT6-repressed enhancers, (Figure 17J), might also participate in the IL-4/STAT6 signaling pathway-mediated transcriptional repression. Thus, we decided to investigate whether HDAC3 influences the IL-4/STAT6 signaling pathway-induced repression in the alternatively polarized BMDMs. Using a microarray dataset from Mullican et al, [114] we identified 1628 IL-4-repressed genes ($p \leq 0.05$) in wild-type BMDMs (Figure 18A). We found an IL-4-repressed gene cluster (Cluster III., 371 genes), which showed diminished repression in HDAC3-deficient macrophages following IL-4 exposure, using K-mean clustering method (Figure 18A and B). Although, the basal expression level of these genes did not show major differences between wild-type and HDAC3-deficient BMDMs but the IL-4-mediated repression was partially or completely abrogated in the absence of HDAC3 (Figure 18A and B).

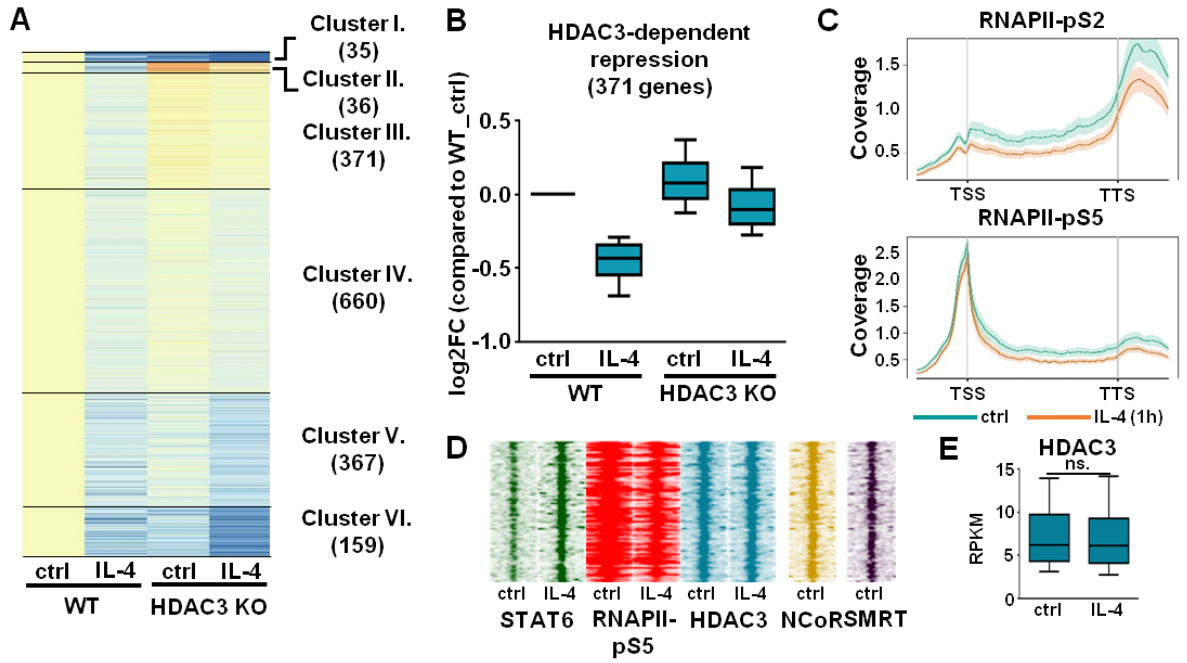

Figure 18. The genome-wide characterization of the potential role of HDAC3 in IL-4/STAT6-mediated transcriptional repression

(A) Heat map representation of IL-4-repressed gene clusters (p≤0.05) in unstimulated and IL-4 stimulated wild-type (WT) and HDAC3 deficient (HDAC3 KO) murine macrophages. Clustering was based on the participation of HDAC3 in the IL-4-mediated repression. Macrophages were treated with IL-4 for 24 hours. (B) Box plot representation of the expression of IL-4/HDAC3-dependently repressed gene set in wild-type (WT) and HDAC3-deficient (HDAC3 KO) mouse macrophages using publicly available microarray results. Macrophages were treated with IL-4 for 24 hours. (C) Metagene plot representation of RNAPII-pS5 and RNAPII-pS2 signals at the gene bodies of IL-4/HDAC3-dependently repressed genes. Coverage is defined as read count per million mapped reads. (D) Read distribution plot of ChIP-seq intensities against RNAPII-pS5, STAT6, HDAC3, NCoR and SMRT around the summit of the detected STAT6 peaks at the IL-4-repressed enhancers (n=325) in the subTADs of HDAC3-dependently repressed genes following 1 hour of IL-4 stimulation. (E) Box plot representation of the average HDAC3 binding intensity on the genomic regions presented on panel D. Changes were considered significant at p<0.00001 using paired t-test and an average fold change cut off value of ≥1.15 was used between ctrl and IL-4 treated samples. # means significant difference, n.s. indicates not significant change.

Furthermore, RNAPII-pS5 and RNAPII-S2 enrichment were also decreased at these gene bodies after 1 hour of IL-4 treatment in wild-type macrophages (Figure 18C). Interestingly, 325 STAT6-repressed enhancers were observed in the same subTAD with IL-4/HDAC3-repressed genes (Figure 18D). These genomic regions were bound by HDAC3 but HDAC3 occupancy was not changed by IL-4 treatment (Figure 18D and E). These results suggest that the presence of HDAC3 at the IL-4/STAT6 signaling pathway-repressed enhancers is required for the IL-4-mediated repression of a specific subset of genes. The investigation of precise mechanism requires further focused studies.

It has been described previously that HDAC3 is one of the key components of NCoR/SMRT corepressor complex [248-250]. Thus, we decided to investigate whether

the NCoR/SMRT corepressor complex itself contributes to IL-4/STAT6/HDAC3-mediated repression as well. First, we examined the occupancy of NCoR and SMRT at HDAC3-bound enhancers using publicly available ChIP-seq data sets [111]. We observed that the IL-4/STAT6/HDAC3 repressed enhancer set was also bound by both NCoR and SMRT in unstimulated BMDMs (Figure 18D).

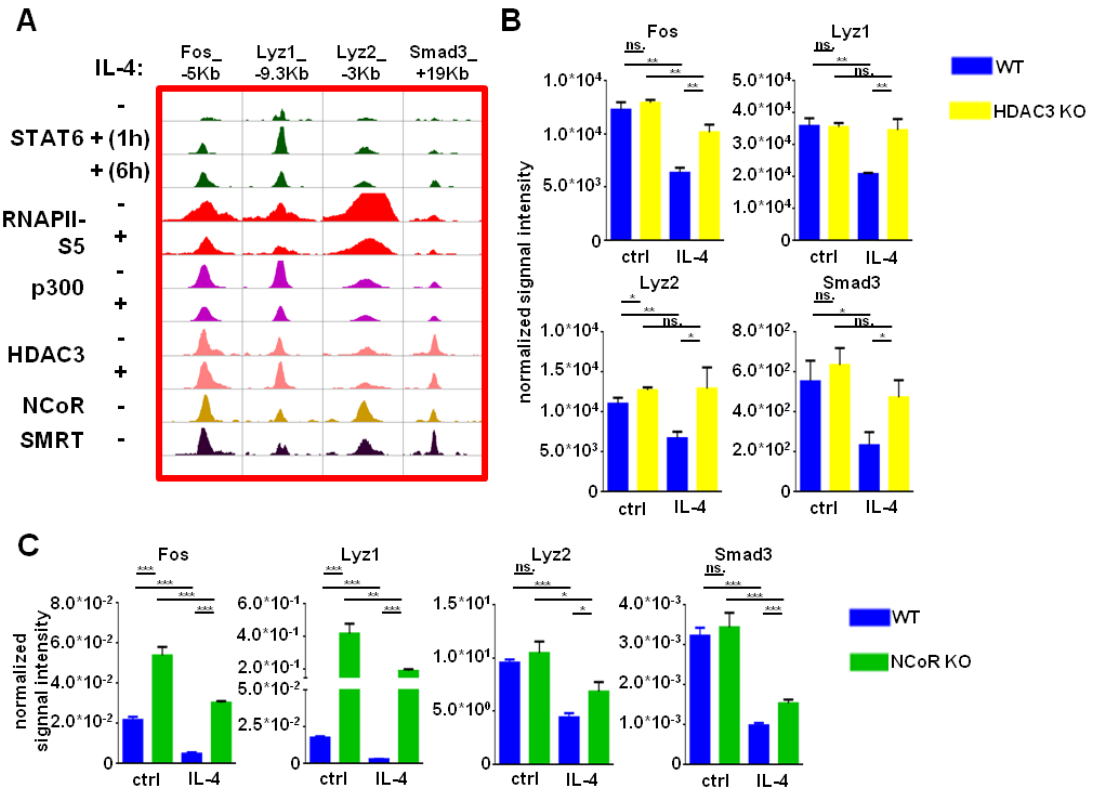

Figure 19. The participation of NCoR/HDAC3 corepressor complex in the IL-4/STAT6 signaling pathway-induced repression of the selecred genes

(A) Representative examples of IL-4/STAT6/HDAC3-repressed genes-associated enhancers. Genome browser view of the merge of STAT6, RNAPII-pS5, p300 and HDAC3-specific ChIP-seq from unstimulated or IL-4-stimulated wild-type (WT) as well as SMRT and NCoR ChIP-seq from unstimulated WT macrophages. (B) Normalized microarray signal intensity values of Fos, Lyz1, Lyz2 and Smad3 genes in unstimulated (ctrl) as well as IL-4 stimulated wild-type (WT) and HDAC3-deficient (HDAC3 KO) mouse macrophages. Each data point represents the mean and SD of three biological replicates. Each data point represents the mean and SD of tree biological replicates. *P<0.05, **P<0.01, ***P<0.001, n.s. indicates no significant difference. (C) RT-qPCR-based measurements of Fos, Lyz1, Lyz2 and Smad3 expression in unstimulated (ctrl) as well as IL-4 stimulated wild-type (WT) and NCoR-deficient (NCoR KO) immortalized bone marrow-derived macrophage cells. Macrophages were treated with IL-4 for 24 hours. Each data point represents the mean and SD of tree biological replicates. *P<0.05, **P<0.01, ***P<0.001, n.s. indicates no significant difference.

Next, we decided to study the requirement of NCoR in the IL-4/STAT6/HDAC3-mediated repression using NCoR-deficient BMDMs. We selected four genes for this analysis, including Fos, Lyz1, Lyz2 and Smad3 based on their IL-4/STAT6/HDAC3-mediated repression and due to the fact that their IL-4/STAT6-signaling pathway-repressed enhancers were bound by HDAC3, NCoR and SMRT (Figure 19A and B). RT-qPCR-based gene expression analysis showed that *Fos* and *Lyz1* genes were

expressed at a significantly higher level in unstimulated macrophages in NCoR-deficient BMDMs compared to wild-type macrophages, while the basal expression of Lyz2 and Smad3 were not changed in the absence of NCoR (Figure 19C). Furthermore, IL-4-mediated repression of these genes was partially abrogated in NCoR-deficient macrophages (Figure 19C). Taken together, our results indicate that IL-4/STAT6 signaling pathway induces transcriptional repression via NCoR/HDAC3 complex at a subset of genes. Thus, we explored at least one of the molecular mechanisms for STAT6-dependent transcriptional repression.

6.1.8. IL-4/STAT6-mediated direct transcriptional repression affects the LPS-induced inflammatory program of macrophages

Next we wanted to investigate whether the repressive action of IL-4 leaves its footprint on the epigenetic signature and if it affects and/or determines the subsequent response of the macrophages to further stimuli. Using KEGG pathway analysis, we identified twelve signaling pathways which were significantly overrepresented exclusively in IL-4-repressed gene cluster (Figure 20A). These pathways included the inflammatory response-associated NOD-like receptor signaling and Toll-like receptor signaling pathways (Figure 20A) [140, 251]. Furthermore, Ingenuity Pathway Analysis (IPA) software-based upstream transcriptional regulator analysis revealed that the inflammatory signals-activated p65 (RelA) is one of the most significantly inhibited transcriptional regulators by IL-4 (Figure 20B).

The majority of IL-4-repressed genes including several members of NOD-like and Toll-like receptor signaling pathways indicated reduced mRNA expression following 24 hours of IL-4 exposure accompanied by decreased STAT6 binding at the repressed enhancers (Figure 10A, B, Figure 20C and D). These results raised the possibility that IL-4 can influence the subsequent inflammatory response of the macrophages via directly repressed enhancers following the dissociation of STAT6.

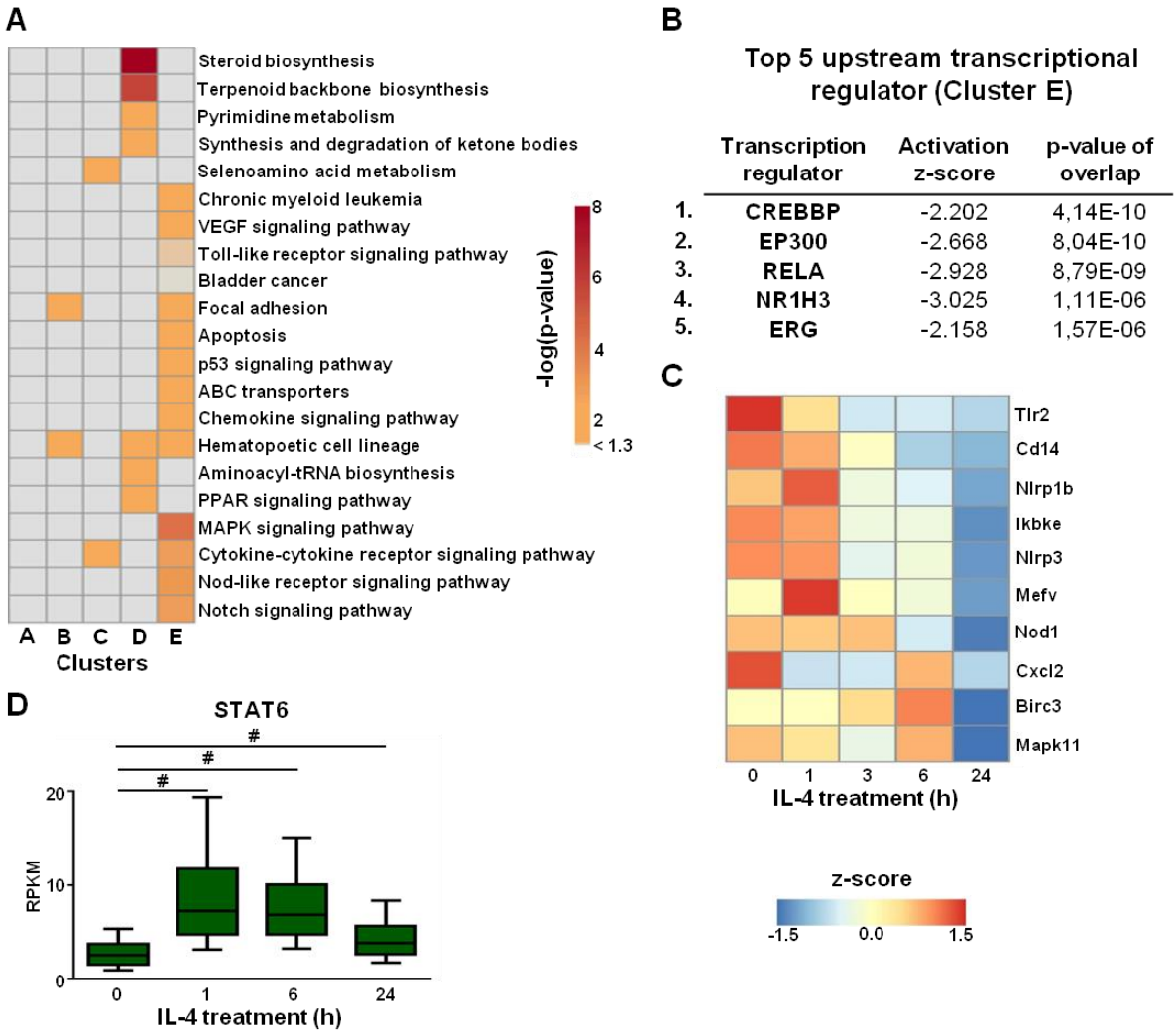

Figure 20. IL-4/STAT6 signaling pathway-dependent repression of inflammatory response activated genes and STAT6 binding dynamics at the repressed regulatory elements

(A) Five IL-4-regulated gene clusters-associated significantly enriched KEGG pathway categories. (B) Ingenuity Pathway Analysis algorithm-based prediction of top upstream transcriptional regulators of IL-4-repressed genes. Transcription regulators showing *p*-value overlap <0.01 and regulation *z*-score >2 or <-2 are shown. (C) Heat map representation of IL-4-regulated gene expression of the selected members of Toll-like and Nod-like receptor pathways in murine BMDMs. Differentiated macrophages were treated with IL-4 for 1, 3, 6 and 24 hours. (D) Box plot representation of STAT6 transcription factor binding at the "repressor" STAT6-occupied RNAPII-pS5^{+} genomic regions in wild-type macrophages. Macrophages were treated with IL-4 for 1, 6 and 24 hours. Changes were considered significant at p<0.00001 using paired t-test and the average of fold differences at the individual enhancers ≥1.15. # p<0.00001 and average fold difference≥1.15, n.s. indicates not significant changes.

In order to investigate whether prior activation of IL-4/STAT6 signaling pathway is able to modulate the inflammatory program of macrophages, we performed RNAPII-pS5, RNAPII-pS2 and p65-specific ChIP-seq as well as RNA-seq experiments on IL-4-pre-treated and LPS-activated mouse BMDMs (experimental design is shown in Figure 21A). Our global transcriptome analysis showed that 1350 genes were significantly upregulated (p≤0.05) in LPS-activated BMDMs compared to unstimulated controls (Figure 21B).

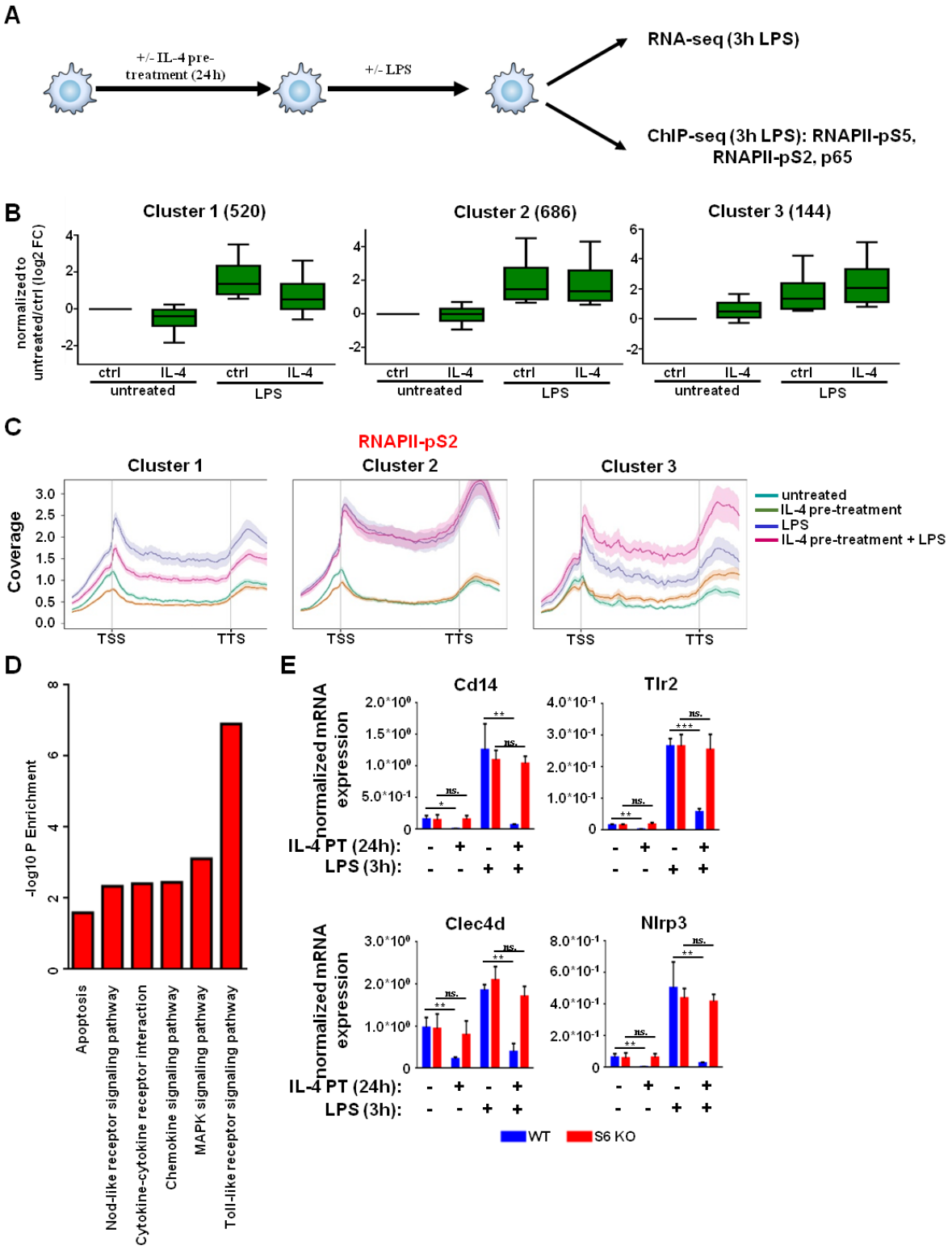

Figure 21. The selective repression of LPS-activated inflammatory program is carried out by IL-4-activated STAT6

(A) Schematic representation of the experimental system used. (B) Box plot representation of the fold changes of LPS-activated genes under the presented conditions determined by RNA-seq. Clustering was performed based on the different LPS-induced gene expression effects on IL-4 pre-treated and untreated macrophages ($p<0.05$). Macrophages were pre-treated with IL-4 for 24 hours or left untreated

followed by 3 hours of LPS exposure. (C) Metagene plot representation of RNAPII-pS2 signals over the gene bodies of the genes found in the clusters introduced on panel B under the presented conditions. Coverage is defined as read count per million mapped reads. (D) IL-4-attenuated LPS-inducible gene cluster-associated significantly enriched KEGG pathway categories. (E) RT-qPCR-based measurements of basal and LPS-induced expression of the selected inflammation-associated genes in IL-4-pre-treated and unstimulated wild-type (WT) and STAT6 deficient (S6KO) BMDMs. Macrophages were pre-treated with IL-4 for 24 hours or left untreated followed by 3 hours of LPS exposure. Each data point represents the mean and SD of four individual animals. *P<0.05, **P<0.01, ***P<0.001, n.s. indicates no significant difference.

Interestingly, 520 genes showed significantly reduced (p≤0.05) LPS-responsiveness following 24 hours IL-4 pre-treatment including the above examined Tlr2, Cd14, Clec4d and Nlrp3 (Figure 21B). Furthermore, LPS-mediated activation of 686 genes was not modulated significantly by IL-4 pre-treatment, while 144 genes showed significantly elevated LPS-dependent inducibility in IL-4-pre-treated BMDMs compared to unstimulated controls (Figure 21B) suggesting that the interaction between the IL-4-activated and LPS-activated signaling pathways is specific and selectively taking place on certain genomic loci and it is not a broad interference or attenuation. Next, we examined whether IL-4/STAT6 signaling pathways influences LPS-dependent inducibility of inflammation responsive genes at the transcriptional or post-transcriptional level. We studied the IL-4 and LPS-regulated RNAPII-pS2 binding at the gene bodies of LPS-activated genes using ChIP-seq. RNAPII-pS2 binding showed a similar pattern to “steady-state” mRNA level in all three LPS inducible gene expression clusters suggesting that IL-4 pre-treatment influences LPS-activated gene expression primarily at the transcriptional level (Figure 21C). Using KEGG patway analysis, we observed that six out of twelve IL-4-attenuated signaling pathways were also significantly overrepresented among the genes that were less activated by LPS following IL-4 pre-treatment, among others the NOD-like receptor and Toll-like receptor signaling pathways (Figure 21D).

In order to determine whether the IL-4-dampended inflammatory responsiveness is STAT6 dependent, we examined the mRNA expression of Tlr2, Cd14, Clec4d and Nlrp3 genes in wild-type and STAT6-deficient macrophages after 24 hours of IL-4 pretreatment followed by 3 hours of LPS-activation. As we expected, IL-4 pre-treatment could not inhibit the LPS-dependent activation of these genes in the absence of STAT6 (Figure 21E). These results raise the possibility that IL-4-activated STAT6 can directly influence the inflammatory responsiveness in macrophages via transcriptional repression of certain components of the LPS-activated inflammation-specific gene expression program.

6.1.9. IL-4/STAT6 signaling pathway-dependent attenuation of inflammatory responsivenes on a specific subset of enhancers

To investigate whether the interaction between IL-4-activated and LPS-activated signaling pathways can also be observed at the enhancer level, we compared the STAT6 and p65 cistromes in the subTADs of IL-4-repressed LPS inducible genes. 961 enhancers were found with overlapping IL-4-activated STAT6 and LPS-activated p65 peaks revealing a partial overlap between the STAT6 and p65 cistromes (Figure 22A and B).

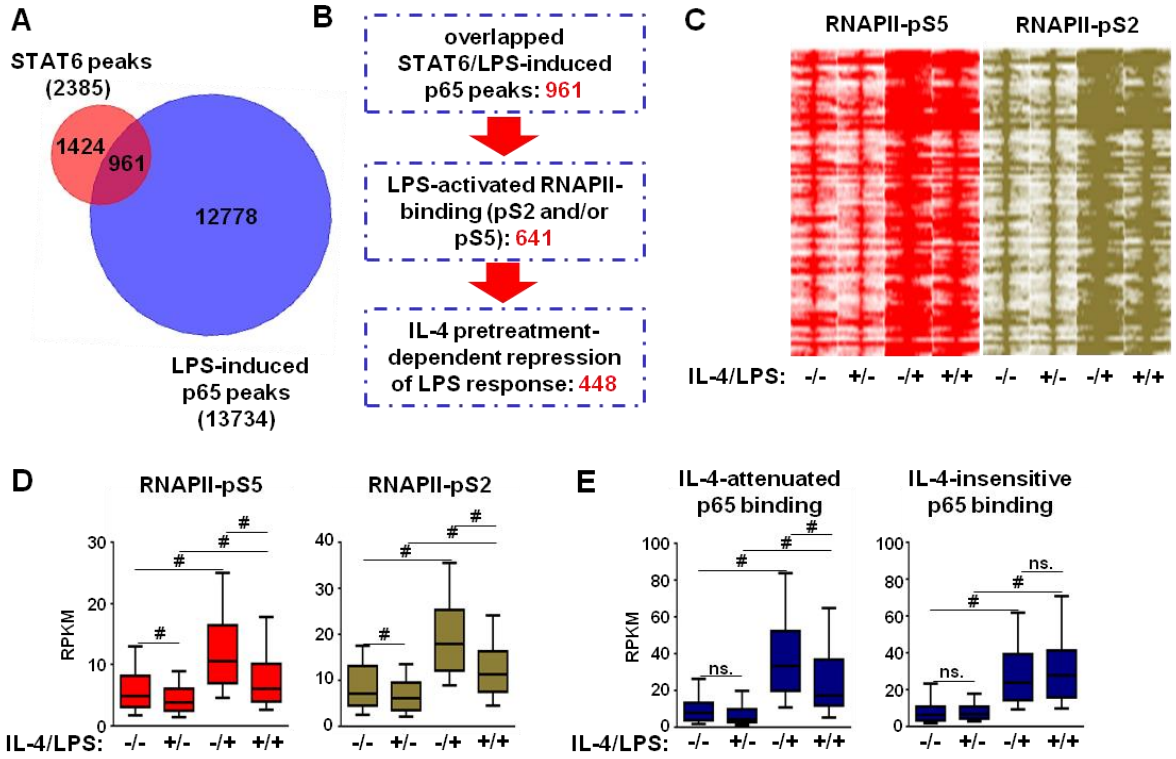

Figure 22. The genome-wide characterization of the IL-4/STAT6 signaling pathway-mediated repression of inflammatory response on a specific subset of enhancers

(A) Venn-diagram depicting the overlap between the STAT6-bound regulatory regions associated to IL-4-inhibited LPS-responsive genes and the LPS-activated p65 cistrome. (B) Flowchart showing the identification of IL-4-repressed, LPS-inducible inflammatory enhancers. Significant changes in RNAPII binding were identified by DiffBind analysis ($p \leq 0.05$). (C) Read distribution plot of ChIP-seq intensities for RNAPII-pS5 and RNAPII-pS2 around the summit of STAT6 peaks on the identified 448 overlapping STAT6 and p65-bound regulatory elements exhibiting IL-4-dependent attenuation of LPS response. (D) Box plot representation of the average read counts (RPKM) for RNAPII-pS5 and RNAPII-pS2 binding at the regulatory regions presented on the read distribution plot on panel C, exhibiting attenuated LPS response in IL-4 pre-treated macrophages. Changes were considered significant at $p<0.00001$ using paired t-test and an average fold change cut off value of ≥1.15 was used between ctrl and IL-4 treated samples. # means significant difference, n.s. indicates not significant difference. (E) Box plot representation of the average read counts (RPKM) for p65 binding at the regulatory regions presented on the read distribution plot on panel C, exhibiting attenuated LPS response in IL-4 pre-treated macrophages. Regulatory regions showing repressed (left) and not influenced (right) p65 binding are shown. Changes were considered significant at $p<0.00001$ using paired t-test and an average fold change cut off value of ≥1.15 was also used between ctrl and IL-4 treated samples. # means significant difference, n.s. indicates not significant difference.

Next, we wanted to examine whether IL-4/STAT6 and inflammatory signaling pathways can interact with each other at the STAT6 and p65-bound enhancers using RNAPII-specific ChIP-seq analysis. 641 out of 961 genomic regions showed significantly increased RNAPII-binding after LPS activation (Figure 22B). Interestingly, 70% (448/641) of LPS-activated enhancers were associated with significantly attenuated basal and LPS-induced RNAPII binding following 24 hours of IL-4 pre-treatment (Figure 22B, C, D and Figure 23A). To further explore the mechanism of IL-4/STAT6 signaling pathway-diminished inflammatory responsiveness, we investigated the LPS-induced p65 binding at this enhancer set in IL-4-pre-treated and unstimulated macrophages. Based on p65 binding, we observed two subsets of these enhancers (Figure 22E and Figure 23A). LPS-induced p65 binding showed significant reduction at 74 IL-4-repressed enhancers, while IL-4-repressed LPS-response was not linked to attenuated p65 binding at 374 enhancers (Figure 22E and Figure 23A).

To further examine the STAT6-dependency of IL-4-attenuated enhancer activity and p65 binding, we selected three-three enhancers for further analysis. RT-qPCR-based measurement of eRNA expression confirmed the IL-4-induced and STAT6-dependent repression of basal and LPS-inducible enhancer activity at the selected enhancers (Figure 23B). Using p65-specific ChIP-qPCR method, we confirmed that IL-4-mediated reduction of LPS-activated p65 binding was completely diminished in the absence of STAT6 on the selected IL-4-reduced p65 binding-associated enhancers (Figure 23C).

Taken together, these results indicate that the activation of IL-4/STAT6 signaling pathway can reduce the inflammatory responsiveness of macrophages through selective, direct repression of a distinct LPS-inducible enhancer set.

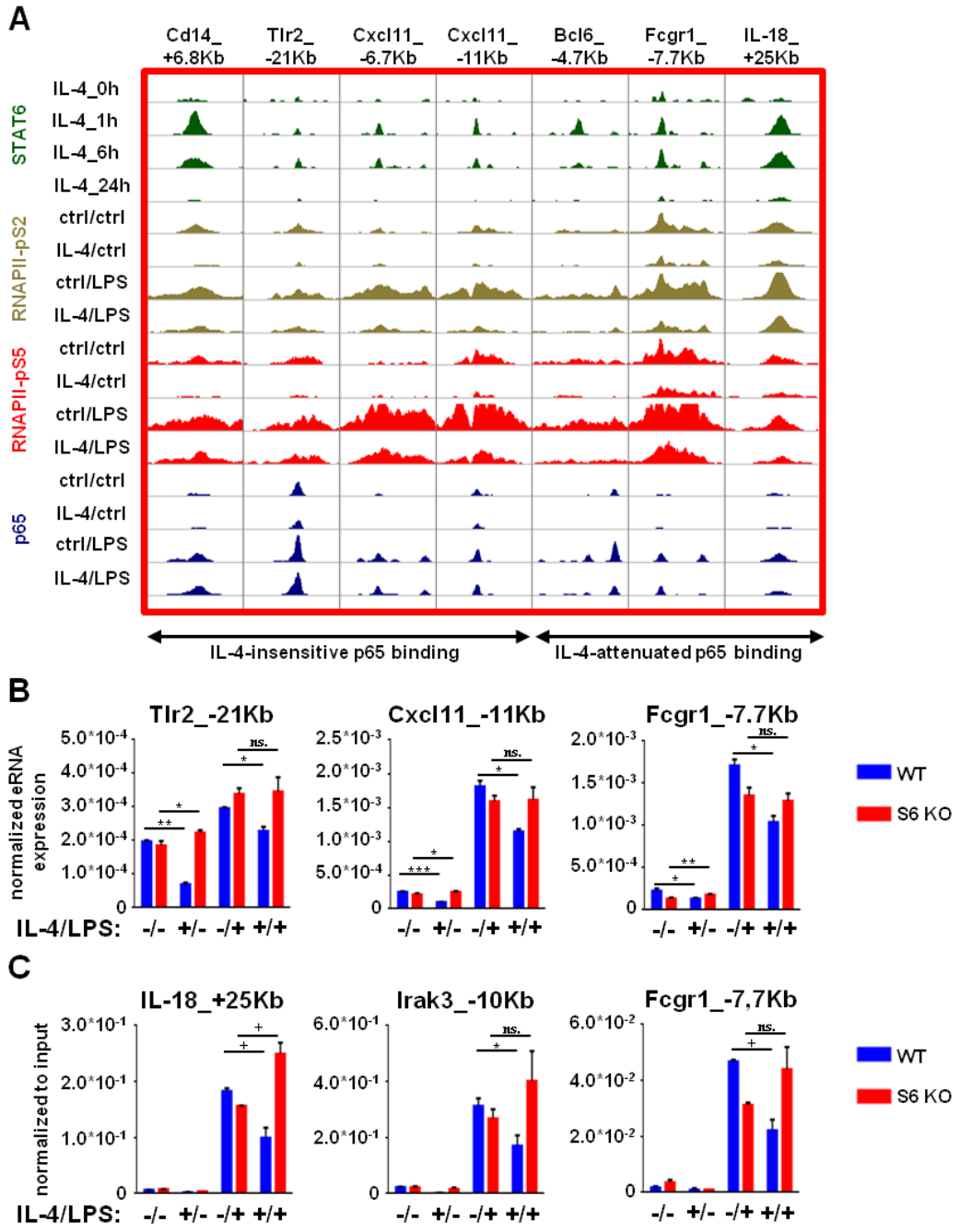

Figure 23. Characterization of the IL-4/STAT6 signaling pathway-attenuted inflammatory responsivness at the selected enhancers

(A) Genome browser views about the IL-4 repressed regulatory regions showing attenuated LPS response in IL-4 pre-treated macrophages. ChIP-seq signals for RNAPII-pS5, RNAPII-pS2 and p65 are shown under the indicated conditions. (B) RT-qPCR-based measurement of basal and LPS-induced eRNA expression at the selected enhancers in IL-4-pre-treated and unstimulated wild-type (WT) and STAT6 deficient (STAT6KO) iBMDMs. Macrophages were treated with IL-4 and LPS for 24 as well as 3 hours. Each data point represents the mean and SD of three biological replicates. *P<0.05, **P<0.01, ***P<0.001, n.s. indicates not significant. (C) ChIP-qPCR-based measurement of p65 binding at the selected IL-4-repressed LPS-responsive enhancers from wild-type (WT) and STAT6-deficient (S6KO) macrophages. Macrophages were treated with IL-4 and LPS for 24 as well as 1 hour. Each data point represents the mean and SD of two biological replicates. ^{+}P<0.1, *P<0.5, n.s. indicates not significant changes.

6.1.10. IL-4-mediated repression of inflammatory response results in attenuated inflammasome activation, decreased IL-1β production and pyroptosis

Genes showing opposing regulation by IL-4 and LPS were mostly associated with inflammation-linked pathways, including NOD-like and Toll-like receptor signaling pathways (Figure 21D). It is known that NOD-like receptors play central role in the inflammasome activation leading to IL-1β secretion and inflammasome-associated cell death, pyroptosis [252]. As shown above, IL-4/STAT6 signaling pathway could repress the basal and LPS-induced expression of a key inflammasome component, *Nlrp3* (Figure 21E). First, we investigated the transcriptional control of *Il1b* expression in IL-4 pre-treated and LPS-activated BMDMs. Interestingly, attenuated basal and LPS-induced RNAPII-pS2 and RNAPII-pS5 binding at *Il1b* gene body as well as *Il1b* mRNA expression were observed in IL-4-pre-treated macrophages (Figure 24A and B). In addition, Il1b_-9.7Kb enhancer was identified within the predicted subTAD of *Il1b* was antagonistically regulated by LPS and IL-4 (Figure 24A). LPS-activated p65-binding at the STAT6-bound Il1b_-9.7Kb enhancer (in case of one out of two p65 peaks) was partially inhibited by IL-4/STAT6 signaling pathway similarly to IL-18_+25Kb and Fcgr1_-7.7Kb enhancers described above (Figure 23C, Figure 24A and C). Consequently, IL-4-mediated repression of basal and LPS-activated eRNA expression was detected at the *Il1b*_-9.7Kb enhancer (Figure 24D). The IL-4-mediated attenuation of basal and LPS-activated *Il1b* eRNA and mRNA expression were completely abolished in STAT6 deficient macrophages (Figure 24B and D). LPS-induced NLRP3 and pro-IL-1β expression were also reduced at the protein level by IL-4/STAT6 signaling pathway (Figure 24E and F), while the expression of additional inflammasome components such as proCaspase-1 and ASC was not changed after IL-4 and LPS stimulation of BMDMs (Figure 24E and F).

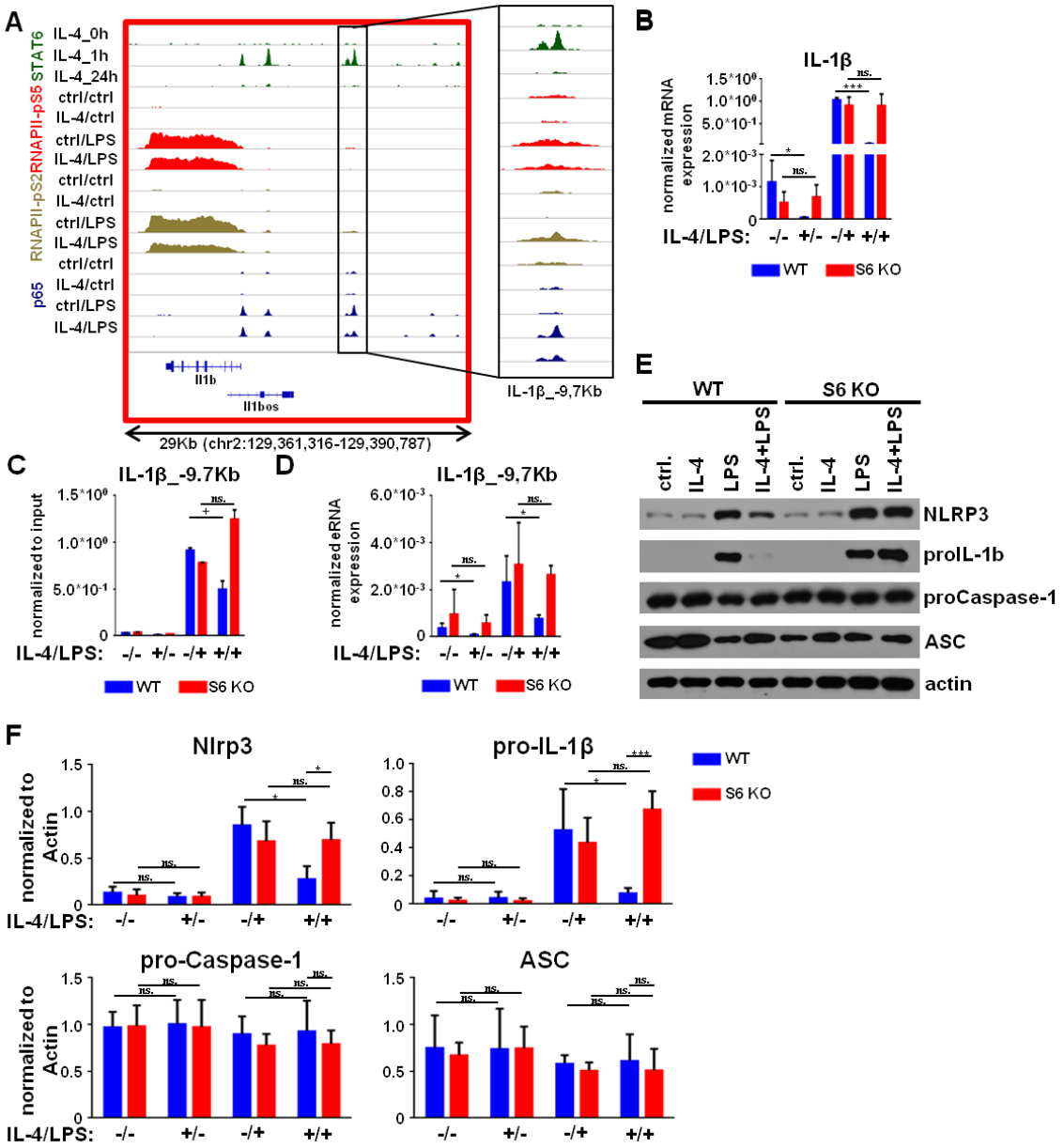

Figure 24. IL-4/STAT6 signaling pathway-dependent repression of inflammatory responsiveness of Nlrp3 and IL-1β at RNA and protein level

(A) Genome browser view of STAT6, RNAPII-pS5, RNAPII-pS2 and p65 specific ChIP-seq signals under the presented treatment conditions on the Il-1b locus. (B) RT-qPCR-based measurement of basal and LPS-induced Il-1b expression in IL-4-pre-treated and unstimulated wild-type (WT) and STAT6-deficient (S6KO) BMDMs. Macrophages were pre-treated with IL-4 for 24 hours or left untreated followed by 3 hours of LPS stimulation. Each data point represents the mean and SD of four individual animals. **P*<0.05, ***P*<0.01, ****P*<0.001, n.s. indicates no significant change. (C) ChIP-qPCR-based measurement of p65 binding at IL-1β_-9.7Kb enhancer from wild-type (WT) and STAT6-deficient (S6KO) BMDMs. Macrophages were pre-treated with IL-4 for 24 hours or left untreated followed by 3 hour of LPS stimulation. Each data point represents the mean and SD of two biological replicates. $^{+}$*P*<0.1, **P*<0.5, n.s. indicates not significant change. (D) RT-qPCR-based measurement of basal and LPS-induced IL-1β_-9.7Kb eRNA expression in IL-4-pre-treated and unstimulated wild-type (WT) and STAT6 deficient (S6KO) bone marrow-derived macrophages. Macrophages were pre-treated with IL-4 for 24 hours or left untreated followed by 3 hours of LPS stimulation. Each data point represents the mean and SD of four individual animals. **P*<0.05, ***P*<0.01, ****P*<0.001, n.s. indicates not significant

change. (E) Western blot-based determination of basal and LPS-regulated Nlrp3, pro-IL-1β, pro-Caspase1, ASC and β-actin expression at protein levels in IL-4-pre-treated and unstimulated wild-type (WT) and STAT6-deficient (STAT6KO) BMDMs. Macrophages were pre-treated with IL-4 for 24 hours or left untreated followed by 3 hours of LPS stimulation. (F) Western blot densitometry analysis of basal and LPS-regulated Nlrp3, pro-IL-1β, pro-Caspase1, ASC and β-actin expression at protein levels in IL-4-pre-treated and unstimulated wild-type (WT) and STAT6 deficient (STAT6KO) mouse bone marrow-derived macrophages. Macrophages were treated with IL-4 and LPS for 24 as well as 3 hours. Each data point represents the mean and SD of five individual animals. *P<0.05, **P<0.01, ***P<0.001, n.s. indicates not significant.

In order to examine whether IL-4-mediated repression of *Nlrp3* expression may result decreased inflammasome activity, we measured the LPS/ATP stimulation-induced Caspase-1 activity in IL-4 pre-treated and unstimulated BMDMs using laser scanning cytometry (Figure 25A).

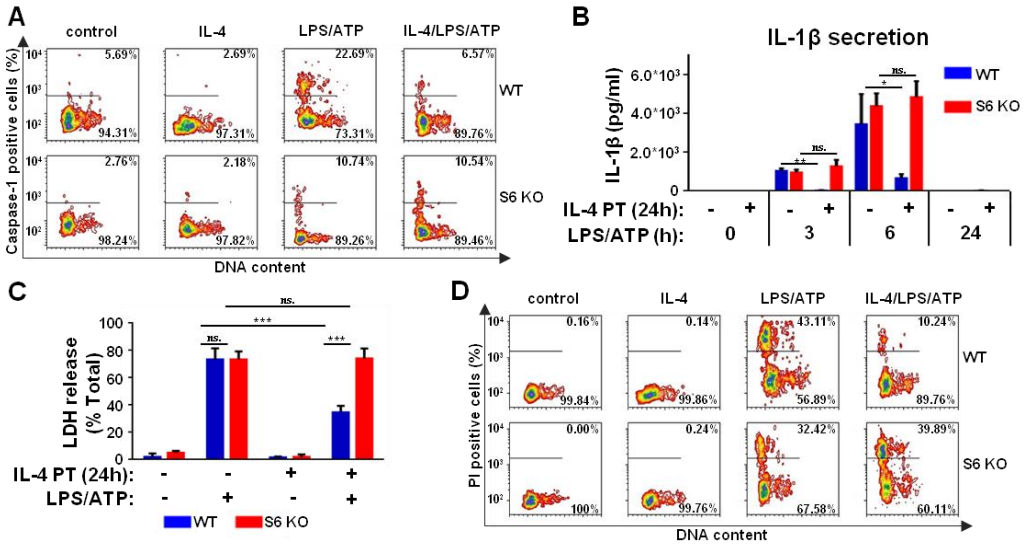

Figure 25. IL-4/STAT6 signaling pathway-repressed inflammasome activation, IL-1β secretion and pyroptotic cell death

(A) Contour map representation of laser-scanning imaging cytometry analysis of Caspase-1 activity in macrophages. Wild-type (WT) and STAT6 deficient (STAT6KO) macrophage were pre-treated with IL-4 for 24 hours or left untreated and LPS stimulation was performed for 3 hours. ATP was added at the last 40 minutes of LPS stimulation. (A representative example of two individual WT and STAT6 KO mice-derived BMDMs is shown.) (B) ELISA-based measurement of IL-1β secretion in IL-4-pre-treated and unstimulated wild-type (WT) and STAT6-deficient (STAT6KO) mouse BMDMs. Macrophages were pre-treated with IL-4 for 24 hours or left untreated and LPS stimulation was performed for 3, 6 and 24 hours. ATP was added in the last 45 minutes of LPS stimulation. Each data point represents the mean and SD of three individual animals. *P<0.05, **P<0.01, ***P<0.001, n.s. indicates no significant change. (C) Lactate dehydrogenase activity assay-based measurement of LPS/ATP co-stimulation-induced LDH release in IL-4-pretreated and unstimulated wild-type (WT) and STAT6-deficient (S6KO) BMDM supernatants. Macrophages were pre-treated with IL-4 for 24 hours or left untreated followed by LPS stimulation for 3 hours. ATP was added for 30 minutes following LPS stimulation. LDH release expressed as the percentage of Triton X-100-liberated total LDH release. Each data point represents the mean and SD of three individual animals. *P<0.05, **P<0.01, ***P<0.001, n.s. indicates no significant change. (D) Contour map representation of laser-scanning imaging cytometry analysis of PI-labelled macrophages. Wild-type (WT) and STAT6-deficient (S6KO) macrophage were pre-treated with IL-4 or

left untreated and LPS stimulation was performed for 3 hours. ATP was added in the last 40 minutes of LPS stimulation. (A representative example of two individual WT and S6KO mice-derived BMDMs are shown.)

As we expected, Caspase-1 activation in wild-type macrophages increased dramatically by LPS/ATP treatment (Figure 25A). In addition, LPS/ATP-induced caspase-1 activity was attenuated significantly following 24 hours of IL-4 pre-treatment, which was completely abolished in the absence of STAT6 (Figure 25A). To evaluate the functional consequence of IL-4/STAT6 signaling pathway-dependent inhibition of inflammasome activation, we measured the LPS and ATP-induced IL-1β secretion in IL-4-pre-treated and untreated wild-type and STAT6 deficient BMDMs. As we expected, IL-1β secretion was induced significantly in wild-type and STAT6 KO macrophages following LPS and ATP treatment (Figure 25B). However, LPS/ATP-dependent induction of IL-1β secretion was partially reduced by IL-4 pre-treatment in a STAT6-dependent manner (Figure 25B). In the next step, we wanted to identfy the role of IL-4/STAT6 signaling pathway in inflammasome activation-induced macrophage cell death, pyroptosis. One of the most typical characteristic of pyroptosis is the insertion of pores into the plasma membrane that can be detected via propidium iodide (PI) staining and LDH activity measurement from macrophage supernatants. IL-4-pretreatment could effectively reduce both LPS-induced LDH release and PI uptake in wild-type but not in STAT6 deficient BMDMs (Figure 25C and D).

Finally, we wanted to investigate whether the inflammatory signals-dependent regulation of Nlrp3 and Il1b genes is modulated *in vivo* by *Heligmosomoides polygyrus* (*H. polygyrus*) infection-induced alternative macrophage activation. Therefore, we injected *Salmonella Typhimurium* or LPS into the peritoneal cavity 9 days after nematode infection. As we expected, the number of the Ym1 positive alternatively activated macrophages was dramatically increased in peritoneal macrophages of *H. polygyrus*-infected mice, confirming alternative macrophage polarization following nematode infection (Figure 26A) [193]. Furthermore, inflammatory marker NOS2 positive macrophage number was highly induced in control and *H. polygyrus*-infected mice following *Salmonella Typhimurium* infection or LPS injection indicating the development of inflammation (Figure 26A). Although Nlrp3 expression was not changed in the used experimental system by LPS injection or *Salmonella* Typhimurium infection, steady-state mRNA level was significantly reduced by *H. polygyrus* infection, and the inhibitory effect of nematode infection was observed in the presence of inflammatory stimuli (Figure 26B). Nematode infection did not influence the basal IL-1β expression in peritoneal macrophages but both LPS injection or *Salmonella Typhimurium* infection induced a robust enhancement in IL-1β mRNA level. This inflammatory signals-induced expression was significantly attenuated in macrophages from *H. polygyrus*-infected mice (Figure 26B).

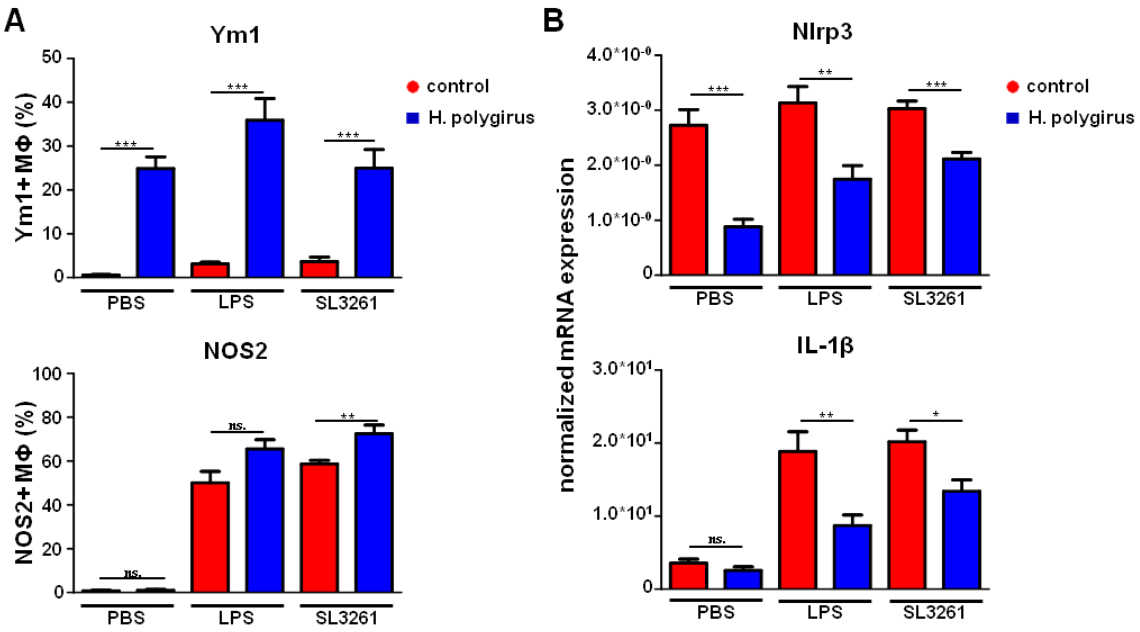

Figure 26. The characterization of inflammatory signals-dependent regulation of Nlrp3 and IL-1β expression in *H. polygyrus*-infected mice-derived *in vivo* alternativre polarized machrophages

(A) The percentage of Ym1 positive and NOS2 positive peritoneal macrophage number in control and *Heligmosomoides polygyrus* (H. polygyrus)-infected mice following PBS and LPS injection as well as *Salmonella* Typhimurium (SL3261)-infection. Each data point represents the mean and SD of four-eleven individual animals. **P*<0.05, ***P*<0.01, ****P*<0.001, n.s. indicates not significant changes. (B) Basal, LPS and *Salmonella* Typhimurium (SL3261)-induced expression of Nlrp3 and Il-1β expression in naïve and *Heligmosomoides polygyrus* (H. polygyrus)-infected mice-derived peritoneal macrophages. Each data point represents the mean and SD of five-six individual animals. **P*<0.05, ***P*<0.01, ****P*<0.001, n.s. indicates no significant change.

Taken together, these findings suggest that prior *in vitro* or *in vivo* alternative macrophage polarization can modulate the subsequent inflammatory response of macrophages, including inflammasome activation, IL-1β secretion as well as pyroptosis through the direct repression of *Nlrp3* and *Il1b* gene expression by IL-4/STAT6 signaling pathway.

6.2. IL-4/STAT6 signaling pathway orchestrates a conserved microRNA signature in human and mouse alternatively polarized macrophages regulating cell survival via miR-342-3p

6.2.1. Identification of the mouse alternatively macrophage polarization-specific miRNA signature

In order to identfy which miRNAs are regulated during mouse alternative macrophage polarization, WT and STAT6 KO mouse BMDMs were differentiated in the presence or the absence of IL-4 then subjected to small RNA-seq analysis. (The differentiation and

activation protocol is shown in Figure 27A). Alternative macrophage polarization of BMDMs was confirmed by FACS- and RT-qPCR-based anayses of known murine alternative macrophage activation markers and by measurement of arginase activity (Figure 27B, C and D).

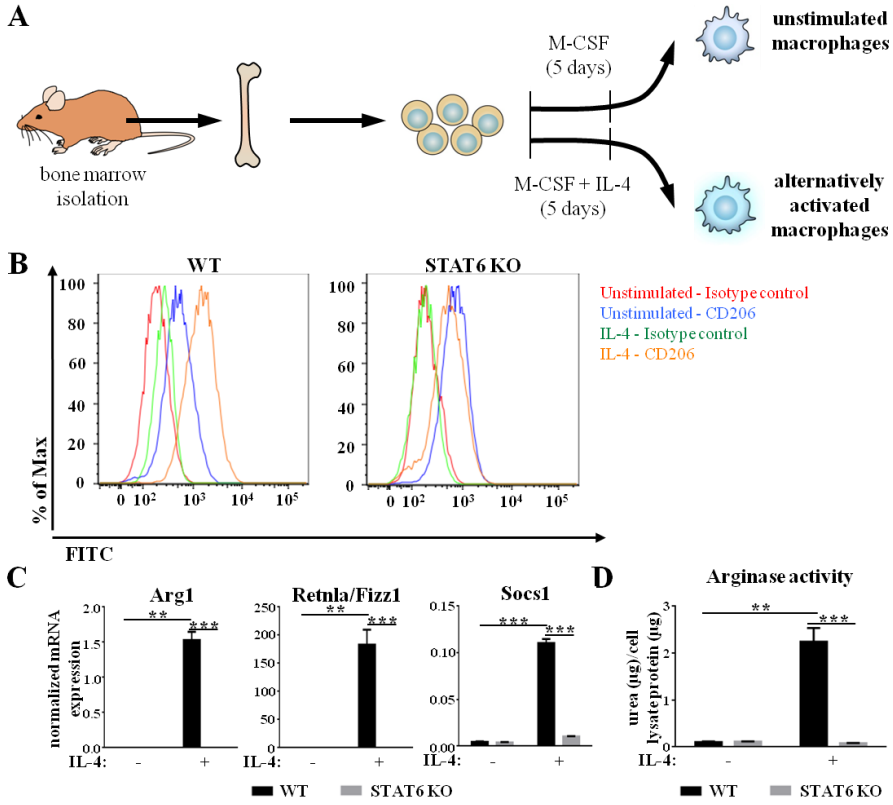

Figure 27. Experimental design and confirmation of alternative macrophage activation in mice (A) Schematic representation of mouse bone marrow isolation and bone marrow-derived macrophage differentiation in the absence or presence of IL-4. (B) Cell surface CD206 expression on IL-4-stimulated or unstimulated WT and STAT6 KO mouse BMDMs. (C) Arg1, Retnla/Fizz1 and Socs1 expression at RNA level in IL-4-stimulated or unstimulated WT and STAT6 KO mouse BMDMs. Each data point represents the mean and SD of three/three (WT/Stat6 KO) individual animals. *P<0.05, **P<0.01, ***P<0.001. (D) Arginase activity in IL-4-stimulated or unstimulated WT and STAT6 KO mouse BMDMs. Each data point represents the mean and SD of three/three (WT/STAT6 KO) individual animals. *P<0.05, **P<0.01, ***P<0.001.

Applying small RNA-seq analysis, we found 162 IL-4-repsonsive miRNAs (76 upregulated and 81 downregulated; FDR<0.1) in alternatively polarized WT macrophages compared to nonpolarized BMDMs (Figure 28A). It is well known that STAT6 transcription factor is a dominant regulator of IL-4-induced transcriptional changes in macrophages [3], we hypothesized that STAT6 might be primarily responsible for the IL-4-mediated miRNA expression changes in BMDMs. In order to investigate the participation of STAT6 in the regulation of the IL-4-responsive miRNAs we compared the IL-4-regulated miRNome between WT and STAT6 KO BMDMs.

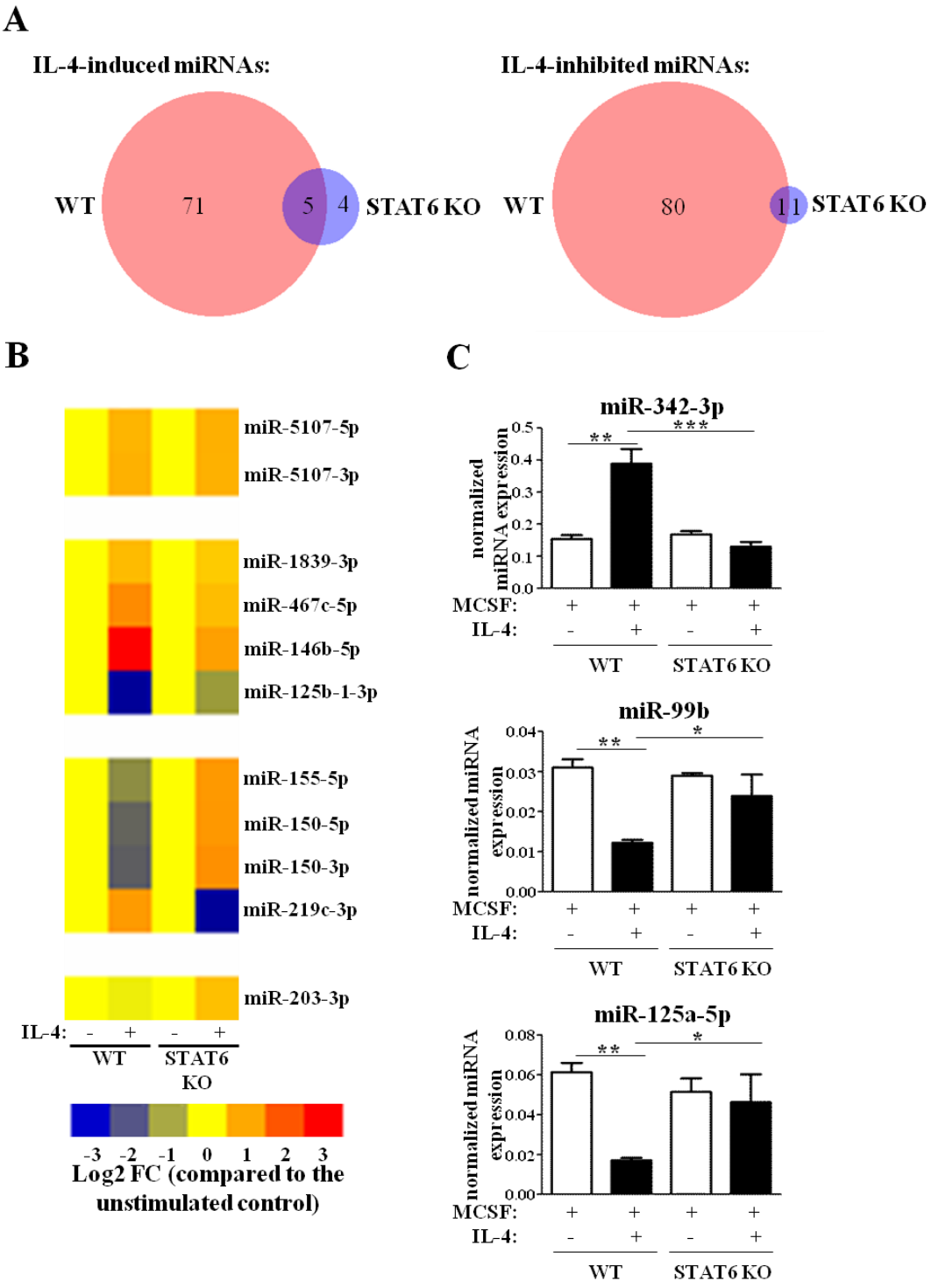

Figure 28. Identification of IL-4/STAT6 signaling pathway-regulated miRNome during in vitro mouse alternative macrophage polarization

(A) Number of miRNAs showing significant (FDR< 0,1) IL-4-dependent regulation in wild-type (WT) and STAT6-deficient (STAT6 KO) macrophages. (B) Heatmap showing average fold changes of IL-4-regulated but STAT6 independent miRNAs in IL-4-stimulated and untreated mouse BMDMs. Colour intensities reflect the fold changes compared to IL-4-stimulated WT to unstimulated WT as well as IL-4-treated STAT6 KO to untreated STAT6 KO macrophages. (C) Stem-loop RT-qPCR-based quantification of miR-342-3p, miR-99b and miR-125a-5p expression in IL-4 stimulated or unstimulated wild-type (WT) and Stat6-deficient (STAT6 KO) mouse bone marrow-derived macrophages. Each data point represents the mean and SD of three individual animals. *P<0.05, **P<0.01, ***P<0.001.

We observed that the majority of the IL-4-responsible miRNAs in WT macrophages were absolutely STAT6-dependent (151 from 157) (Figure 28A). Intriguingly, we only identified 11 miRNAs that showed change in expression following IL-4 exposure in STAT6-deficient BMDMs (Figure 28A and B). We decided to further examine three selected IL-4/STAT6 signaling patway-regulated miRNAs including the IL-4-induced miR-342-3p as well as the IL-4-repressed miR-99b and miR-125a-5p. The miRNA selection was based on the published miRNA-associated functions which might be relevant linked to the alternative macrophage polarization. The IL-4-induced mir-342-3p plays pro-apoptotic and anti-proliferative role in different tumor types raising the possibility that it may act as a potential negative feedback regulator of IL-4-induced macrophage proliferation [190, 253-255]. Furthermore, the selected two IL-4-repressed miRNAs including miR-99b and miR-125a-5p are the members of miR-99b-125a miRNA polycistron and contribute to the control of phenotypic and functional features in macrophages but their role is controversial during the regulation of alternative macrophage polarization [180, 184, 185]. Our stem-loop RT-qPCR-based validation confirmed that the IL-4-mediated upregulation of miR-342-3p and downregulation of miR-99b and miR-125a-5p were completely STAT6-dependent (Figure 28C).

In order to investigate the IL-4-induced miRNA expression changes *in vivo*, we used a filarial nematode infection-based mouse model of alternative macrophage polarization. It was previously described that intraperitoneal implantation of the filarial nematode *Brugia malayi* induces the accumulation of macrophages with alternative macrophage polarization-like characteristics including elevated expression of Ym1, Fizz1/RELM-α and Arg1 [236, 256]. Based on this, we measured miR-342-3p, miR-99b and miR-125a-5p expression in nematode-elicited macrophages at different time points after infection. (The experimental design is shown in Figure 29A). Similarly to our *in vitro* results, miR-342-3p expression was elevated in nematode-elicited macrophages three days after *B. malayi* implantation as compared to naïve cells, and its continuously decreasing kinetics was observed at later time points (Figure 29B). In addition, both miR-99b and miR-125a-5p expression were attenuated during *B. malayi*-induced alternative macrophage activation, also reinforcing our *in vitro* findings (Figure 29B). Collectively, these results indicate that these miRNAs are regulated exclusively via the IL-4/STAT6 signaling pathway during *in vitro* and *in vivo* alternative macrophage activation.

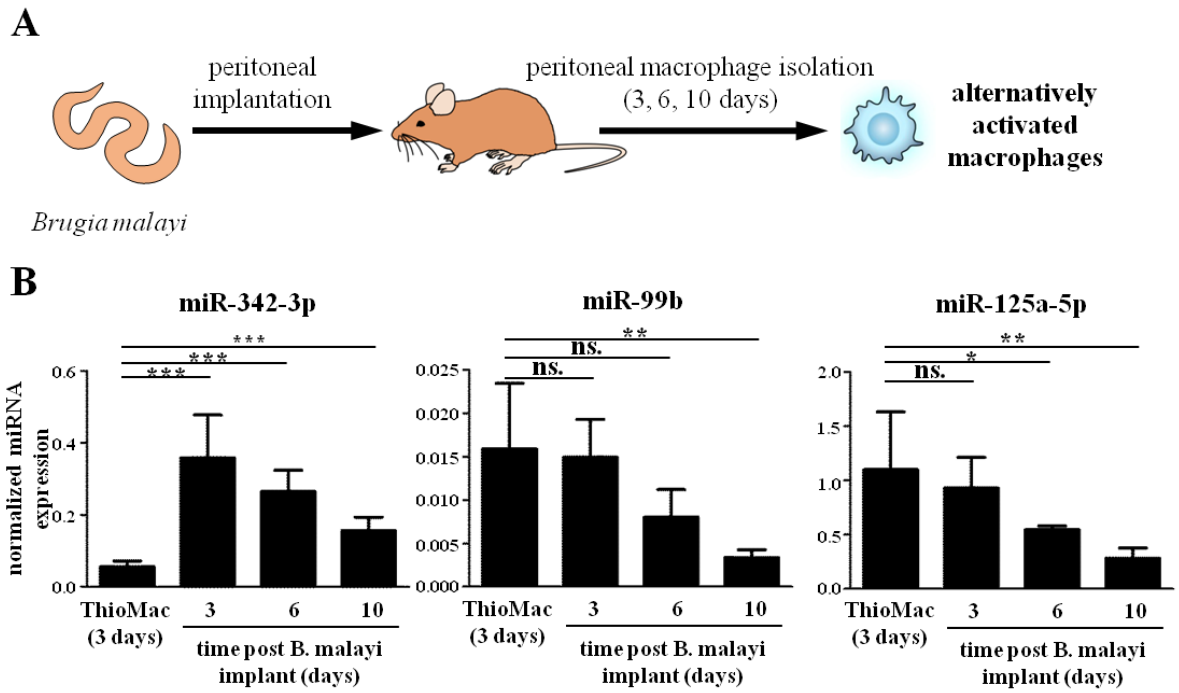

Figure 29. Mir-342-3p, miR-99b and miR-125a-5p expression in Brugia malayi-implanted mice-derived *in vivo* alternatively polarized macrophages

(A) Schematic representation of parasite implantation-induced *in vivo* alternative macrophage activation in mice. (B) Stem-loop RT-qPCR-based quantification of miR-342-3p, miR-99b and miR-125a-5p in mouse thioglycolate-elicited and *in vivo* alternatively activated macrophages. Each data point represents the mean and SD of five individual animals. *P<0.05, **P<0.01, ***P<0.001, n.s. indicates not significant.

6.2.2. Conserved IL-4-dependent regulation of miR-342-3p, miR-99b and miR-125a-5p expression during *in vitro* human alternative macrophage activation

In order to examine the IL-4-dependent regulation of miR-342-3p, miR-99b and miR-125a-5p expression in differentiating human macrophages, $CD14^+$ monocytes were separated from human peripheral blood and exposed to IL-4 for 72 hours then subjected to stem-loop RT-qPCR analysis (The experimental design is shown in Figure 30A).

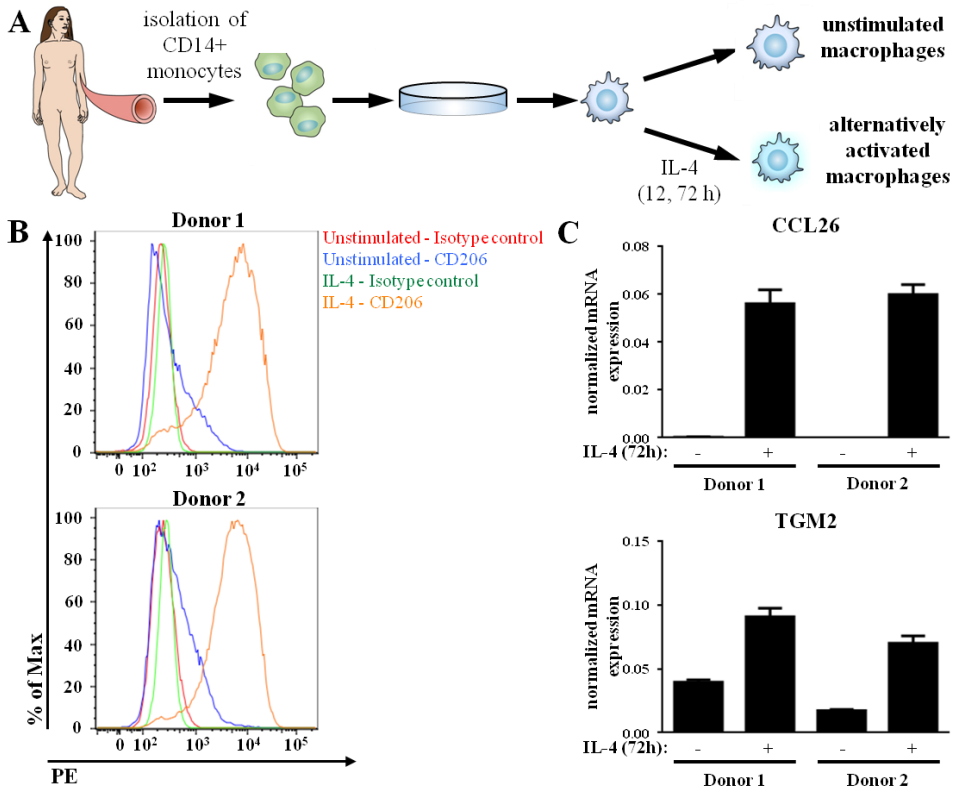

Figure 30. Experimental design and confirmation of alternative macrophage activation in human (A) Schematic representation of human CD14+ monocyte isolation from peripheral blood and the experimental conditions of macrophage differentiation as well as alternative macrophage activation. (B) Cell surface CD206 expression on two independent human donor-derived 72 hours nontreated and IL-4-stimulated macrophages. (C) CCL26 and TGM2 expression at mRNA level in two independent human donor-derived 72 hours nontreated and IL-4-stimulated macrophages. Error bars indicate the standard deviation (SD) of the three technical replicates.

The IL-4-dependent induction of human alternative macrophage polarization markers was confirmed by RT-qPCR and FACS analyses in human macrophages (Figure 30B and C).

Our results from four independent human donors indicated that the expression of miR-342-3p was not changed during monocyte-to-macrophage transition while induced dramatically in response to IL-4 (Figure 31).

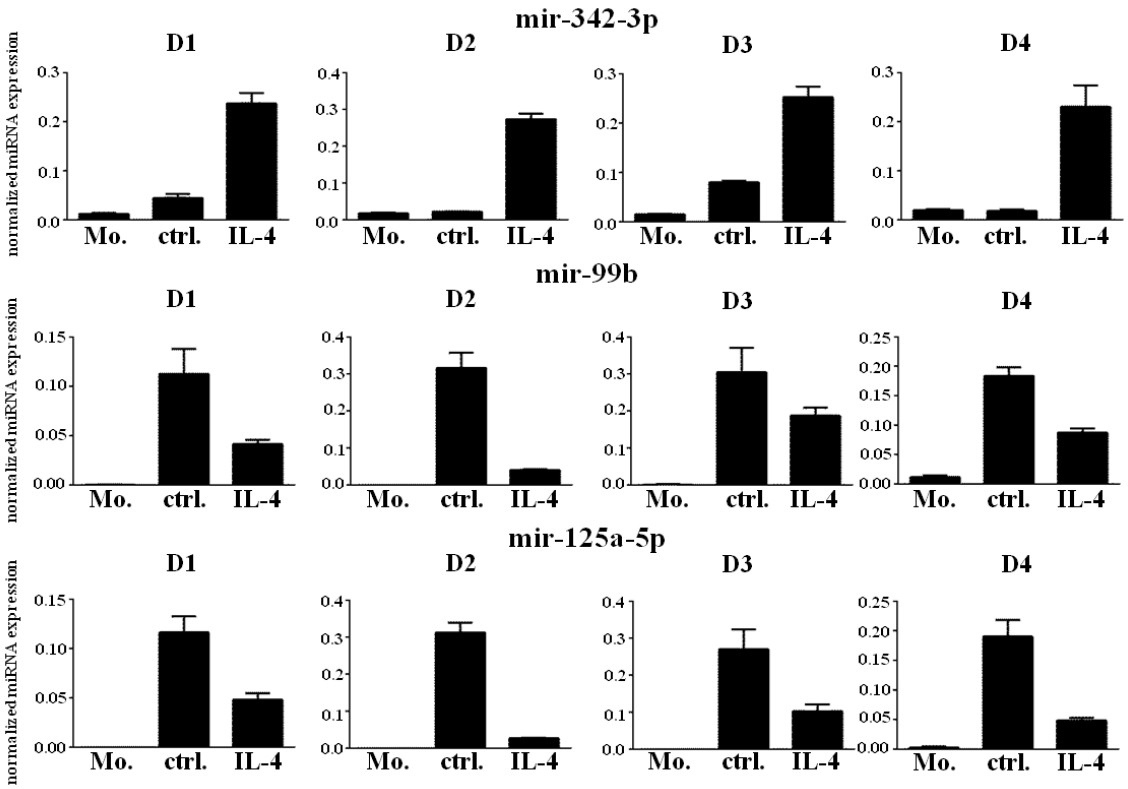

Figure 31. IL-4-dependent regulation of miR-342-3p, miR-99b and miR-125a-5p expression during *in vitro* human alternative macrophage polarization

MiR-342-3p, miR-193b, miR-99b and miR-125a-5p expression in four (D1-D4) independent human donor-derived monocytes, 72 hours nontreated and IL-4 stimulated macrophages. Error bars indicate the standard deviation (SD) of the three technical replicates.

In contrast, miR-99b and miR-125a-5p were induced significantly during monocyte-macrophage differentiation (Figure 31). However, the monocyte-macrophage transition-induced miR-99b and miR-125a-5p expressions were attenuated in all four human donors by IL-4 (Figure 31). Taken together, these findings suggest that the IL-4-dependent regulation of miR-342-3p, miR-99b and miR-125a-5p expression is conserved in mice and humans.

6.2.3. Direct Stat6-dependent induction of miR-342-3p and its host gene EVL during alternative activation of murine and human macrophages

It was previously described that miR-342-3p is located within the third intron of the EVL gene in humans and mice, and their expressions showed coordinated regulation in different tumor types [257, 258]. Thus, we decided to further examine the potential regulatory mechanism controlling the expression of EVL and miR-342-3p during human and mouse alternative macrophage polarization.

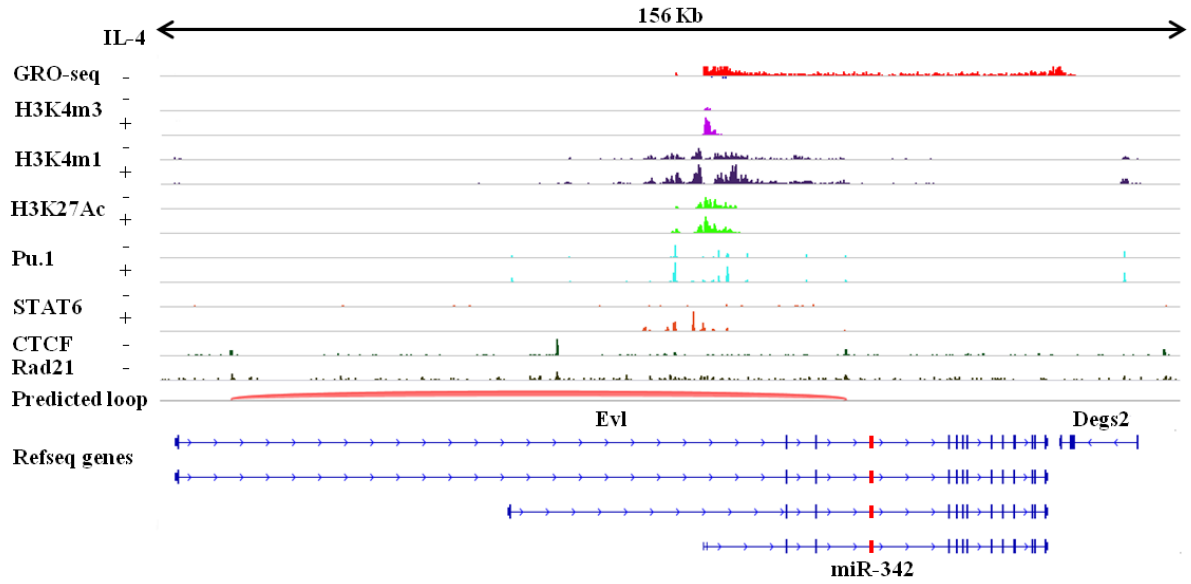

Figure 32. Nascent RNA expression, post-translational histone modification enrichment and transcription factor/cofactor binding at the genomic locus of mouse Evl/miR-342

Strand-specific GRO-Seq, CTCF and Rad21-specific ChIP-seq signals in unstimulated as well as H3K4m3, H3K4m1, H3K27Ac, Pu.1 and Stat6 ChIP-Seq signals in IL-4-stimulated and unstimulated mouse macrophages at the EVL locus visualized by the Integrative Genomics Viewer.

Therefore, we analyzed publicly available GRO-seq from unstimulated and ChIP-seq datasets from both IL-4-exposed and unstimulated mouse BMDMs [97, 108]. The analysis of transcription of nascent RNA (GRO-seq) and the location of active TSS-mark H3K4m3 (ChIP-seq) data indicated that the shortest known transcript variant of *Evl* (NM_001163396) was expressed in resting mouse macrophages (Figure 32). In addition, H3K4m3 enrichment was increased at the TSS of *Evl* in IL-4-stimulated BMDMs compared to unstimulated cells (Figure 32). Interestingly, H3K4m3 enrichment was not detected in the intronic region of Evl around the miR-342-3p coding region indicating that Evl and miR-342-3p utilized the common TSS in resting and alternatively polarized mouse BMDMs (Figure 32).

To further study the IL-4-mediated control of miR-342-3p and Evl expression in mice, we measured both mature miRNA and its host gene expression in mouse bone-marrow cells as well as in IL-4-exposed and unstimulated BMDMs. Both Evl and miR-342-3p expression level were elevated during mouse BMDM differentiation that was further enhanced by IL-4 in a STAT6-dependent manner (Figure 33A and B). In addition, we investigated the macrophage-specific LDTF Pu.1 and IL-4-activated STAT6 binding at the EVL-associated subTAD (Figure 32).

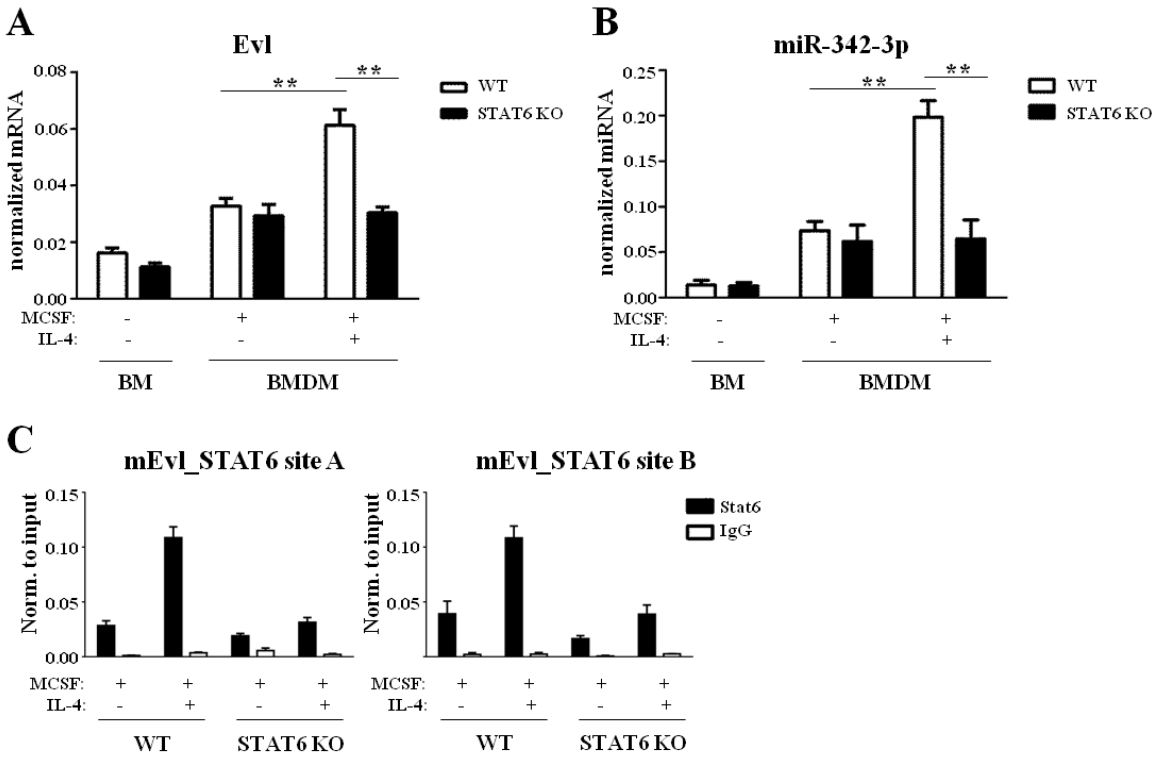

Figure 33. Direct IL-4/STAT6 signaling pathway-dependent regulation of EVL and miR-342-3p expression in mouse BMDMs

(A) RT-qPCR-based measurement of Evl expression in bone marrow cells and IL-4 stimulated or unstimulated bone marrow-derived macrophages in wild-type (WT) or Stat6-deficient (STAT6 KO) mice. Each data point represents the mean and SD of three individual animals. ***P*<0.01. (B) Stem-loop RT-qPCR-based quantification of miR-342-3p expression in bone marrow cells and IL-4 stimulated or unstimulated bone marrow-derived macrophages in wild type (WT) or Stat6-deficient (STAT6 KO) mice. Each data point represents the mean and SD of three individual animals. ***P*<0.01. (C) IL-4-induced Stat6 binding of two regulatory regions of the mouse EVL gene in wild-type (WT) and Stat6-defficient (STAT6 KO) mouse macrophages measured by ChIP-qPCR. Columns represent mean arbitrary units described in the Methods section ±SD.

Although, Pu.1-bound genomic sites were observed within the predicted subTAD in both unstimulated and IL-4-treated BMDMs but Pu.1 binding was not modulated by IL-4 stimulation (Figure 32). Moreover, IL-4-induced Stat6 binding was detected at both upstream and downstream genomic regions from the TSS of the Evl gene [108] (Figure 32). Next, we validated two Stat6-bound distal regulatory regions -4 Kb (mEvl_Stat6 site A) and +4 Kb (mEVL_Stat6 site B) from the TSS. ChIP-qPCR results indicated an IL-4-induced enrichment of Stat6 binding at these regions in WT macrophages relative to untreated WT and IL-4-exposed STAT6-deficient BMDMs as well as IgG controls (Figure 33C).

In order to investigate whether IL-4-induced co-regulation of EVL and miR-342-3p is conserved between human and mouse, we examined their expression in human monocyte-derived unstimulated and IL-4-exposed differentiating macrophages at different time points. Intriguingly, IL-4-induced EVL expression was already observed in all three donors after 12 hours but it was reduced at later time points (Figure 34A).

The expression of miR-342-3p followed similar but delayed kinetics in IL-4-treated human differentiating macrophages, its elevated expression was only observed after 24 hours (Figure 34B). In order to identify whether STAT6 binding is detectable at the genomic locus of human EVL, we used publicly available human STAT6 ChIP-seq datasets from IL-4 stimulated Th2-type T-cells [259]. Interestingly, STAT6 binding was detected +0.3 Kb from the TSS of the EVL gene in these cells. Therefore, we hypothesized that this region might also be bound by STAT6 in IL-4-treated human differentiating macrophages. We could confirm our hypothesis by ChIP-qPCR in two independent human donors (D1 and D2) (Figure 34C). These results suggest that miR-342-3p and its host gene EVL are coordinately regulated by IL-4 via direct DNA binding of STAT6 in both mouse and human macrophages.

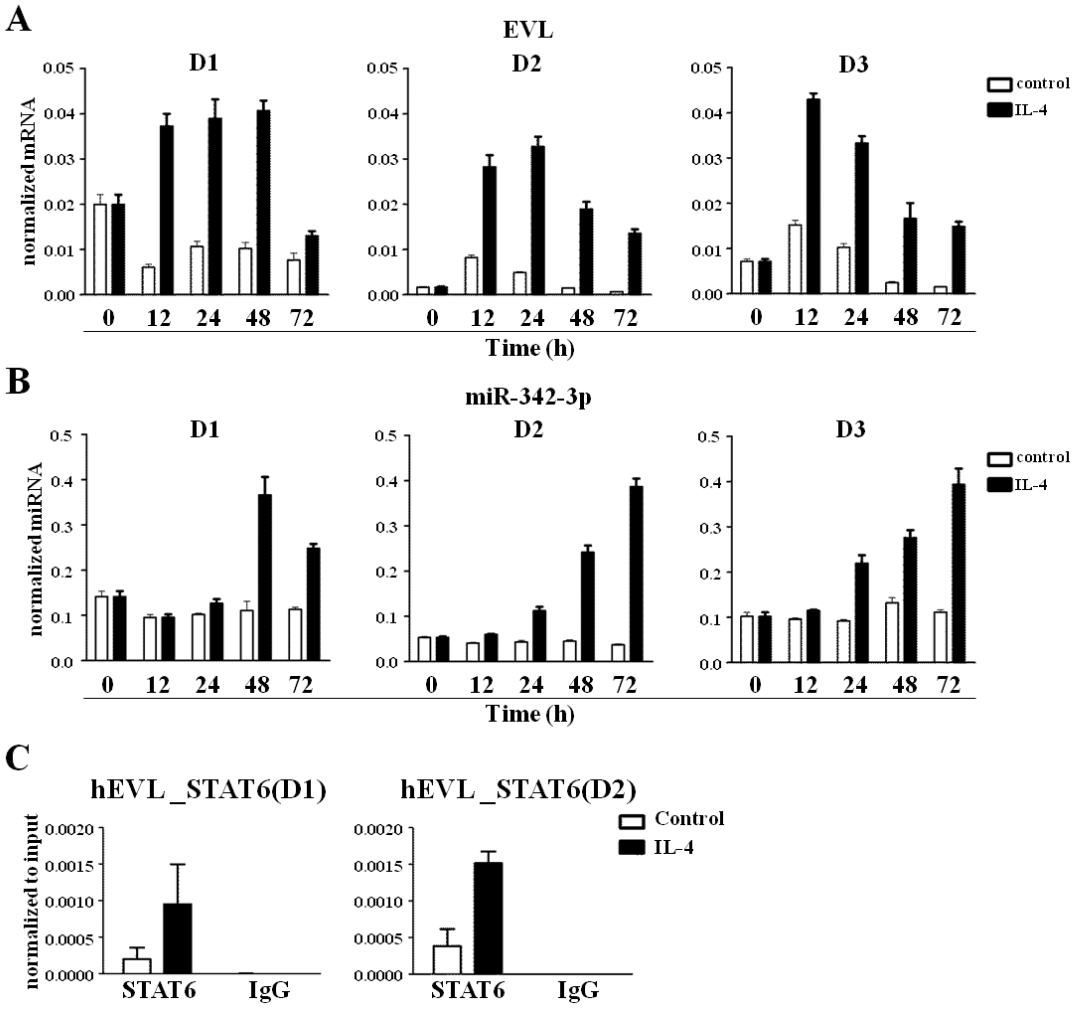

Figure 34. Direct IL-4/STAT6 signaling pathway-dependent regulation of EVL and miR-342-3p expression in human macrophages

(A) RT-qPCR-based measurement of EVL expression during human macrophage differentiation in the absence or presence of IL-4. (B) Stem-loop RT-qPCR-based quantification of miR-342-3p expression during human macrophage differentiation in the absence or presence of IL-4. (C) IL-4-induced recruitment of STAT6 to the EVL locus in macrophages obtained from two independent human donors (D1, D2) measured by ChIP-qPCR. Data are expressed as mean ±SD.

6.2.4. MiR-342-3p regulates cell proliferation and apoptosis-associated signaling pathways at the post- transcriptional level in macrophages

In order to study the miR-342-3p-regulated molecular pathways, we investigated the global transcriptome of miR-342-3p-transfected RAW264.7 macrophages using microarray analysis and identified a set of repressed miR-342-3p direct target genes with computational and biochemical approaches. (The flowchart of experimental approaches is shown in Figure 35.*)* Based on the microarray analysis, 2640 downregulated and 2341 upregulated genes (FDR<0.1) were identified in mi-342-3p overexpressing macrophages compared to negative-control-transfected cells (Figure 35).

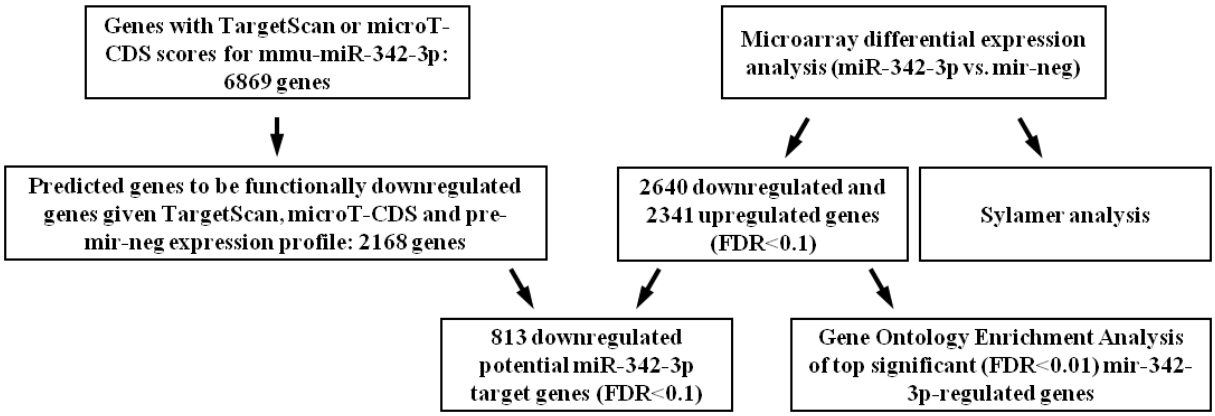

Figure 35 Schematic representation of combined microarray-based and computational miR-342-3p target gene identification

To identify the miR-342-3p-regulated biological processes, we analyzed the list of most significantly regulated genes (FDR≤0.01) applying the ClueGO Cytoscape plugin [260]. We found cellular metabolism and regulation of viable cell number including cell proliferation and cell death as the most significantly overrepresented miR-342-3p-regulated GO categories (Figure 36A). Furthermore, Sylamer analysis of miR-342-3p and miR-negative control-transfected cells-derived microarrays indicated that the complementary sequence of the 8mer seed region of miR-342-3p was enriched within the 3'UTR of downregulated genes in miR-342-3p-transfected cells, showing the specificity of the miR-342-3p-induced transcriptomic changes (Figure 36B). For the investigation of functionally relevant miRNA:mRNA interactions we applyed TargetExpress method [224] which combines TargetScan [225] and microT-CDS [226] target prediction algorthms with the gene expression profile of the negative control condition. The resulting predicted miR-342-3p targets showed the best correlation with miR-342-3p-dependent repression of gene expression in our experimental system (Figure 36C). 813 predicted miR-342-3p target genes were significantly repressed in pre-miR-342-3p-transfected cells (Figure 35). These results raise the possibility, that these genes are repressed directly in this experimental system by miR-342-3p. However, further experimental verification is necessary for the demonstration of direct miR-342-3p-dependent repression.

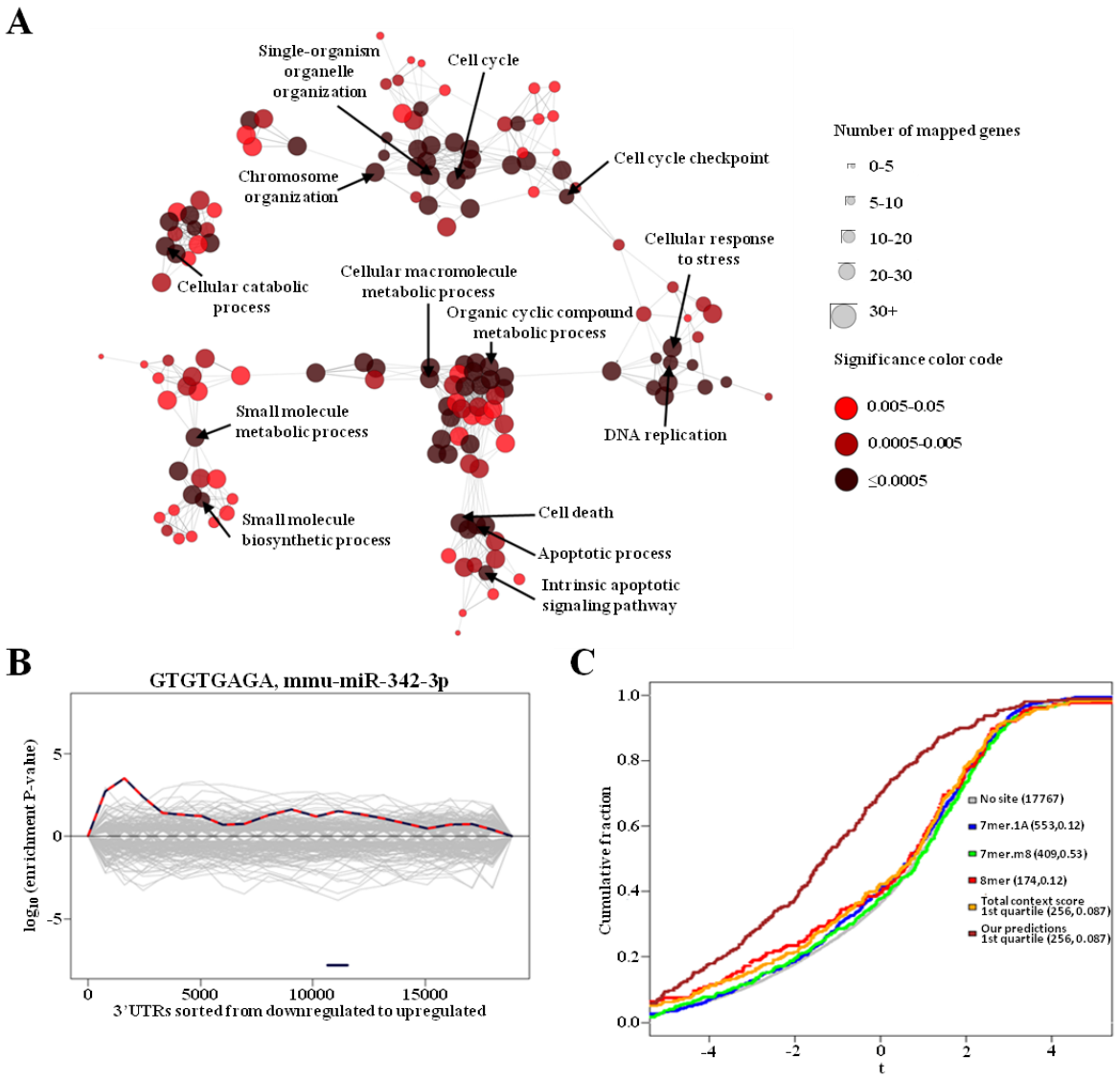

Figure 36. The *in silico* analysis-based miR-342-3p target gene identification

(A) Network visualization of Gene Ontology Enrichment Analysis of genes differentially expressed in miR-342-3p-transfected RAW264.7 mouse macrophages (FDR≤0.01) using ClueGO Cytoscape plugin. Nodes represent enriched Gene Ontology Biological Process terms, node colors represent corresponding FDR values (Benjamini-Hochberg method), node sizes represent the number of genes associated with the GO term. Only the label of the most significant term per group is shown. Nodes without second degree connections are omitted for clarity. (B) Sylamer analysis revealed that only *miR-342-3p 8-mer s*eed matches were enriched among downregulated genes in miR-342-3p-transfected macrophages compared to mir-negative control-treated cells. *MiR-342-3p* and murine microRNA seed matches are represented as red dashed and gray lines, respectively. (C) Cumulative distributions of relative change (t statistic) for different sets of potential miR-342-3p target genes: with 7mer.1A (blue), 7mer.m8 (green), 8mer (red) seeds, or the top 1000 TargetScan (Total context+, orange) or microT-CDS (miTG, purple) and TargetExpress (brown) predictions to be functionally down-regulated. Set size and statistical significance of each set being more repressed than genes with no potential target site are shown in brackets.

6.2.5. MiR-342-3p acts as a regulator of macrophage cell number via reduction of cell viability and induction of apoptosis

Our microarray analysis indicated that cellular proliferation and cell death may be regulated in macrophages by miR-342-3p. It has been previously demonstrated that proliferation of local macrophage population is induced by IL-4-mediated Th2-type inflammation [190]. Furthermore, it has also been described that miR-342-3p was aberrantly downregulated in different tumor types including colorectal and breast cancers [253, 257]. Finally, overexpression of miR-342-3p was able to induce apoptosis and block cancer cell proliferation [255, 257]. Therefore, we hypothesized that IL-4/STAT6 signaling pathway-induced miR-342-3p expression could be a member of the potential negative feedback mechanism controlling macrophage proliferation upon Th2-type cytokine stimulus.

In order to test this hypothesis we examined the functional effects of miR-342-3p on macrophage proliferation and/or apoptosis in RAW264.7 cells transfected with miR-342-3p or miR-negative control miRNA mimics. Macrophage numbers were determined at various time points following miRNA mimic transfection by propidium iodide staining of permeabilized adherent cells [230]. Overexpression of miR-342-3p induced the 40 and more than 80 percent reduction in the macrophage number at 24 and 48 hours post-transfection, respectively, as compared to the miR-negative control-transfected cells (Figure 37A).

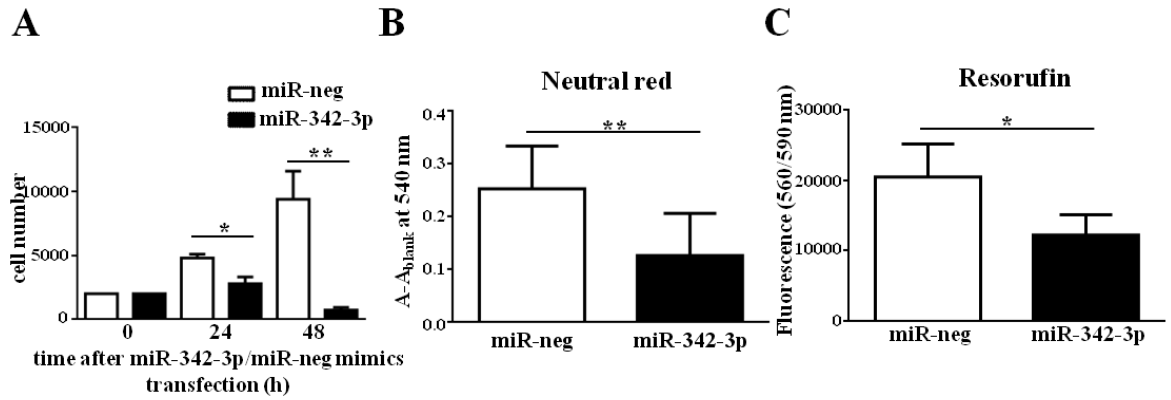

Figure 37. Reduced macrophage viability by miR-342-3p overexpression

(A) PI staining-based cell number analysis of RAW264.7 cells at different time points following miR-342-3p mimic transfection. Each data point represents the mean and SEM of five parallel samples from two independent experiments. *P<0.05, **P<0.01 (B) Neutral red-based cell viability analysis of miR negative control (miR-neg) and miR-342-3p (miR-342-3p) mimics-transfected RAW264.7 cells 48h after miRNA mimics transfection. Each data point represents the mean and SEM of four independent experiments. *P<0.05. (C) Resorufin-based cell viability analysis of miR negative control (miR-neg) and miR-342-3p (miR-342-3p) mimics-transfected RAW264.7 cells 48h after miRNA mimics transfection. Each data point represents the mean and SEM of four independent experiments. *P<0.05.

Next, we wanted to confirm our results with independent methods including resazurin reduction and neutral red uptake-based *in vitro* cell viability assays [231]. The miR-

342-3p overexpression was able to reduce viable macrophage numbers by 40 and 55% at 48 hours following the transfection in the resazurin and neutral red uptake assays, respectively (Figure 37B and C). In order to investigate whether the decreased viable cell number is the result of impaired progression of the cells through the cell cycle or the consequence of increased cellular death, we performed cell cycle analysis by PI staining and a necrosis/apoptosis assay by Annexin V/PI double-staining of the miR-342-3p and miR-negative control mimics-transfected RAW264.7 macrophages. The Hoechst staining and slide-based imaging cytometry-based analysis revealed that miR-342-3p overexpression caused a slight but not significant increase in the number of cells in S-phase (Figure 38A).

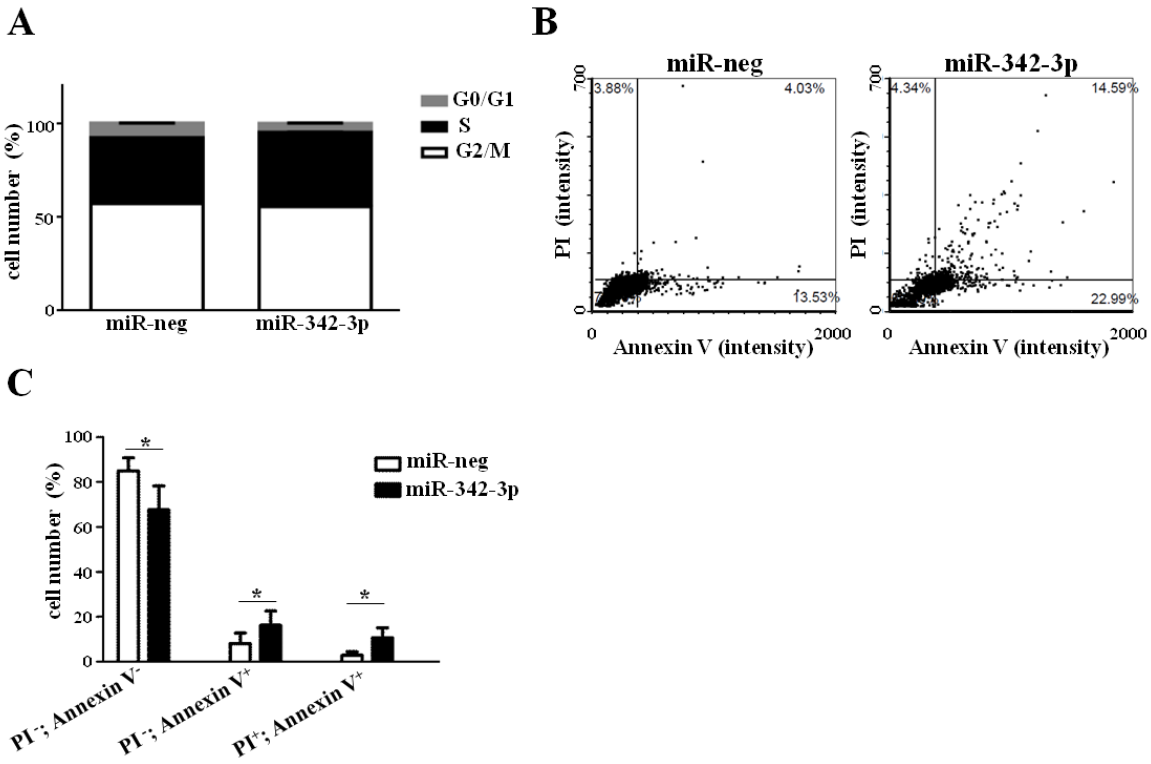

Figure 38. Mir-342-3p overexpression-induced apoptosis by miR-342-3p in macrophages

(A) Effect of miR-342-3p on cell cycle progression in RAW264.7 cells. Cell cycle distribution was evaluated by slide-based imaging cytometry after PI staining. Each data point represents the mean and SD of three independent experiments. *P<0.05. (B) Representative dot plots of laser-scanning imaging cytometry analysis of Annexin V and PI labelled miR negative control (miR-neg) and miR-342-3p (miR-342-3p) mimics-transfected RAW264.7 cells 48h after miRNA mimics transfection. (C) Viable (PI-, Annexin V-), early apoptotic (PI-, Annexin V+) and late apoptotic (PI+, Annexin V+) cell distribution 48h following miR-negative control (miR-neg) and miR-342-3p (miR-342-3p) mimics transfection into RAW264.7 cells. Each data point represents the mean and SD of three independent experiments. *P<0.05.

In contrast, miR-342-3p overexpression significantly enhanced the number of both Annexin V positive/PI negative early (Figure 38B, lower right quadrants) and Annexin V/PI double positive late (Figure 38B, upper right quadrants) apoptotic cells (Figure

38B and C). These results suggest that miR-342-3p regulates macrophage cell numbers via induction of apoptosis.

Interestingly, the negative regulators of apoptosis Gene Ontology (GO) category (GO:0043066) involved 23 genes from the downregulated potential miR-342-3p target genes (Figure 39A). We applied GeneMANIA to identify the potential interactions between the miR-342-3p-attenuated anti-apoptotic genes and found that 19 out of 23 potential miR-342-3p target genes formed an anti-apoptotic gene network indicating extensive predicted interactions and colocalization [261] (Figure 39B). To identify the direct miRNA:mRNA interactions we selected Bcl2l1 as one of the central members of the miR-342-3p-regulated anti-apoptotic gene network for additional analysis. *In silico* target prediction analysis using TargetScan algorithm showed two predicted mir-342-3p binding sites within the 3'UTR of Bcl2l1 (Figure39C, miR-342-3p_I and miR-342-3p_II) [262]. We created luciferase expression constructs with the predicted miR-342-3p binding sites-containing 3'UTR regions of Bcl2l1 or their 9 nucleotides lenght deletion-containing mutated versions (Figure 39C). We transfected these constructs with miR-342-3p or miRNA negative-control mimics into HEK293T cells. Small but statistically significant repression of luciferase activity was detected in miR-342-3p_I binding site-containing construct-transfected cells in the presence of miR-342-3p mimic compared to miR-negative control (Figure 39C). MiR-342-3p mimic-induced reduction of luciferase activity was completely diminished when miR-342-3p_I-binding site was deleted (Figure 38C). In contrast, luciferase activity of the construct containing the miR-342-3p_II binding site was not affected significantly by miR-342-3p mimic transfection. Collectively, our *in silico* and experimental analyses suggest the miR-342-3p-dependent direct repression of Bcl2l1 expression.

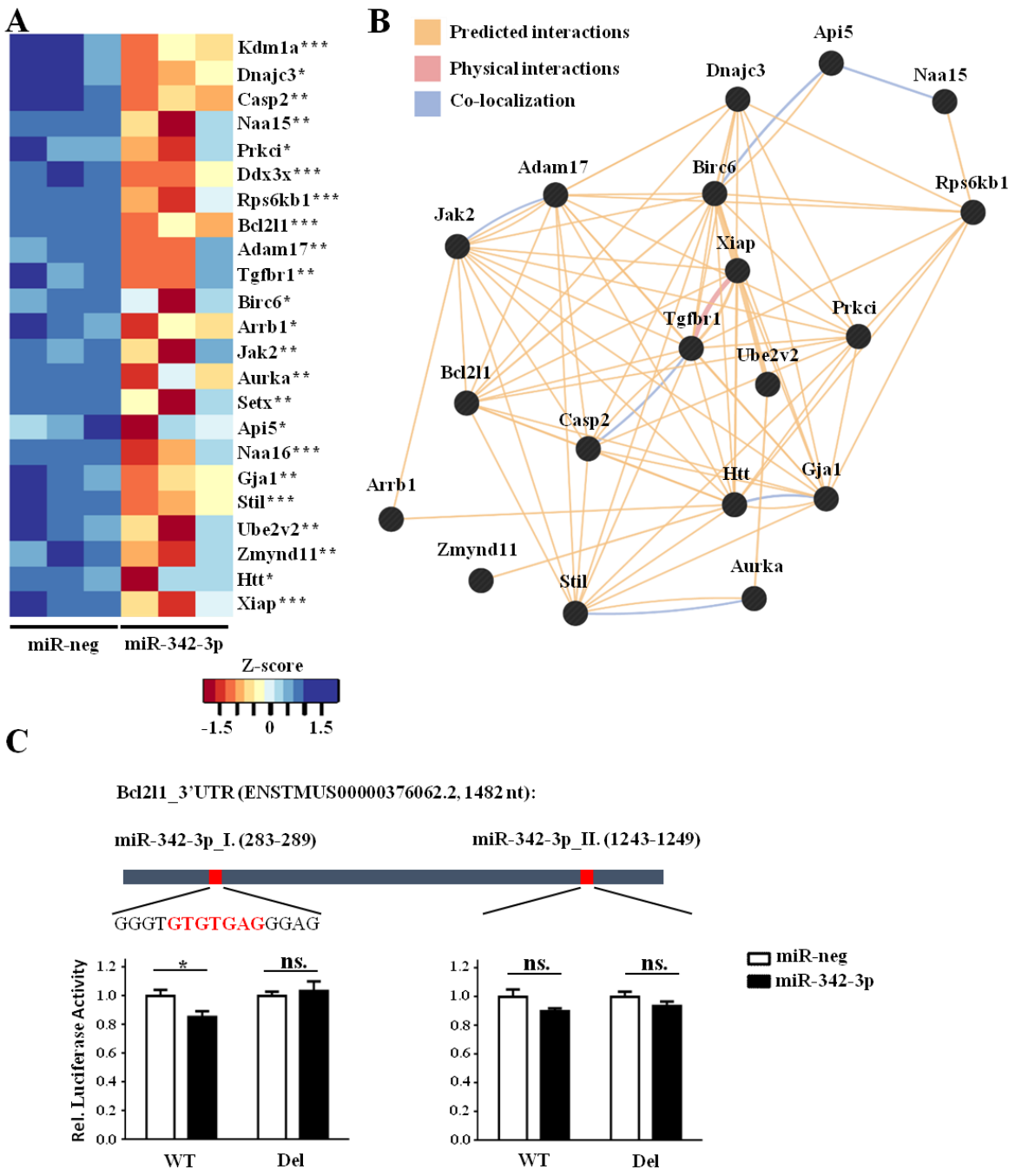

Figure 39. MiR-342-3p-repressed anti-apoptotic gene network in macrophages

(A) Relative expression heatmap of selected potential anti-apoptotic miR-342-3p target genes expression in miR-negative control (pre-miR-neg) and miR-342-3p overexpressing RAW264.7 cells 18h after miRNA mimics transfection in three independent experiments (significance of repression is indicated after the gene name: *FDR<=0.1, **FDR<=0.05, ***FDR<=0.01). (B) GeneMANIA-based identification of miR-342-3p-repressed, anti-apoptoic gene network. (C) Luciferase activity in HEK293T cells cotransfected with luciferase expression constructs containing WT/mutated(Del) miR-342-3p binding sites of Bcl2l1 and miR-342-3p/miRNA negative-control mimics (n=6). *P<0.05.

6.3. Dynamic transcriptional control of macrophage miRNA signature via inflammation responsive enhancers revealed using a combination of next generation sequencing-based approaches

6.3.1. Characterization of the transcriptional basis of inflammation responsive miRNA signature in macrophages

In order to investigate which macrophage-expressed miRNAs are regulated by inflammatory stimuli, we stimulated mouse BMDMs with LPS for 3 hours and performed small RNA sequencing (small RNA seq). We found that 261 miRNAs were expressed in unstimulated BMDMs (data not shown) and 17 miRNAs were regulated significantly different by LPS (p-value<0.05 and FDR<0.1; 4 downregulated and 13 upregulated; Table 5).

	miRNA	logFC	PValue	FDR
LPS-activated miRNAs	**mmu-miR-155-3p**	6,799093	7,99E-160	2,05E-157
	mmu-miR-125a-3p	2,160694	7,28E-25	9,36E-23
	mmu-miR-146a-3p	2,434241	6,31E-23	5,41E-21
	mmu-let-7e-3p	1,898633	8,11E-16	5,21E-14
	mmu-miR-222-5p	1,807565	2,82E-15	1,45E-13
	mmu-miR-221-5p	0,946709	5,64E-15	2,42E-13
	mmu-miR-155-5p	2,759894	5,64E-11	1,81E-09
	mmu-miR-210-5p	0,575059	2,99E-05	0,000769
	mmu-miR-222-3p	0,529486	0,0001	0,002269
	mmu-miR-21a-3p	0,79779	0,000308	0,005923
	mmu-let-7i-3p	0,815987	0,000323	0,005923
	mmu-miR-147-3p	1,550421	0,000393	0,006728
LPS-repressed miRNAs	**mmu-miR-27a-5p**	-1,84618	1,30E-13	4,78E-12
	mmu-miR-223-5p	-0,83427	4,74E-06	0,000135
	mmu-miR-26b-3p	-0,63833	0,000106	0,002269
	mmu-miR-30c-1-3p	-0,77286	0,002015	0,030461

Table 5. List of the LPS-regulated mature miRNAs in mouse BMDMs

To identify the potential regulatory mechanisms controlling LPS-responsive miRNA expression, we investigated the pri-miRNA transcripts using the combination of publicly available GRO-seq and active promoter mark H3K4m3-specific ChIP-seq datasets from control and LPS-exposed BMDMs [108, 118]. We found 518 sense nascent RNA transcripts overlapping with 568 miRNA-coding genomic regions in the absence and/or presence of LPS stimulus (data not shown). 12 identified nascent RNA transcripts were overlapped with the genes of 17 LPS-regulated miRNAs (data not shown).

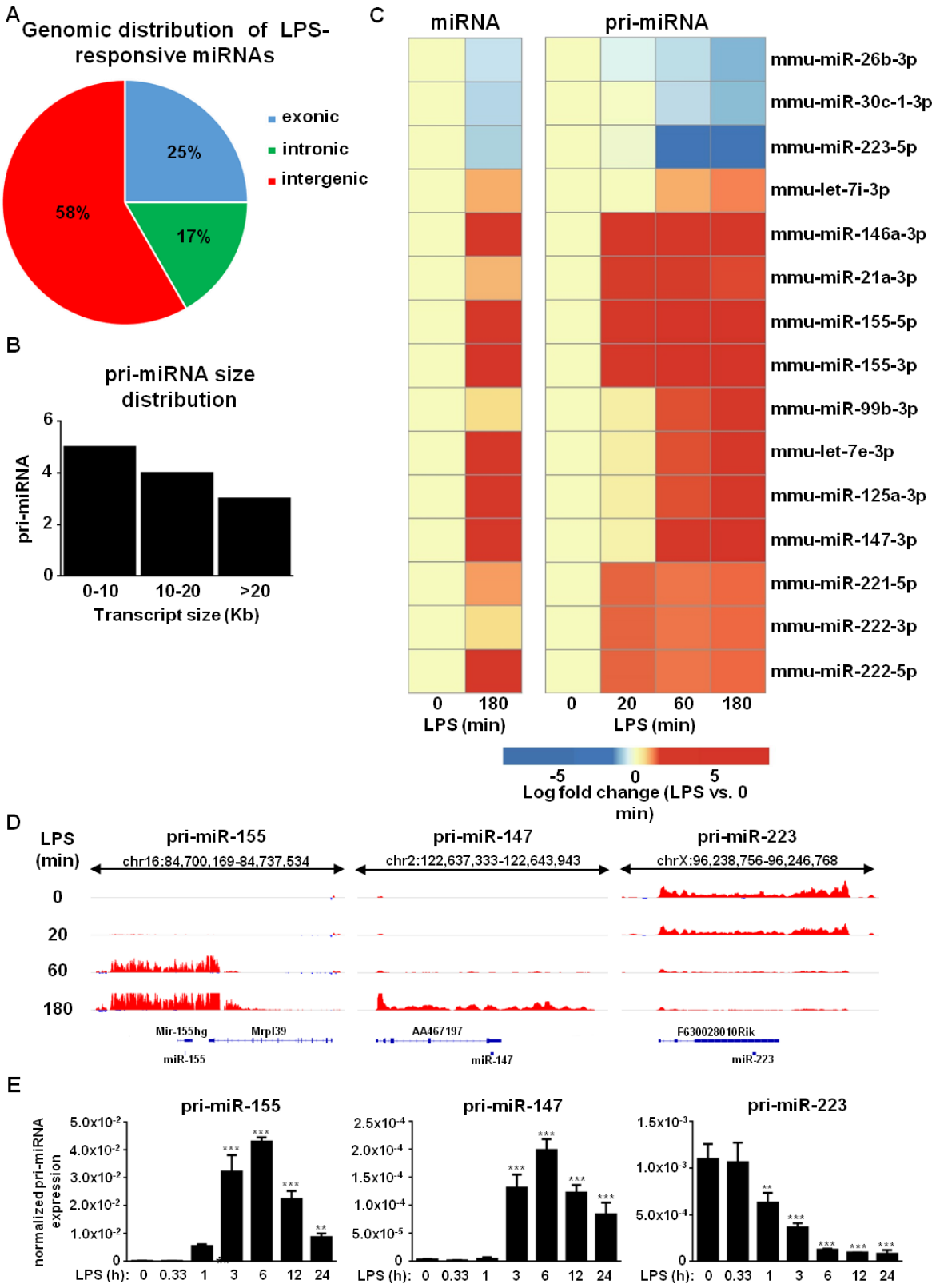

Figure 40. Identification of transcriptionally regulated miRNAs in LPS-stimulated mouse BMDMs

(A) The ratio of transcribed intergenic, intronic and exonic LPS responsive miRNAs. (B) Primary transcript size distribution of LPS-regulated miRNAs. (C) Heat map showing fold changes of transcriptionally regulated miRNA expression at mature (left panel) and pri-miRNA (right panel) levels in LPS-stimulated macrophages compared with unstimulated control. (D) Genome browser view of

GRO-seq data showing the primary RNA transcripts of selected LPS-regulated miRNAs in unstimulated and LPS-stimulated mouse macrophages. Macrophages were treated with LPS for 20, 60 and 180 minutes. (E) RT-qPCR-based validation of pri-miRNA expression in LPS-stimulated and unstimulated macrophages. Macrophages were treated with LPS for 20 minutes as well as 1, 3, 6, 12 and 24 hours. Each data point represents the mean and SD of three biological replicates. *P<0.05, **P<0.01, ***P<0.001 compared with the unstimulated control marked as 0.

Next, we determined the genomic location and primary transcript size of LPS-regulated miRNAs. 58% of them were intergenic, while 25% and 17% showed exonic and intronic location, respectively (Figure 40A). The length distribution of primary-miRNA transcripts was very diverse (ranging from 5,6 to 73 Kb) but the majority of these transcripts (9/12) fell within the range of 5,6-20Kb (Figure 40B). To identfy the transcriptional or posttranscriptional regulatory mechanisms of inflammatory stimuli, we determined the LPS-induced pri-miRNA expression changes using the same GRO-seq datasets [118]. 15 out of 17 transcribed LPS-responsive miRNAs (3 down-regulated and 12 upregulated) showed similar expression patterns with their pri-miRNAs (3 down-regulated and 7 up-regulated; 3 LPS-induced pri-miRNAs contained more than one miRNAs) indicating dominantly transcriptional regulation of miRNA expression in LPS-exposed macrophages (Figure 40C). For validation purposes, we selected three previously described LPS-responsive miRNAs, including the LPS-activated miR-155 and miR-147 as well as the LPS-repressed miR-223 (Figure 40D) [167, 169, 171, 173, 186, 263, 264]. Time course experiments confirmed the LPS-dependent induction of pri-miR-155 and pri-miR-147 and the repression of pri-miR-223 expression (Figure 40E).

Collectively, these findings suggest that the majority of inflammation responsive miRNAs are regulated at the transcriptional level in macrophages.

6.3.2. Transcription start sites of inflammation responsive pri-miRNAs are associated with general active promoter marks and RNA polymerase II binding

It is well characterized that specific epigenetic marks including H3K27Ac and H3K4m3 as well RNAPII binding are associated with the promoters of transcriptionally active protein-coding genes [69, 242]. The active promoter-specific H3K4m3 enrichment and RNAPII binding has been also used for the identification of pri-miRNA promoter regions [265, 266]. In order to investigate whether LPS-regulated pri-miRNA genes have similar epigenetic signatures, we analyzed publicly available H3K4m3, H3K27Ac and RNAPII-specific ChIP-seq datasets from both unstimulated and LPS-exposed mouse BMDMs [108]. As we expected, the TSSs of the inflammation-regulated pri-miRNA genes were associated with H3K4m3, H3K27Ac and RNAPII enrichments (Figure 41A and B). LPS stimulation induced H3K27Ac enrichment and RNAPII binding on the TSSs of LPS-activated pri-miRNAs, including pri-miR-155 and pri-miR-147 (Figure 41A and B). In contrast, LPS-dependent attenuation of H3K27Ac enrichment and RNAPII

binding were observed at the TSSs of inflammation-repressed pri-miRNA genes such as pri-miR-223, without the alteration of H3K4m3 enrichment (Figure 41A and B).

Taken together, these findings suggest that (i) LPS sensitive miRNA genes have similar epigenetic features as protein-coding genes and (ii) their transcription seems to be dependent on RNAPII.

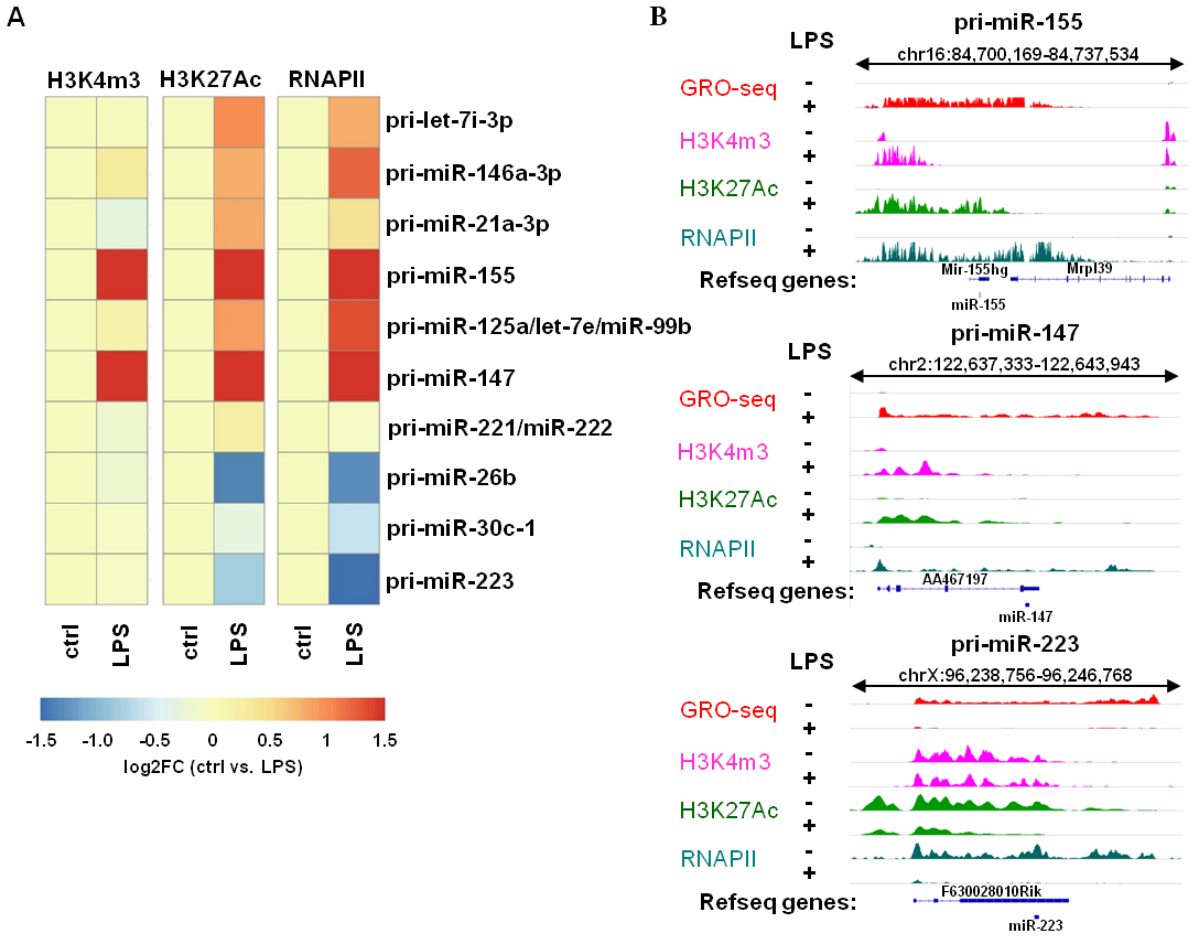

Figure 41. Characterization of transcriptional start sites of LPS-responsive pri-miRNAs in mouse BMDMs

(A) Heat map representation of H3K4m3 and H3K27Ac enrichments as well as RNAPII binding at the TSSs of activated and repressed pri-miRNAs in LPS-stimulated and unstimulated mouse BMDMs. Macrophages were treated with LPS for 4 hours. (B) Strand-specific GRO-Seq, H3K4m3, H3K27Ac and RNAPII-specific ChIP-seq signals in LPS-stimulated and unstimulated mouse macrophages at TSSs and gene bodies of the selected inflammation responsive pri-miRNAs visualized by the Integrative Genomics Viewer.

6.3.3. LPS-regulated pri-miRNAs are associated with an inflammation-responsive enhancer network

The protein-coding genes-associated enhancers are marked by specific post-translational histone modifications including H3K4m1, H3K4m2 and eRNA expression

(Reviewed in [267] and [240]). Enhancers have also been described to regulate pri-miRNA expression in many cell types and tissues [268, 269]. These pri-miRNA-linked distal regulatory regions have general enhancer-like features including enhancer-specific H3K4m1 enrichment and eRNA expression [268, 269]. Based on these findings, we aimed to investigate whether LPS-responsive enhancers can be found in the same subTADs with pri-miRNA genes by using publicly available H3K4m1-specific ChIP-seq and GRO-seq data sets [108, 118]. We performed subTAD prediction based on mouse BMDM-derived CTCF and Rad21 data sets, applying a previously described algorithm [91, 97, 237-239].

As we expected, the LPS responsive pri-miRNA genes were associated with H3K4m1 and eRNA "positive" enhancers (Figure 42A and B). Our global analysis identified 33 induced and 11 repressed distal regulatory regions in the subTADs of LPS-regulated pri-miRNA genes (Figure 41B).

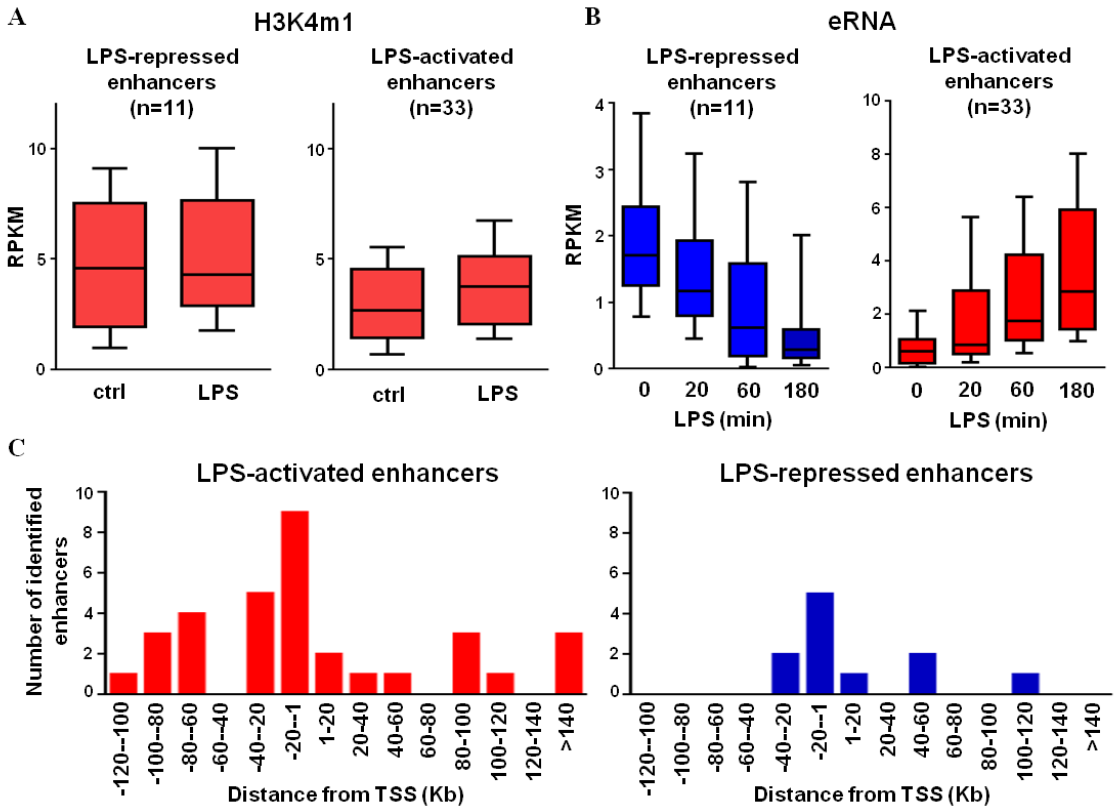

Figure 42. Identification of LPS-regulated enhancers associated with inflammation responsive miRNA genes in mouse BMDMs with the combination of GRO-seq and H3K4m1-specific ChIP-seq datasets

(A) Box plot representation of H3K4m1 at the activated and repressed pri-miRNA-associated enhancers in LPS-stimulated and unstimulated mouse BMDMs. Macrophages were treated with LPS for 4 hours. (B) Box plot representation of eRNA expression at the activated and repressed pri-miRNA-associated enhancers in LPS-stimulated and unstimulated mouse BMDMs. Macrophages were treated with LPS for 20, 60 and 180 minutes. (C) Distribution of enhancers relative to TSSs of the identified LPS-regulated pri-miRNAs.

The investigation of genomic location of LPS-regulated enhancers relative to the TSS of pri-miRNAs indicated that 67% (22/33) of activated enhancers were upstream from the corresponding TSSs (Figure 42C). Furthermore, 48% (16/33) of LPS-activated enhancers were located more than 40 Kb from TSSs (Figure 42C). LPS-attenuated distal regulatory regions also showed asymmetric genomic distribution around the TSS but 73% (8/11) of them were located within 40 Kb relative to TSS (Figure 42C), suggesting that repressive mechanisms more often operate at closer distal regulatory elements compared to the activating ones.

Next, we wanted to study the inflammation-regulated enhancers in the annotated sub-TADs of LPS responsive miR-155, miR-147 and miR-223 genes. We found 9 and 2 H3K4m1 positive enhancers, showing LPS-enhanced eRNA expression in the pri-miR-155 and pri-miR-147-associated sub-TADs, respectively (Figure 43A). In addition, the genomic locus of LPS-repressed pri-miR-223 gene also contained 3 LPS-repressed enhancers (Figure 43A). For all three pri-miRNAs, we selected 2-2 enhancers for further investigation by eRNA-specific RT-qPCR measurements. LPS-mediated activation of the selected pri-miR-155-associated enhancers was correlated with pri-miR-155 expression (Figure 40E and 43B). Similarly, significantly increased eRNA expression was observed at pri-miR-147_+14 Kb and +27Kb enhancers after LPS exposure, followed by induced pri-miR-147 expression (Figure 40E and 43B). However, the studied pri-miR-147-associated enhancers were associated with different activation kinetics at later time points (12 and 24 hours) of LPS treatment. The pri-miR-147_+27 Kb enhancer activity was significantly reduced compared to its maximal expression level following 12 and 24 hours of LPS exposure (Figure 43B). In contrast, eRNA expression remained at a high level at the latest (12 and 24 hours) time points of LPS stimulation at pri-miR-147_+14 Kb enhancer (Figure 43B). Finally, the eRNA expression at the selected pri-miR-223-associated enhancers was attenuated significantly as early as 1 hour after LPS treatment and showed repressed expression level at the 24 hour time point similarly to pri-miR-223 expression (Figure 40E and 43B).

Taken together, these findings indicate that LPS-sensitive miRNA genes are associated with distal regulatory regions showing similar LPS-mediated eRNA expression kinetics with pri-miRNA expression. These obsevations are consistent with studies focusing on mRNA-associated enhancers, thus indicate that enhancers are able to participate in the transcriptional regulation of the inflammation responsive miRNA expression, analogous to mRNAs [110, 270].

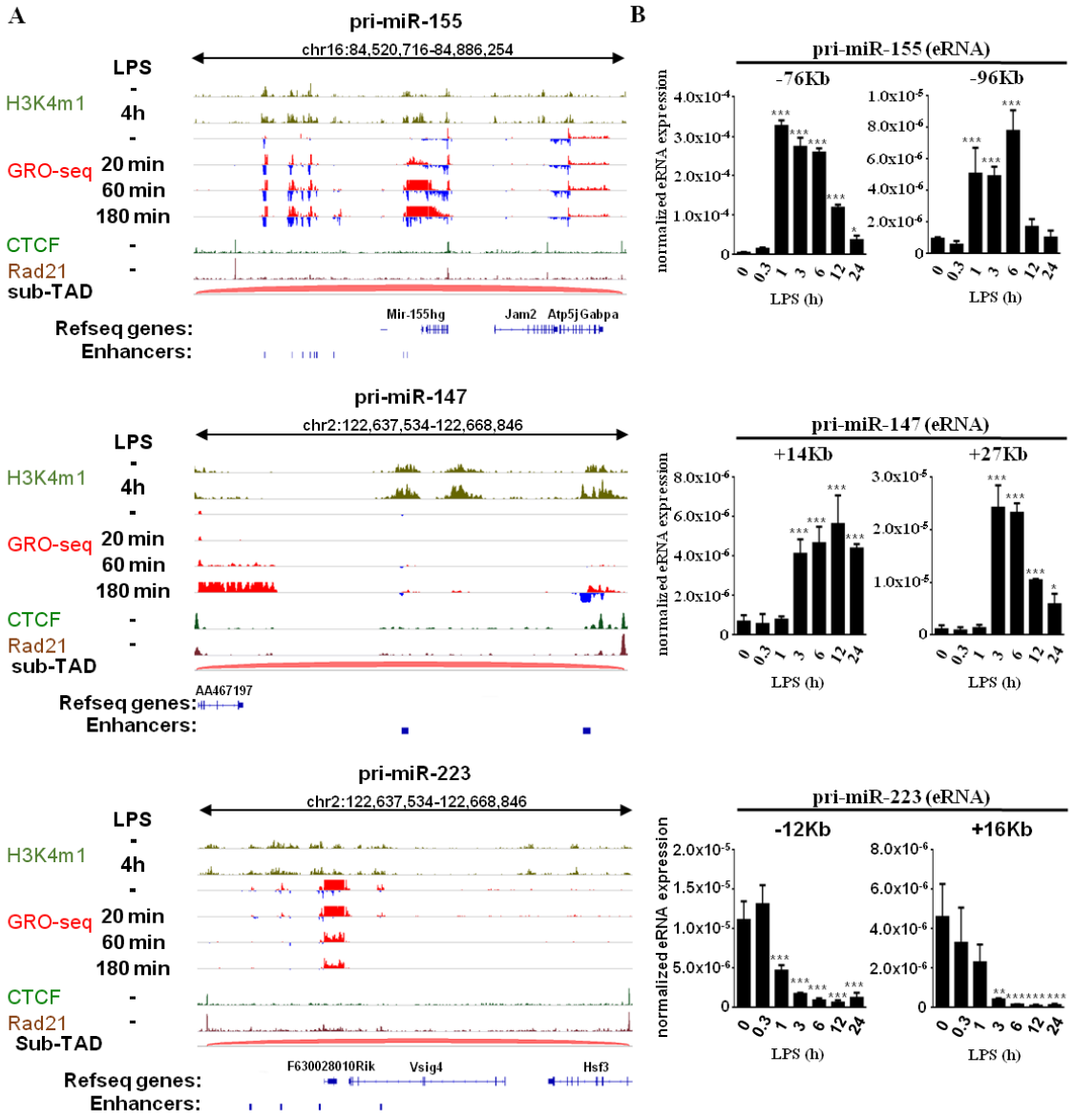

Figure 43. Characterization of pri-miR-155, pri-miR-147 and pri-miR-223 genes-associated enhancers in mouse BMDMs

(A) Strand-specific GRO-Seq, H3K4m1, CTCF and Rad21-specific ChIP-seq signals in LPS-stimulated and unstimulated mouse macrophages at the genomic loci of miR-155, miR-147 and miR-223 are visualized by the Integrative Genomics Viewer. (B) RT-qPCR-based measurement of eRNA expression of 2-2 selected miR-155, miR-147 and miR-223-associated enhancers in LPS-stimulated and unstimulated macrophages. Macrophages were treated with LPS for 20 minutes as well as 1, 3, 6, 12 and 24 hours. Each data point represents the mean and SD of three biological replicates. *P<0.05, **P<0.01, ***P<0.001 compared with the unstimulated control marked as 0.

6.3.4. Classification of inflammation responsive pri-miRNA-associated enhancers based on NFkB-p65 binding

LPS stimulation leads to the activation of many SRTFs including NFkB and AP-1 transcription factor complexes resulting in dramatic changes in the chromatin structure, epigenomic signature and transcriptome in macrophages [75]. To study the participation of NFkB and AP-1 transcription factor complexes in the LPS-dependent regulation of pri-miRNAs expression, we analyzed the binding of NFkB subunit p65 and AP-1 complex member JunB at the LPS-responsive enhancers using publicly available ChIP-seq data sets [108, 110]. As we expected, p65 binding proved to be negligible in unstimulated macrophages, while LPS treatment induced the recruitment of p65 to 13961 genomic regions (Table 6).

		NFkB-p65		Jun B	
		ctrl	**LPS**	**ctrl**	**LPS**
All peaks		531	13961	6497	47054
LPS-activated enhancers	**p65^{high}**	0	17	7	16
	p65^{low}	0	0	1	10
LPS-repressed enhancers		0	2	2	6

Table 6. The number of peaks determined for NFkB-p65 and Jun B at LPS-activated and repressed enhancers in unstimulated and LPS-stimulated mouse BMDMs

In contrast, JunB binding was observed at 6497 genomic sites in resting BMDMs, and the JunB peak number was increased to 47057 after LPS exposure (Table 6). By focusing on the pri-miRNA-linked LPS-activated enhancers, we found that p65 binding was detected at 51,5% (17/33) of them ("p65^{high}" enhancers) while p65 peaks were not detected at the remaining 48,5% (16/33; "p65^{low}" enhancers) (Table 6, Figure 44A and B). In contrast, we did not detect p65 binding at the majority (9/11) of LPS-repressed pri-miRNAs-associated enhancers (Table 6, Figure 44A and B). Interestingly, we found that basal and LPS-induced JunB binding was elevated at LPS-activated p65^{high} enhancers compared to p65^{low} distal regulatory regions (Table 6, Figure 44C). Similarly, LPS-repressed enhancers showed low JunB binding both in resting and LPS-exposed BMDMs (Table 6, Figure 44C).

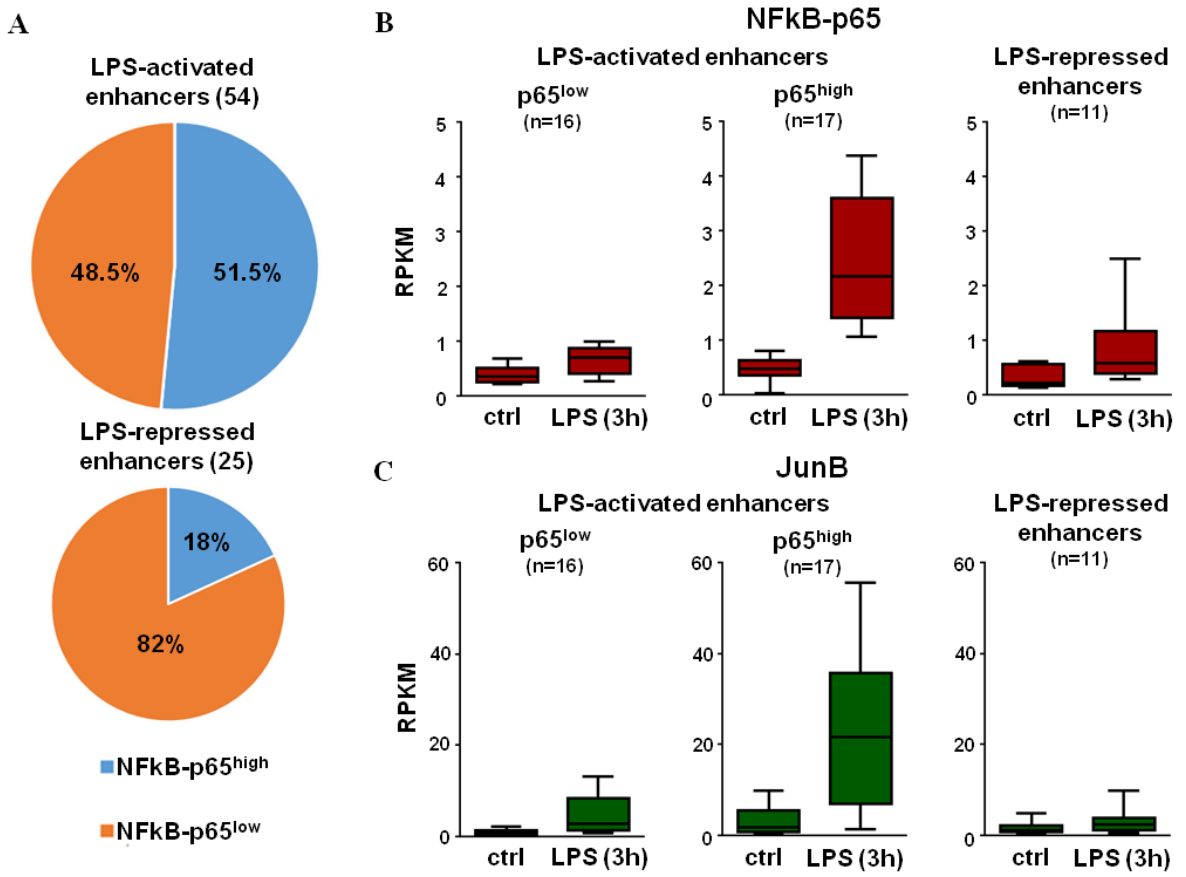

Figure 44. NFKB-p65 binding-based classification of LPS-responsive pri-miRNA-associated enhancers

(A) The ratio of NFkB subunit p65-bound ($p65^{high}$) and un-bound ($p65^{low}$) LPS-activated and repressed pri-miRNA-associated enhancers in mouse BMDMs. (B) Box plot representation of NFkB-p65 binding at $p65^{high}$ and $p65^{low}$ LPS-activated as well as LPS-repressed enhancers in LPS-stimulated and unstimulated (ctrl) mouse macrophages. Macrophages were treated with LPS for 3 hours. (C) Box plot representation of JunB binding at $p65^{high}$ and $p65^{low}$ LPS-activated as well as LPS-repressed enhancers in LPS-stimulated and unstimulated mouse macrophages. Macrophages were treated with LPS for 4 hours.

As we expected, *de novo* motif analysis under NFkB-p65 and JunB peaks showed that NFkB-p65 and Jun-AP1 motifs were significantly enriched at these genomic regions (Figure 45A and B). Targeted motif search indicated that both NFkB-p65 and Jun-AP1 motifs were observed a higher number at the LPS-activated $p65^{high}$ enhancers compared to the LPS-activated $p65^{low}$ and LPS-repressed distal regulatory regions (Figure 45C). Intriguingly, Jun-AP1 motif number (30) was higher at LPS-activated $p65^{high}$ enhancers compared to NFkB-p65 motif number (8) despite the fact that JunB and p65 binding were similar in LPS-exposed BMDMs (Table 6, Figure 44B, C and Figure 45C). Taken together, these findings demonstrate that LPS-activated pri-miRNAs-linked enhancers show different p65 and JunB binding patterns, whereas LPS-repressed enhancers are associated with low p65 and JunB binding, indicating the role of p65 and JunB-independent indirect repressive mechanisms.

A

	P-value	% of Targets	% of Background	Motif
1. Pu.1	1e-1781	37.62%	9.84%	
2. NFkB-p65	1e-1707	19.29%	2.21%	
3. CEBPb	1e-1115	18.00%	3.27%	
4. Jun-AP1	1e-952	21.18%	5.37%	
5. Oct4	1e-282	6.14%	1.43%	

B

	P-value	% of Targets	% of Bg	Motif
1. Jun-AP1	1e-7811	35.30%	4.70%	
2. Pu.1	1e-3593	36.60%	11.51%	
3. CEBPa	1e-1604	21.26%	7.51%	
4. cJun-CRE	1e-1501	15.12%	4.29%	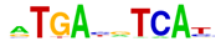
5. IRF1	1e-475	6.46%	2.20%	

C

	Motif	LPS-activated enhancers		LPS-repressed enhancers
		p65^{high}	p65^{low}	
NFkB-p65		8/5	5/3	0/0
Jun-AP1		30/12	18/7	6/3

Figure 45. De novo and targeted binding motif analysis under NFKB-p65 and JunB peaks

(A) Top 5 de novo identified motifs under all NFkB-p65 peaks from ChIP-seq data using HOMER. "%of Targets" refers to the ratio of the peaks having the given motif, and "% of Bg" refers to the ratio of a random background. (B) Top 5 de novo identified motifs under all JunB peaks from ChIP-seq data using HOMER. "%of Targets" refers to the ratio of the peaks having the given motif, and "% of Bg" refers to the ratio of a random background. (C) Targeted NFkB-p65 and Jun-AP1 binding motif identification at p65^{high} and p65^{low} LPS-activated as well as LPS-repressed enhancers (identified motif number/motif "positive" enhancers).

6.3.5. LPS-activated p65^{high} and p65^{low} pri-miRNA-linked enhancers have different epigenetic characteristics

In order to study whether the functional properties of LPS-responsive enhancers are determined by p65 and JunB binding, we analyzed publicly available H3K4m1, H3K27Ac and RNAPII-specific ChIP-seq as well as ATAC-seq datasets from resting and LPS-exposed mouse BMDMs [108, 271]. Intriguingly, the chromatin accessibility was higher at p65^{high} compared to p65^{low} LPS-activated enhancers in unstimulated macrophages (Figure 46A).

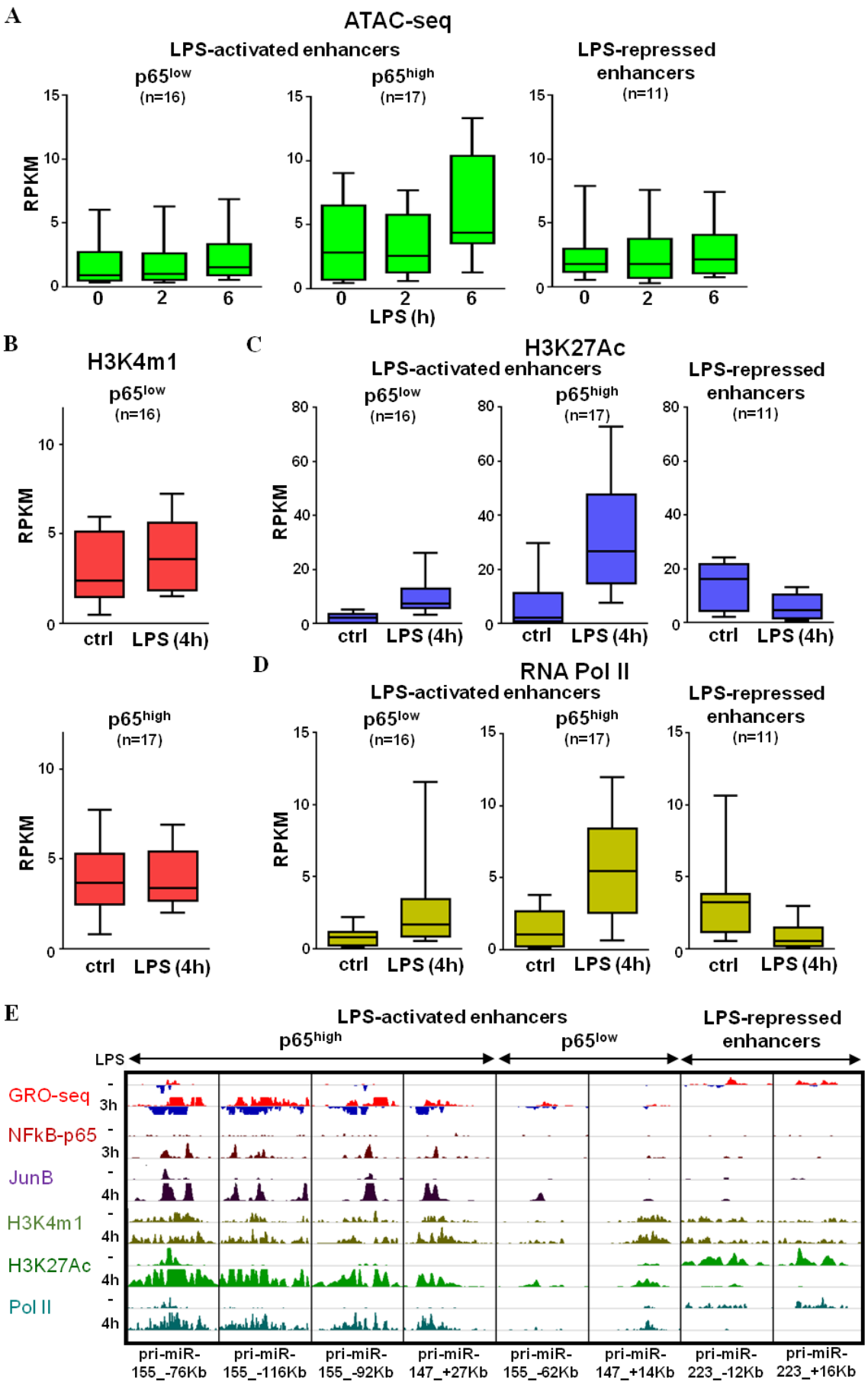
A
ATAC-seq
LPS-activated enhancers
LPS-repressed enhancers
p65low (n=16)
p65high (n=17)
(n=11)
RPKM
LPS (h)
B
H3K4m1
C
H3K27Ac
D
RNA Pol II
ctrl
LPS (4h)
E
LPS-activated enhancers
LPS-repressed enhancers
LPS
GRO-seq
NFkB-p65
JunB
H3K4m1
H3K27Ac
Pol II
pri-miR-155_-76Kb
pri-miR-155_-116Kb
pri-miR-155_-92Kb
pri-miR-147_+27Kb
pri-miR-155_-62Kb
pri-miR-147_+14Kb
pri-miR-223_-12Kb
pri-miR-223_+16Kb

Figure 46. Characterization of p65^{high} and p65^{low} pri-miRNA-associated enhancers in mouse BMDMs

(A) Box plot representation of the ATAC-seq intensities at p65^{high} and p65^{low} LPS-activated as well as LPS-repressed enhancers in unstimulated and LPS-stimulated macrophages. Macrophages were treated with LPS for 2 and 6 hours. (B) Box plot representation of H3K4m1 enrichment at p65^{high} and p65^{low} LPS-activated enhancers in LPS-stimulated and unstimulated mouse macrophages. Macrophages were treated with LPS for 4 hours. (C) Box plot representation of H3K27Ac enrichment at p65^{high} and p65^{low} LPS-activated as well as LPS-repressed enhancers in unstimulated and LPS-stimulated macrophages. Macrophages were treated with LPS for 4 hours. (D) Box plot representation of RNA Pol II binding at p65^{high} and p65^{low} LPS-activated as well as LPS-repressed enhancers in unstimulated and LPS-stimulated macrophages. Macrophages were treated with LPS for 4 hours. (E) Strand-specific GRO-Seq, H3K4m1, H3K27Ac, NFkB-p65, JunB and RNA Pol II ChIP-Seq signals at the selected p65^{high} and p65^{low} LPS-activated as well as LPS-repressed enhancers in LPS-stimulated and unstimulated mouse macrophages. GRO-seq as well as ChIP-seq for the indicated factors and post-translational histone modifications are visualized by the Integrative Genomics Viewer.

Although, the chromatin accessibility was enhanced at both p65^{high} and p65^{low} enhancers following LPS treatment, a greater increase was detected at p65^{high} enhancers compared to p65^{low} enhancers after 6 hours of LPS exposure (Figure 46A). In contrast, both basal and LPS-modulated H3K4m1 enrichments proved to be similar at p65^{high} and p65^{low} LPS-activated distal regulatory regions (Figure 46B). In addition, higher basal and LPS-induced H3K27Ac enrichment and RNAPII binding were detected at LPS-activated p65^{high} enhancers compared to p65^{low} enhancers (Figure 46C, D and E). As we expected, both H3K27Ac enrichment and RNAPII binding were attenuated, while H3K4m1 enrichment and chromatin accessibility were not changed at LPS-repressed enhancers following LPS exposure (Figure 42A, Figure 46A, C, D and E).

In order to investigate the additional characteristics of p65/JunB-dependent and independent activation of LPS-induced pri-miRNA-associated enhancers, we selected four p65^{high} enhancers (pri-miR-155_-76Kb, pri-miR-155_-116Kb, pri-miR-155_-92Kb, pri-miR-147_+27Kb) and two p65^{low} enhancers (pri-miR-155_-62Kb, pri-miR-147_+14Kb) for further study (Figure 46E). We investigated the binding kinetics of p65, PU.1, p300 and RNAPII at the selected enhancers in unstimulated and LPS- exposed mouse BMDMs using ChIP-qPCR. LPS-mediated maximal induction of p65 binding was achieved at 1 hour and it was continuously decreased at later time points (6 and 24 hours) (Figure 47). As we expected, p65-binding was weakly detectable at p65^{low} enhancers in LPS-exposed macrophages (Figure 47). In contrast to NFkB-p65 binding, Pu.1-binding was similar at p65^{high} and p65^{low} enhancers in resting macrophages and all the enhancers were associated with LPS-induced Pu.1 occupancy after 1 hour of LPS stimulation which remained nearly unchanged at later time points (6 and 24 hours) (Figure 47). Finally, we examined the binding kinetics of p300 and two phosporylated forms of RNAPII including transcription initiation-specific RNAPII-pS5 (serine 5 phosphorylated) and elongation-specific RNAPII-pS2 (serine 2 phosphorylated) at the selected enhancers. LPS stimulus-induced p300, RNAPII-S5 and S2 binding were higher at the p65^{high} compared to the p65^{low} enhancers (Figure 47).

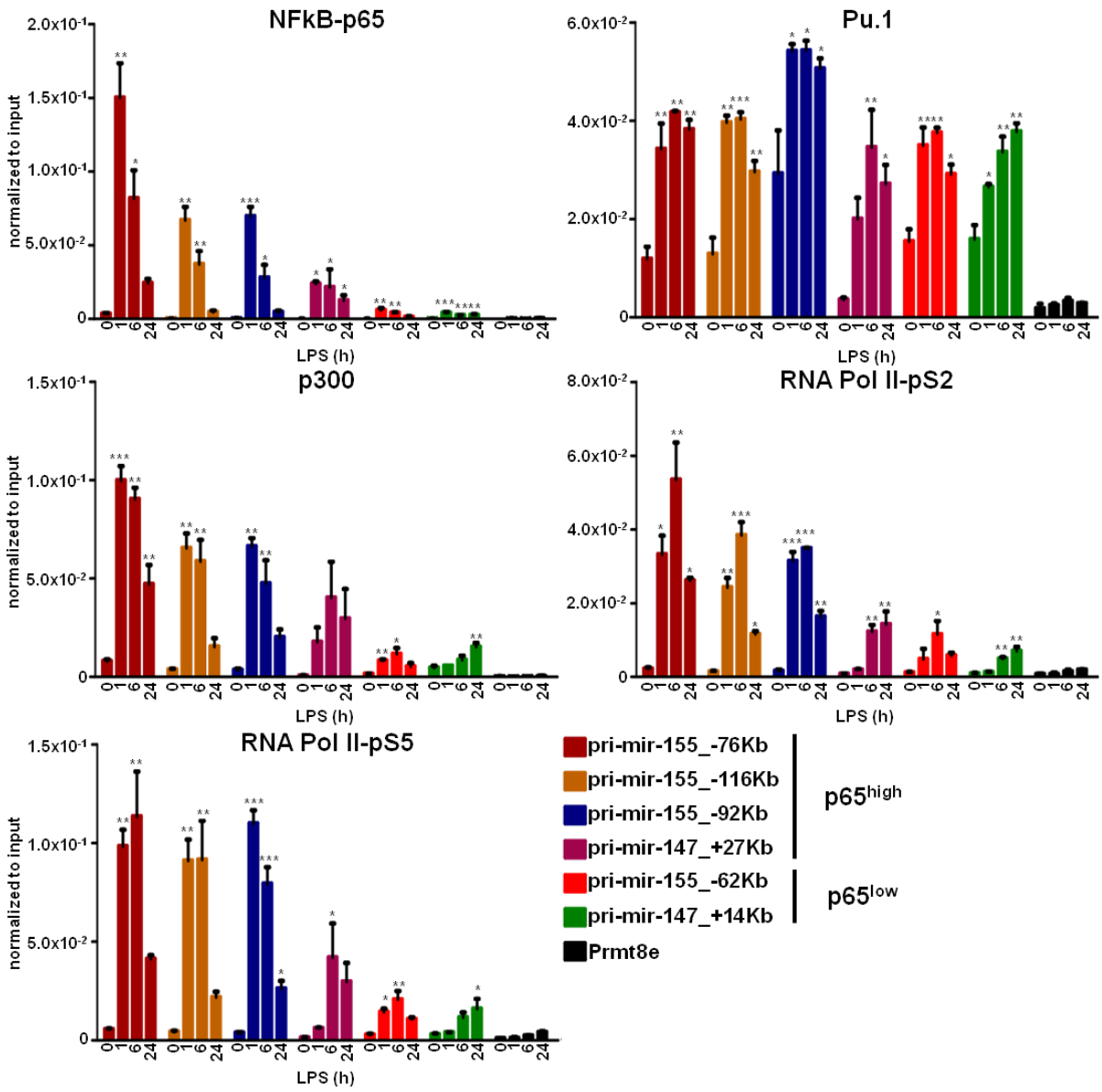

Figure 47. Functional characterization of selected pri-miR-155 and pri-miR-147-associated LPS-activated p65^{high} and p65^{low} enhancers in mouse inflammatory macrophages

ChIP-qPCR measurements against RNA Pol II-pS5, RNA Pol II-pS2, Pu.1, NFkB-p65 and p300 on selected LPS-activated enhancers and negative control Prmt8 enhancer (Prmt8e) regions from wild-type unstimulated and LPS- stimulated macrophages. Macrophages were treated with LPS for 1, 6 and 24 hours. The mean and ±SD of two biological replicates are shown. *P<0.05, **P<0.01, ***P<0.001 compared with the unstimulated control marked as 0.

Intriguingly, we found temporal differences in RNAPII binding between pri-miR-155 and pri-miR-147-linked enhancers. Pri-miR-155-associated enhancers indicated rapid RNAPII p-S2 and p-S5 recruitment after 1 hour of LPS treatment (Figure 46), while pri-miR-147-linked enhancers were associated with a delayed RNAPII recruitment peaking at 6 hours (Figure 47). Taken together, our findings indicate that p65-dependent and independent processes equally contribute to the control of inflammatory pri-miRNA gene/enhancer signature. Interestingly, H3K4m1 enrichment and LPS-induced PU.1 binding do not show major differences between the selected

p65^{low} and p65^{high} enhancers but chromatin accessibility, H3K27Ac enrichment, p300 and RNAPII-binding are positively correlated with the strength of p65 and JunB-binding at the LPS-induced pri-miRNAs-associated enhancers. Finally, the temporal kinetics of RNAPII binding following LPS exposure shows pri-miRNA locus specificity.

6.3.6. Genome architectural context of inflammation-induced pri-miR-155 expression

Mapping of the pri-miR-155-associated, LPS-responsive enhancers showed that these enhancers are located far away (between -54 and -116 Kb) from the TSS of pri-miR-155-coding genomic region. Thus, we wanted to examine whether these distal regulatory elements are located in close spatial proximity to the TSS of pri-miR-155 gene following inflammatory stimulus. To investigate the basal and LPS-induced chromatin interactions, we performed 3C-seq using bait in the region of the most upstream LPS-activated enhancer located -116 Kb from the TSS of miRNA gene in the predicted sub-TAD. We could identfy both constitutive and LPS-induced interactions within the sub-TAD of pri-miR-155 (Figure 48). Permanent interaction was detected between the TSS of pri-miR-155 and the -116Kb enhancer (Figure 48; red arrow). Furtherrmore, LPS-triggered interactions were observed between pri-miR-155_-116 Kb and other LPS-activated enhancers within the sub-TAD (Figure 48; blue arrows). Collectively, our results indicate that (i) the identified inflammation activated enhancers interact with each other and the TSS of pri-miR-155; (ii) the architecture of pri-miR-155-linked sub-TAD undergoes inflammation-mediated spatial reorganization in mouse macrophages.

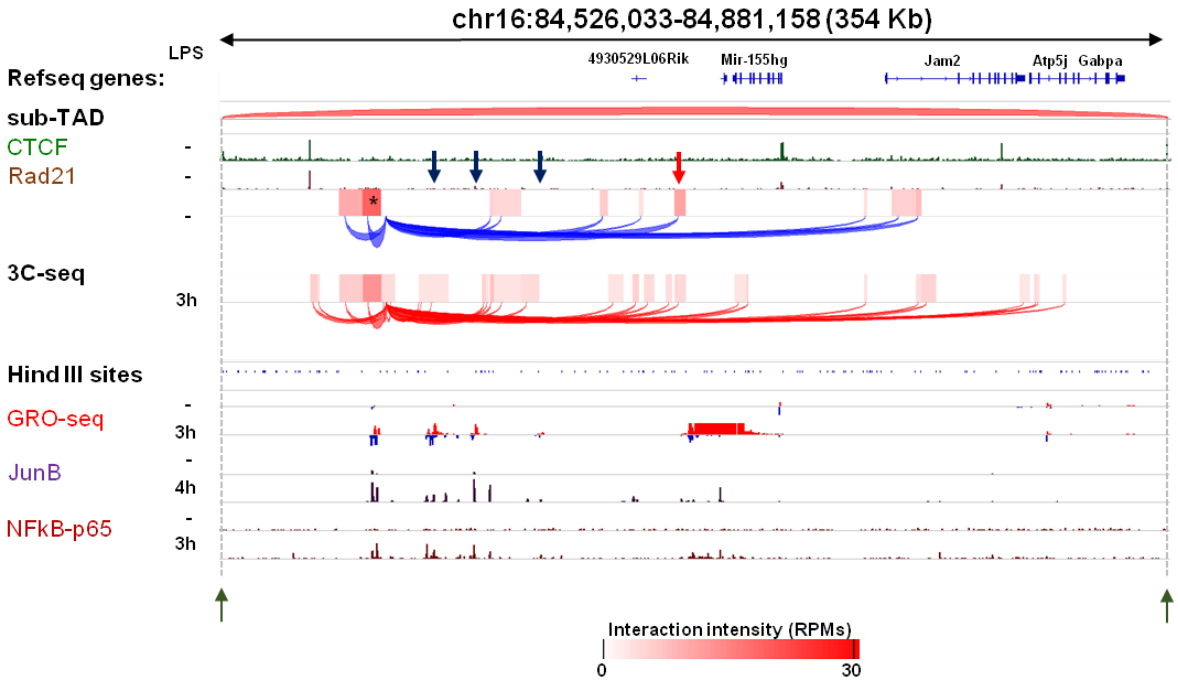

Figure 48. Basal and inflammation-induced chromatin interactions between the LPS-activated enhancers and the TSS of pri-miR155 within the miR-155-associated sub-TAD

Genome browser view of the *pri-miR-155* locus containing proximal interacting regions of the intergenic bait in LPS-stimulated and unstimulated mouse BMDMs as well as loop predictions generated based on CTCF/RAD21-cobound regions. Asterisks show the site of the specific bait. GRO-seq and ChIP-seq for the indicated factors are shown. Green arrowheads and gray dashed lines indicate the predicted domain borders.

7. Discussion

The functional diversity and plasitcity of macrophages are largely dependent on the microenvironmental signals including inflammatory mediators, cytokines and lipids both in physiological and pathological conditions [4, 272, 273]. In the last decade, many microenvironmental signals-induced molecular and epigenetic mechanisms including SRTF-mediated transcriptional activation or miRNA-mediated post-transcriptional repression have been intensively characterized in macrophages [75, 274, 275]. However, many issues remain unanswered in connection with macrophage polarization signals-activated transcriptional and post-transcriptional regulatory mechanisms. On the one hand, large gene sets are repressed by macrophage polarization signals but the mechanisms of SRTF activation-dependent repression is largely unknown [42, 44, 54]. On the other hand, although the biological functions of macrophage polarization signals-responsive miRNAs are well studied, their transcriptional regulation remians poorly understood. In our work, we identified the novel transcriptional repressor activity of IL-4-activated STAT6 transcription factor and characterized the transcriptional regulation of IL-4 and LPS-responsive miRNAs using the combination of NGS-based genomic approaches.

The application of global transcriptome analyses have limitations in the ability to analyze macrophage polarization signals-induced repression and to separate primary repressive events from subsequent ones. Global assessment of nascent RNA expression provided a novel opportunity to detect primary transcriptional changes. It has been demonstrated, that sequencing of subcellular RNA fractions reveal reduced expression of several nascent RNAs following only 30 minutes of lipid A stimulation in macrophages [117]. LPS-dependent reduction of enhancer activity has been also observed at several super enhancers in mouse macrophages. These LPS-repressed super enhancers are associted with different key master transcription factor composition including lower p65 binding compared to the LPS-activated super enhancers [118]. In addition, TNFα-dependent reduction of enhancer activity is also observed in adipocytes in the absence of p65 binding [276]. These findings suggest the general role of transcriptional repression in different cell types following inflammatory stimuli but its exact molecular background remains largely obscure. In our work, we show that IL-4 can also induce the transcriptional repression of large set of genes during alternative macrophage polarization. In contrast with the inflammatory signals-induced repression, IL-4-activated STAT6 transcription factor binding is detected at the IL-4-repressed enhancers suggesting that direct STAT6-mediated repression also contributes to alternative macrophage polarization.

The comprehensive analysis of STAT6-mediated direct transcriptional regulation shows that repressed enhancers are associated with lower STAT6 occupancy and underrepresented STAT6 *de novo* motif enrichment compared to activated enhancers. These findings suggest that IL-4-activated STAT6 acts as a transcriptional repressor either (i) by recognizing non-canonical STAT6-binding motif or (ii) without direct DNA

binding. Interestingly, both mechanisms of SRTF-mediated transcriptional repression are known in macrophage biology. Specific NF-κB-binding motif can be found in the promoter regions of tolerogenic inflammation responsive genes controling the LPS tolerance by binding of p50-NCoR-HDAC3 repressosome complex [277]. The SRTF-mediated, direct DNA binding-independent transcriptional repression is also described in macrophages. The SUMOylated lipid sensing nuclear receptors including PPARs and LXRs can reduce the activity of inflammatory SDTFs through transrepression, carried out by direct protein-protein interactions without direct DNA binding [109, 278, 279]. In case of IL-4/STAT6 signaling pathway-mediated transcriptional repression, it remains to be investigated which mechanisms contribute in these process. In addition, if STAT6 binding to the DNA is indirect, which DNA-bound factor interacts with STAT6. Although, our *de novo* motif analysis suggests that PU.1 and CEBPA are the most likely candidates but both LDTF binding also attenuated at STAT6-repressed enhancers. Thus this requires further investigations.

As far as the molecular mechanism of the repressor activity is concerned, STAT6-mediated repression appears to be distinct from the above mentioned repressive mechanisms in this regard as well. Histone acetylation and gene expression tightly depend on HAT:HDAC ratio [243]. Several studies demonstrated that the HDACs-containing co-repressor complexes play important role in the limitation of transcriptional activation by cytokine-activated STAT proteins [245-247, 280]. In addition, it is also described that STAT5 plays dual role in the regulation of megakaryocyte differentiation. The tyrosine-unphosporylated STAT5 colocalizes with DNA-bound CTCFs and represses the megakaryocytic transcription program while trombopoietin-induced phosphorylation of STAT5 leads to its genomic redistribution and activation of megakaryocyte differentiation program [281]. However, these observations do not explain the molecular mechanisms of STAT6-mediated direct transcriptional repression following IL-4 activation. Our ChIP-seq studies show reduced p300 binding at the IL-4/STAT6 signaling pathway-repressed enhancers in IL-4-stimulated macrophages, exhibiting the potential role of attenuated p300 binding in the STAT6 transcription factor-mediated direct transcriptional repression. Furthermore, we also show that all classical HDACs including HDAC1, 2 and 3 were already bound at STAT6-repressed enhancers in the absence of IL-4 but their occupancies are not influenced by IL-4 stimulation. In spite of all these, we found that the distinct subset of IL-4-repressed genes are regulated HDAC3-dependent manner by IL-4/STAT6 signaling pathway. Although, the molecular basis of IL-4/STAT6 signaling pathway-enhanced HDAC3 activity is not konwn in alternatively polarized macrophages but several studies rasie the potential role of post-translational modifications and or allosteric regulators in the modulation of histone deacteylase activity of different HDACs [282-284]. The mechanistic background of both enhanced HDAC3 activity and non-HDAC3-dependent repression remain to be identified.

In spite of the well characterized functional participation of miRNA-mediated post-transcriptional repression in macrophage polarization, the molecular bases of polarization signals-dependent transcriptional and/or post-transcriptional regulation of

miRNA expression are less investigated. The novel NGS-based methods such as GRO-seq, ChIP-seq and ATAC-seq may provide useful tool for the precise identification of pri-miRNA-coding genes and their regulatory regions. Furthermore, the combination of these techniques with miRNA expression profiling methods may contribute to the better understanding of transcriptional regulation of macrophage polarization signals responsive miRNAs (Figure 49). ChIP-seq-based identification of active pri-miRNA promoter regions has been published in some studies using active promoter mark H3K4m3 and RNAPII-specific ChIP-seq data sets [265, 266, 285, 286].

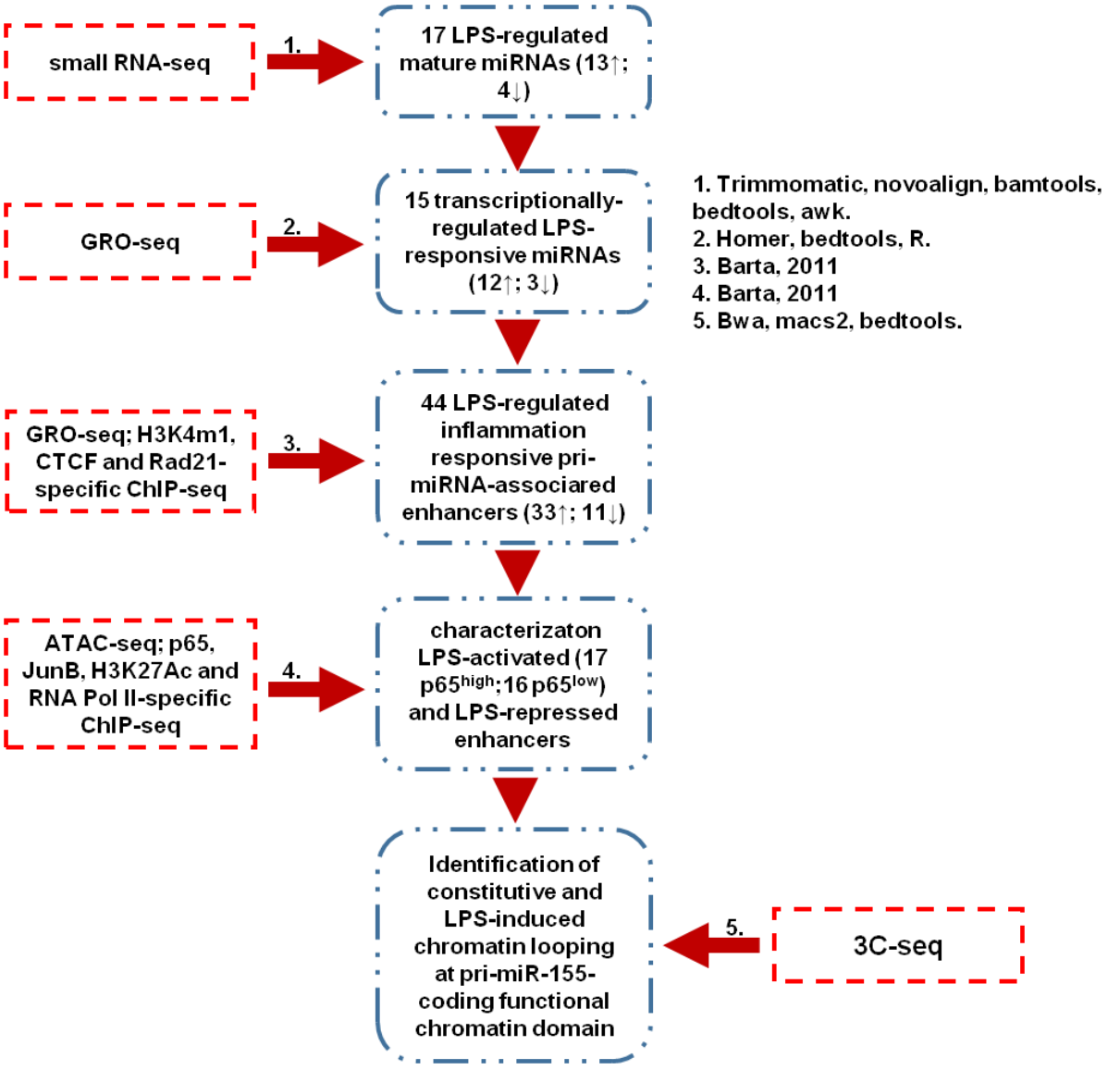

Figure 49. Schematic representation of the experimental and bioinformatic approaches for the investigation of transcriptional regulation of inflammatory responsive miRNAs

Flowchart showing genomics and bioinformatics pipeline utilized in the characterization of transcriptionally-regulated LPS-responsive miRNAs in mouse macrophages.

In addition, the recently developed FANTOM5 miRNA expression and promoter atlas contains the large amount of genomic information about human and mouse miRNA promoters [287]. Nevertheless, the TSSs of some LPS-responsive miRNAs including

miR-221/222 polycistron and miR-146a are unidentified. Here we identified the exact genomic location of TSSs of both primary transcripts using GRO-seq and H3K4m3-specific ChIP-seq data sets from mouse BMDMs. Our analysis also shows that the LPS-repressed miR-30c-1 has macrophage-specific promoter region/TSS which is located more than 10 Kb from the previously published TSS by FANTOM5. The intronic miRNAs and their host genes are often coregulated but the recent studies show that several intronic miRNAs are regulated by their own promoter independently from their host genes [288-290]. Interestingly, we could not identify own H3K4m3 and divergent nascent RNA transcription positive promoters for the LPS-responsive intronic miRNAs and the IL-4-induced intronic miR-342-3p suggesting their coordinated regulation with their host genes. Indeed, we observed the IL-4-induced coregulation of miR-342-3p and its host gene EVL in both human and mice.

Compared to the inflammation responsive protein-coding genes, the involvement of distal regulatory elements is less understood in the transcriptional control of inflammatory miRNAs in macrophages. Here we show that the pri-miRNA-coding regions of both transcriptionally repressed and activated LPS-responsive miRNAs are located with H3K4m1 and eRNA positive enhancers in same sub-TADs. H3K27Ac enrichment and eRNA expression at pri-miRNA genes-associated enhancers are regulated similarly to the pri-miRNAs/mature miRNAs by LPS. Based on LPS-activated SRTF NFkB-p65 binding, the LPS activated pri-miRNAs-linked enhancers was could be further divided into two sub-classes including NFkB-p65^{high} and NFkB-p65^{low} enhancers, which were associated with different epigenetic and functional properties. In addition, the LPS-repressed pri-miRNA-linked enhancers were associated with weak NFkB-p65 binding as previously described [118]. Taken together, these findings raised the possibility of the functional connection between these distal regulatory regions and the LPS-dependent regulation of pri-miRNA expression.

We selected the LPS-responsive miR-155 for further investigation of the interaction of distal enhancers and pri-mR-155-linked promoter region. MiR-155 is one of the well-studied inflammatory miRNAs with conserved immunomodulatory role in many cell types in response to inflammatory signals by limiting the pro-inflammatory gene expression program [167, 171, 173, 264, 291]. By combining GRO-seq and H3K4m1 ChIP-seq data, we identified 11 LPS-activated enhancers associated with the miR-155 gene, which clustered into enhancer clusters (super-enhancers). Interestingly, a similar miR-155-associated enhancer cluster was observed in TNFα-stimulated human HUVEC cells [292]. Our 3C-seq analysis indicated the LPS-induced reorganization of the miR-155-coding genomic locus and formation of interactions between the activated enhancer clusters, the sub-TAD border and the TSS of pri-miR-155. These findings suggest that transcriptional induction of miR-155 expression following inflammatory stimuli involves the activation of miR-155 gene-associated distal regulatory regions and the extensive rearrangement of chromosome structure around the pri-miR-155-coding genomic region (Figure 50).

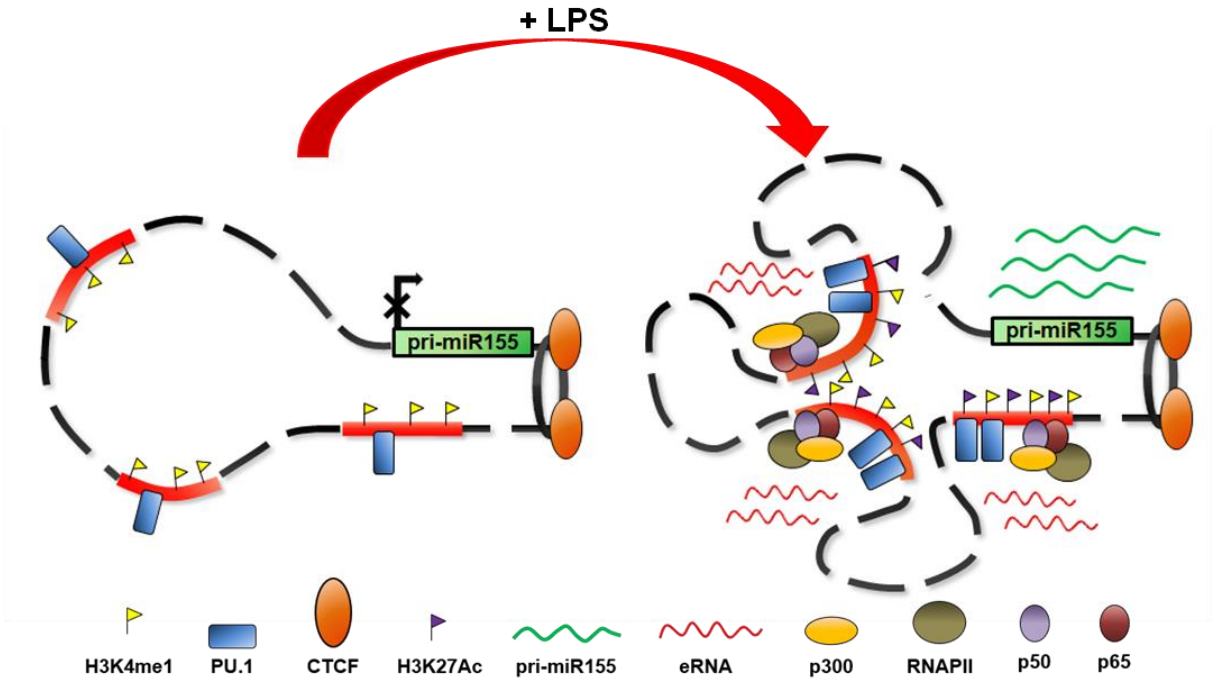

Figure 50. Schematic representation of the proposed mechanism of LPS-induced pri-miR-155 transcription in mouse macrophages

Similarly to LPS-activated miR-155, the alternative macrophage polarization signal IL-4-induced miR-342-3p is also regulated directly by SRTF. Our findings show that IL-4-activated SRTF Stat6-binding is observed at an adjacent genomic region of miR-342 host gene Evl in mouse and human macrophages (+4 Kb and -4 Kb in mouse; +0.3 Kb in human). In addition, both IL-4-induced Evl and miR-342-3p expression were completely STAT6-dependent in mouse BMDMs suggesting that Evl and miR-342 are direct targets of IL-4/STAT6 signaling pathway in both human and murine alternative macrophage activation. Interestingly, increased expression of miR-342-5p (derived from the 5' strand of pre-miR-342 miRNA precursor) in inflammatory macrophages has been linked to the formation of atherosclerotic lesions and INFγ-induced miR-342-5p contributes to broad cell-intrinsic antiviral response via the regulation of sterol pathway [293, 294]. These results suggest that both pri-miRNA expression and miRNA strand selection may be regulated differently in macrophages by external stimuli.

Alternatively polarized macrophages are required for effective protection against different nematode infections reducing parasite number and inhibiting nematode-induced tissue damage [295, 296]. However, nematode infection-induced Th2-type inflammation can also influence the immune response against other pathogens and the prevalence of autoimmune or inflammatory diseases [193, 296, 297]. Therefore, a better understanding of the potential interactions between Th2 and Th1-type inflammation-activated signaling pathways has a great importance in macrophage biology and also in immune-inflammatory pathologies. It has been previously published that the IL-4/STAT6 signaling pathway can suppress M1-polarization signal-activated genes in macrophages *in vitro* mainly through the competition between STAT6 and inflammatory signal-activated transcription factors for binding at the same regulatory

regions [49, 298-301]. The common feature of these studies is the application of IL-4 and INFγ/LPS co-treatment or short (15-30 minutes) IL-4 pre-treatment examining the potential interactions between simultaneous M1 and M2 polarization signals [49, 298-301]. It has also been shown recently with IL-4 and IFNγ co-stimulation-based *in vitro* modeling of complex immunological microenvironment that the IFNγ-induced transcriptional activation via auxiliary transcription factors including AP-1 and CEBPβ is attenuated by IL-4, while the STAT1 and IRF1 transcription factors-mediated effects of IFNγ are resistant to IL-4-mediated inhibition in mouse macrophages [302]. Our findings provide evidence that IL-4/STAT6 signaling pathway induces epigenetic changes that persist following the release of STAT6 from the DNA, leading to attenuated activation of inflammatory enhancers (Figure 51).

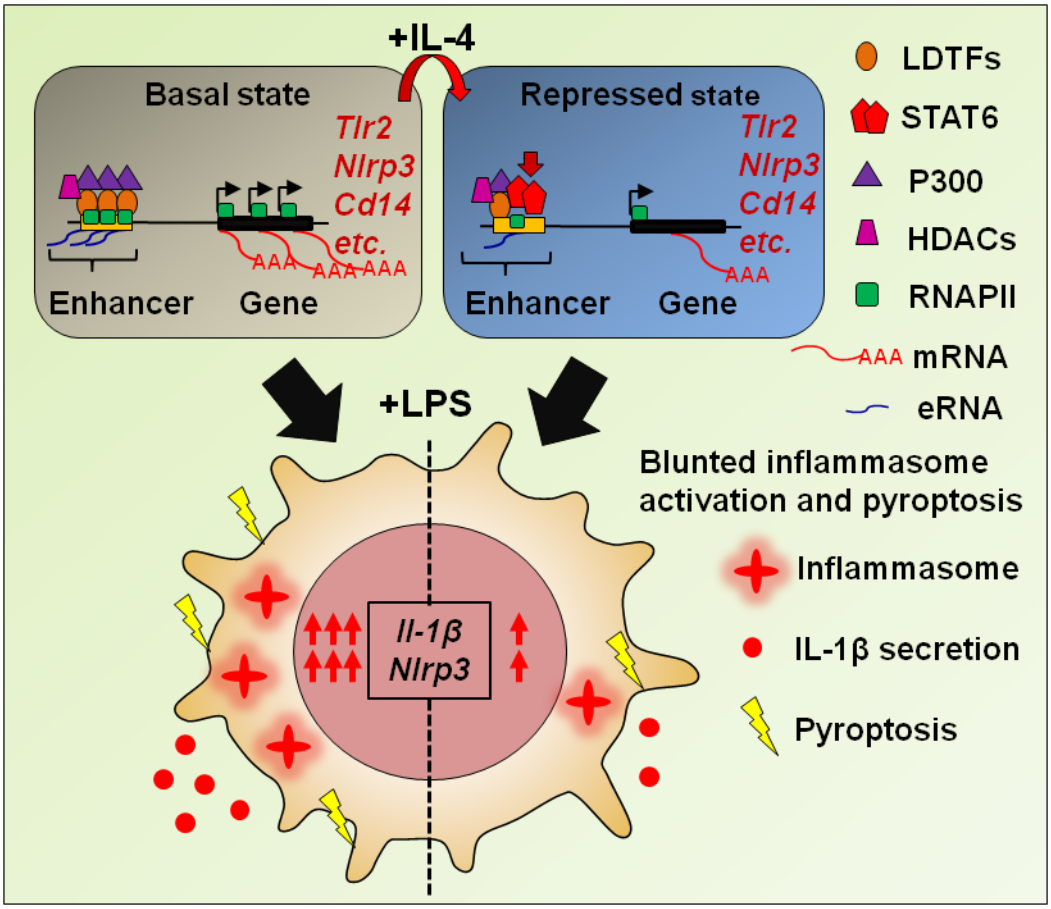

Figure 51. Schematic representation of the proposed mechanism and biological consequence of the IL-4/STAT6 signaling pathway-mediated direct repression at the specific subset of inflammation responsive enhancers in macrophages

The consequence of IL-4 priming-induced repression of inflammatory enhancers is the decreased responsiveness to inflammatory signals via diminished basal and LPS-induced expression of key components of Toll-like and Nod-like receptor signaling pathways including TLR2 or NLRP3. In addition, the majority of IL-4/STAT6-repressed genes including *Tlr2* and *Nlrp3* show diminished expression in macrophages derived from *Brugia malayii*-implanted mice compared to thioglycollate-elicited macrophages. This formally suggests that alternative polarization likely induces partial desensitization

of macrophages to further inflammatory signals *in vivo*. Accordingly, M2-type macrophages have been shown to protect mice against chemically-induced colitis [303-305]. In addition, a growing body of evidence indicates that clinically controlled helminth infection is able to ameliorate inflammatory bowel disease (IBD) [305]. Several IL-4-repressed genes including *Tlr2* and *Nlrp3* are associated with a regulatory role in the development of chronic intestinal inflammation. *Tlr2* controls mucosal inflammation and plays protective role against DSS-induced colitis in mice [306]. In contrast, the role of *Nlrp3* is currently controversial in different murine colitis models [307, 308].

Pathogen infections and inflammation induce rapid macrophage accumulation locally at the site of infection or tissue damage [272]. The general paradigm of macrophage accumulation is that the circulating monocytes are recruited to sites of inflammation and differentiate into macrophages [309, 310] but the rapid proliferation of resident macrophages were also observed in adipose tissue of obese animals or atherosclerotic lesions [311, 312]. Furthermore, local IL-4-induced macrophage proliferation was detected following nematode infections in mice [190]. Some miRNAs associated with anti-proliferative or pro-apoptotic properties in immune or cancer cells, which are able to function as a negative-feedback mechanism controlling local cell proliferation. Specifically, E2F1 transcription factor can facilitates cell cycle progression but also induces apoptotic cell death via up-regulating pro-apoptotic miR-449a/b expression [313]. In addition, nematode infection-induced Th2-type inflammation leads to the local macrophage proliferation and enhanced anti-proliferative miR-378 expression simultaneously indicating a complex regulation of *in situ* macrophage proliferation [177]. MiR-342-3p also associated with anti-proliferative and pro-apoptotic role in breast and colorectal cancer cells [253, 255, 257]. We observed elevated miR-342-3p expression in parallel with local macrophage proliferation at the early stage of *B. malayi*-induced *in vivo* alternative macrophage polarization suggesting a potential role of miR-342-3p in the control of local viable macrophage number [177]. Indeed, our *in vitro* functional studies confirmed that miR-342-3p over-expression diminished viable macrophage number trough induction of apoptosis. Furthermore, the miR-342-3p-repressed anti-apoptotic gene network was identified with well known inhibitors of apoptosis including Birc6, Xiap, Api5 and Bcl2l1 in RAW 264.7 macrophages using a combination of *in silico* target prediction algorithms and miRNA-mimics experiments. Finally, we provided evidence that Bcl2l1 is directly repressed by miR-342-3p. These results raise the possibility that the IL-4-induced miR-342-3p plays a central role in the regulation of macrophage cell number via induction of apoptosis as a potent negative feedback regulator. Thus, the IL-4-mediated proliferative response of macrophages might be controlled by the simultaneous induction of counteracting cellular processes, generating an endogenous limit of macrophage abundance. The suggested dual role of IL-4 is further supported by the previously decribed observation that IL-4 is capable of sensitizing macrophages to rapamycin-induced apoptosis [314]. Interestingly, increased expression of miR-342-3p in the liver is associated with the enhanced macrophage apoptosis in malaria-infected mice [315, 316]. These results suggest the

tight connection between macrophage apoptosis and Th2-type inflammation-dependent induction of miR-342-3p expression.

8. Summary

The complex molecular microenvironment tightly determines the phenotypic and functional features of macrophages in different physiological and pathological conditions. The macrophage exposure to different polarization signals including cytokines and pathogen-derived molecules leads to the activation of signal specific gene expression program via SRTFs. Our systematic genome-wide analysis revealed that the alternative macrophage polarization signal IL-4 represses large gene set at the transcriptional level. IL-4-activated STAT6 binds the repressed genes-linked distal regulatory elements. The STAT6-binding was associated with reduced chromatin openess, LDTF, p300 and RNAPII binding as well as decreased eRNA expression. These results suggest the IL-4-activated STAT6 transcriptional factor can act as a transcriptional repressor in macrophages. In addition, we found that the IL-4/STAT6 signaling pathway-mediated transcriptional repression diminishes the inflammatory responsiveness of macrophages including NLRP3 inflammasome activation, IL-1β production and pyroptosis. Taken together, these results suggest that complex bidirectional interactions exist between alternative macrophage polarization and inflammatory signals that influence the responsiveness and sensitivity of macrophages toward microbial-, stress-, and damage-associated endogenous signals.

The miRNA-mediated post-transcriptional repression also contributes in the regulation of macrophage function. Here, we identified that miR-342-3p and their host gene EVL are directly induced in human and mice by IL-4/STAT6 signaling pathway. Interestingly, miR-342-3p can reduce macrophage survival via direct targeting of anti-apoptotic gene pathway including Bcl2l1. These results suggest that IL-4/STAT6 signaling pathway-induced miR-342-3p potentially participate in the negative feed-back regulation of IL-4-mediated macrophage proliferation.

Finally, we characterized the transcriptional regulation of the inflammation responsive miRNome including miR-155, miR-147 and miR-223 using an integrated NGS-based approach. Here we show that LPS-dependent transcriptional induction of miR-155 expression is based on an intensive communication between the distal anhancers and the pri-miR-155-linked TSS and associated with the reorganization of the pri-miR-155-coding genomic locus.

9. Összefoglalás

A komplex molekuláris mikrokörnyezet szigorúan szabályozza a mkrofágok fenotípusos és funkcinális sajátosságait különböző fiziológiás és patológiás körülmények között. A makrofágok stimulációja különböző polarizációs szignálokkal, köztük citokinekkel és patogén eredetű molekulákkal, a szignálok által aktivált transzkripciós faktorokon keresztül a szignálokra specifikus génexpressziós program bekapcsolásához vezet. Szisztematikus teljes genom szintű analízis segítségével kimutattuk, az alternatív makrofág polarizációs szignálok közé tartozó IL-4 egy nagy géncsoport kifejeződését gátolja a transzkripció szintjén. Az IL-4 által aktivált STAT6 transzkripciós faktor kötődik a gátolt génekhez tartozó ehanszerekhez. Ezeken a helyeken a STAT6 kötődés együtt jár a csökkent kromatin nyitottsággal, kisebb LDTF, p300 és RNS Polimeráz II kötődéssel, valamint alacsonyabb eRNS kifejeződéssel. Ezek az eredmények azt mutatják, hogy az IL-4 által aktivált STAT6 transzkripciós faktor képes represszorként működni a makrofágokban. Továbbá megfigyeltük, hogy az IL-4/STAT6 szignálútvonal által kiváltott represszió képes csökkenteni a makrofágok gyulladásos válaszkészségét, köztük az NLRP3 inflammaszóma aktivációt, az IL-1βtermelődést és a piroptózist. Összességében ezek az eredmények felvetik egy kétirányú kölcsönhatás lehetőségét az alternatív makrofág polarizáció és a gyulladásos szignálok között, amely jelentősen befolyásolhatja a makrofágok különböző mikrobiális, stressz és sérülés eredetű szignálokkal szembeni érzékenységét és válaszkészségét.

A miRNS-ek által kiváltott poszt-transzkripciós gátlás szintén hozzájárul a makrofágok funkciójának szabályozásához. A munkánk során azonosítottuk, a miR-342-3p-nek és EVL gazdagénjének IL-4/STAT6 szignálútvonal által kiváltott közvetlen indukcióját. Érdekes módon a miR-342-3p csökkenti a makrofág életképességet közvetlenül szabályozva egy a Bcl2l1 gént is magában foglaló antiapoptotikus génhálózatot. Ezek az eredmények azt mutatják, hogy IL-4/STAT6 szignálútvonal által indukált miR-342-3p részt vesz az IL-4 által kiváltott sejtosztódás szabályozásában a folyamat negatív regulátoraként.

Végül feltérképeztük a gyulladásos miRNS-ek, köztük a miR-155, miR-147 és miR-223 transzkripciós szabályozását egy integrált új-generációs szekvenálás alapú megközelítés alkalmazásával. Kimutattuk, hogy a miR-155 kifejeződésének LPS által kiváltott aktiválása a pri-miR-155 transzkripciós starthelye és távoli enhenszerei közötti intenzív kommunikáción alapszik, amely együtt jár a miR-155-öt kódoló genomi régió gyulladásos szignál által kiváltott átrendeződésével.

10. New Findings

- IL-4-activated STAT6 transcription factor acts as a transcriptional repressor in alternatively polarized macrophages.
- IL-4/STAT6 signaling pathway-repressed enhancers are associated with reduced RNAPII, LDTF and p300 binding as well as eRNA expression.
- IL-4 pretreatment attenuates the inflammatory responsiveness in macrophages.
- IL-4 pretreatment limits the LPS-induced NLRP3 inflammasome activation, IL-1β production and pyroptotic cell death
- IL-4/STAT6 signaling pathway regulates a conserved miRNA signature in human and mouse macrophages.
- Mir-342-3p and its host gene EVL are coordinately induced in both human and mouse macrophages by IL4.
- EVL is a direct target of STAT6.
- Mir-342-3p regulates macrophage survival through targeting an anti-apoptotic gene network including Bcl2l1.
- Integrated, next-generation sequencing-based approach was developed to investigate the external signals-mediated transcriptional regulation of miRNA expression.
- 15 transcriptionally regulated miRNAs were found in LPS-exposed macrophages.
- LPS responsive pri-miRNAs are associated with thirty-three activated and eleven repressed enhancers.
- Based on LPS-activated p65 (and JunB) binding, two distinct LPS-activated enhancer subsets are distinguishable with different functional characteristics.
- The architecture of pri-miR-155-coding genomic region undergoes LPS-dependent spatial reorganization.

11. List of Keywords

epigenetics, enhancer, next-generation sequencing, inflammation, alternative macrophage polarization, IL-4, STAT6, transcriptional repression, inflammasome activation, pyroptosis, miRNA, pri-miRNA, post-transcriptional repression, apoptosis, LPS, p65, miR-155

12. Tárgyszavak

epigenetika, enhanszer, új-generációs szekvenálás, gyulladás, alternatív makrofág polarizáció, IL-4, STAT6, transzkripciós gátlás, inflammaszóma aktiváció, pirotózis, miRNS, pri-miRNS, poszt-transzkripcionális represszió, apotózis, LPS, p65, miR-155

13. Acknowledgements

First of all I would like to thank my supervisor Prof. László Nagy for his continuous support, patience and motivation during my PhD studies and research. He was an excellent mentor whose main goal to lead me towards becoming a real scientist.

I am grateful to Prof. József Tőzser and Prof. Laszló Fésüs the current and former leaders of the Department of Boichemistry and Molecular Biology for the opportunity to work in well-equipped environment with highly skilled colleagues.

I would like to thank my advisory committee: Dr. Árpád Lányi and Dr. Sándor Bíró for their encouragement and insightful comments.

Special thanks to Dr. Bence Dániel, Attila Horváth and Dr. Máté Kiss for their excellent work and selfless help as well as and the all members of the Nagy Laboratory for their support during my work.

My gratitude also goes to Tímea Silye-Cseh, Ágnes Kriston, Beáta Kovács-Szalka. Márta Béládi and Ibolya Fürtös for their excellent technical assistance.

I am also thankful to many collaborators: Dr. Szilvia Benkő, Dr. Marietta Budai, Dr. Béla Nagy Jr., Dr. Jean-Francois Deleuze, Dr. Éva Várallyay, Prof. Judith Allen, Dr. Dominik Rückerl, Dr. Zsolt Bacsó, Dr. Quang Minh Doan-Xuan, Csaba Bankó, Dr. Ira G. Schulman, Dr. Sacha Sauer, Dr. Cei Abreu-Goodger, Dr. Cesaré Ovando Vázquez, Dr. Matthew N. Poy, Dr. Sudhir Gopal Tattikota and Dr. Xin Yan.

Last but not the least, I am very grateful to my family and friends who has supported me throughout the entire process.

14. References

[1] S.H. Kaufmann, Immunology's foundation: the 100-year anniversary of the Nobel Prize to Paul Ehrlich and Elie Metchnikoff, Nat Immunol, 9 (2008) 705-712.

[2] P.J. Murray, T.A. Wynn, Protective and pathogenic functions of macrophage subsets, Nature reviews. Immunology, 11 (2011) 723-737.

[3] S. Gordon, F.O. Martinez, Alternative activation of macrophages: mechanism and functions, Immunity, 32 (2010) 593-604.

[4] D.M. Mosser, J.P. Edwards, Exploring the full spectrum of macrophage activation, Nature reviews. Immunology, 8 (2008) 958-969.

[5] S. Gordon, A. Pluddemann, Tissue macrophages: heterogeneity and functions, BMC biology, 15 (2017) 53.

[6] F. Ginhoux, M. Guilliams, Tissue-Resident Macrophage Ontogeny and Homeostasis, Immunity, 44 (2016) 439-449.

[7] D. Hashimoto, A. Chow, C. Noizat, P. Teo, M.B. Beasley, M. Leboeuf, C.D. Becker, P. See, J. Price, D. Lucas, M. Greter, A. Mortha, S.W. Boyer, E.C. Forsberg, M. Tanaka, N. van Rooijen, A. Garcia-Sastre, E.R. Stanley, F. Ginhoux, P.S. Frenette, M. Merad, Tissue-resident macrophages self-maintain locally throughout adult life with minimal contribution from circulating monocytes, Immunity, 38 (2013) 792-804.

[8] C.C. Bain, A. Bravo-Blas, C.L. Scott, E.G. Perdiguero, F. Geissmann, S. Henri, B. Malissen, L.C. Osborne, D. Artis, A.M. Mowat, Constant replenishment from circulating monocytes maintains the macrophage pool in the intestine of adult mice, Nature immunology, 15 (2014) 929-937.

[9] T. Satoh, K. Nakagawa, F. Sugihara, R. Kuwahara, M. Ashihara, F. Yamane, Y. Minowa, K. Fukushima, I. Ebina, Y. Yoshioka, A. Kumanogoh, S. Akira, Identification of an atypical monocyte and committed progenitor involved in fibrosis, Nature, 541 (2017) 96-101.

[10] T.A. Wynn, K.M. Vannella, Macrophages in Tissue Repair, Regeneration, and Fibrosis, Immunity, 44 (2016) 450-462.

[11] S. Nucera, D. Biziato, M. De Palma, The interplay between macrophages and angiogenesis in development, tissue injury and regeneration, The International journal of developmental biology, 55 (2011) 495-503.

[12] P.J. Murray, J.E. Allen, S.K. Biswas, E.A. Fisher, D.W. Gilroy, S. Goerdt, S. Gordon, J.A. Hamilton, L.B. Ivashkiv, T. Lawrence, M. Locati, A. Mantovani, F.O. Martinez, J.L. Mege, D.M. Mosser, G. Natoli, J.P. Saeij, J.L. Schultze, K.A. Shirey, A. Sica, J. Suttles, I. Udalova, J.A. van Ginderachter, S.N. Vogel, T.A. Wynn, Macrophage activation and polarization: nomenclature and experimental guidelines, Immunity, 41 (2014) 14-20.

[13] P.J. Murray, Macrophage Polarization, Annual review of physiology, 79 (2017) 541-566.

[14] A. Sica, A. Mantovani, Macrophage plasticity and polarization: in vivo veritas, J Clin Invest, 122 (2012) 787-795.

[15] J. Xue, S.V. Schmidt, J. Sander, A. Draffehn, W. Krebs, I. Quester, D. De Nardo, T.D. Gohel, M. Emde, L. Schmidleithner, H. Ganesan, A. Nino-Castro, M.R. Mallmann, L. Labzin, H. Theis, M. Kraut, M. Beyer, E. Latz, T.C. Freeman, T. Ulas, J.L. Schultze, Transcriptome-based network analysis reveals a spectrum model of human macrophage activation, Immunity, 40 (2014) 274-288.

[16] T. Varga, R. Mounier, A. Horvath, S. Cuvellier, F. Dumont, S. Poliska, H. Ardjoune, G. Juban, L. Nagy, B. Chazaud, Highly Dynamic Transcriptional Signature of Distinct Macrophage Subsets during Sterile Inflammation, Resolution, and Tissue Repair, Journal of immunology, 196 (2016) 4771-4782.

[17] F.O. Martinez, S. Gordon, The M1 and M2 paradigm of macrophage activation: time for reassessment, F1000prime reports, 6 (2014) 13.

[18] M.D. Kraaij, E.J. Vereyken, P.J. Leenen, T.P. van den Bosch, F. Rezaee, M.G. Betjes, C.C. Baan, A.T. Rowshani, Human monocytes produce interferon-gamma upon stimulation with LPS, Cytokine, 67 (2014) 7-12.

[19] N. Choudhry, F. Petry, N. van Rooijen, V. McDonald, A protective role for interleukin 18 in interferon gamma-mediated innate immunity to Cryptosporidium parvum that is independent of natural killer cells, The Journal of infectious diseases, 206 (2012) 117-124.
[20] X. Hu, L.B. Ivashkiv, Cross-regulation of signaling pathways by interferon-gamma: implications for immune responses and autoimmune diseases, Immunity, 31 (2009) 539-550.
[21] M. Muller, S. Carter, M.J. Hofer, I.L. Campbell, Review: The chemokine receptor CXCR3 and its ligands CXCL9, CXCL10 and CXCL11 in neuroimmunity--a tale of conflict and conundrum, Neuropathology and applied neurobiology, 36 (2010) 368-387.
[22] C.S. Hsieh, S.E. Macatonia, C.S. Tripp, S.F. Wolf, A. O'Garra, K.M. Murphy, Development of TH1 CD4+ T cells through IL-12 produced by Listeria-induced macrophages, Science, 260 (1993) 547-549.
[23] Y. Wu, Z. Tian, H. Wei, Developmental and Functional Control of Natural Killer Cells by Cytokines, Frontiers in immunology, 8 (2017) 930.
[24] M.B. Lutz, Induction of CD4(+) Regulatory and Polarized Effector/helper T Cells by Dendritic Cells, Immune network, 16 (2016) 13-25.
[25] Y. Liu, K.N. Stewart, E. Bishop, C.J. Marek, D.C. Kluth, A.J. Rees, H.M. Wilson, Unique expression of suppressor of cytokine signaling 3 is essential for classical macrophage activation in rodents in vitro and in vivo, Journal of immunology, 180 (2008) 6270-6278.
[26] C.E. Arnold, C.S. Whyte, P. Gordon, R.N. Barker, A.J. Rees, H.M. Wilson, A critical role for suppressor of cytokine signalling 3 in promoting M1 macrophage activation and function in vitro and in vivo, Immunology, 141 (2014) 96-110.
[27] K. Takeda, S. Akira, TLR signaling pathways, Seminars in immunology, 16 (2004) 3-9.
[28] M. Yamamoto, K. Takeda, Current views of toll-like receptor signaling pathways, Gastroenterology research and practice, 2010 (2010) 240365.
[29] A.P. West, I.E. Brodsky, C. Rahner, D.K. Woo, H. Erdjument-Bromage, P. Tempst, M.C. Walsh, Y. Choi, G.S. Shadel, S. Ghosh, TLR signalling augments macrophage bactericidal activity through mitochondrial ROS, Nature, 472 (2011) 476-480.
[30] J. Henao-Mejia, E. Elinav, C.A. Thaiss, R.A. Flavell, Inflammasomes and metabolic disease, Annual review of physiology, 76 (2014) 57-78.
[31] V. Motta, F. Soares, T. Sun, D.J. Philpott, NOD-like receptors: versatile cytosolic sentinels, Physiological reviews, 95 (2015) 149-178.
[32] V.A. Rathinam, K.A. Fitzgerald, Inflammasome Complexes: Emerging Mechanisms and Effector Functions, Cell, 165 (2016) 792-800.
[33] K. Yakimchuk, C. Roura-Mir, K.G. Magalhaes, A. de Jong, A.G. Kasmar, S.R. Granter, R. Budd, A. Steere, V. Pena-Cruz, C. Kirschning, T.Y. Cheng, D.B. Moody, Borrelia burgdorferi infection regulates CD1 expression in human cells and tissues via IL1-beta, European journal of immunology, 41 (2011) 694-705.
[34] M. Schenk, M. Fabri, S.R. Krutzik, D.J. Lee, D.M. Vu, P.A. Sieling, D. Montoya, P.T. Liu, R.L. Modlin, Interleukin-1beta triggers the differentiation of macrophages with enhanced capacity to present mycobacterial antigen to T cells, Immunology, 141 (2014) 174-180.
[35] B. Wegiel, R. Larsen, D. Gallo, B.Y. Chin, C. Harris, P. Mannam, E. Kaczmarek, P.J. Lee, B.S. Zuckerbraun, R. Flavell, M.P. Soares, L.E. Otterbein, Macrophages sense and kill bacteria through carbon monoxide-dependent inflammasome activation, The Journal of clinical investigation, 124 (2014) 4926-4940.
[36] S.L. Fink, B.T. Cookson, Caspase-1-dependent pore formation during pyroptosis leads to osmotic lysis of infected host macrophages, Cellular microbiology, 8 (2006) 1812-1825.
[37] A. Lehtonen, H. Ahlfors, V. Veckman, M. Miettinen, R. Lahesmaa, I. Julkunen, Gene expression profiling during differentiation of human monocytes to macrophages or dendritic cells, Journal of leukocyte biology, 82 (2007) 710-720.
[38] T. Roszer, Understanding the Mysterious M2 Macrophage through Activation Markers and Effector Mechanisms, Mediators of inflammation, 2015 (2015) 816460.
[39] T. Satoh, O. Takeuchi, A. Vandenbon, K. Yasuda, Y. Tanaka, Y. Kumagai, T. Miyake, K. Matsushita, T. Okazaki, T. Saitoh, K. Honma, T. Matsuyama, K. Yui, T. Tsujimura, D.M. Standley, K. Nakanishi, K.

Nakai, S. Akira, The Jmjd3-Irf4 axis regulates M2 macrophage polarization and host responses against helminth infection, Nature immunology, 11 (2010) 936-944.
[40] X. Liao, N. Sharma, F. Kapadia, G. Zhou, Y. Lu, H. Hong, K. Paruchuri, G.H. Mahabeleshwar, E. Dalmas, N. Venteclef, C.A. Flask, J. Kim, B.W. Doreian, K.Q. Lu, K.H. Kaestner, A. Hamik, K. Clement, M.K. Jain, Kruppel-like factor 4 regulates macrophage polarization, The Journal of clinical investigation, 121 (2011) 2736-2749.
[41] O.M. Pello, M. De Pizzol, M. Mirolo, L. Soucek, L. Zammataro, A. Amabile, A. Doni, M. Nebuloni, L.B. Swigart, G.I. Evan, A. Mantovani, M. Locati, Role of c-MYC in alternative activation of human macrophages and tumor-associated macrophage biology, Blood, 119 (2012) 411-421.
[42] A. Szanto, B.L. Balint, Z.S. Nagy, E. Barta, B. Dezso, A. Pap, L. Szeles, S. Poliska, M. Oros, R.M. Evans, Y. Barak, J. Schwabe, L. Nagy, STAT6 transcription factor is a facilitator of the nuclear receptor PPARgamma-regulated gene expression in macrophages and dendritic cells, Immunity, 33 (2010) 699-712.
[43] Z. Czimmerer, T. Varga, S. Poliska, I. Nemet, A. Szanto, L. Nagy, Identification of novel markers of alternative activation and potential endogenous PPARgamma ligand production mechanisms in human IL-4 stimulated differentiating macrophages, Immunobiology, 217 (2012) 1301-1314.
[44] F.O. Martinez, L. Helming, R. Milde, A. Varin, B.N. Melgert, C. Draijer, B. Thomas, M. Fabbri, A. Crawshaw, L.P. Ho, N.H. Ten Hacken, V. Cobos Jimenez, N.A. Kootstra, J. Hamann, D.R. Greaves, M. Locati, A. Mantovani, S. Gordon, Genetic programs expressed in resting and IL-4 alternatively activated mouse and human macrophages: similarities and differences, Blood, 121 (2013) e57-69.
[45] G. Raes, R. Van den Bergh, P. De Baetselier, G.H. Ghassabeh, C. Scotton, M. Locati, A. Mantovani, S. Sozzani, Arginase-1 and Ym1 are markers for murine, but not human, alternatively activated myeloid cells, Journal of immunology, 174 (2005) 6561; author reply 6561-6562.
[46] M.J. Fenton, J.A. Buras, R.P. Donnelly, IL-4 reciprocally regulates IL-1 and IL-1 receptor antagonist expression in human monocytes, Journal of immunology, 149 (1992) 1283-1288.
[47] F. Colotta, F. Re, M. Muzio, R. Bertini, N. Polentarutti, M. Sironi, J.G. Giri, S.K. Dower, J.E. Sims, A. Mantovani, Interleukin-1 type II receptor: a decoy target for IL-1 that is regulated by IL-4, Science, 261 (1993) 472-475.
[48] S. Lacraz, L. Nicod, B. Galve-de Rochemonteix, C. Baumberger, J.M. Dayer, H.G. Welgus, Suppression of metalloproteinase biosynthesis in human alveolar macrophages by interleukin-4, The Journal of clinical investigation, 90 (1992) 382-388.
[49] Y. Ohmori, T.A. Hamilton, STAT6 is required for the anti-inflammatory activity of interleukin-4 in mouse peritoneal macrophages, The Journal of biological chemistry, 273 (1998) 29202-29209.
[50] J. Ehrchen, L. Steinmuller, K. Barczyk, K. Tenbrock, W. Nacken, M. Eisenacher, U. Nordhues, C. Sorg, C. Sunderkotter, J. Roth, Glucocorticoids induce differentiation of a specifically activated, anti-inflammatory subtype of human monocytes, Blood, 109 (2007) 1265-1274.
[51] M.D. van de Garde, F.O. Martinez, B.N. Melgert, M.N. Hylkema, R.E. Jonkers, J. Hamann, Chronic exposure to glucocorticoids shapes gene expression and modulates innate and adaptive activation pathways in macrophages with distinct changes in leukocyte attraction, Journal of immunology, 192 (2014) 1196-1208.
[52] T.T. Antoniv, K.H. Park-Min, L.B. Ivashkiv, Kinetics of IL-10-induced gene expression in human macrophages, Immunobiology, 210 (2005) 87-95.
[53] K.H. Park-Min, T.T. Antoniv, L.B. Ivashkiv, Regulation of macrophage phenotype by long-term exposure to IL-10, Immunobiology, 210 (2005) 77-86.
[54] F.O. Martinez, S. Gordon, M. Locati, A. Mantovani, Transcriptional profiling of the human monocyte-to-macrophage differentiation and polarization: new molecules and patterns of gene expression, Journal of immunology, 177 (2006) 7303-7311.
[55] L.A. Borthwick, L. Barron, K.M. Hart, K.M. Vannella, R.W. Thompson, S. Oland, A. Cheever, J. Sciurba, T.R. Ramalingam, A.J. Fisher, T.A. Wynn, Macrophages are critical to the maintenance of IL-13-dependent lung inflammation and fibrosis, Mucosal immunology, 9 (2016) 38-55.

[56] R.M. Anthony, J.F. Urban, Jr., F. Alem, H.A. Hamed, C.T. Rozo, J.L. Boucher, N. Van Rooijen, W.C. Gause, Memory T(H)2 cells induce alternatively activated macrophages to mediate protection against nematode parasites, Nature medicine, 12 (2006) 955-960.
[57] K. Pfeffer, T. Matsuyama, T.M. Kundig, A. Wakeham, K. Kishihara, A. Shahinian, K. Wiegmann, P.S. Ohashi, M. Kronke, T.W. Mak, Mice deficient for the 55 kd tumor necrosis factor receptor are resistant to endotoxic shock, yet succumb to L. monocytogenes infection, Cell, 73 (1993) 457-467.
[58] E. Jouanguy, R. Doffinger, S. Dupuis, A. Pallier, F. Altare, J.L. Casanova, IL-12 and IFN-gamma in host defense against mycobacteria and salmonella in mice and men, Current opinion in immunology, 11 (1999) 346-351.
[59] G.R. Thomas, M. McCrossan, M.E. Selkirk, Cytostatic and cytotoxic effects of activated macrophages and nitric oxide donors on Brugia malayi, Infection and immunity, 65 (1997) 2732-2739.
[60] A. Varin, S. Mukhopadhyay, G. Herbein, S. Gordon, Alternative activation of macrophages by IL-4 impairs phagocytosis of pathogens but potentiates microbial-induced signalling and cytokine secretion, Blood, 115 (2010) 353-362.
[61] M. Benoit, B. Desnues, J.L. Mege, Macrophage polarization in bacterial infections, Journal of immunology, 181 (2008) 3733-3739.
[62] R. Noy, J.W. Pollard, Tumor-associated macrophages: from mechanisms to therapy, Immunity, 41 (2014) 49-61.
[63] Y. Zhang, A. Jeltsch, The application of next generation sequencing in DNA methylation analysis, Genes, 1 (2010) 85-101.
[64] M. Tsompana, M.J. Buck, Chromatin accessibility: a window into the genome, Epigenetics & chromatin, 7 (2014) 33.
[65] G.A. Maston, S.G. Landt, M. Snyder, M.R. Green, Characterization of enhancer function from genome-wide analyses, Annual review of genomics and human genetics, 13 (2012) 29-57.
[66] N. Hah, W.L. Kraus, Hormone-regulated transcriptomes: lessons learned from estrogen signaling pathways in breast cancer cells, Molecular and cellular endocrinology, 382 (2014) 652-664.
[67] B. Daniel, G. Nagy, L. Nagy, The intriguing complexities of mammalian gene regulation: how to link enhancers to regulated genes. Are we there yet?, FEBS letters, 588 (2014) 2379-2391.
[68] T. Juven-Gershon, J.T. Kadonaga, Regulation of gene expression via the core promoter and the basal transcriptional machinery, Developmental biology, 339 (2010) 225-229.
[69] A. Barski, S. Cuddapah, K. Cui, T.Y. Roh, D.E. Schones, Z. Wang, G. Wei, I. Chepelev, K. Zhao, High-resolution profiling of histone methylations in the human genome, Cell, 129 (2007) 823-837.
[70] X. Xie, J. Lu, E.J. Kulbokas, T.R. Golub, V. Mootha, K. Lindblad-Toh, E.S. Lander, M. Kellis, Systematic discovery of regulatory motifs in human promoters and 3' UTRs by comparison of several mammals, Nature, 434 (2005) 338-345.
[71] M.A. Zabidi, A. Stark, Regulatory Enhancer-Core-Promoter Communication via Transcription Factors and Cofactors, Trends in genetics : TIG, 32 (2016) 801-814.
[72] N.D. Heintzman, R.K. Stuart, G. Hon, Y. Fu, C.W. Ching, R.D. Hawkins, L.O. Barrera, S. Van Calcar, C. Qu, K.A. Ching, W. Wang, Z. Weng, R.D. Green, G.E. Crawford, B. Ren, Distinct and predictive chromatin signatures of transcriptional promoters and enhancers in the human genome, Nature genetics, 39 (2007) 311-318.
[73] W.A. Whyte, D.A. Orlando, D. Hnisz, B.J. Abraham, C.Y. Lin, M.H. Kagey, P.B. Rahl, T.I. Lee, R.A. Young, Master transcription factors and mediator establish super-enhancers at key cell identity genes, Cell, 153 (2013) 307-319.
[74] D. Hnisz, B.J. Abraham, T.I. Lee, A. Lau, V. Saint-Andre, A.A. Sigova, H.A. Hoke, R.A. Young, Super-enhancers in the control of cell identity and disease, Cell, 155 (2013) 934-947.
[75] C.K. Glass, G. Natoli, Molecular control of activation and priming in macrophages, Nature immunology, 17 (2016) 26-33.
[76] Y. Zhu, L. Sun, Z. Chen, J.W. Whitaker, T. Wang, W. Wang, Predicting enhancer transcription and activity from chromatin modifications, Nucleic acids research, 41 (2013) 10032-10043.

[77] O. Bogdanovic, A. Fernandez-Minan, J.J. Tena, E. de la Calle-Mustienes, C. Hidalgo, I. van Kruysbergen, S.J. van Heeringen, G.J. Veenstra, J.L. Gomez-Skarmeta, Dynamics of enhancer chromatin signatures mark the transition from pluripotency to cell specification during embryogenesis, Genome research, 22 (2012) 2043-2053.
[78] R.L. Schiltz, C.A. Mizzen, A. Vassilev, R.G. Cook, C.D. Allis, Y. Nakatani, Overlapping but distinct patterns of histone acetylation by the human coactivators p300 and PCAF within nucleosomal substrates, The Journal of biological chemistry, 274 (1999) 1189-1192.
[79] H.J. Szerlong, J.E. Prenni, J.K. Nyborg, J.C. Hansen, Activator-dependent p300 acetylation of chromatin in vitro: enhancement of transcription by disruption of repressive nucleosome-nucleosome interactions, The Journal of biological chemistry, 285 (2010) 31954-31964.
[80] Q. Jin, L.R. Yu, L. Wang, Z. Zhang, L.H. Kasper, J.E. Lee, C. Wang, P.K. Brindle, S.Y. Dent, K. Ge, Distinct roles of GCN5/PCAF-mediated H3K9ac and CBP/p300-mediated H3K18/27ac in nuclear receptor transactivation, The EMBO journal, 30 (2011) 249-262.
[81] A. Visel, M.J. Blow, Z. Li, T. Zhang, J.A. Akiyama, A. Holt, I. Plajzer-Frick, M. Shoukry, C. Wright, F. Chen, V. Afzal, B. Ren, E.M. Rubin, L.A. Pennacchio, ChIP-seq accurately predicts tissue-specific activity of enhancers, Nature, 457 (2009) 854-858.
[82] S. Ghisletti, I. Barozzi, F. Mietton, S. Polletti, F. De Santa, E. Venturini, L. Gregory, L. Lonie, A. Chew, C.L. Wei, J. Ragoussis, G. Natoli, Identification and characterization of enhancers controlling the inflammatory gene expression program in macrophages, Immunity, 32 (2010) 317-328.
[83] V. Perissi, K. Jepsen, C.K. Glass, M.G. Rosenfeld, Deconstructing repression: evolving models of co-repressor action, Nature reviews. Genetics, 11 (2010) 109-123.
[84] R. Margueron, D. Reinberg, The Polycomb complex PRC2 and its mark in life, Nature, 469 (2011) 343-349.
[85] W.A. Whyte, S. Bilodeau, D.A. Orlando, H.A. Hoke, G.M. Frampton, C.T. Foster, S.M. Cowley, R.A. Young, Enhancer decommissioning by LSD1 during embryonic stem cell differentiation, Nature, 482 (2012) 221-225.
[86] A.D. Schmitt, M. Hu, B. Ren, Genome-wide mapping and analysis of chromosome architecture, Nature reviews. Molecular cell biology, 17 (2016) 743-755.
[87] S. Sati, G. Cavalli, Chromosome conformation capture technologies and their impact in understanding genome function, Chromosoma, 126 (2017) 33-44.
[88] A.S. Hansen, C. Cattoglio, X. Darzacq, R. Tjian, Recent evidence that TADs and chromatin loops are dynamic structures, Nucleus, (2017) 1-13.
[89] B.A. Bouwman, W. de Laat, Getting the genome in shape: the formation of loops, domains and compartments, Genome biology, 16 (2015) 154.
[90] W. de Laat, D. Duboule, Topology of mammalian developmental enhancers and their regulatory landscapes, Nature, 502 (2013) 499-506.
[91] S.S. Rao, M.H. Huntley, N.C. Durand, E.K. Stamenova, I.D. Bochkov, J.T. Robinson, A.L. Sanborn, I. Machol, A.D. Omer, E.S. Lander, E.L. Aiden, A 3D map of the human genome at kilobase resolution reveals principles of chromatin looping, Cell, 159 (2014) 1665-1680.
[92] R.E. Thurman, E. Rynes, R. Humbert, J. Vierstra, M.T. Maurano, E. Haugen, N.C. Sheffield, A.B. Stergachis, H. Wang, B. Vernot, K. Garg, S. John, R. Sandstrom, D. Bates, L. Boatman, T.K. Canfield, M. Diegel, D. Dunn, A.K. Ebersol, T. Frum, E. Giste, A.K. Johnson, E.M. Johnson, T. Kutyavin, B. Lajoie, B.K. Lee, K. Lee, D. London, D. Lotakis, S. Neph, F. Neri, E.D. Nguyen, H. Qu, A.P. Reynolds, V. Roach, A. Safi, M.E. Sanchez, A. Sanyal, A. Shafer, J.M. Simon, L. Song, S. Vong, M. Weaver, Y. Yan, Z. Zhang, Z. Zhang, B. Lenhard, M. Tewari, M.O. Dorschner, R.S. Hansen, P.A. Navas, G. Stamatoyannopoulos, V.R. Iyer, J.D. Lieb, S.R. Sunyaev, J.M. Akey, P.J. Sabo, R. Kaul, T.S. Furey, J. Dekker, G.E. Crawford, J.A. Stamatoyannopoulos, The accessible chromatin landscape of the human genome, Nature, 489 (2012) 75-82.
[93] Y. Shen, F. Yue, D.F. McCleary, Z. Ye, L. Edsall, S. Kuan, U. Wagner, J. Dixon, L. Lee, V.V. Lobanenkov, B. Ren, A map of the cis-regulatory sequences in the mouse genome, Nature, 488 (2012) 116-120.

[94] M.H. Kagey, J.J. Newman, S. Bilodeau, Y. Zhan, D.A. Orlando, N.L. van Berkum, C.C. Ebmeier, J. Goossens, P.B. Rahl, S.S. Levine, D.J. Taatjes, J. Dekker, R.A. Young, Mediator and cohesin connect gene expression and chromatin architecture, Nature, 467 (2010) 430-435.
[95] F. Fang, Y. Xu, K.K. Chew, X. Chen, H.H. Ng, P. Matsudaira, Coactivators p300 and CBP maintain the identity of mouse embryonic stem cells by mediating long-range chromatin structure, Stem cells, 32 (2014) 1805-1816.
[96] N. Hah, C.G. Danko, L. Core, J.J. Waterfall, A. Siepel, J.T. Lis, W.L. Kraus, A rapid, extensive, and transient transcriptional response to estrogen signaling in breast cancer cells, Cell, 145 (2011) 622-634.
[97] B. Daniel, G. Nagy, N. Hah, A. Horvath, Z. Czimmerer, S. Poliska, T. Gyuris, J. Keirsse, C. Gysemans, J.A. Van Ginderachter, B.L. Balint, R.M. Evans, E. Barta, L. Nagy, The active enhancer network operated by liganded RXR supports angiogenic activity in macrophages, Genes & development, 28 (2014) 1562-1577.
[98] F.L. Meng, Z. Du, A. Federation, J. Hu, Q. Wang, K.R. Kieffer-Kwon, R.M. Meyers, C. Amor, C.R. Wasserman, D. Neuberg, R. Casellas, M.C. Nussenzweig, J.E. Bradner, X.S. Liu, F.W. Alt, Convergent transcription at intragenic super-enhancers targets AID-initiated genomic instability, Cell, 159 (2014) 1538-1548.
[99] M.U. Kaikkonen, N.J. Spann, S. Heinz, C.E. Romanoski, K.A. Allison, J.D. Stender, H.B. Chun, D.F. Tough, R.K. Prinjha, C. Benner, C.K. Glass, Remodeling of the enhancer landscape during macrophage activation is coupled to enhancer transcription, Molecular cell, 51 (2013) 310-325.
[100] M.T. Lam, H. Cho, H.P. Lesch, D. Gosselin, S. Heinz, Y. Tanaka-Oishi, C. Benner, M.U. Kaikkonen, A.S. Kim, M. Kosaka, C.Y. Lee, A. Watt, T.R. Grossman, M.G. Rosenfeld, R.M. Evans, C.K. Glass, Rev-Erbs repress macrophage gene expression by inhibiting enhancer-directed transcription, Nature, 498 (2013) 511-515.
[101] C.A. Melo, J. Drost, P.J. Wijchers, H. van de Werken, E. de Wit, J.A. Oude Vrielink, R. Elkon, S.A. Melo, N. Leveille, R. Kalluri, W. de Laat, R. Agami, eRNAs are required for p53-dependent enhancer activity and gene transcription, Molecular cell, 49 (2013) 524-535.
[102] C.L. Hsieh, T. Fei, Y. Chen, T. Li, Y. Gao, X. Wang, T. Sun, C.J. Sweeney, G.S. Lee, S. Chen, S.P. Balk, X.S. Liu, M. Brown, P.W. Kantoff, Enhancer RNAs participate in androgen receptor-driven looping that selectively enhances gene activation, Proceedings of the National Academy of Sciences of the United States of America, 111 (2014) 7319-7324.
[103] D. Gosselin, C.K. Glass, Epigenomics of macrophages, Immunological reviews, 262 (2014) 96-112.
[104] S. Heinz, C. Benner, N. Spann, E. Bertolino, Y.C. Lin, P. Laslo, J.X. Cheng, C. Murre, H. Singh, C.K. Glass, Simple combinations of lineage-determining transcription factors prime cis-regulatory elements required for macrophage and B cell identities, Molecular cell, 38 (2010) 576-589.
[105] S.R. McKercher, B.E. Torbett, K.L. Anderson, G.W. Henkel, D.J. Vestal, H. Baribault, M. Klemsz, A.J. Feeney, G.E. Wu, C.J. Paige, R.A. Maki, Targeted disruption of the PU.1 gene results in multiple hematopoietic abnormalities, The EMBO journal, 15 (1996) 5647-5658.
[106] A. Mancino, A. Termanini, I. Barozzi, S. Ghisletti, R. Ostuni, E. Prosperini, K. Ozato, G. Natoli, A dual cis-regulatory code links IRF8 to constitutive and inducible gene expression in macrophages, Genes & development, 29 (2015) 394-408.
[107] S. Heinz, C.E. Romanoski, C. Benner, K.A. Allison, M.U. Kaikkonen, L.D. Orozco, C.K. Glass, Effect of natural genetic variation on enhancer selection and function, Nature, 503 (2013) 487-492.
[108] R. Ostuni, V. Piccolo, I. Barozzi, S. Polletti, A. Termanini, S. Bonifacio, A. Curina, E. Prosperini, S. Ghisletti, G. Natoli, Latent enhancers activated by stimulation in differentiated cells, Cell, 152 (2013) 157-171.
[109] E. Treuter, R. Fan, Z. Huang, T. Jakobsson, N. Venteclef, Transcriptional repression in macrophages-basic mechanisms and alterations in metabolic inflammatory diseases, FEBS letters, 591 (2017) 2959-2977.

[110] G.D. Barish, R.T. Yu, M. Karunasiri, C.B. Ocampo, J. Dixon, C. Benner, A.L. Dent, R.K. Tangirala, R.M. Evans, Bcl-6 and NF-kappaB cistromes mediate opposing regulation of the innate immune response, Genes & development, 24 (2010) 2760-2765.
[111] G.D. Barish, R.T. Yu, M.S. Karunasiri, D. Becerra, J. Kim, T.W. Tseng, L.J. Tai, M. Leblanc, C. Diehl, L. Cerchietti, Y.I. Miller, J.L. Witztum, A.M. Melnick, A.L. Dent, R.K. Tangirala, R.M. Evans, The Bcl6-SMRT/NCoR cistrome represses inflammation to attenuate atherosclerosis, Cell metabolism, 15 (2012) 554-562.
[112] P. Li, N.J. Spann, M.U. Kaikkonen, M. Lu, D.Y. Oh, J.N. Fox, G. Bandyopadhyay, S. Talukdar, J. Xu, W.S. Lagakos, D. Patsouris, A. Armando, O. Quehenberger, E.A. Dennis, S.M. Watkins, J. Auwerx, C.K. Glass, J.M. Olefsky, NCoR repression of LXRs restricts macrophage biosynthesis of insulin-sensitizing omega 3 fatty acids, Cell, 155 (2013) 200-214.
[113] S. Ghisletti, W. Huang, S. Ogawa, G. Pascual, M.E. Lin, T.M. Willson, M.G. Rosenfeld, C.K. Glass, Parallel SUMOylation-dependent pathways mediate gene- and signal-specific transrepression by LXRs and PPARgamma, Molecular cell, 25 (2007) 57-70.
[114] S.E. Mullican, C.A. Gaddis, T. Alenghat, M.G. Nair, P.R. Giacomin, L.J. Everett, D. Feng, D.J. Steger, J. Schug, D. Artis, M.A. Lazar, Histone deacetylase 3 is an epigenomic brake in macrophage alternative activation, Genes & development, 25 (2011) 2480-2488.
[115] X. Chen, I. Barozzi, A. Termanini, E. Prosperini, A. Recchiuti, J. Dalli, F. Mietton, G. Matteoli, S. Hiebert, G. Natoli, Requirement for the histone deacetylase Hdac3 for the inflammatory gene expression program in macrophages, Proceedings of the National Academy of Sciences of the United States of America, 109 (2012) E2865-2874.
[116] R. Fan, A. Toubal, S. Goni, K. Drareni, Z. Huang, F. Alzaid, R. Ballaire, P. Ancel, N. Liang, A. Damdimopoulos, I. Hainault, A. Soprani, J. Aron-Wisnewsky, F. Foufelle, T. Lawrence, J.F. Gautier, N. Venteclef, E. Treuter, Loss of the co-repressor GPS2 sensitizes macrophage activation upon metabolic stress induced by obesity and type 2 diabetes, Nature medicine, 22 (2016) 780-791.
[117] D.M. Bhatt, A. Pandya-Jones, A.J. Tong, I. Barozzi, M.M. Lissner, G. Natoli, D.L. Black, S.T. Smale, Transcript dynamics of proinflammatory genes revealed by sequence analysis of subcellular RNA fractions, Cell, 150 (2012) 279-290.
[118] N. Hah, C. Benner, L.W. Chong, R.T. Yu, M. Downes, R.M. Evans, Inflammation-sensitive super enhancers form domains of coordinately regulated enhancer RNAs, Proceedings of the National Academy of Sciences of the United States of America, 112 (2015) E297-302.
[119] M. Ghildiyal, P.D. Zamore, Small silencing RNAs: an expanding universe, Nature reviews. Genetics, 10 (2009) 94-108.
[120] D.P. Bartel, MicroRNAs: genomics, biogenesis, mechanism, and function, Cell, 116 (2004) 281-297.
[121] V.N. Kim, J. Han, M.C. Siomi, Biogenesis of small RNAs in animals, Nature reviews. Molecular cell biology, 10 (2009) 126-139.
[122] Y. Lee, M. Kim, J. Han, K.H. Yeom, S. Lee, S.H. Baek, V.N. Kim, MicroRNA genes are transcribed by RNA polymerase II, The EMBO journal, 23 (2004) 4051-4060.
[123] G.M. Borchert, W. Lanier, B.L. Davidson, RNA polymerase III transcribes human microRNAs, Nature structural & molecular biology, 13 (2006) 1097-1101.
[124] Y. Lee, C. Ahn, J. Han, H. Choi, J. Kim, J. Yim, J. Lee, P. Provost, O. Radmark, S. Kim, V.N. Kim, The nuclear RNase III Drosha initiates microRNA processing, Nature, 425 (2003) 415-419.
[125] J. Han, Y. Lee, K.H. Yeom, Y.K. Kim, H. Jin, V.N. Kim, The Drosha-DGCR8 complex in primary microRNA processing, Genes & development, 18 (2004) 3016-3027.
[126] M. Landthaler, A. Yalcin, T. Tuschl, The human DiGeorge syndrome critical region gene 8 and Its D. melanogaster homolog are required for miRNA biogenesis, Current biology : CB, 14 (2004) 2162-2167.
[127] Y. Wang, R. Medvid, C. Melton, R. Jaenisch, R. Blelloch, DGCR8 is essential for microRNA biogenesis and silencing of embryonic stem cell self-renewal, Nature genetics, 39 (2007) 380-385.
[128] R.I. Gregory, K.P. Yan, G. Amuthan, T. Chendrimada, B. Doratotaj, N. Cooch, R. Shiekhattar, The Microprocessor complex mediates the genesis of microRNAs, Nature, 432 (2004) 235-240.

[129] A.M. Denli, B.B. Tops, R.H. Plasterk, R.F. Ketting, G.J. Hannon, Processing of primary microRNAs by the Microprocessor complex, Nature, 432 (2004) 231-235.
[130] Y.K. Kim, V.N. Kim, Processing of intronic microRNAs, The EMBO journal, 26 (2007) 775-783.
[131] J. Han, J.S. Pedersen, S.C. Kwon, C.D. Belair, Y.K. Kim, K.H. Yeom, W.Y. Yang, D. Haussler, R. Blelloch, V.N. Kim, Posttranscriptional crossregulation between Drosha and DGCR8, Cell, 136 (2009) 75-84.
[132] E. Lund, S. Guttinger, A. Calado, J.E. Dahlberg, U. Kutay, Nuclear export of microRNA precursors, Science, 303 (2004) 95-98.
[133] M.T. Bohnsack, K. Czaplinski, D. Gorlich, Exportin 5 is a RanGTP-dependent dsRNA-binding protein that mediates nuclear export of pre-miRNAs, Rna, 10 (2004) 185-191.
[134] G. Hutvagner, J. McLachlan, A.E. Pasquinelli, E. Balint, T. Tuschl, P.D. Zamore, A cellular function for the RNA-interference enzyme Dicer in the maturation of the let-7 small temporal RNA, Science, 293 (2001) 834-838.
[135] S.W. Knight, B.L. Bass, A role for the RNase III enzyme DCR-1 in RNA interference and germ line development in Caenorhabditis elegans, Science, 293 (2001) 2269-2271.
[136] J. Winter, S. Jung, S. Keller, R.I. Gregory, S. Diederichs, Many roads to maturity: microRNA biogenesis pathways and their regulation, Nature cell biology, 11 (2009) 228-234.
[137] S.M. Hammond, S. Boettcher, A.A. Caudy, R. Kobayashi, G.J. Hannon, Argonaute2, a link between genetic and biochemical analyses of RNAi, Science, 293 (2001) 1146-1150.
[138] T. Kawamata, Y. Tomari, Making RISC, Trends in biochemical sciences, 35 (2010) 368-376.
[139] A. Khvorova, A. Reynolds, S.D. Jayasena, Functional siRNAs and miRNAs exhibit strand bias, Cell, 115 (2003) 209-216.
[140] H.Y. Hu, Z. Yan, Y. Xu, H. Hu, C. Menzel, Y.H. Zhou, W. Chen, P. Khaitovich, Sequence features associated with microRNA strand selection in humans and flies, BMC genomics, 10 (2009) 413.
[141] E. Berezikov, W.J. Chung, J. Willis, E. Cuppen, E.C. Lai, Mammalian mirtron genes, Molecular cell, 28 (2007) 328-336.
[142] J.G. Ruby, C.H. Jan, D.P. Bartel, Intronic microRNA precursors that bypass Drosha processing, Nature, 448 (2007) 83-86.
[143] M. Xie, M. Li, A. Vilborg, N. Lee, M.D. Shu, V. Yartseva, N. Sestan, J.A. Steitz, Mammalian 5'-capped microRNA precursors that generate a single microRNA, Cell, 155 (2013) 1568-1580.
[144] J.E. Babiarz, J.G. Ruby, Y. Wang, D.P. Bartel, R. Blelloch, Mouse ES cells express endogenous shRNAs, siRNAs, and other Microprocessor-independent, Dicer-dependent small RNAs, Genes & development, 22 (2008) 2773-2785.
[145] D. Cifuentes, H. Xue, D.W. Taylor, H. Patnode, Y. Mishima, S. Cheloufi, E. Ma, S. Mane, G.J. Hannon, N.D. Lawson, S.A. Wolfe, A.J. Giraldez, A novel miRNA processing pathway independent of Dicer requires Argonaute2 catalytic activity, Science, 328 (2010) 1694-1698.
[146] J.S. Yang, T. Maurin, N. Robine, K.D. Rasmussen, K.L. Jeffrey, R. Chandwani, E.P. Papapetrou, M. Sadelain, D. O'Carroll, E.C. Lai, Conserved vertebrate mir-451 provides a platform for Dicer-independent, Ago2-mediated microRNA biogenesis, Proceedings of the National Academy of Sciences of the United States of America, 107 (2010) 15163-15168.
[147] J. Krol, I. Loedige, W. Filipowicz, The widespread regulation of microRNA biogenesis, function and decay, Nature reviews. Genetics, 11 (2010) 597-610.
[148] M.R. Fabian, N. Sonenberg, W. Filipowicz, Regulation of mRNA translation and stability by microRNAs, Annual review of biochemistry, 79 (2010) 351-379.
[149] D.P. Bartel, MicroRNAs: target recognition and regulatory functions, Cell, 136 (2009) 215-233.
[150] W. Filipowicz, S.N. Bhattacharyya, N. Sonenberg, Mechanisms of post-transcriptional regulation by microRNAs: are the answers in sight?, Nature reviews. Genetics, 9 (2008) 102-114.
[151] A. Grimson, K.K. Farh, W.K. Johnston, P. Garrett-Engele, L.P. Lim, D.P. Bartel, MicroRNA targeting specificity in mammals: determinants beyond seed pairing, Molecular cell, 27 (2007) 91-105.
[152] J.G. Doench, P.A. Sharp, Specificity of microRNA target selection in translational repression, Genes & development, 18 (2004) 504-511.

[153] M. Wakiyama, K. Takimoto, O. Ohara, S. Yokoyama, Let-7 microRNA-mediated mRNA deadenylation and translational repression in a mammalian cell-free system, Genes & development, 21 (2007) 1857-1862.
[154] A. Zdanowicz, R. Thermann, J. Kowalska, J. Jemielity, K. Duncan, T. Preiss, E. Darzynkiewicz, M.W. Hentze, Drosophila miR2 primarily targets the m7GpppN cap structure for translational repression, Molecular cell, 35 (2009) 881-888.
[155] G. Mathonnet, M.R. Fabian, Y.V. Svitkin, A. Parsyan, L. Huck, T. Murata, S. Biffo, W.C. Merrick, E. Darzynkiewicz, R.S. Pillai, W. Filipowicz, T.F. Duchaine, N. Sonenberg, MicroRNA inhibition of translation initiation in vitro by targeting the cap-binding complex eIF4F, Science, 317 (2007) 1764-1767.
[156] B. Wang, A. Yanez, C.D. Novina, MicroRNA-repressed mRNAs contain 40S but not 60S components, Proceedings of the National Academy of Sciences of the United States of America, 105 (2008) 5343-5348.
[157] T.P. Chendrimada, K.J. Finn, X. Ji, D. Baillat, R.I. Gregory, S.A. Liebhaber, A.E. Pasquinelli, R. Shiekhattar, MicroRNA silencing through RISC recruitment of eIF6, Nature, 447 (2007) 823-828.
[158] P.A. Maroney, Y. Yu, J. Fisher, T.W. Nilsen, Evidence that microRNAs are associated with translating messenger RNAs in human cells, Nature structural & molecular biology, 13 (2006) 1102-1107.
[159] C.P. Petersen, M.E. Bordeleau, J. Pelletier, P.A. Sharp, Short RNAs repress translation after initiation in mammalian cells, Molecular cell, 21 (2006) 533-542.
[160] S. Nottrott, M.J. Simard, J.D. Richter, Human let-7a miRNA blocks protein production on actively translating polyribosomes, Nature structural & molecular biology, 13 (2006) 1108-1114.
[161] I. Behm-Ansmant, J. Rehwinkel, T. Doerks, A. Stark, P. Bork, E. Izaurralde, mRNA degradation by miRNAs and GW182 requires both CCR4:NOT deadenylase and DCP1:DCP2 decapping complexes, Genes & development, 20 (2006) 1885-1898.
[162] K.D. Taganov, M.P. Boldin, K.J. Chang, D. Baltimore, NF-kappaB-dependent induction of microRNA miR-146, an inhibitor targeted to signaling proteins of innate immune responses, Proceedings of the National Academy of Sciences of the United States of America, 103 (2006) 12481-12486.
[163] C.E. Monk, G. Hutvagner, J.S. Arthur, Regulation of miRNA transcription in macrophages in response to Candida albicans, PloS one, 5 (2010) e13669.
[164] A.K. Schnitger, A. Machova, R.U. Mueller, A. Androulidaki, B. Schermer, M. Pasparakis, M. Kronke, N. Papadopoulou, Listeria monocytogenes infection in macrophages induces vacuolar-dependent host miRNA response, PloS one, 6 (2011) e27435.
[165] Y. Singh, V. Kaul, A. Mehra, S. Chatterjee, S. Tousif, V.P. Dwivedi, M. Suar, L. Van Kaer, W.R. Bishai, G. Das, Mycobacterium tuberculosis controls microRNA-99b (miR-99b) expression in infected murine dendritic cells to modulate host immunity, The Journal of biological chemistry, 288 (2013) 5056-5061.
[166] R.M. O'Connell, K.D. Taganov, M.P. Boldin, G. Cheng, D. Baltimore, MicroRNA-155 is induced during the macrophage inflammatory response, Proceedings of the National Academy of Sciences of the United States of America, 104 (2007) 1604-1609.
[167] E. Tili, J.J. Michaille, A. Cimino, S. Costinean, C.D. Dumitru, B. Adair, M. Fabbri, H. Alder, C.G. Liu, G.A. Calin, C.M. Croce, Modulation of miR-155 and miR-125b levels following lipopolysaccharide/TNF-alpha stimulation and their possible roles in regulating the response to endotoxin shock, Journal of immunology, 179 (2007) 5082-5089.
[168] Y. Cheng, W. Kuang, Y. Hao, D. Zhang, M. Lei, L. Du, H. Jiao, X. Zhang, F. Wang, Downregulation of miR-27a* and miR-532-5p and upregulation of miR-146a and miR-155 in LPS-induced RAW264.7 macrophage cells, Inflammation, 35 (2012) 1308-1313.
[169] G. Liu, A. Friggeri, Y. Yang, Y.J. Park, Y. Tsuruta, E. Abraham, miR-147, a microRNA that is induced upon Toll-like receptor stimulation, regulates murine macrophage inflammatory responses, Proceedings of the National Academy of Sciences of the United States of America, 106 (2009) 15819-15824.

[170] X.Q. Cheng, L.J. Song, H. Li, H. Di, Y.Y. Zhang, D.F. Chen, Beneficial effect of the polysaccharides from Bupleurum smithii var. parvifolium on "two-hit" acute lung injury in rats, Inflammation, 35 (2012) 1715-1722.
[171] K.A. Jablonski, A.D. Gaudet, S.A. Amici, P.G. Popovich, M. Guerau-de-Arellano, Control of the Inflammatory Macrophage Transcriptional Signature by miR-155, PloS one, 11 (2016) e0159724.
[172] F. Xu, Y. Kang, H. Zhang, Z. Piao, H. Yin, R. Diao, J. Xia, L. Shi, Akt1-mediated regulation of macrophage polarization in a murine model of Staphylococcus aureus pulmonary infection, The Journal of infectious diseases, 208 (2013) 528-538.
[173] R.M. O'Connell, A.A. Chaudhuri, D.S. Rao, D. Baltimore, Inositol phosphatase SHIP1 is a primary target of miR-155, Proceedings of the National Academy of Sciences of the United States of America, 106 (2009) 7113-7118.
[174] M. Nazari-Jahantigh, Y. Wei, H. Noels, S. Akhtar, Z. Zhou, R.R. Koenen, K. Heyll, F. Gremse, F. Kiessling, J. Grommes, C. Weber, A. Schober, MicroRNA-155 promotes atherosclerosis by repressing Bcl6 in macrophages, The Journal of clinical investigation, 122 (2012) 4190-4202.
[175] M. He, Z. Xu, T. Ding, D.M. Kuang, L. Zheng, MicroRNA-155 regulates inflammatory cytokine production in tumor-associated macrophages via targeting C/EBPbeta, Cellular & molecular immunology, 6 (2009) 343-352.
[176] R.T. Martinez-Nunez, F. Louafi, T. Sanchez-Elsner, The interleukin 13 (IL-13) pathway in human macrophages is modulated by microRNA-155 via direct targeting of interleukin 13 receptor alpha1 (IL13Ralpha1), The Journal of biological chemistry, 286 (2011) 1786-1794.
[177] D. Ruckerl, S.J. Jenkins, N.N. Laqtom, I.J. Gallagher, T.E. Sutherland, S. Duncan, A.H. Buck, J.E. Allen, Induction of IL-4Ralpha-dependent microRNAs identifies PI3K/Akt signaling as essential for IL-4-driven murine macrophage proliferation in vivo, Blood, 120 (2012) 2307-2316.
[178] T. Veremeyko, S. Siddiqui, I. Sotnikov, A. Yung, E.D. Ponomarev, IL-4/IL-13-dependent and independent expression of miR-124 and its contribution to M2 phenotype of monocytic cells in normal conditions and during allergic inflammation, PloS one, 8 (2013) e81774.
[179] D. Karo-Atar, M. Itan, M. Pasmanik-Chor, A. Munitz, MicroRNA profiling reveals opposing expression patterns for miR-511 in alternatively and classically activated macrophages, The Journal of asthma : official journal of the Association for the Care of Asthma, 52 (2015) 545-553.
[180] J.W. Graff, A.M. Dickson, G. Clay, A.P. McCaffrey, M.E. Wilson, Identifying functional microRNAs in macrophages with polarized phenotypes, The Journal of biological chemistry, 287 (2012) 21816-21825.
[181] B. Tang, B. Xiao, Z. Liu, N. Li, E.D. Zhu, B.S. Li, Q.H. Xie, Y. Zhuang, Q.M. Zou, X.H. Mao, Identification of MyD88 as a novel target of miR-155, involved in negative regulation of Helicobacter pylori-induced inflammation, FEBS letters, 584 (2010) 1481-1486.
[182] J. Hou, P. Wang, L. Lin, X. Liu, F. Ma, H. An, Z. Wang, X. Cao, MicroRNA-146a feedback inhibits RIG-I-dependent Type I IFN production in macrophages by targeting TRAF6, IRAK1, and IRAK2, Journal of immunology, 183 (2009) 2150-2158.
[183] A.A. Chaudhuri, A.Y. So, N. Sinha, W.S. Gibson, K.D. Taganov, R.M. O'Connell, D. Baltimore, MicroRNA-125b potentiates macrophage activation, Journal of immunology, 187 (2011) 5062-5068.
[184] S.W. Kim, K. Ramasamy, H. Bouamar, A.P. Lin, D. Jiang, R.C. Aguiar, MicroRNAs miR-125a and miR-125b constitutively activate the NF-kappaB pathway by targeting the tumor necrosis factor alpha-induced protein 3 (TNFAIP3, A20), Proceedings of the National Academy of Sciences of the United States of America, 109 (2012) 7865-7870.
[185] S. Banerjee, H. Cui, N. Xie, Z. Tan, S. Yang, M. Icyuz, V.J. Thannickal, E. Abraham, G. Liu, miR-125a-5p regulates differential activation of macrophages and inflammation, The Journal of biological chemistry, 288 (2013) 35428-35436.
[186] Q. Chen, H. Wang, Y. Liu, Y. Song, L. Lai, Q. Han, X. Cao, Q. Wang, Inducible microRNA-223 down-regulation promotes TLR-triggered IL-6 and IL-1beta production in macrophages by targeting STAT3, PloS one, 7 (2012) e42971.
[187] Y. Chen, S.X. Wang, R. Mu, X. Luo, Z.S. Liu, B. Liang, H.L. Zhuo, X.P. Hao, Q. Wang, D.F. Fang, Z.F. Bai, Q.Y. Wang, H.M. Wang, B.F. Jin, W.L. Gong, T. Zhou, X.M. Zhang, Q. Xia, T. Li, Dysregulation

of the miR-324-5p-CUEDC2 axis leads to macrophage dysfunction and is associated with colon cancer, Cell reports, 7 (2014) 1982-1993.
[188] M.L. Squadrito, F. Pucci, L. Magri, D. Moi, G.D. Gilfillan, A. Ranghetti, A. Casazza, M. Mazzone, R. Lyle, L. Naldini, M. De Palma, miR-511-3p modulates genetic programs of tumor-associated macrophages, Cell reports, 1 (2012) 141-154.
[189] C. Baer, M.L. Squadrito, D. Laoui, D. Thompson, S.K. Hansen, A. Kiialainen, S. Hoves, C.H. Ries, C.H. Ooi, M. De Palma, Suppression of microRNA activity amplifies IFN-gamma-induced macrophage activation and promotes anti-tumour immunity, Nature cell biology, 18 (2016) 790-802.
[190] S.J. Jenkins, D. Ruckerl, P.C. Cook, L.H. Jones, F.D. Finkelman, N. van Rooijen, A.S. MacDonald, J.E. Allen, Local macrophage proliferation, rather than recruitment from the blood, is a signature of TH2 inflammation, Science, 332 (2011) 1284-1288.
[191] C.J. Johnston, E. Robertson, Y. Harcus, J.R. Grainger, G. Coakley, D.J. Smyth, H.J. McSorley, R. Maizels, Cultivation of Heligmosomoides polygyrus: an immunomodulatory nematode parasite and its secreted products, Journal of visualized experiments : JoVE, (2015) e52412.
[192] S.K. Hoiseth, B.A. Stocker, Aromatic-dependent Salmonella typhimurium are non-virulent and effective as live vaccines, Nature, 291 (1981) 238-239.
[193] D. Ruckerl, S.M. Campbell, S. Duncan, T.E. Sutherland, S.J. Jenkins, J.P. Hewitson, T.A. Barr, L.H. Jackson-Jones, R.M. Maizels, J.E. Allen, Macrophage origin limits functional plasticity in helminth-bacterial co-infection, PLoS pathogens, 13 (2017) e1006233.
[194] L. Gandino, L. Varesio, Immortalization of macrophages from mouse bone marrow and fetal liver, Experimental cell research, 188 (1990) 192-198.
[195] G.D. Barish, M. Downes, W.A. Alaynick, R.T. Yu, C.B. Ocampo, A.L. Bookout, D.J. Mangelsdorf, R.M. Evans, A Nuclear Receptor Atlas: macrophage activation, Mol Endocrinol, 19 (2005) 2466-2477.
[196] J.D. Buenrostro, P.G. Giresi, L.C. Zaba, H.Y. Chang, W.J. Greenleaf, Transposition of native chromatin for fast and sensitive epigenomic profiling of open chromatin, DNA-binding proteins and nucleosome position, Nat Methods, 10 (2013) 1213-1218.
[197] C. Trapnell, D.G. Hendrickson, M. Sauvageau, L. Goff, J.L. Rinn, L. Pachter, Differential analysis of gene regulation at transcript resolution with RNA-seq, Nature biotechnology, 31 (2013) 46-53.
[198] A. Subramanian, P. Tamayo, V.K. Mootha, S. Mukherjee, B.L. Ebert, M.A. Gillette, A. Paulovich, S.L. Pomeroy, T.R. Golub, E.S. Lander, J.P. Mesirov, Gene set enrichment analysis: a knowledge-based approach for interpreting genome-wide expression profiles, Proceedings of the National Academy of Sciences of the United States of America, 102 (2005) 15545-15550.
[199] W. Huang da, B.T. Sherman, R.A. Lempicki, Systematic and integrative analysis of large gene lists using DAVID bioinformatics resources, Nature protocols, 4 (2009) 44-57.
[200] R. Stadhouders, P. Kolovos, R. Brouwer, J. Zuin, A. van den Heuvel, C. Kockx, R.J. Palstra, K.S. Wendt, F. Grosveld, W. van Ijcken, E. Soler, Multiplexed chromosome conformation capture sequencing for rapid genome-scale high-resolution detection of long-range chromatin interactions, Nature protocols, 8 (2013) 509-524.
[201] H. Li, R. Durbin, Fast and accurate short read alignment with Burrows-Wheeler transform, Bioinformatics, 25 (2009) 1754-1760.
[202] U.M. Thongjuea S, Medicine WIoM, Oxford Uo and UK, r3Cseq: Analysis of Chromosome Conformation Capture and Next-generation Sequencing (3C-seq). (2016).
[203] P. Flicek, M.R. Amode, D. Barrell, K. Beal, K. Billis, S. Brent, D. Carvalho-Silva, P. Clapham, G. Coates, S. Fitzgerald, L. Gil, C.G. Giron, L. Gordon, T. Hourlier, S. Hunt, N. Johnson, T. Juettemann, A.K. Kahari, S. Keenan, E. Kulesha, F.J. Martin, T. Maurel, W.M. McLaren, D.N. Murphy, R. Nag, B. Overduin, M. Pignatelli, B. Pritchard, E. Pritchard, H.S. Riat, M. Ruffier, D. Sheppard, K. Taylor, A. Thormann, S.J. Trevanion, A. Vullo, S.P. Wilder, M. Wilson, A. Zadissa, B.L. Aken, E. Birney, F. Cunningham, J. Harrow, J. Herrero, T.J. Hubbard, R. Kinsella, M. Muffato, A. Parker, G. Spudich, A. Yates, D.R. Zerbino, S.M. Searle, Ensembl 2014, Nucleic acids research, 42 (2014) D749-755.
[204] A. Kozomara, S. Griffiths-Jones, miRBase: annotating high confidence microRNAs using deep sequencing data, Nucleic Acids Res, 42 (2014) D68-73.

[205] B. Langmead, C. Trapnell, M. Pop, S.L. Salzberg, Ultrafast and memory-efficient alignment of short DNA sequences to the human genome, Genome Biol, 10 (2009) R25.
[206] M. Lawrence, W. Huber, H. Pages, P. Aboyoun, M. Carlson, R. Gentleman, M.T. Morgan, V.J. Carey, Software for computing and annotating genomic ranges, PLoS computational biology, 9 (2013) e1003118.
[207] R.C. Team, R: A language and environment for statistical computing., in, 2015.
[208] X. Zhou, H. Lindsay, M.D. Robinson, Robustly detecting differential expression in RNA sequencing data using observation weights, Nucleic Acids Res, 42 (2014) e91.
[209] Y.B.a.Y. Hochberg, Controlling the False Discovery Rate: A Practical and Powerful Approach to Multiple Testing, Journal of the Royal Statistical Society. Series B (Methodological), 57 (1995) 289 – 300.
[210] E. Barta, Command line analysis of ChIP-seq results, 2011.
[211] Y. Zhang, T. Liu, C.A. Meyer, J. Eeckhoute, D.S. Johnson, B.E. Bernstein, C. Nusbaum, R.M. Myers, M. Brown, W. Li, X.S. Liu, Model-based analysis of ChIP-Seq (MACS), Genome biology, 9 (2008) R137.
[212] E.P. Consortium, An integrated encyclopedia of DNA elements in the human genome, Nature, 489 (2012) 57-74.
[213] C.S. Ross-Innes, R. Stark, A.E. Teschendorff, K.A. Holmes, H.R. Ali, M.J. Dunning, G.D. Brown, O. Gojis, I.O. Ellis, A.R. Green, S. Ali, S.F. Chin, C. Palmieri, C. Caldas, J.S. Carroll, Differential oestrogen receptor binding is associated with clinical outcome in breast cancer, Nature, 481 (2012) 389-393.
[214] H.A. Kestler, A. Muller, J.M. Kraus, M. Buchholz, T.M. Gress, H. Liu, D.W. Kane, B.R. Zeeberg, J.N. Weinstein, VennMaster: area-proportional Euler diagrams for functional GO analysis of microarrays, BMC bioinformatics, 9 (2008) 67.
[215] H. Thorvaldsdottir, J.T. Robinson, J.P. Mesirov, Integrative Genomics Viewer (IGV): high-performance genomics data visualization and exploration, Briefings in bioinformatics, 14 (2013) 178-192.
[216] L. Shen, N. Shao, X. Liu, E. Nestler, ngs.plot: Quick mining and visualization of next-generation sequencing data by integrating genomic databases, BMC genomics, 15 (2014) 284.
[217] A.S. Hinrichs, D. Karolchik, R. Baertsch, G.P. Barber, G. Bejerano, H. Clawson, M. Diekhans, T.S. Furey, R.A. Harte, F. Hsu, J. Hillman-Jackson, R.M. Kuhn, J.S. Pedersen, A. Pohl, B.J. Raney, K.R. Rosenbloom, A. Siepel, K.E. Smith, C.W. Sugnet, A. Sultan-Qurraie, D.J. Thomas, H. Trumbower, R.J. Weber, M. Weirauch, A.S. Zweig, D. Haussler, W.J. Kent, The UCSC Genome Browser Database: update 2006, Nucleic acids research, 34 (2006) D590-598.
[218] L. Gautier, L. Cope, B.M. Bolstad, R.A. Irizarry, affy--analysis of Affymetrix GeneChip data at the probe level, Bioinformatics, 20 (2004) 307-315.
[219] M. Carlson, org.Mm.eg.db: Genome wide annotation for Mouse.
[220] T.B. Project, mogene10stv1cdf: mogene10stv1cdf.
[221] R.A. Irizarry, B. Hobbs, F. Collin, Y.D. Beazer-Barclay, K.J. Antonellis, U. Scherf, T.P. Speed, Exploration, normalization, and summaries of high density oligonucleotide array probe level data, Biostatistics, 4 (2003) 249-264.
[222] G.K. Smyth, Linear models and empirical bayes methods for assessing differential expression in microarray experiments, Stat Appl Genet Mol Biol, 3 (2004) Article3.
[223] S. van Dongen, C. Abreu-Goodger, A.J. Enright, Detecting microRNA binding and siRNA off-target effects from expression data, Nat Methods, 5 (2008) 1023-1025.
[224] C. Ovando-Vazquez, D. Lepe-Soltero, C. Abreu-Goodger, Improving microRNA target prediction with gene expression profiles, BMC genomics, 17 (2016) 364.
[225] D.M. Garcia, D. Baek, C. Shin, G.W. Bell, A. Grimson, D.P. Bartel, Weak seed-pairing stability and high target-site abundance decrease the proficiency of lsy-6 and other microRNAs, Nature structural & molecular biology, 18 (2011) 1139-1146.
[226] M. Reczko, M. Maragkakis, P. Alexiou, I. Grosse, A.G. Hatzigeorgiou, Functional microRNA targets in protein coding sequences, Bioinformatics, 28 (2012) 771-776.
[227] M. Carlson, TxDb.Mmusculus.UCSC.mm10.ensGene: Annotation package for TxDb object(s).

[228] M. Lawrence, R. Gentleman, V. Carey, rtracklayer: an R package for interfacing with genome browsers, Bioinformatics, 25 (2009) 1841-1842.
[229] I.M. Corraliza, M.L. Campo, G. Soler, M. Modolell, Determination of arginase activity in macrophages: a micromethod, J Immunol Methods, 174 (1994) 231-235.
[230] A. Prowse, E. Wolvetang, P. Gray, A rapid, cost-effective method for counting human embryonic stem cell numbers as clumps, Biotechniques, 47 (2009) 599-606.
[231] G. Repetto, A. del Peso, J.L. Zurita, Neutral red uptake assay for the estimation of cell viability/cytotoxicity, Nat Protoc, 3 (2008) 1125-1131.
[232] E. Miko, Z. Margitai, Z. Czimmerer, I. Varkonyi, B. Dezso, A. Lanyi, Z. Bacso, B. Scholtz, miR-126 inhibits proliferation of small cell lung cancer cells by targeting SLC7A5, FEBS Lett, 585 (2011) 1191-1196.
[233] M.X. Doan, A.K. Sarvari, P. Fischer-Posovszky, M. Wabitsch, Z. Balajthy, L. Fesus, Z. Bacso, High content analysis of differentiation and cell death in human adipocytes, Cytometry A, (2013).
[234] M.N. Poy, L. Eliasson, J. Krutzfeldt, S. Kuwajima, X. Ma, P.E. Macdonald, S. Pfeffer, T. Tuschl, N. Rajewsky, P. Rorsman, M. Stoffel, A pancreatic islet-specific microRNA regulates insulin secretion, Nature, 432 (2004) 226-230.
[235] H. Dickensheets, N. Vazquez, F. Sheikh, S. Gingras, P.J. Murray, J.J. Ryan, R.P. Donnelly, Suppressor of cytokine signaling-1 is an IL-4-inducible gene in macrophages and feedback inhibits IL-4 signaling, Genes and immunity, 8 (2007) 21-27.
[236] G.D. Thomas, D. Ruckerl, B.H. Maskrey, P.D. Whitfield, M.L. Blaxter, J.E. Allen, The biology of nematode- and IL4Ralpha-dependent murine macrophage polarization in vivo as defined by RNA-Seq and targeted lipidomics, Blood, 120 (2012) e93-e104.
[237] T. Xiao, J. Wallace, G. Felsenfeld, Specific sites in the C terminus of CTCF interact with the SA2 subunit of the cohesin complex and are required for cohesin-dependent insulation activity, Mol Cell Biol, 31 (2011) 2174-2183.
[238] S. Sofueva, E. Yaffe, W.C. Chan, D. Georgopoulou, M. Vietri Rudan, H. Mira-Bontenbal, S.M. Pollard, G.P. Schroth, A. Tanay, S. Hadjur, Cohesin-mediated interactions organize chromosomal domain architecture, EMBO J, 32 (2013) 3119-3129.
[239] V.C. Seitan, A.J. Faure, Y. Zhan, R.P. McCord, B.R. Lajoie, E. Ing-Simmons, B. Lenhard, L. Giorgetti, E. Heard, A.G. Fisher, P. Flicek, J. Dekker, M. Merkenschlager, Cohesin-based chromatin interactions enable regulated gene expression within preexisting architectural compartments, Genome Res, 23 (2013) 2066-2077.
[240] G. Natoli, J.C. Andrau, Noncoding transcription at enhancers: general principles and functional models, Annu Rev Genet, 46 (2012) 1-19.
[241] W. Li, D. Notani, M.G. Rosenfeld, Enhancers as non-coding RNA transcription units: recent insights and future perspectives, Nature reviews. Genetics, 17 (2016) 207-223.
[242] D. Shlyueva, G. Stampfel, A. Stark, Transcriptional enhancers: from properties to genome-wide predictions, Nature reviews. Genetics, 15 (2014) 272-286.
[243] E. Calo, J. Wysocka, Modification of enhancer chromatin: what, how, and why?, Molecular cell, 49 (2013) 825-837.
[244] G. Legube, D. Trouche, Regulating histone acetyltransferases and deacetylases, EMBO Rep, 4 (2003) 944-947.
[245] L. Icardi, R. Mori, V. Gesellchen, S. Eyckerman, L. De Cauwer, J. Verhelst, K. Vercauteren, X. Saelens, P. Meuleman, G. Leroux-Roels, K. De Bosscher, M. Boutros, J. Tavernier, The Sin3a repressor complex is a master regulator of STAT transcriptional activity, Proceedings of the National Academy of Sciences of the United States of America, 109 (2012) 12058-12063.
[246] I. Nusinzon, C.M. Horvath, Interferon-stimulated transcription and innate antiviral immunity require deacetylase activity and histone deacetylase 1, Proceedings of the National Academy of Sciences of the United States of America, 100 (2003) 14742-14747.
[247] S. Ray, C. Lee, T. Hou, I. Boldogh, A.R. Brasier, Requirement of histone deacetylase1 (HDAC1) in signal transducer and activator of transcription 3 (STAT3) nucleocytoplasmic distribution, Nucleic acids research, 36 (2008) 4510-4520.

[248] J. Li, J. Wang, J. Wang, Z. Nawaz, J.M. Liu, J. Qin, J. Wong, Both corepressor proteins SMRT and N-CoR exist in large protein complexes containing HDAC3, EMBO J, 19 (2000) 4342-4350.
[249] M.G. Guenther, O. Barak, M.A. Lazar, The SMRT and N-CoR corepressors are activating cofactors for histone deacetylase 3, Mol Cell Biol, 21 (2001) 6091-6101.
[250] P. Karagianni, J. Wong, HDAC3: taking the SMRT-N-CoRrect road to repression, Oncogene, 26 (2007) 5439-5449.
[251] K. Takeda, T. Kaisho, S. Akira, Toll-like receptors, Annu Rev Immunol, 21 (2003) 335-376.
[252] N.M. de Vasconcelos, N. Van Opdenbosch, M. Lamkanfi, Inflammasomes as polyvalent cell death platforms, Cell Mol Life Sci, (2016).
[253] D.M. Cittelly, P.M. Das, N.S. Spoelstra, S.M. Edgerton, J.K. Richer, A.D. Thor, F.E. Jones, Downregulation of miR-342 is associated with tamoxifen resistant breast tumors, Mol Cancer, 9 (2010) 317.
[254] B.M. Engels, G. Hutvagner, Principles and effects of microRNA-mediated post-transcriptional gene regulation, Oncogene, 25 (2006) 6163-6169.
[255] H. Wang, J. Wu, X. Meng, X. Ying, Y. Zuo, R. Liu, Z. Pan, T. Kang, W. Huang, MicroRNA-342 inhibits colorectal cancer cell proliferation and invasion by directly targeting DNA methyltransferase 1, Carcinogenesis, 32 (2011) 1033-1042.
[256] P. Loke, M.G. Nair, J. Parkinson, D. Guiliano, M. Blaxter, J.E. Allen, IL-4 dependent alternatively-activated macrophages have a distinctive in vivo gene expression phenotype, BMC Immunol, 3 (2002) 7.
[257] W.M. Grady, R.K. Parkin, P.S. Mitchell, J.H. Lee, Y.H. Kim, K.D. Tsuchiya, M.K. Washington, C. Paraskeva, J.K. Willson, A.M. Kaz, E.M. Kroh, A. Allen, B.R. Fritz, S.D. Markowitz, M. Tewari, Epigenetic silencing of the intronic microRNA hsa-miR-342 and its host gene EVL in colorectal cancer, Oncogene, 27 (2008) 3880-3888.
[258] D. Ronchetti, M. Lionetti, L. Mosca, L. Agnelli, A. Andronache, S. Fabris, G.L. Deliliers, A. Neri, An integrative genomic approach reveals coordinated expression of intronic miR-335, miR-342, and miR-561 with deregulated host genes in multiple myeloma, BMC Med Genomics, 1 (2008) 37.
[259] L.L. Elo, H. Jarvenpaa, S. Tuomela, S. Raghav, H. Ahlfors, K. Laurila, B. Gupta, R.J. Lund, J. Tahvanainen, R.D. Hawkins, M. Oresic, H. Lahdesmaki, O. Rasool, K.V. Rao, T. Aittokallio, R. Lahesmaa, Genome-wide profiling of interleukin-4 and STAT6 transcription factor regulation of human Th2 cell programming, Immunity, 32 (2010) 852-862.
[260] G. Bindea, B. Mlecnik, H. Hackl, P. Charoentong, M. Tosolini, A. Kirilovsky, W.H. Fridman, F. Pages, Z. Trajanoski, J. Galon, ClueGO: a Cytoscape plug-in to decipher functionally grouped gene ontology and pathway annotation networks, Bioinformatics, 25 (2009) 1091-1093.
[261] J. Montojo, K. Zuberi, H. Rodriguez, G.D. Bader, Q. Morris, GeneMANIA: Fast gene network construction and function prediction for Cytoscape, F1000Research, 3 (2014) 153.
[262] V. Agarwal, G.W. Bell, J.W. Nam, D.P. Bartel, Predicting effective microRNA target sites in mammalian mRNAs, eLife, 4 (2015).
[263] J. Wang, X. Bai, Q. Song, F. Fan, Z. Hu, G. Cheng, Y. Zhang, miR-223 Inhibits Lipid Deposition and Inflammation by Suppressing Toll-Like Receptor 4 Signaling in Macrophages, International journal of molecular sciences, 16 (2015) 24965-24982.
[264] L.N. Schulte, A.J. Westermann, J. Vogel, Differential activation and functional specialization of miR-146 and miR-155 in innate immune sensing, Nucleic acids research, 41 (2013) 542-553.
[265] F. Ozsolak, L.L. Poling, Z. Wang, H. Liu, X.S. Liu, R.G. Roeder, X. Zhang, J.S. Song, D.E. Fisher, Chromatin structure analyses identify miRNA promoters, Genes & development, 22 (2008) 3172-3183.
[266] C.H. Chien, Y.M. Sun, W.C. Chang, P.Y. Chiang-Hsieh, T.Y. Lee, W.C. Tsai, J.T. Horng, A.P. Tsou, H.D. Huang, Identifying transcriptional start sites of human microRNAs based on high-throughput sequencing data, Nucleic acids research, 39 (2011) 9345-9356.
[267] S. Heinz, C.E. Romanoski, C. Benner, C.K. Glass, The selection and function of cell type-specific enhancers, Nature reviews. Molecular cell biology, 16 (2015) 144-154.

[268] D. Chen, L.Y. Fu, Z. Zhang, G. Li, H. Zhang, L. Jiang, A.P. Harrison, H.P. Shanahan, C. Klukas, H.Y. Zhang, Y. Ruan, L.L. Chen, M. Chen, Dissecting the chromatin interactome of microRNA genes, Nucleic acids research, 42 (2014) 3028-3043.
[269] J.H. Cheng, D.Z. Pan, Z.T. Tsai, H.K. Tsai, Genome-wide analysis of enhancer RNA in gene regulation across 12 mouse tissues, Scientific reports, 5 (2015) 12648.
[270] P. Li, N.J. Spann, M.U. Kaikkonen, M. Lu, Y. Oh da, J.N. Fox, G. Bandyopadhyay, S. Talukdar, J. Xu, W.S. Lagakos, D. Patsouris, A. Armando, O. Quehenberger, E.A. Dennis, S.M. Watkins, J. Auwerx, C.K. Glass, J.M. Olefsky, NCoR repression of LXRs restricts macrophage biosynthesis of insulin-sensitizing omega 3 fatty acids, Cell, 155 (2013) 200-214.
[271] M.K. Atianand, W. Hu, A.T. Satpathy, Y. Shen, E.P. Ricci, J.R. Alvarez-Dominguez, A. Bhatta, S.A. Schattgen, J.D. McGowan, J. Blin, J.E. Braun, P. Gandhi, M.J. Moore, H.Y. Chang, H.F. Lodish, D.R. Caffrey, K.A. Fitzgerald, A Long Noncoding RNA lincRNA-EPS Acts as a Transcriptional Brake to Restrain Inflammation, Cell, 165 (2016) 1672-1685.
[272] S. Gordon, P.R. Taylor, Monocyte and macrophage heterogeneity, Nature reviews. Immunology, 5 (2005) 953-964.
[273] B. Ruffell, N.I. Affara, L.M. Coussens, Differential macrophage programming in the tumor microenvironment, Trends in immunology, 33 (2012) 119-126.
[274] M.L. Squadrito, M. Etzrodt, M. De Palma, M.J. Pittet, MicroRNA-mediated control of macrophages and its implications for cancer, Trends in immunology, 34 (2013) 350-359.
[275] G. Liu, E. Abraham, MicroRNAs in immune response and macrophage polarization, Arteriosclerosis, thrombosis, and vascular biology, 33 (2013) 170-177.
[276] S.F. Schmidt, B.D. Larsen, A. Loft, R. Nielsen, J.G. Madsen, S. Mandrup, Acute TNF-induced repression of cell identity genes is mediated by NFkappaB-directed redistribution of cofactors from super-enhancers, Genome research, 25 (2015) 1281-1294.
[277] Q. Yan, R.J. Carmody, Z. Qu, Q. Ruan, J. Jager, S.E. Mullican, M.A. Lazar, Y.H. Chen, Nuclear factor-kappaB binding motifs specify Toll-like receptor-induced gene repression through an inducible repressosome, Proceedings of the National Academy of Sciences of the United States of America, 109 (2012) 14140-14145.
[278] C.K. Glass, K. Saijo, Nuclear receptor transrepression pathways that regulate inflammation in macrophages and T cells, Nature reviews. Immunology, 10 (2010) 365-376.
[279] S.J. Bensinger, P. Tontonoz, Integration of metabolism and inflammation by lipid-activated nuclear receptors, Nature, 454 (2008) 470-477.
[280] H. Nakajima, P.K. Brindle, M. Handa, J.N. Ihle, Functional interaction of STAT5 and nuclear receptor co-repressor SMRT: implications in negative regulation of STAT5-dependent transcription, The EMBO journal, 20 (2001) 6836-6844.
[281] H.J. Park, J. Li, R. Hannah, S. Biddie, A.I. Leal-Cervantes, K. Kirschner, D. Flores Santa Cruz, V. Sexl, B. Gottgens, A.R. Green, Cytokine-induced megakaryocytic differentiation is regulated by genome-wide loss of a uSTAT transcriptional program, The EMBO journal, 35 (2016) 580-594.
[282] G.H. Eom, H. Kook, Posttranslational modifications of histone deacetylases: implications for cardiovascular diseases, Pharmacology & therapeutics, 143 (2014) 168-180.
[283] R.A. Mathias, A.J. Guise, I.M. Cristea, Post-translational modifications regulate class IIa histone deacetylase (HDAC) function in health and disease, Molecular & cellular proteomics : MCP, 14 (2015) 456-470.
[284] M. Vogelauer, A.S. Krall, M.A. McBrian, J.Y. Li, S.K. Kurdistani, Stimulation of histone deacetylase activity by metabolites of intermediary metabolism, The Journal of biological chemistry, 287 (2012) 32006-32016.
[285] C. Nepal, M. Coolen, Y. Hadzhiev, D. Cussigh, P. Mydel, V.M. Steen, P. Carninci, J.B. Andersen, L. Bally-Cuif, F. Muller, B. Lenhard, Transcriptional, post-transcriptional and chromatin-associated regulation of pri-miRNAs, pre-miRNAs and moRNAs, Nucleic acids research, 44 (2016) 3070-3081.
[286] H. Suzuki, S. Takatsuka, H. Akashi, E. Yamamoto, M. Nojima, R. Maruyama, M. Kai, H.O. Yamano, Y. Sasaki, T. Tokino, Y. Shinomura, K. Imai, M. Toyota, Genome-wide profiling of chromatin

signatures reveals epigenetic regulation of MicroRNA genes in colorectal cancer, Cancer research, 71 (2011) 5646-5658.
[287] D. de Rie, I. Abugessaisa, T. Alam, E. Arner, P. Arner, H. Ashoor, G. Astrom, M. Babina, N. Bertin, A.M. Burroughs, A.J. Carlisle, C.O. Daub, M. Detmar, R. Deviatiiarov, A. Fort, C. Gebhard, D. Goldowitz, S. Guhl, T.J. Ha, J. Harshbarger, A. Hasegawa, K. Hashimoto, M. Herlyn, P. Heutink, K.J. Hitchens, C.C. Hon, E. Huang, Y. Ishizu, C. Kai, T. Kasukawa, P. Klinken, T. Lassmann, C.H. Lecellier, W. Lee, M. Lizio, V. Makeev, A. Mathelier, Y.A. Medvedeva, N. Mejhert, C.J. Mungall, S. Noma, M. Ohshima, M. Okada-Hatakeyama, H. Persson, P. Rizzu, F. Roudnicky, P. Saetrom, H. Sato, J. Severin, J.W. Shin, R.K. Swoboda, H. Tarui, H. Toyoda, K. Vitting-Seerup, L. Winteringham, Y. Yamaguchi, K. Yasuzawa, M. Yoneda, N. Yumoto, S. Zabierowski, P.G. Zhang, C.A. Wells, K.M. Summers, H. Kawaji, A. Sandelin, M. Rehli, F. Consortium, Y. Hayashizaki, P. Carninci, A.R.R. Forrest, M.J.L. de Hoon, An integrated expression atlas of miRNAs and their promoters in human and mouse, Nature biotechnology, 35 (2017) 872-878.
[288] A. Rodriguez, S. Griffiths-Jones, J.L. Ashurst, A. Bradley, Identification of mammalian microRNA host genes and transcription units, Genome Res, 14 (2004) 1902-1910.
[289] H.K. Saini, S. Griffiths-Jones, A.J. Enright, Genomic analysis of human microRNA transcripts, Proc Natl Acad Sci U S A, 104 (2007) 17719-17724.
[290] A. Marsico, M.R. Huska, J. Lasserre, H. Hu, D. Vucicevic, A. Musahl, U. Orom, M. Vingron, PROmiRNA: a new miRNA promoter recognition method uncovers the complex regulation of intronic miRNAs, Genome biology, 14 (2013) R84.
[291] M. Ceppi, P.M. Pereira, I. Dunand-Sauthier, E. Barras, W. Reith, M.A. Santos, P. Pierre, MicroRNA-155 modulates the interleukin-1 signaling pathway in activated human monocyte-derived dendritic cells, Proceedings of the National Academy of Sciences of the United States of America, 106 (2009) 2735-2740.
[292] Q. Duan, X. Mao, Y. Xiao, Z. Liu, Y. Wang, H. Zhou, Z. Zhou, J. Cai, K. Xia, Q. Zhu, J. Qi, H. Huang, J. Plutzky, T. Yang, Super enhancers at the miR-146a and miR-155 genes contribute to self-regulation of inflammation, Biochimica et biophysica acta, 1859 (2016) 564-571.
[293] Y. Wei, M. Nazari-Jahantigh, L. Chan, M. Zhu, K. Heyll, J. Corbalan-Campos, P. Hartmann, A. Thiemann, C. Weber, A. Schober, The microRNA-342-5p fosters inflammatory macrophage activation through an Akt1- and microRNA-155-dependent pathway during atherosclerosis, Circulation, 127 (2013) 1609-1619.
[294] K.A. Robertson, W.Y. Hsieh, T. Forster, M. Blanc, H. Lu, P.J. Crick, E. Yutuc, S. Watterson, K. Martin, S.J. Griffiths, A.J. Enright, M. Yamamoto, M.M. Pradeepa, K.A. Lennox, M.A. Behlke, S. Talbot, J. Haas, L. Dolken, W.J. Griffiths, Y. Wang, A. Angulo, P. Ghazal, An Interferon Regulated MicroRNA Provides Broad Cell-Intrinsic Antiviral Immunity through Multihit Host-Directed Targeting of the Sterol Pathway, PLoS biology, 14 (2016) e1002364.
[295] J.E. Allen, T.E. Sutherland, Host protective roles of type 2 immunity: parasite killing and tissue repair, flip sides of the same coin, Semin Immunol, 26 (2014) 329-340.
[296] P. Salgame, G.S. Yap, W.C. Gause, Effect of helminth-induced immunity on infections with microbial pathogens, Nature immunology, 14 (2013) 1118-1126.
[297] D.E. Elliott, J.V. Weinstock, Helminth-host immunological interactions: prevention and control of immune-mediated diseases, Ann N Y Acad Sci, 1247 (2012) 83-96.
[298] W. Deng, Y. Ohmori, T.A. Hamilton, Mechanisms of IL-4-mediated suppression of IP-10 gene expression in murine macrophages, J Immunol, 153 (1994) 2130-2136.
[299] Y. Ohmori, T.A. Hamilton, IL-4-induced STAT6 suppresses IFN-gamma-stimulated STAT1-dependent transcription in mouse macrophages, J Immunol, 159 (1997) 5474-5482.
[300] V.T. Nguyen, E.N. Benveniste, IL-4-activated STAT-6 inhibits IFN-gamma-induced CD40 gene expression in macrophages/microglia, J Immunol, 165 (2000) 6235-6243.
[301] Y. Ohmori, T.A. Hamilton, Interleukin-4/STAT6 represses STAT1 and NF-kappa B-dependent transcription through distinct mechanisms, J Biol Chem, 275 (2000) 38095-38103.

[302] V. Piccolo, A. Curina, M. Genua, S. Ghisletti, M. Simonatto, A. Sabo, B. Amati, R. Ostuni, G. Natoli, Opposing macrophage polarization programs show extensive epigenomic and transcriptional cross-talk, Nature immunology, 18 (2017) 530-540.
[303] S.B. Weisser, H.K. Brugger, N.S. Voglmaier, K.W. McLarren, N. van Rooijen, L.M. Sly, SHIP-deficient, alternatively activated macrophages protect mice during DSS-induced colitis, J Leukoc Biol, 90 (2011) 483-492.
[304] M.M. Hunter, A. Wang, K.S. Parhar, M.J. Johnston, N. Van Rooijen, P.L. Beck, D.M. McKay, In vitro-derived alternatively activated macrophages reduce colonic inflammation in mice, Gastroenterology, 138 (2010) 1395-1405.
[305] J.V. Weinstock, D.E. Elliott, Translatability of helminth therapy in inflammatory bowel diseases, Int J Parasitol, 43 (2013) 245-251.
[306] E. Cario, G. Gerken, D.K. Podolsky, Toll-like receptor 2 controls mucosal inflammation by regulating epithelial barrier function, Gastroenterology, 132 (2007) 1359-1374.
[307] C. Bauer, P. Duewell, C. Mayer, H.A. Lehr, K.A. Fitzgerald, M. Dauer, J. Tschopp, S. Endres, E. Latz, M. Schnurr, Colitis induced in mice with dextran sulfate sodium (DSS) is mediated by the NLRP3 inflammasome, Gut, 59 (2010) 1192-1199.
[308] M.H. Zaki, K.L. Boyd, P. Vogel, M.B. Kastan, M. Lamkanfi, T.D. Kanneganti, The NLRP3 inflammasome protects against loss of epithelial integrity and mortality during experimental colitis, Immunity, 32 (2010) 379-391.
[309] O. Soehnlein, L. Lindbom, Phagocyte partnership during the onset and resolution of inflammation, Nat Rev Immunol, 10 (2010) 427-439.
[310] C. Auffray, M.H. Sieweke, F. Geissmann, Blood monocytes: development, heterogeneity, and relationship with dendritic cells, Annu Rev Immunol, 27 (2009) 669-692.
[311] S.U. Amano, J.L. Cohen, P. Vangala, M. Tencerova, S.M. Nicoloro, J.C. Yawe, Y. Shen, M.P. Czech, M. Aouadi, Local proliferation of macrophages contributes to obesity-associated adipose tissue inflammation, Cell Metab, 19 (2014) 162-171.
[312] C.S. Robbins, I. Hilgendorf, G.F. Weber, I. Theurl, Y. Iwamoto, J.L. Figueiredo, R. Gorbatov, G.K. Sukhova, L.M. Gerhardt, D. Smyth, C.C. Zavitz, E.A. Shikatani, M. Parsons, N. van Rooijen, H.Y. Lin, M. Husain, P. Libby, M. Nahrendorf, R. Weissleder, F.K. Swirski, Local proliferation dominates lesional macrophage accumulation in atherosclerosis, Nat Med, 19 (2013) 1166-1172.
[313] M. Lize, S. Pilarski, M. Dobbelstein, E2F1-inducible microRNA 449a/b suppresses cell proliferation and promotes apoptosis, Cell Death Differ, 17 (2010) 452-458.
[314] I. Capua, A. Mercalli, M.S. Pizzuto, A. Romero-Tejeda, S. Kasloff, C. De Battisti, F. Bonfante, L.V. Patrono, E. Vicenzi, V. Zappulli, V. Lampasona, A. Stefani, C. Doglioni, C. Terregino, G. Cattoli, L. Piemonti, Influenza A viruses grow in human pancreatic cells and cause pancreatitis and diabetes in an animal model, Journal of virology, 87 (2013) 597-610.
[315] S. Al-Quraishy, M.A. Dkhil, D. Delic, A.A. Abdel-Baki, F. Wunderlich, Organ-specific testosterone-insensitive response of miRNA expression of C57BL/6 mice to Plasmodium chabaudi malaria, Parasitol Res, 111 (2012) 1093-1101.
[316] U. Frevert, E. Nardin, Cellular effector mechanisms against Plasmodium liver stages, Cell Microbiol, 10 (2008) 1956-1967.

15. Publications Related to Dissertation

UNIVERSITY AND NATIONAL LIBRAY
UNIVERSITY OF DEBRECEN
H-4002 Egyetem tér 1, Debrecen
Phone: +3652/410-443, email: publikaciok@lib.unideb.hu

Registry number: DEENK/28/2018.PL
Subject: PhD Publikációs Lista

Candidate: Zsolt Czimmerer
Neptun ID: J06DZW
Doctoral School: Doctoral School of Molecular Cellular and Immune Biology
MTMT ID: 10038295

List of publications related to the dissertation

1. Czimmerer, Z., Horváth, A., Dániel, B., Nagy, G., Cuaranta-Monroy, I., Kiss, M., Kolostyák, Z., Póliska, S., Steiner, L., Giannakis, N., Varga, T., Nagy, L.: Dynamic transcriptional control of macrophage miRNA signature via inflammation responsive enhancers revealed using a combination of next generation sequencing-based approaches.
Biochim. Biophys. Acta-Gene Regul. Mech. 1861 (1), 14-28, 2018.
DOI: http://dx.doi.org/10.1016/j.bbagrm.2017.11.003
IF: 5.018 (2016)

2. Czimmerer, Z., Dániel, B., Horváth, A., Rückerl, D., Nagy, G., Kiss, M., Peloquin, M., Budai, M. M., Cuaranta-Monroy, I., Simándi, Z., Steiner, L., Nagy, B., Póliska, S., Bankó, C., Bacsó, Z., Schulman, I. G., Sauer, S., Deleuze, J. F., Allen, J. E., Benkő, S., Nagy, L.: The Transcription Factor STAT6 Mediates Direct Repression of Inflammatory Enhancers and Limits Activation of Alternatively Polarized Macrophages.
Immunity. 48 (1), 75-90, 2018.
DOI: http://dx.doi.org/10.1016/j.immuni.2017.12.010
IF: 22.845 (2016)

3. Czimmerer, Z., Varga, T., Kiss, M., Vázquez, C. O., Doan-Xuan, Q. M., Rückerl, D., Tattikota, S. G., Yan, X., Nagy, Z. S., Dániel, B., Póliska, S., Horváth, A., Nagy, G., Varallyay, É., Poy, M. N., Allen, J. E., Bacsó, Z., Abreu-Goodger, C., Nagy, L.: The IL-4/STAT6 signaling axis establishes a conserved microRNA signature in human and mouse macrophages regulating cell survival via miR-342-3p.
Genome Med. 8 (1), 1-22, 2016.
DOI: http://dx.doi.org/10.1186/s13073-016-0315-y
IF: 7.071

16. List of Other Publications

UNIVERSITY AND NATIONAL LIBRAY
UNIVERSITY OF DEBRECEN
H-4002 Egyetem tér 1, Debrecen
Phone: +3652/410-443, email: publikaciok@lib.unideb.hu

List of other publications

4. Czimmerer, Z., Nagy, Z. S., Nagy, G., Horváth, A., Silye-Cseh, T., Kriston, Á., Jonás, D., Sauer, S., Steiner, L., Dániel, B., Deleuze, J. F., Nagy, L.: Extensive and functional overlap of the STAT6 and RXR cistromes in the active enhancer repertoire of human CD14+ monocyte derived differentiating macrophages.
Mol. Cell. Endocrinol. [Epub ahead of print], 2017.
DOI: http://dx.doi.org/10.1016/j.mce.2017.07.034
IF: 3.754 (2016)

5. Fejes, Z., Póliska, S., Czimmerer, Z., Káplár, M., Penyige, A., Gál Szabó, G., Bekéné Debreceni, I., Kunapuli, S. P., Kappelmayer, J., Nagy, B.: Hyperglycemia suppresses microRNA expression in platelets to increase P2RY12 and SELP levels in type 2 diabetes mellitus.
Thromb. Haemost. 117 (3), 529-542, 2017.
DOI: http://dx.doi.org/10.1160/TH16-04-0322
IF: 5.627 (2016)

6. Kiss, M., Czimmerer, Z., Nagy, G., Bieniasz-Krzywiec, P., Ehling, M., Pap, A., Póliska, S., Botó, P., Tzerpos, P., Horváth, A., Kolostyák, Z., Dániel, B., Szatmári, I., Mazzone, M., Nagy, L.: Retinoid X receptor suppresses a metastasis-promoting transcriptional program in myeloid cells via a ligand-insensitive mechanism.
Proc. Natl. Acad. Sci. U. S. A. 114 (40), 10725-10730, 2017.
DOI: http://dx.doi.org/10.1073/pnas.1700785114
IF: 9.661 (2016)

7. Gyöngyösi, A., Dócs, O., Czimmerer, Z., Orosz, L., Horváth, A., Török, O., Méhes, G., Nagy, L., Bálint, B. L.: Measuring expression levels of small regulatory RNA molecules from body fluids and formalin-fixed, paraffin-embedded samples.
Methods Mol. Biol. 1182, 105-119, 2014.
DOI: http://dx.doi.org/10.1007/978-1-4939-1062-5_10

8. Dániel, B., Nagy, G., Hah, N., Horváth, A., Czimmerer, Z., Póliska, S., Gyuris, T., Keirsse, J., Gysemans, C., Van Ginderachter, J. A., Bálint, B. L., Evans, R. M., Barta, E., Nagy, L.: The active enhancer network operated by liganded RXR supports angiogenic activity in macrophages.
Genes Dev. 28 (14), 1562-1577, 2014.
DOI: http://dx.doi.org/10.1101/gad.242685.114
IF: 10.798

9. Czimmerer, Z., Hulvely, J., Simándi, Z., Varallyay, É., Havelda, Z., Szabó, E., Varga, A., Dezső, B., Balogh, M., Horváth, A., Domokos, B., Török, Z., Nagy, L., Bálint, B. L.: A versatile method to design stem-loop primer-based quantitative PCR assays for detecting small regulatory RNA molecules.
PLoS One. 8 (1), 1-10, 2013.
DOI: http://dx.doi.org/10.1371/journal.pone.0055168
IF: 3.534

10. Nagy, Z., Czimmerer, Z., Nagy, L.: Nuclear receptor mediated mechanisms of macrophage cholesterol metabolism.
Mol. Cell. Endocrinol. 368 (1-2), 85-98, 2013.
DOI: http://dx.doi.org/10.1016/j.mce.2012.04.003
IF: 4.241

11. Nagy, Z., Czimmerer, Z., Szántó, A., Nagy, L.: Pro-inflammatory cytokines negatively regulate PPARγ mediated gene expression in both human and murine macrophages via multiple mechanisms.
Immunobiology. 218 (11), 1336-1344, 2013.
DOI: http://dx.doi.org/10.1016/j.imbio.2013.06.011
IF: 3.18

12. Brignull, L. M., Czimmerer, Z., Saidi, H., Dániel, B., Villela, I., Bartlett, N. W., Johnston, S. L., Meira, L. B., Nagy, L., Nohturfft, A.: Reprogramming of lysosomal gene expression by interleukin-4 and Stat6.
BMC Genomics. 14 (1), 1-20, 2013.
DOI: http://dx.doi.org/10.1186/1471-2164-14-853
IF: 4.041

13. Kiss, M., Czimmerer, Z., Nagy, L.: The role of lipid-activated nuclear receptors in shaping macrophage and dendritic cell function: from physiology to pathology.
J. Allergy Clin. Immunol. 132 (2), 264-286, 2013.
DOI: http://dx.doi.org/10.1016/j.jaci.2013.05.044
IF: 11.248

14. Czimmerer, Z., Varga, T., Póliska, S., Német, I., Szántó, A., Nagy, L.: Identification of novel markers of alternative activation and potential endogenous PPARgamma ligand production mechanisms in human IL-4 stimulated differentiating macrophages.
Immunobiology. 217 (12), 1301-1314, 2012.
DOI: http://dx.doi.org/10.1016/j.imbio.2012.08.270
IF: 2.814

15. Varga, T., Czimmerer, Z., Nagy, L.: PPARs are a unique set of fatty acid regulated transcription factors controlling both lipid metabolism and inflammation.
Biochim. Biophys. Acta Mol. Basis Dis. 1812 (8), 1007-1022, 2011.
DOI: http://dx.doi.org/10.1016/j.bbadis.2011.02.014
IF: 5.387

16. Oberoi, J., Fairall, L., Watson, P. J., Yang, J. C., Czimmerer, Z., Kampmann, T., Goult, B. T., Greenwood, J. A., Gooch, J. T., Kallenberger, B. C., Nagy, L., Neuhaus, D., Schwabe, J. W. R.: Structural basis for the assembly of the SMRT/NCoR core transcriptional repression machinery.
Nat. Struct. Mol. Biol. 18 (2), 177-184, 2011.
DOI: http://dx.doi.org/10.1038/nsmb.1983
IF: 12.712

17. Mikó, E., Margitai, Z., Czimmerer, Z., Várkonyi, I., Dezső, B., Lányi, Á., Bacsó, Z., Scholtz, B.: miR-126 inhibits proliferation of small cell lung cancer cells by targeting SLC7A5.
FEBS Lett. 585 (8), 1191-1196, 2011.
DOI: http://dx.doi.org/10.1016/j.febslet.2011.03.039
IF: 3.538

UNIVERSITY AND NATIONAL LIBRAY
UNIVERSITY OF DEBRECEN
H-4002 Egyetem tér 1, Debrecen
Phone: +3652/410-443, email: publikaciok@lib.unideb.hu

18. Mikó, E., Czimmerer, Z., Csánky, E., Boros, G., Buslig, J., Dezső, B., Scholtz, B.: Differentially expressed microRNAs in small cell lung cancer.
Exp. Lung Res. 35 (8), 646-664, 2009.
DOI: http://dx.doi.org/10.3109/01902140902822312
IF: 1.177

19. Rőszer, T., Jenei, Z., Gáll, T., Nagy, O., Czimmerer, Z., Serfőző, Z., Elekes, K., Bánfalvi, G.: A possible stimulatory effect of FMRFamide on neural nitric oxide production in the central nervous system of Helix lucorum L.
Brain. Behav. Evol. 63 (1), 23-33, 2004.
IF: 1.954

20. Rőszer, T., Czimmerer, Z., Szentmiklósi, J. A., Bánfalvi, G.: Nitric oxide synthesis is blocked in the enteral nervous system during dormant periods of the snail Helix lucorum L.
Cell Tissue Res. 316, 255-262, 2004.
IF: 2.67

21. Rőszer, T., Jenei, Z., Serfőző, Z., Czimmerer, Z., Bánfalvi, G.: Structural diversity of NADPH diaphorase-reactive enteral networks in Stylommatophora (Gastropoda, Pulmonata).
Invertebr. Biol. 123 (2), 128-135, 2004.
IF: 0.754

Total IF of journals (all publications): 122,024
Total IF of journals (publications related to the dissertation): 34,934

The Candidate's publication data submitted to the iDEa Tudóstér have been validated by DEENK on the basis of Web of Science, Scopus and Journal Citation Report (Impact Factor) databases.

26 January, 2018